

Sheffield Hallam University

Lattice models of amphiphile and solvent mixtures.

BRINDLE, David.

Available from the Sheffield Hallam University Research Archive (SHURA) at:

<http://shura.shu.ac.uk/19397/>

A Sheffield Hallam University thesis

This thesis is protected by copyright which belongs to the author.

The content must not be changed in any way or sold commercially in any format or medium without the formal permission of the author.

When referring to this work, full bibliographic details including the author, title, awarding institution and date of the thesis must be given.

Please visit <http://shura.shu.ac.uk/19397/> and <http://shura.shu.ac.uk/information.html> for further details about copyright and re-use permissions.



339856

Sheffield City Polytechnic Library

REFERENCE ONLY

ProQuest Number: 10694278

All rights reserved

INFORMATION TO ALL USERS

The quality of this reproduction is dependent upon the quality of the copy submitted.

In the unlikely event that the author did not send a complete manuscript and there are missing pages, these will be noted. Also, if material had to be removed, a note will indicate the deletion.



ProQuest 10694278

Published by ProQuest LLC (2017). Copyright of the Dissertation is held by the Author.

All rights reserved.

This work is protected against unauthorized copying under Title 17, United States Code
Microform Edition © ProQuest LLC.

ProQuest LLC.
789 East Eisenhower Parkway
P.O. Box 1346
Ann Arbor, MI 48106 – 1346

LATTICE MODELS OF AMPHIPHILE AND SOLVENT MIXTURES

DAVID BRINDLE, BSc

A thesis submitted in partial fulfilment of the requirements
of the Council for National Academic Awards for the degree of
Doctor of Philosophy

August 1991

Division of Applied Physics, Sheffield City Polytechnic
in collaboration with Albright and Wilson Ltd., Whitehaven.

ABSTRACT

Materials based on amphiphilic molecules have a wide range of industrial applications and are of fundamental importance in the structure of many biological systems. Their importance derives from their behaviour as surface-active agents in solubilization applications and because of their ability to form systems with varying degrees of structural order such as micelles, bilayers and liquid crystal phases. The nature of the molecular ordering is of importance both during the processing of these materials and in their final application.

A Monte Carlo simulation of a three dimensional lattice model of an amphiphile and solvent mixture has been developed as an extension of earlier work in two dimensions. In the earlier investigation the simulation was carried out with three segment amphiphiles on a two dimensional lattice and cluster size distributions were determined for a range of temperatures, amphiphile concentrations and intermolecular interaction energies.

In the current work, a wider range of structures are observed including micelles, bilayers and a vesicle. The structures are studied as a function of temperature, chain length, amphiphile concentration and intermolecular interaction energies. Clusters are characterised according to their shape, size and surface roughness. A detailed temperature-concentration phase diagram is presented for a system with four segment amphiphiles. The phase diagram shows a critical micelle concentration (c.m.c) at low amphiphile concentrations and a transition from a bicontinuous to lamellar region at amphiphile concentrations around 50%. At high amphiphile concentrations, there is some evidence for the formation of a gel. The results obtained question the validity of current models of the c.m.c.

The Monte Carlo simulations require extensive computing power and the simulation was carried out on a transputer array, where the parallel architecture allows high speed. The development of a suitable parallel algorithm is discussed.

A mean field model of a bilayer is presented which has similar interaction potentials as the Monte Carlo model. The ordering of the bilayer is examined as a function of chain length, bilayer thickness, temperature and inter molecular interaction energies. In this approximation a phase transition to the ordered bilayer is observed.

ACKNOWLEDGEMENTS

I would like to thank my supervisors at the Polytechnic, Dr. C. M. Care and Dr. R. M. Wood for their continuing help and guidance in my work and to thank E. Messenger and the staff at Albright and Wilson Ltd. for their support.

I also wish to thank the staff at the National Transputer Centre for their assistance in the early stages of my work and the technical staff at the Polytechnic for their help.

Finally I wish to acknowledge the support and tolerance of my family and friends, particularly during the 'writing up' stages.

ADVANCED STUDIES

As part of the course of study I attended an under graduate course on colloids in the Chemistry Department of the Polytechnic. The following conferences were attended:

CCP5 Annual Meeting, Birbeck College, London, January 1988

CCP5, Workshop on Parallel Computers in Molecular Simulation,
June 1988

NATO Advanced Studies Institute, Computer Modelling of Fluids,
Polymers and Solids, Bath, September 1988

CCP5 Annual Meeting, Cambridge, December 1989

CONTENTS

1 INTRODUCTION

1.1 AIMS

1.2 OVERVIEW OF CHAPTERS

2 AMPHIPHILIC SYSTEMS

2.1 THE AMPHIPHILE

2.2 LIQUID CRYSTAL PHASES

2.3 PHASE DIAGRAMS

3 SIMULATION AND STATISTICAL MECHANICAL MODELS OF MICELLES AND LYOTROPIC LIQUID CRYSTAL PHASES

3.1 INTRODUCTION

3.1.1 Model Classification

3.2 MODEL PROPERTIES

3.2.1 System Properties

3.2.2 Bond Order Parameters

3.2.3 Density Profiles

3.2.4 Principal Moments Of Inertia

3.3 SIMULATIONS

3.3.1 Molecular Dynamics

3.3.2 Monte Carlo Simulations

3.4 STATISTICAL MECHANICAL MODELS

3.4.1 Analytical Treatments

3.4.2 Phenomenological And Decorated Lattice Models

4 THE MONTE CARLO SIMULATION

4.1 INTRODUCTION

4.2 THE MODEL

4.3 THE SIMULATION

- 4.3.1 The Metropolis Algorithm
- 4.3.2 Describing The Amphiphiles
- 4.3.3 Random Number Generation
- 4.3.4 Moving The Amphiphile
- 4.3.5 The Internal Energy Change
- 4.3.6 The Boltzmann Weighting Factor
- 4.3.7 Accepting The Move
- 4.3.8 Data Analysis
- 4.3.9 Cluster Size
- 4.3.10 Principal Moments Of Inertia
- 4.3.11 Surface Roughness
- 4.3.12 Bond Order Parameters

4.4 CHOICE OF PARALLEL ALGORITHM

- 4.4.1 Processor Farm
- 4.4.2 Geometric Parallelism
- 4.4.3 Algorithmic Parallelism

4.5 IMPLEMENTATION OF PARALLEL SYSTEM

- 4.5.1 The Monte Carlo Process
- 4.5.2 The Statistics Process
- 4.5.3 The Host Process

5 THE MONTE CARLO RESULTS

5.1 INTRODUCTION

5.2 TESTING THE SIMULATION IN 2-D

5.3 COMPARISON OF 2-D AND 3-D

5.4 PRELIMINARY INVESTIGATION

5.5 HEAD-SOLVENT POTENTIAL, γ

- 5.5.1 Low Concentration
- 5.5.2 High Concentration
- 5.5.3 Summary

5.6 THE $s=4$, $\gamma=-2.0$ SYSTEM

- 5.6.1 The Micellar Region
- 5.6.2 The Phase Diagram
- 5.6.3 The Principal Moments Of Inertia
- 5.6.4 The Mean Cluster Size
- 5.6.5 The Surface Roughness
- 5.6.6 Comparison With Experiment
- 5.6.7 Effect Of Lattice Dimension
- 5.6.8 Summary

6 MEAN FIELD MODEL

6.1 INTRODUCTION

6.2 LATTICE MODELS

6.3 OFF LATTICE MODELS

6.4 EXTENSION TO MODEL

6.5 THE PROGRAM

6.5.1 Generating Chain Conformations

6.5.2 Determining The Degeneracies

6.5.3 Conformational Probabilities

6.5.4 Head Roughness

6.6 RESULTS

6.6.1 The Head-Solvent Interaction, γ

6.6.2 Effect Of Chain Length

6.6.3 The Bilayer Thickness

6.6.4 Comparison With Simulation

6.7 SUMMARY

7 SUMMARY AND CONCLUSIONS

8 FUTURE WORK

REFERENCES

APPENDIX A

APPENDIX B

Materials based on amphiphilic molecules have applications in a wide range of manufacturing and service industries where they behave as surface-active agents in solubilization processes. They are able to form systems with varying degrees of structural order such as micelles, bilayers and other lyotropic liquid crystal phases. The nature of the molecular ordering is of importance both during the processing of these materials and in their final application.

Although much experimental work has been performed in order to characterise the structures appearing in the various phases of aqueous-amphiphile systems, the relative importance of the fundamental driving forces of ordering have yet to be put on a sound basis. One way of contributing to this objective is to model an amphiphile and solvent system. The fundamental driving forces of ordering are more clearly observable in a model with idealised molecular structures and potentials. However the model should be detailed enough to show the molecular ordering seen in real systems. Computer simulations of models with simplified molecules are able to show self-assembly of amphiphiles.

1.1 AIMS

The aims of the project were:

1. To develop a simple three dimensional lattice model of an amphiphile-solvent mixture which displays the essential features of real lyotropic systems. The model, which is developed as an extension of earlier work in two dimensions [Care 1987a,b], is examined using Monte

Carlo simulation and by a mean field approximation for comparison.

2. To investigate the types of phases that the model is able to produce when monomers are allowed to freely assemble into the preferred structure and to develop ways of characterising these phases. The model is to be investigated for evidence of a critical micelle concentration. The effects of chain length, amphiphile concentration, intermolecular potentials and temperature on the phase diagram are also to be investigated.

3. To compare the phase diagram exhibited by the model with that observed experimentally.

1.2 OVERVIEW OF CHAPTERS

Chapter 2 is an introduction to amphiphiles and lyotropic liquid crystal structures. An introduction into the concept of a critical micelle concentration is also given.

Chapter 3 is a review of simulations and statistical mechanical models of amphiphile and solvent systems. The review pays special attention to simulations and lattice models as these are most relevant to the work presented in the following chapters. Similarly little attention is given to results of dynamic properties as these are not available from Monte Carlo simulations. Mean field models are reviewed separately in chapter 6 as they have a direct bearing on the model proposed there.

Chapter 4 introduces the proposed model and gives details of the Monte Carlo simulation. This includes a description of the development of a parallel simulation algorithm and of the configurational properties measured.

Chapter 5 presents the results from the Monte Carlo simulation. The results of a preliminary investigation into the effect of changing the system parameters, ie. chain length, amphiphile concentration, molecular interaction potentials and temperature are presented. A temperature-concentration phase diagram is presented for a system containing amphiphile with a chain length of 4. The evidence for the different phase regions, and for the existence of a critical micelle concentration, is discussed.

The first part of Chapter 6 reviews previous mean field models of amphiphilic systems. The review presents the separate approaches of lattice and off-lattice mean field models. Ideas from both these areas are used to present an adapted lattice model in which there are amphiphile-solvent interactions. These interactions are similar to those used in the Monte Carlo simulation and cause the mean field model to show evidence of a phase transition to a bilayer on cooling. A comparison is made between this transition and the equivalent transition obtained from the Monte Carlo simulation.

Finally, Chapter 7 summarises the work presented here and reports the conclusions, and Chapter 8 discusses possible future work.

2.1 THE AMPHIPHILE

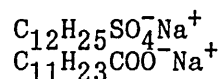
An amphiphile is typically a hydrocarbon which has two distinct parts. When immersed in a solvent, one section has an affinity for the solvent and is said to be solvophilic whilst the other section is solvophobic i.e. is repelled by the solvent. When, as is most common, the solvent is water, the terms hydrophilic and hydrophobic are used. Typically the solvophobic part is a hydrocarbon chain and the solvophilic section is polar or ionic and shorter than the hydrocarbon chain. The hydrophilic section is usually called the head and the hydrophobic section is called the tail.

Each amphiphile may only contain one polar head, but there may be several tails which may be either hydrocarbon or fluorocarbon and linear or branched. Amphiphiles with a single chain are most common. The minimum polarity for a head group is a single CH_3OH group.

Amphiphiles are normally classified according to the nature of the head group. They can be anionic, cationic, nonionic or zwitterionic. Some common examples of each are given below. [Ottewill 1983]

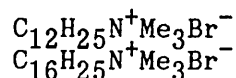
Anionic

Sodium dodecyl sulphate (SDS)
Sodium dodecanoate



Cationic

Dodecyltrimethylammonium bromide (DTAB)
Hexadecyltrimethylammonium bromide (HTAB)



Nonionic

Dodecylhexaoxyethylene glycol monoether $C_{12}H_{25}[OCH_2CH_2]_6OH$
Dodecyl sulphanyl ethanol $C_{12}H_{25}SOCH_2CH_2OH$

Zwitterionic

3-dimethyldodecylamine propane sulphonate $C_{12}H_{25}-\overset{+}{N}(Me)_2-C_2H_4CH_2SO_3^-$

Anionics are the most widely used surfactants because of cost and performance. Cationics are expensive, but their germicidal action makes them useful for some applications [Ottewill 1983]. An advantage enjoyed by nonionics is that the lengths of both solvophilic and solvophobic groups can be varied, thus changing the physical properties of the surfactant system which extends their application.

When amphiphiles, are immersed in a nonpolar/polar liquid mixture they will tend to aggregate at the liquid interface with the tails in the nonpolar medium and the heads in the polar medium. This is often explained as limiting the solvophobic interaction between the tail and polar medium. However, it is better viewed as increasing the solvophilic interaction between the surfactant heads and the polar liquid, as the solvophobic interaction is often slightly attractive but much less so than the solvophilic interaction. (See Tanford (1980)). The surface aggregation effect is also seen at an air/water interface, figure 2.1a.

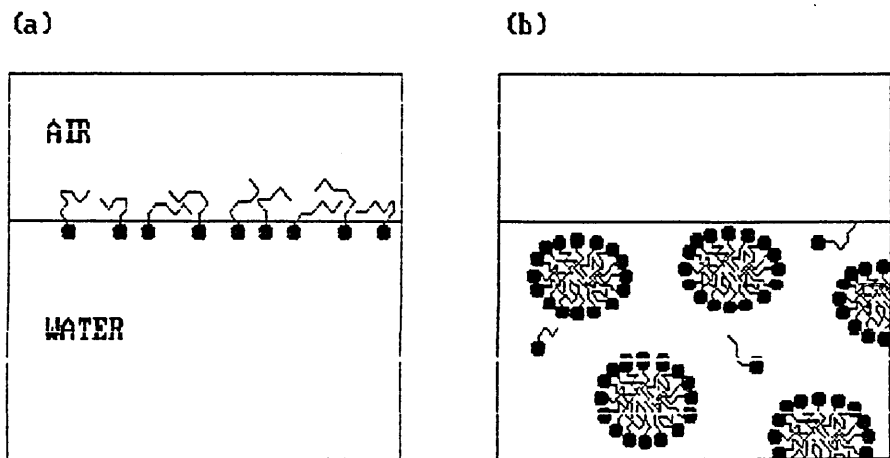


Figure 2.1 : (a) surface aggregation at an air/water interface
(b) schematic representation of the micellar system

At a certain concentration of the amphiphiles in the solvent, aggregates of amphiphiles will form within the bulk solvent, see figure 2.1b. These aggregates are termed "micelles" and first appear within a narrow concentration range called "the critical micelle concentration", or c.m.c. Evidence for this formation of aggregates can be obtained by monitoring a range a physical properties as shown in figure 2.2 [Lindman 1983].

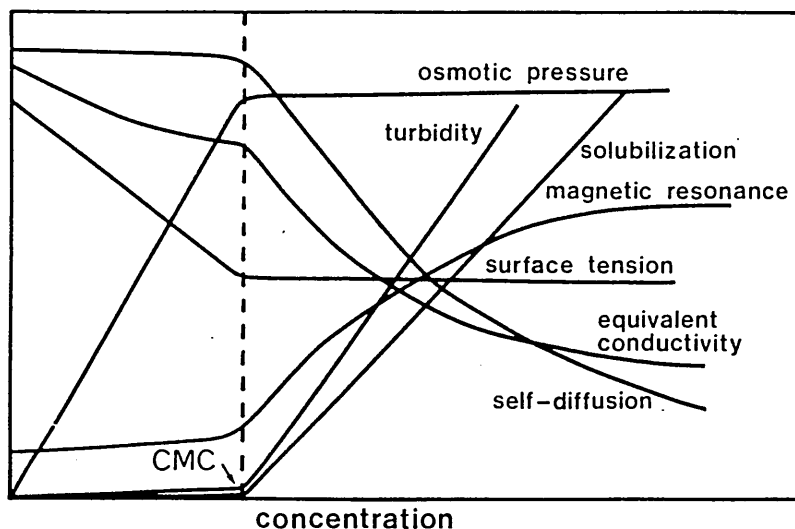


Figure 2.2 : The critical micelle concentration [Lindman 1983]

Micelle formation does not represent the formation of a new macroscopic phase, and is therefore not characterised by a single critical transition point. The use of the term c.m.c. can therefore be misleading. In some systems, e.g. bile salts where hydrophilic and hydrophobic groups are not well separated [O'Connor 1984], micelle sizes are known to increase over a relatively wide concentration range and it may be better not to use the term at all. However, when there is only a narrow range, the use of a c.m.c. to characterise the system becomes convenient. It must also be understood that no unique experimental definition exists for the c.m.c. Values measured will depend upon the experimental technique used.

Two classes of thermodynamic models proposed to describe micelle formation are the phase separation models and the equilibrium models. The phase separation model is useful even though, as described above, micellar systems are one phase systems. This is because the micellar association is thought to be highly cooperative. The relation between

the monomeric concentration in solution and the total amphiphile concentration for true phase separation is shown in figure 2.3(a). The figure displays a sharp transition at the c.m.c.

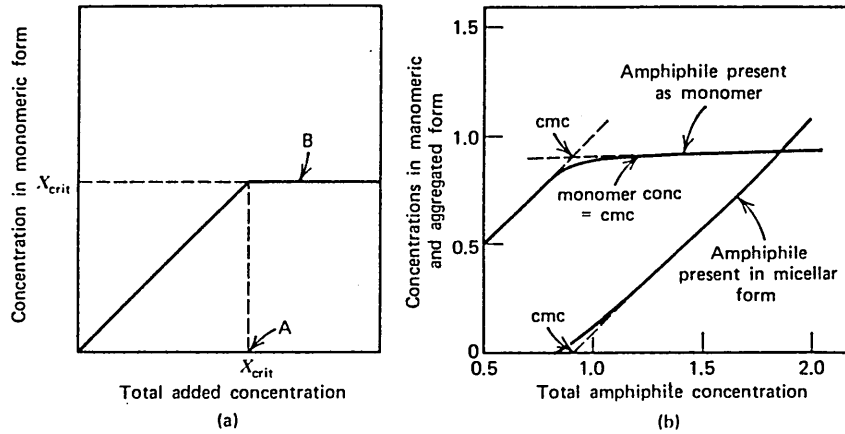


Figure 2.3 : Relation between the concentration of monomers and total amphiphile concentration for (a) phase separation (b) mass action model [Tanford 1980]

An example of an equilibrium model is the mass action model. In this model, it is assumed that m monomers are in thermal equilibrium with a single micellar aggregate, M_m , of size m .



The equilibrium constant for this system is given by

$$K = (f_m X_m / m) / (f_1 X_1)^m \quad (2.2)$$

where the f 's are the activity coefficients and X_m is the fraction of monomers in an aggregate of size m . Figure 2.3(b) shows the monomer versus total amphiphile concentration as given by equation (2.2) with

the activity coefficients set to unity and $m=50$ [Wennerström & Lindman 1979]. It is seen that the mass action model predicts a smooth transition through the c.m.c region as obtained experimentally. For this reason equilibrium models are generally preferred.

As a consequence of the marked cooperativity thought to characterise micelle formation, the micelle size distribution is predicted to show a minimum and a maximum. This is shown schematically in figure 2.4 [Wennerström & Lindman 1979].

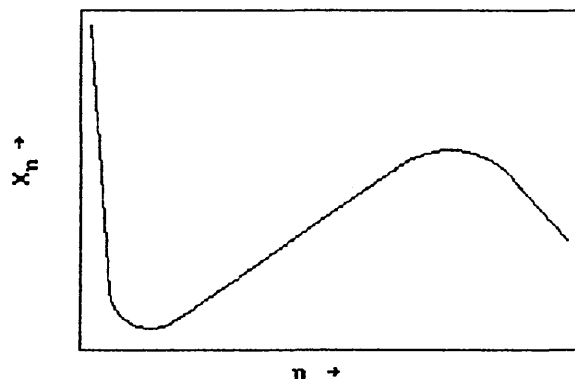


Figure 2.4 : Schematic size distribution curve for a typical micelle forming amphiphile. The aggregate concentration X_n is plotted on a logarithmic scale versus the aggregation number n .

The maximum occurs for aggregation numbers typically between 50 and 100. The presence of the minimum in the size distribution has been suggested as a criterion for proper micelle formation [Wennerström & Lindman 1979]. It is important to note, however, that the size distribution is never available experimentally. Only the number average or weight average micelle size and the total amphiphile in micelle form

are measured.

The c.m.c varies with changing physical and chemical conditions. There is a strong decrease in the c.m.c as the tail length increases. This decrease is logarithmic and is much more rapid for nonionic than for ionic surfactants; ionics generally having a higher c.m.c than nonionics. Fluorocarbon tail surfactants have lower c.m.c. values than the corresponding hydrocarbon tail surfactants. The effect of temperature and pressure is only slight; the c.m.c often having a minimum around room temperature.

In dilute solutions micelles have very little interaction with each other. However, as the concentration is increased above the c.m.c, the number of micelles increases causing interactions between the micelles which result in a dramatic alteration in solution properties. The disordered micellar solution changes to an ordered liquid crystalline phase or mesophase. Unlike the micellar solutions, the liquid crystalline phases usually have high viscosity, although at the molecular level the mobility is high, being not much slower than that of ordinary liquids. An exception to this are solvent rich lamellar phases which can have low viscosities. Changes of phase can also be induced by adding a third component, e.g. alcohol or electrolyte.

2.2 LIQUID CRYSTAL PHASES

A good review of the different liquid crystal phases is given in Tiddy (1985). Although commonly referred to as liquid crystal phases, the different structures observed are in reality mesophases. The simplest

lyotropic liquid crystal systems are those composed of the surfactant and water i.e. a binary system. The models presented in this thesis are restricted to such binary models. There are three frequently occurring liquid crystal phases in such systems: the hexagonal phase, the cubic mesophase and the lamellar phase. As with micelles, the hexagonal phase and cubic mesophases may be normal or reversed. The liquid crystal phases are shown schematically below. Reversed micelles occur when some surfactants, mixed with a little water, are dissolved in excess oil. They have similar properties to normal micelles.

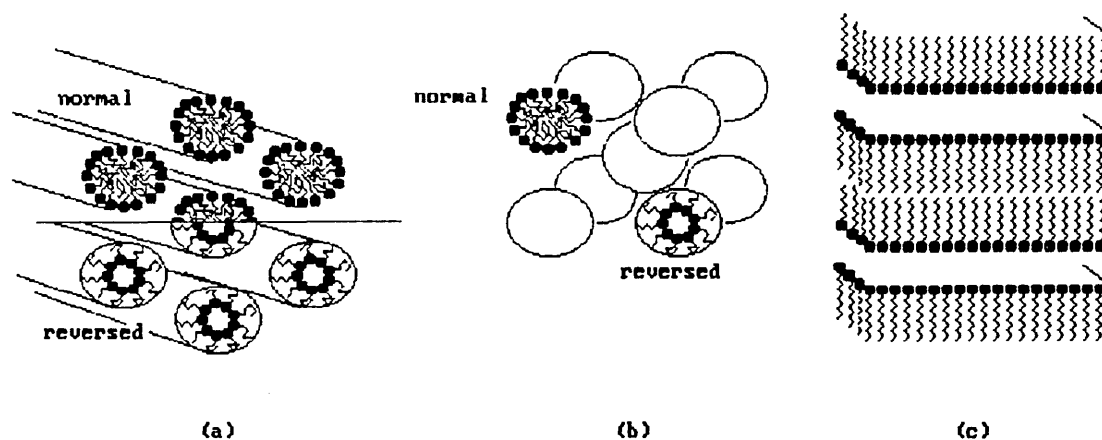


Figure 2.5 : (a) Hexagonal phase (normal and reversed)
 (b) Cubic mesophase (normal and reversed)
 (c) lamellar phase

The lamellar liquid crystal phase (Fig 2.5c) consists of ordered bilayers separated by water layers which can vary in thickness from 10 > 100 Å according to surfactant type and composition. The layered nature of the phase can often be seen when pouring the sample, and gives a characteristic parabolic focal conic texture when viewed under crossed polarised light.

The hexagonal phase (figure 2.5a) is made up out of long, hexagonally packed cylindrical micelles. It is characterised by a very high viscosity, and shows a characteristic speckled effect when viewed under polarised light.

The cubic mesophase occurs between other liquid crystal phases; an example of which is the face-centred cubic structure shown in figure 2.5b. While it is certain that two very distinct classes of cubic mesophase occur, their exact structures remain to be fully elucidated. One group occurs at compositions between micellar solutions and hexagonal phases. Another is formed at compositions between lamellar and hexagonal phases. In both groups, at least two different varieties are known to exist [Tiddy 1982][Adam 1984][Walsh 1983]. However, the exact structures remain to be solved. The cubic mesophases are optically isotropic and have extremely high viscosity, being higher than both lamellar and hexagonal phases.

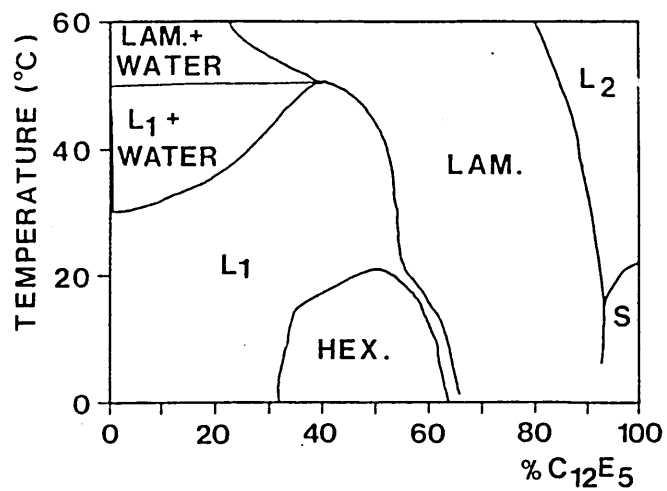
Other lyotropic liquid crystal phases known to exist include nematic phases, gels and vesicle and liposome dispersions. Nematic phases were first reported by Lawson & Flautt (1967). They occur in a minority of surfactant-water systems between micellar and hexagonal or between micellar and lamellar phases. They are optically birefringent and their viscosity is much lower than that of other lyotropic mesophases. Gels consist of lamellar structures where the surfactant chains are partially frozen in all-trans conformation and occur at temperatures below those at which lamellar phases occur. They have hexagonal packing. Vesicle and liposome dispersions may be formed by mixing lamellar phases with excess water. Liposomes are multi-bilayer walled spheroids

which comprise the disperse phase of a water-continuous lamellar/water emulsion. This is obviously a two phase system. Vesicles are roughly spherical with a surface comprising of a single curved bilayer. Their diameters lie in the range 250Å to \approx 1 micron. Most vesicle solutions are unstable, reverting eventually to a lamellar phase dispersion. It is a matter of controversy as to whether small vesicles (diam. \approx 250Å) can ever be at thermodynamic equilibrium [Tiddy 1985].

In addition to the phases described above, intermediate phases which are birefringent and form at compositions between hexagonal and lamellar have been suggested. However, many of these require further work to establish that they differ significantly from those of the well-established phases.

2.3 PHASE DIAGRAMS

In many cases it is convenient to portray the different phases using a phase diagram. Figure 2.6 shows a typical phase diagram of the binary water-(dodecane-pentaoxyethylene dodecylether) system [Harusawa *et al* 1974]. At temperatures below 20°C there is a transition from an isotropic solution, through a hexagonal phase to a lamellar region as the amphiphile concentration is increased. This is typical of many surfactant systems. The region L_1 is the micellar region and the region L_2 is the surfactant solution in which water is dissolved. The solid region occurs because the melting point of the surfactant is 21.5 °C.



L₁, L₂ : isotropic solution phases
 S : Solid

Figure 2.6 : binary phase diagram of C₁₂E₅-H₂O [Harusawa 1974]

3.1 INTRODUCTION

Statistical mechanical models involve the determination of macroscopic thermodynamic parameters from a microscopic model of a system. This frequently involves the derivation of the partition function for an appropriate ensemble. The canonical ensemble, for example, is the appropriate ensemble for a closed, isothermal (constant NVT) system, and the canonical partition function, Q , is frequently used to calculate the Helmholtz free energy, F , of such a system where

$$F = - kT \ln Q \quad (3.1)$$

The partition function can also be used to derive any other thermodynamic property.

This chapter is a review of statistical mechanical models of micelles and lyotropic liquid crystal phases. For these systems, as with many others, it is not possible to calculate the exact partition function analytically. Approximate solutions of the partition function have been made using analytical and mean field approximations. Other techniques, e.g Monte Carlo and molecular dynamics simulations estimate thermodynamic averages without explicitly deriving the partition function.

The mean field approximations are reviewed separately in Chapter 6.

3.1.1 Model Classification

Statistical mechanical treatments of amphiphilic systems may be classified according to their description of the amphiphilic chains and whether they consider single or multiple clusters. In addition the systems may be confined to a lattice. Figure 3.1 shows a classification hierarchy.

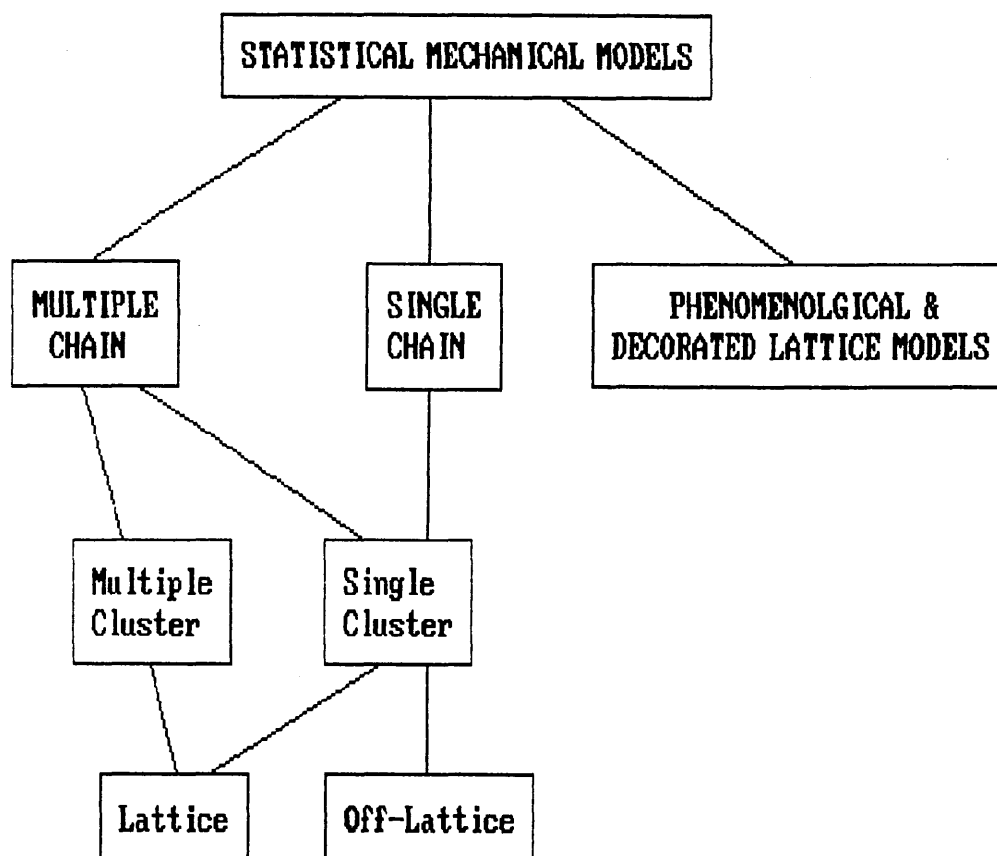


Figure 3.1 : Hierarchy of model classification.

Some treatments undertake simulations with many amphiphilic chains

present whereas others consider a single amphiphile in an idealised mean field appropriate to a given cluster geometry.

In many of the models the system may be either on or off lattice. Lattice models are often used as they have advantages over other types of model in that they are computationally less expensive and are easier to analyse. They have been previously shown to be successful for studying phase transitions, examples being magnetic materials, binary alloys, ferroelectrics and liquid crystals [Binder 1979,1987].

Lattice models are relatively simple but few are exactly soluble by analytical methods [Baxter 1982]. Those that cannot be solved exactly may be solved either by using analytical approximations such as the Bragg-Williams or quasi-chemical approximations, or by computer simulation. For a clear explanation of the Bragg-Williams and quasi-chemical theories, see chapter 14, Hill (1962).

Statistical mechanical models of amphiphiles may also be classified according to whether they consider single or multiple aggregates. The distinction is important as single aggregate models have constraints on the aggregate geometry, whereas multiple aggregate models allow self assembly of aggregates from a random starting configuration. Multiple aggregate models also allow system properties to be determined in addition to single cluster and chain properties.

There is much literature on models of amphiphilic systems and to review all models in detail here is impractical. The models of most relevance are the simulations and lattice models and thus these are considered in most detail.

3.2 MODEL PROPERTIES

Simulations and statistical mechanical models permit various properties of the amphiphilic systems to be derived as a function of temperature, amphiphile concentration, the amphiphile chain length, head type and amphiphile-solvent interactions. The properties derived from these models may concern the system as a whole, the micelle structure or the chains themselves. Properties obtained from a given model are compared with those obtained from other models and where possible with experiment.

3.2.1 System Properties

The cluster size distribution, the critical micelle concentration (c.m.c) and the phase diagram of a system may be found. These properties have been determined by a wide range of experimental techniques. It is difficult for simulation techniques to examine the c.m.c. because of the low concentrations involved.

3.2.2 Bond Order Parameters

The most common characteristic of chain organisation in amphiphilic aggregates are the "P₂" order parameters of the bonds along the chain. The order parameter of the kth bond is given by

$$S_k = \langle P_2(\cos\theta_k) \rangle = \langle 3/2 \cos^2\theta_k - 1/2 \rangle \quad (3.2)$$

where θ_k is the angle the k^{th} bond makes with the normal of the aggregate surface. S_k is thus a measure of how the chain bonds orientate with respect to the normal of the aggregate. When $S_k = 0$ all bond directions are equiprobable. For $1 \geq S_k > 0$ there is preferential ordering along the normal to the aggregate surface, whilst for $-0.5 \leq S_k < 0$ there is preferential ordering parallel to the surface. Order parameters in alkyl chains can be measured experimentally by various magnetic resonance techniques for different aggregates. Alternatively θ_k may be measured with respect to the first bond in the chain.

Bond order parameters, $S(r)$, may also be measured as a function of the distance, r , from the aggregate centre.

$$S(r) = \langle 3/2 \cos^2\theta - 1/2 \rangle \quad (3.3)$$

where θ is the angle formed by the bond vector between chain segment centres and the radius vector from the aggregate centre of mass to the bond centre.

3.2.3 Density Profiles

The number density of CH_3 groups, $\rho(r)$, as a function of the distance r from the aggregate centre of mass is readily obtained from the results of simulations. It can be used to predict the scattering amplitudes of methyl tail groups which have been measured experimentally by small angle neutron scattering experiments (e.g. Bendedouch *et al* (1983), Cabane *et al* (1985)). The scattering function, $A(q)$, of scattering vector, q , is given by the sine Fourier transform of the CH_3 density multiplied by r

$$A(q)/A(0) = 1/q \int_r \rho(r) \sin(qr) r dr \quad (3.4)$$

3.2.4 Principal Moments Of Inertia

The size and shape of aggregates is often described in terms of the principal components of the moments of the inertia tensor I , where

$$I = \int_r r^2 \rho(r) dr \quad (3.5)$$

If the three components I_x , I_y and I_z are equal the aggregate is spherical. The ratio of the largest to smallest moments has been used as a measure of aggregate shape fluctuation (e.g. Woods *et al* (1986)).

3.3 SIMULATIONS

The two distinct classes of simulations used to model amphiphilic systems are molecular dynamics and Monte Carlo simulations. In molecular dynamics, the equations of motion of a system of interacting particles are solved and equilibrium properties are determined from time averages taken over a sufficiently long time interval.

Monte Carlo simulations allow the estimation of expectation values of time independent configurational properties of systems in thermal equilibrium with their surroundings.

For a system observed in the canonical, (constant NVT), ensemble in a state x with energy $U(x)$, the expectation value of a configurational

property, $\langle A \rangle$, is given by

$$\langle A \rangle = \frac{\int_x A(x) \exp\{-U(x)/kT\} dx}{\int_x \exp\{-U(x)/kT\} dx} \quad (3.6)$$

where k is the Boltzmann factor and T is the temperature in Kelvin. The denominator normalises the expectation value and is the partition function, Q .

In most cases equation (3.6) cannot be calculated analytically. Monte Carlo techniques allow the determination of expectation values without calculating the partition function. The technique uses importance sampling in which random numbers are sampled from a non-uniform distribution which allows the function evaluation to be concentrated in the regions of phase space which make important contributions to the integral.

The method developed by Metropolis *et al* (1953) sets up a Markov chain of states of the liquid such that its limiting distribution is the Boltzmann distribution. A Markov chain is a sequence of trials in which the outcome of each trial depends only on the outcome of the preceding trial. It is described in terms of a transition probability matrix, π , whose elements, π_{ij} , are the probability of moving from a state i to a state j . The elements have the following properties:

$$\sum_i \rho_i \pi_{ij} = \rho_j \quad (3.7)$$

$$\sum_j \pi_{ij} = 1 \quad (3.8)$$

where ρ_i is the probability of the system being in a state i . π is the transition matrix for an ergodic chain in which every state can eventually be reached from another state.

It is possible to determine elements of the transition matrix which satisfy the above equations by using the unnecessarily strong condition of microscopic reversibility:

$$\rho_i \pi_{ij} = \rho_j \pi_{ji} \quad (3.9)$$

The Metropolis Monte Carlo Method satisfies (3.8) and (3.9) using a sampling scheme described in section 4.3.1.

The set of configurations are sampled from phase-space such that the configurations are weighted according to the Boltzmann distribution. Thus equation (3.6) may be written

$$\langle A \rangle = \frac{1}{M} \sum_{j=1}^M A^j \quad (3.10)$$

where M is the number of configurations sampled and A^j is the value of the property of interest i in the j^{th} configuration. M should be large to reduce the uncertainty in $\langle A \rangle$.

Molecular dynamics has the major advantage that it allows the study of time dependent processes. However, in some studies, the Monte Carlo method may be preferable because it is able to equilibrate much quicker than the equivalent molecular dynamics simulation using techniques

not permitted in the latter case. In some systems, e.g. lattice models, it is not possible to use molecular dynamics.

3.3.1 Molecular Dynamics

In recent years the increase in available computing power has led to attempts to model relatively realistic models of micelles and bilayers. These exclusively consider single clusters and are mostly studied off-lattice by molecular dynamics simulations.

Even with today's powerful computers it is not feasible to simulate the self-assembly micelles in an amphiphile and solvent system using realistic molecular potentials. Thus prior assumptions have to be made about the geometry of the clusters. Typically the amphiphiles are restricted to a planar structure (bilayer) or sphere (micelle) and the head groups are usually confined to an outer shell of the plane or sphere. In more recent works greater freedom is given to the motion of the head groups.

Molecular dynamics simulations can provide both static and dynamic results. Since we are reviewing them here primarily for comparison with lattice models, which do not provide dynamic results, we concentrate on static properties. Static results include the behaviour of the order parameters, the radial distribution of the head groups and the density profile across the aggregate.

Molecular dynamics simulations have been applied to rough models of monolayers [Cotterill 1976] [Toxvaerd 1977] [Kox *et al* 1980]. Van der

Ploeg & Berendsen (1982)(1983) extended these simulations to a realistic representation of a lipid bilayer. They modelled the decanoate decanol - water system which has been thoroughly investigated by x-ray diffraction and NMR techniques [Seelig 1977].

In the 1982 model a system is considered consisting of two layers of 16 decane molecules each; periodic in two dimensions. This system is shown to be too small to exclude artifacts produced by the periodic boundaries. To overcome this, the 1983 work models a bilayer of 2 x 64 decane molecules in a unit cell 2 x 2 nm.

The molecules are described by a united atom model (mass $\text{CH}_2 = 14\text{u}$, $\text{CH}_3 = 15\text{u}$) with explicit potentials for non-bonded interactions up to 1 nm range, bond angle distortion and dihedral angle rotation. Head groups are of a larger size and mass (44 u) and are bound by a harmonic potential to their average position in each layer. This is meant to represent a rough mean force potential for hydrophilic head groups (COO^-) in contact with water. A small external force is exerted on the head groups in order to impose an external pressure of 10^5 Pa. Verlet's algorithm [Verlet 1976] is used for integration of Newton's equations of motion, using the SHAKE algorithm [Ryckaert *et al* 1977] to conserve bond length constraints.

The simulation is run at two different temperatures (300 and 325 K) and two different values of surface area per head group (0.25 and 0.276 nm^2). The initial configurations are obtained from the 1981 system, copying it four times, followed by an equilibration run of 80 ps to get rid of any correlations between the four quadrants. The simulation is then run for a further 80 ps.

Figure 3.2 shows order parameters for the four simulations. The S_{CD} order parameters describe the C-H bond directions relative to the normal of the bilayer plane. Good agreement is given with the neutron magnetic resonance experiments of Seelig & Niederberger (1974) for a head group surface area of 0.25 nm^2 .

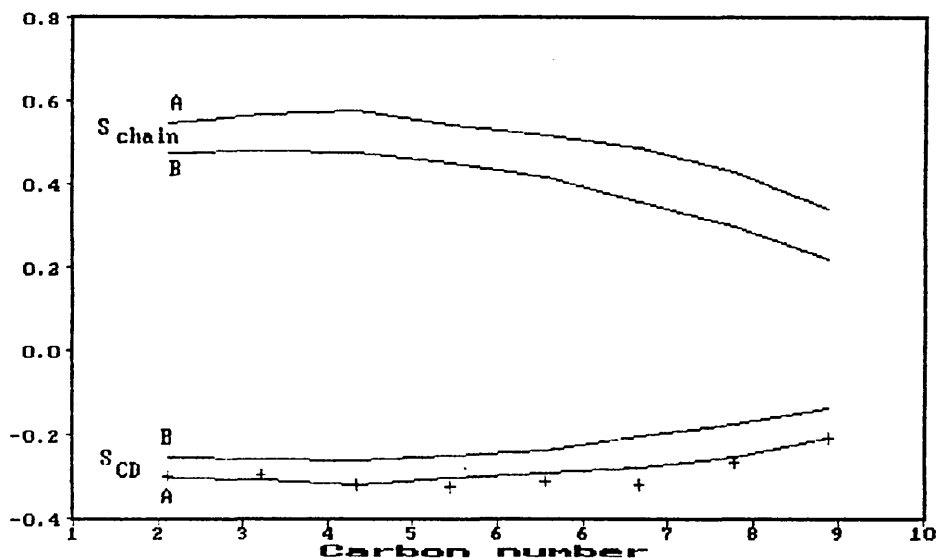


Figure 3.2 : Order parameters for each carbon atom in MD simulations of 2×64 decane molecules. Lines A have surface area per group $A_S = 0.25 \text{ nm}^2$ and $T = 300 \text{ K}$. Lines B have $A_S = 0.276 \text{ nm}^2$ and $T = 308 \text{ K}$. [van der Ploeg & Berendsen 1983]. Data points (+) are the neutron magnetic resonance experiments of Seelig & Niederberger (1974)

The S_{chain} order parameter is for the vector from C_{i-1} to C_{i+1} , where i is the carbon number incrementing from $i=1$ at the head. It relates to the local ordering of the long molecular axis relative to the normal of the bilayer plane. The figure shows that chain segments nearest the head group are best aligned to the plane normal. Both S_{chain} and S_{CD} show only a slight dependence on temperature but de-

crease strongly with increasing surface area.

The density of CH₂ groups is not homogeneous over the bilayer. Figure 3.3 shows a density profile with a distinct trough in the middle of the bilayer. There is some evidence for this density dip from x-ray diffraction measurements [Levine *et al* 1968,1971] [Caspar & Kirschner 1971].

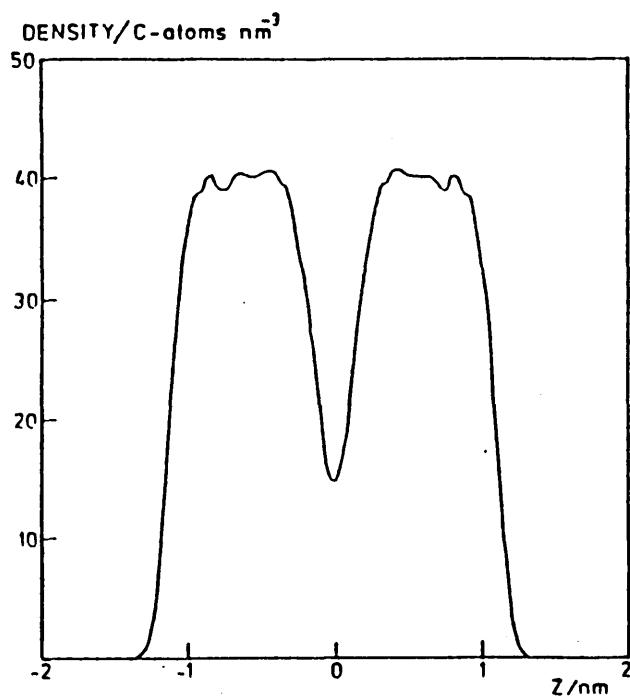


Figure 3.3 : Density profile over the depth of the bilayer [van der Ploeg & Berendsen 1983].

The bilayer membrane model, described above, was adapted to describe the internal structure of a micelle by Haile & O'Connell (1984), Woods *et al* (1986). The Haile model consists of 40 (later 52) thirteen member alkane chains, including the head group. Each member of the chain may be considered to be a soft sphere which interacts with intermolecular forces through a Lennard-Jones pair potential, and interacts with intramolecular forces through harmonic potentials for

bond vibration and bond angle bending. The hydrocarbon-solvent interaction is modelled by confining the aggregate to a spherical shell of radius 20 Å, using a repulsive r^{-12} potential acting between the shell and hydrocarbon tail groups.

In the Haile 1984 model the head groups are fixed in a spherical shell and there are no explicit head-head and head-solvent interactions. In the later work, the head-solvent and head-head interactions are included and the head groups allowed to move freely on the surface of the repulsive shell. Here only the later model [Woods *et al* 1986] is referred to, although the simulation technique in the earlier work was similar.

The head-solvent interaction is a harmonic potential acting normal to the shell surface

$$u_{\text{HS}}(r) = \gamma\epsilon(r^* - 1)^2 \quad (3.11)$$

The Lennard-Jones energy parameter, ϵ , is set at 419 J/mol, and $r^* = r/r_m$ is the reduced distance between the head group and the shell, with $r_m = 4$ Å, the distance to the minimum in the Lennard-Jones potential. The harmonic force constant, γ , is set to 30 allowing the head group to fluctuate between 2.5 and 8 Å from the shell at the run temperature of 300 K.

The head-head interactions are of the form

$$u_{\text{HH}}(r) = \epsilon[r^{*-3} + r^{*-12}] \quad (3.12)$$

which includes both dipole-like repulsion and excluded volume effects.

Initially the head groups are fixed on a spherical shell, of radius 32 Å, with the hydrocarbon chains fully extended and pointing towards the centre of the micelle and value of the bond rotational potential is set to one-tenth of its final value. The density of the micelle is then slowly increased by shrinking the micelle to a radius of 16 Å, corresponding to the liquid alkane density. After collapsing the system is allowed to relax.

The final part of the initialisation is to finely tune the radius of the confining spherical shell to satisfy the criterion of mechanical equilibrium on the shell. In all the initialisation takes 40000 time steps with further 40000 time steps of full simulation to reach equilibrium. Each time step corresponds to 0.002 ps of real time.

Results are obtained relating to both local structure and to conformational structure. For local structure this includes singlet distribution functions, average positions of groups, and distribution of tail groups. The conformational structure is reported in terms of gauche bond distributions and bond orientation.

The singlet distribution function is determined from the simulation using the relationship

$$\rho_i(r) = \langle N_i(r) \rangle / 4\pi r^2 \Delta r \quad (3.13)$$

where i refers to the chain segment number, r is the radius of a

spherical shell of thickness Δr measured relative to the centre of mass of the aggregate and $\langle N_i(r) \rangle$ is the time averaged number of segments of type i at a radius r . The singlet distribution function is a probability density and is used to provide primary measures of local structure within the aggregate for the CH_2 , CH_3 and head groups. It is related to $P_i(r)$, the probability of a group of type i being found at radius r by

$$\rho_i(r) 4\pi r^2 \Delta r / N = P_i(r) \quad (3.14)$$

where N is the total number of molecules in the aggregate. Figure 3.4 shows a plot of $r^2 \rho_i(r)$ vs. r [Woods *et al* 1986]. (Note this is proportional to $P_i(r)$). The results show that groups away from the head group have an increasingly ill defined most probable position. Indeed, groups 12 and 13 show a nearly uniform probability for being at any point beyond a few angstroms from the centre.

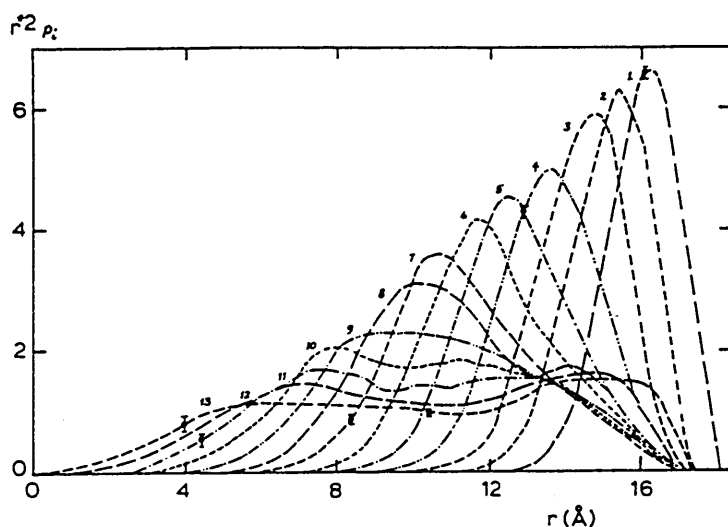


Figure 3.4 : Group probability distributions from the model of Woods *et al* (1986)

The Fourier transform of the singlet distribution for methyl tail groups is used to determine the scattering amplitude of the tail groups, see equation 3.4. There is good qualitative agreement with scattering amplitudes measured by Bendedouch *et al* (1982) using small angle neutron scattering.

Bond order parameters (equation 3.3) are calculated as a function of the radius r of the aggregate and for each segment in the chain. As shown in figure 3.5 [Woods *et al* 1986], preferential ordering is found at the micelle centre and at the chain-solvent interface. The former is a geometrical effect as only chains with tail bonds parallel to the micelle radius can reach the centre. The latter ordering is due in part to the effects of the confining shell.

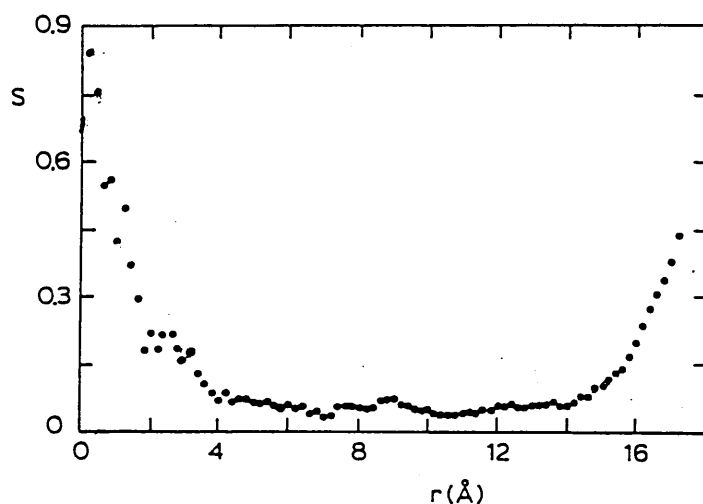


Figure 3.5 : Bond order parameters [Woods *et al* 1986]

The segment bond order is shown to be highest for bonds nearest the head groups decreasing towards the tails. This behaviour was similar to that found from NMR measurements [Walderhaug *et al* 1984].

The fluctuation in shape of the aggregate with time is determined by evaluating the principal components of the inertia tensor I ; I_x , I_y , I_z . The ratio of the largest to smallest principal component is examined with time. The fluctuations are shown to be rapid but small, although the confinement of the chains to a spherical volume suppresses high fluctuations.

In contrast to the traditional description of intramicellar structure, it is found that only a very small fraction of the hydrocarbon chains are in an all-trans conformation.

The work of Ploeg *et al* (1983) and Woods *et al* (1986) is limited because prior assumptions are made about the structure in that the head groups are confined to an "average plane". This assumption is likely to be more significant in the model of the micellar system than in that of the bilayer where the surface interface is smaller.

The work of Jönsson *et al* (1986) has attempted to overcome the problem of confining heads to a plane by explicitly including water molecules and counterions. Their simulation is of a sodium octanoate micelle consisting of 15 amphiphiles with surrounding water and counterions. The main difference between their work and the work of Haile and coworkers is that the micelle is kept in place by the surrounding water rather than by a spherical shell. This inclusion of surrounding molecules, however, results in an increase in computing time by an order of magnitude.

The micelle is initialised to a structure with the chain in an all-trans position, extending radially from the centre. The 1094 water molecules are placed on the bases of a primitive cubic lattice surrounding the amphiphiles. Fifteen randomly chosen water molecules are then exchanged for 15 sodium ions.

The water molecules are represented by the empirical simple point charge of Berendsen *et al* (1981). The authors claim this gives inadequate screening of the ionic interactions of the system which impairs the proper aggregation of the amphiphiles. To overcome this runs are made with the ionic interactions of the Na^+ and COO^- ions reduced to half their real values. These runs are referred to as RC (reduced charge) as opposed to FC (full charge).

Figure 3.6 [Jönsson *et al* 1986] shows the total carbon density as a function of the distance from the aggregate centre obtained from both RC and FC runs. The hydrocarbon density decays smoothly from its maximum value down to zero suggesting that the micelle has a rough surface.

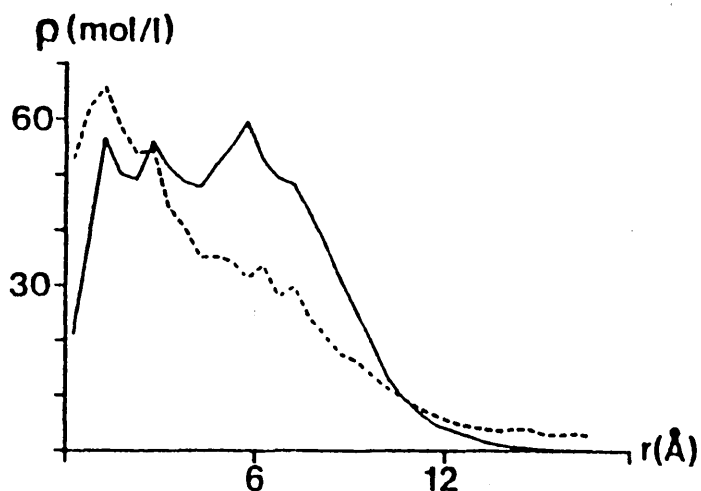


Figure 3.6 : Total carbon density for FC (dashed line) and RC (solid line) models [Jönsson *et al* 1986]

The average radius of the micelle is calculated to be 11.9 ± 1.0 Å in the FC case and 9.5 ± 1.7 Å in the RC model. Using neutron scattering experiments the average radius of a SDS micelle has been measured at 18.4 Å with a 10% standard deviation [Cabane *et al* 1985]. However the micelle in the experiment contains a greater number of chains, which are also longer than those used in the simulation.

Figures 3.7(a)(b) show the density of the different hydrocarbon groups

as a function of distance from the centre of the micelle [Jönsson *et al* 1986].

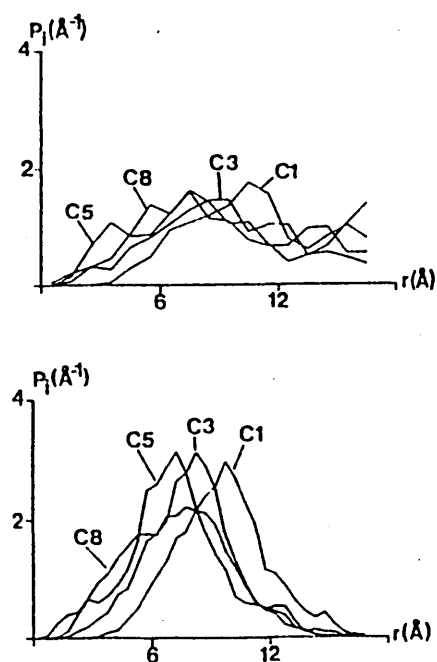


Figure 3.7 : Probability distribution for different carbon atoms for (a) FC model and (b) RC model [Jönsson *et al* 1986]

In the RC case, which the authors consider to be most realistic, there are distinct peaks for the different distributions, although each distribution is broad cf. Woods *et al* (1986). The average radial positions of the first five positions are shown to be similar to those expected for a close packed micelle. As with Haile *et al* (1984) scattering amplitudes for methyl tail groups are calculated and give good correspondence with the SANS results of Bendedouch *et al*' (1983).

The same sodium octanoate micelle in aqueous solution system was later modelled by Watanabe *et al* (1988). Their system is the same size as Jönsson's, but equilibrated differently. The octanoate ions are initially equilibrated without solvent by constraining the head groups

onto the surface of the sphere and reducing the sphere radius in a similar way to Haile *et al* (1984). The solvent is prepared independently by equilibrating 1331 water molecules in a box with side length 43.2 Å. The micelle is then inserted into the centre of the box, removing all overlapping water molecules. Next, fifteen sodium ions are substituted for water molecules and the whole system equilibrated with head groups constrained in a spherical shell. At this point the full simulation commenced.

The results of Watanabe *et al* (1988), are in good agreement with the work of Woods *et al* (1986), who did not explicitly include the solvent, but differed from those of Jönsson *et al* (1986). It appears that the results depend more on the equilibrium method than on the inclusion of water molecules. The probability distribution of the different carbon atoms with respect to the micelle centre is shown in figure 3.8 [Watanabe *et al* 1988].

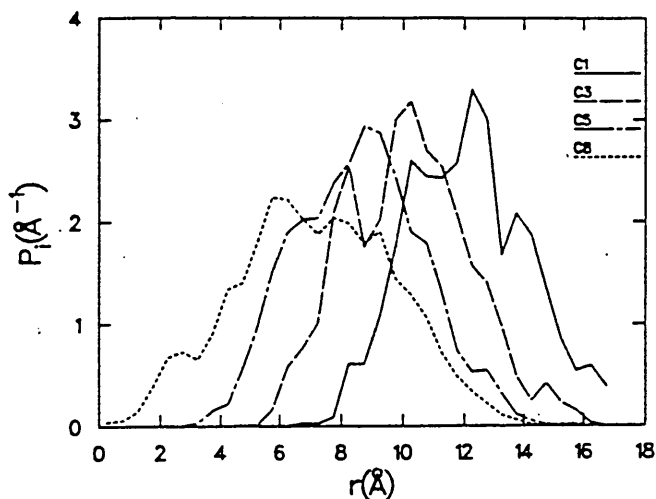


Figure 3.8 : Probability distribution of different carbon atoms
[Watanabe *et al* 1988]

The authors claim that Jönsson's use of scaled charges to account for the inadequate screening of the SPC water is not justified. The claim is made on the basis of a calculation of the dielectric permittivity of the SPC water that Jönsson claimed is too low to yield adequate screening of the ionic interactions.

Karaboni and O'Connell (1990) did a molecular dynamics simulation similar to that of Woods *et al* (1986) to study the effects of various intermolecular potentials. Two significant developments were made to the 1986 model. The first of these is that a finite energy barrier is imposed on the hydrocarbon chains equal to the energy of solubilization of hydrocarbon segments in water and is negligible inside the core

$$u_{CS}^*(r) = \kappa / (1 + \rho(r^*/r_{CS}^*)^\tau) \quad (3.15)$$

where κ controls the height of the barrier, and $\rho = 0.76$ and $\kappa = -46$ control the steepness. This potential is considered more realistic than the infinite wall and allows chain segments with sufficient energy to leave the aggregate.

The second development was to replace the harmonic head-solvent interaction with a finite energy potential

$$u_{hs}^*(r) = \begin{cases} \beta / (1 + \alpha(2 - r^*/r_{hs}^*)^\lambda), & r^* < 2r_{hs}^* \\ 0, & r^* \geq 2r_{hs}^* \end{cases} \quad (3.16)$$

where the values $\alpha=0.76$ and $\lambda=-46$ are chosen to provide a sharp barrier transition and β is used to control the barrier height. The harmonic potential used previously was thought to be unrealistic because the head group feels increasing repulsion in both directions from the core boundary.

Simulations were performed with different chain-solvent and head-solvent interaction potentials. The different interaction potentials produced noticeable effects on the head group distributions, but there were little differences for segments along the chain. The tail distributions agree with both experimental data and with the results of the molecular dynamics simulations of Jönsson *et al* (1986) and Watanabe *et al* (1988). The first bond in the chain tends to be preferentially ordered, while the others show little order. This agrees with the NMR data of Chevalier & Chachaty (1985). Even though the micelles are partially confined to a sphere, their shape is to some degree non-spherical.

The molecular dynamics simulation of an amphiphile and solvent system by Gunn & Dawson (1989) takes a different approach from the above molecular dynamics simulations and strictly speaking is not a multiple chain model as the amphiphiles are represented by ellipsoids. The solvent molecules are represented by spheres. The group do not try to model accurate inter- and intra molecular potentials and claim to show self-assembly to a bilayer.

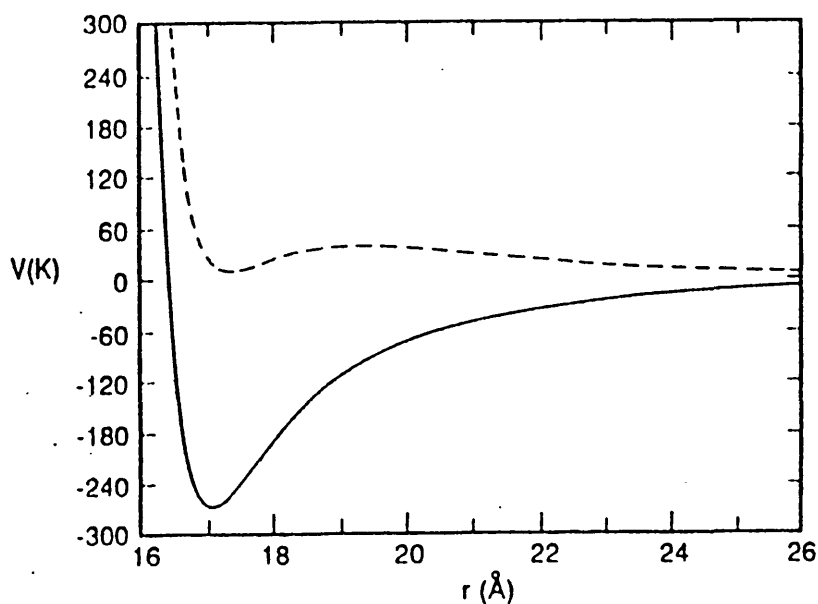


Figure 3.9 : Plots of the two extremes of amphiphile-water potential, the hydrophilic case (solid line) and the hydrophobic case (dashed line). [Gunn & Dawson 1989]

Amphiphile-amphiphile, amphiphile-solvent and solvent-solvent potentials are represented by Lennard-Jones type functions. The anisotropic shape of the amphiphile molecules is achieved by making the function parameters dependent on the orientation of the molecules. An extra term was added to the amphiphile potential to favour solvation at one

end of the amphiphile. Figure 3.9 shows the form of the amphiphile-solvent potential in both hydrophilic and hydrophobic cases.

The simulations were carried out with 500 amphiphiles and 10,000 solvent molecules. Initially the molecules were placed on a cubic lattice with a bilayer geometry and assigned random initial velocities. The system was then run until the cubic structure was destroyed. This disrupted configuration was used for the starting point of the simulation. Figure 3.10 shows schematic plots of the amphiphiles only from snapshots of simulations at different temperatures and amphiphile-amphiphile potentials.

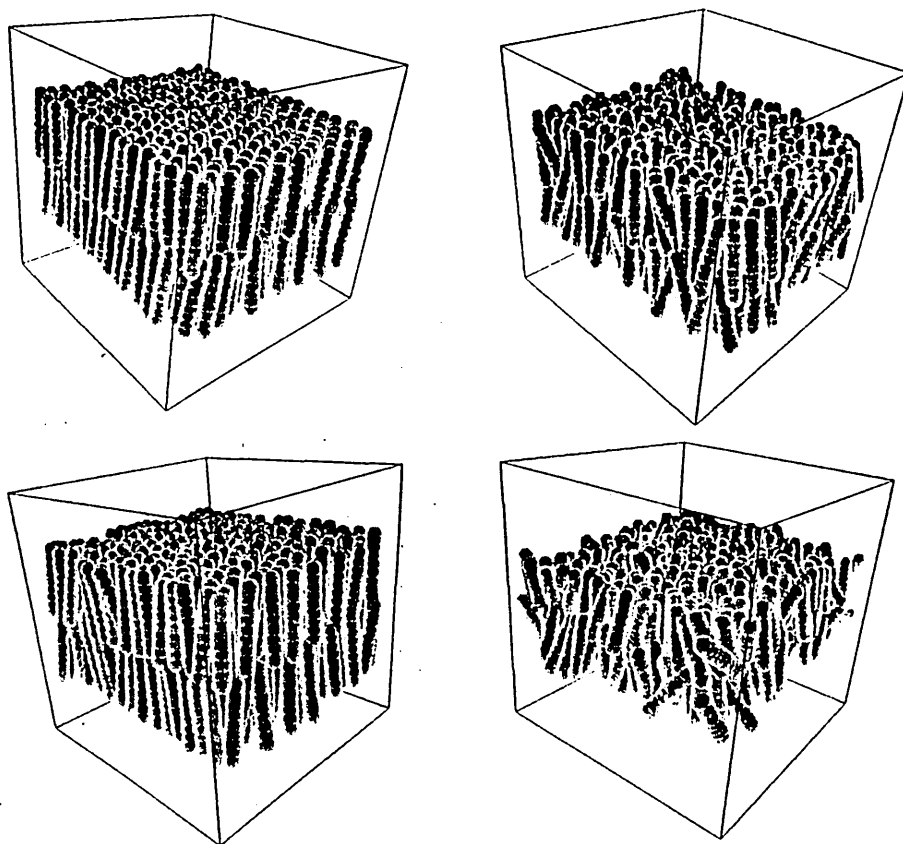


Figure 3.10 : Schematic plots of amphiphile organisation [Gunn & Dawson 1989]

The figures show good alignment in the bilayer with strong amphiphile-amphiphile potentials and low temperatures. The bilayer becomes more disordered with higher temperature and when using a weak potential.

With the exception of the Gunn & Dawson model described above, molecular dynamics models have attempted to model bilayers and micelles with realistic molecular structures and interactions. These models have shown good agreement with experimental results. However, the head-solvent interactions are difficult to model and, particularly in the simulation of micelles, the results of the simulation are dependent on the method of equilibration used.

3.3.2 Monte Carlo Simulations

Unlike the molecular dynamics simulations described above, Monte Carlo (MC) simulations have mainly not attempted to use realistic potentials. They can be single micelle or multi micelle simulations.

An example which does try to use realistic potentials is the work of Vacatello & Yoon (1990). They consider a Monte Carlo study of a micelle similar to that described in the molecular dynamics simulations of Woods *et al* (1986). The micelle is spherical with 52 amphiphiles represented as sequences of $N_c = 13$ units connected according to the RIS model. The amphiphiles are confined to a spherical region by the repulsive interactions of the tail group units with a solvent field.

The total chain energy is the sum of the intra-chain interactions, the

inter-chain interactions and the chain-solvent interactions. The intra-chain interactions consist of the gauche bond energy, $n_g E_g$, where n_g is the number of gauche bonds and $E_g=2100$ J/mol is the energy of a gauche bond, and of nonbonded interactions between CH_2 groups separated by more than three bonds given by

$$E_{\text{nb}}(d) = - E_m [(d_m/d)^{12} - 2(d_m/d)^6] \quad (3.17)$$

where d is the distance between units, $d_m=0.4$ nm is the value of d for which E_{nb} is a minimum and $E_m=580$ J/mol is that minimum energy.

The inter-chain interactions are those used by Woodset *al* (1986). The chain-solvent repulsion is a function of the distance r from the micelle centre

$$E_{\text{CS}} = \epsilon(r^*/(R_s-r))^{12} \quad (3.18)$$

and the head groups are forced on the outside of the micelle by the potential

$$E_{\text{HS}} = \gamma \epsilon(((R_s-r)/r)^* - 1)^2 \quad (3.19)$$

where $\epsilon=419$ J/mol, $\gamma=30$ and $r^*=0.4$ nm are as in Woods *et al* (1986). The values are chosen empirically to produce a reasonable distribution of head groups along the micelle radius. The dipole-like head-head repulsions of Woods *et al* (1986) are not used as their effect is small and obscured by the fact that the solvent is not explicitly modelled.

The system is initialised as a sphere with large radius $R_s = 10\text{nm}$ in

which the chains are randomly placed. This is equilibrated at 300K and R_s is reduced successively until it reaches 2.0 nm, equilibrating at each reduction. After equilibration of the $R_s = 2.0$ nm micelle configurations are sampled of 50 cycles of moves, where a cycle consists of 8000 attempts to translate an amphiphile, 8000 attempts to rotate an amphiphile and 80000 attempts a reflecting a gauche bond.

Figure 3.11 shows the variation of C-C bond order parameters with distance from the micelle centre. They show fairly good agreement in the micelle core with the results of Woods *et al* (1986), although in the outer shell these results show the order parameter to be small, whereas Woods *et al* (1986) predict a comparatively large increase in the order parameter.

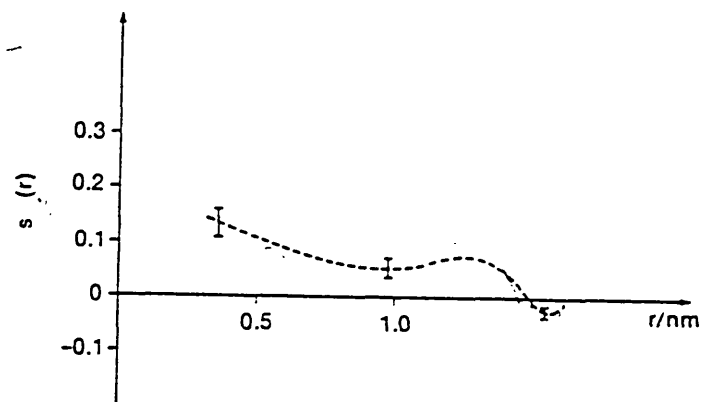


Figure 3.11 : The bond order parameters in the micelle
[Vacatello & Yoon 1990]

Haan & Pratt (1981), Owenson & Pratt (1984) also model a single mi-

celle. They considered a diamond lattice with aggregates of $\approx 20-50$ chains. The initial configuration of the aggregate was placed in a simple ordered arrangement in which all chains had at least one site in nearest neighbour contact with another. All vacant sites on the lattice were occupied by solvent molecules. The energy of the aggregate was given by

$$U = n_{TT}E_{TT} + n_{TH}E_{TH} + n_{HH}E_{HH} + n_gE_g \quad (3.20)$$

where n_{TT} , E_{TT} , n_{TH} , E_{TH} , n_{HH} and E_{HH} are the numbers and energies of tail-tail, tail-head and head-head nearest neighbour bonds, and n_g is the number of gauche bonds of energy E_g .

Analytical calculations they carried out lead them to suggested that the stability of finite micellar aggregates is due mainly to the long range of repulsive interaction between the head groups. Figure 3.12 [Haan & Pratt 1981] shows the density profiles obtained for heads (lower curve) and total density (upper curve). The head site distribution was shown to be much broader than commonly assumed and the aggregate had a compact centre. These factors suggest micelles with a dry hydrophobic core but with substantial surface roughness fluctuations.

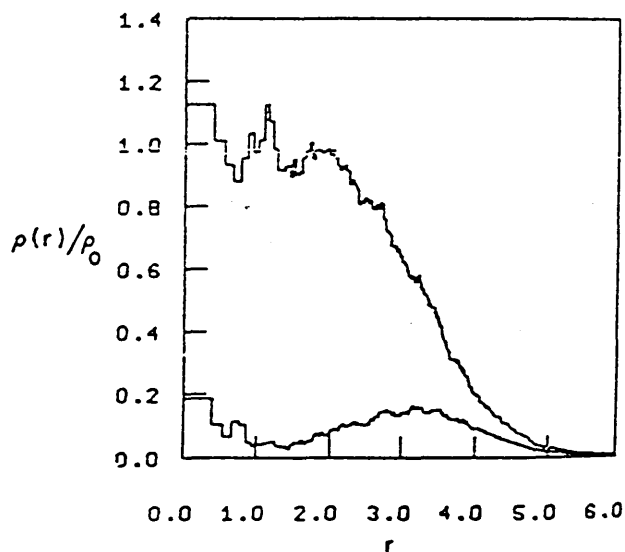


Figure 3.12 : Density profile for (a) heads and (b) total density [Haan & Pratt 1981].

Although more simplified calculations are used, the head group and total density profiles of Pratt *et al* are in good agreement with the molecular dynamics simulations of Watanabe *et al* (1988).

The principal values of the moments of inertia were calculated to examine the average aggregate shape. These are shown in table 3.1, where I_1 , I_2 and I_3 are the principal values in descending order and indicate that the aggregates were highly irregular.

	N = 20	N = 30	N = 40
I_1	3.35×10^2	6.95×10^2	3.29×10^3
I_2	1.76×10^2	3.51×10^2	6.45×10^2
I_3	1.10×10^2	2.07×10^2	4.32×10^2

Table 3.1 : Principal values of moments of inertia for aggregates of 20, 30 and 40 chains. [Haan & Pratt 1981]

In the case of multiple micelle MC, realistic potentials are not

attempted, but the molecules are allowed to self assemble into the microstructure they prefer. Only three groups are known to be taking this approach; Care (1987a,b) (see chapter 4), Larson *et al* (1985),(1988) and Kazakov & Kazakova (1990a,b).

Larson *et al* have simulated oil-water-amphiphile systems in 2 and 3 dimensions [Larson *et al* 1985][Larson 1988]. The amphiphiles had an equal number of head and tail sites (either 2 or 4) and the oil and water molecules occupied single sites on a square lattice. The potentials assigned to the head units were the same as those assigned to the water and the potentials of the tail units were equal to those of the oil. The net energy of mixing was thus given by a multiple of

$$W = E_{LH} - 1/2E_{LL} - 1/2E_{HH} \quad (3.21)$$

where E_{LH} , E_{LL} and E_{HH} are the interaction energies of hydrophilic-lyophilic, lyophilic-lyophilic and hydrophilic- hydrophilic interactions respectively.

Of particular interest here are the results obtained for a run in 3D in which water was omitted resulting in a two phase system [Larson 1988]. Because of the symmetry of the model the results were the same as would be found for the 2 phase amphiphile-water system. Results were reported for amphiphile concentrations between 80% and 30% on a lattice of 15 X 15 X 15 sites.

At 80% concentration the author reported that the lattice had a lamellar structure in which most slices through the lattice were similar to

figure 3.13a. Decreasing the amphiphile concentration to 60% produced a transition to a state in which most slices of the lattice displayed discrete patches of head groups, figure 3.13b, which connected to each other forming cylinders. For amphiphile concentrations of 40% and 30% spherical aggregates were observed. The results thus suggested a transition from lamellar to cylindrical then spherical phases as the amphiphile concentration was reduced. (In the three phase system only lamellar morphologies were observed).

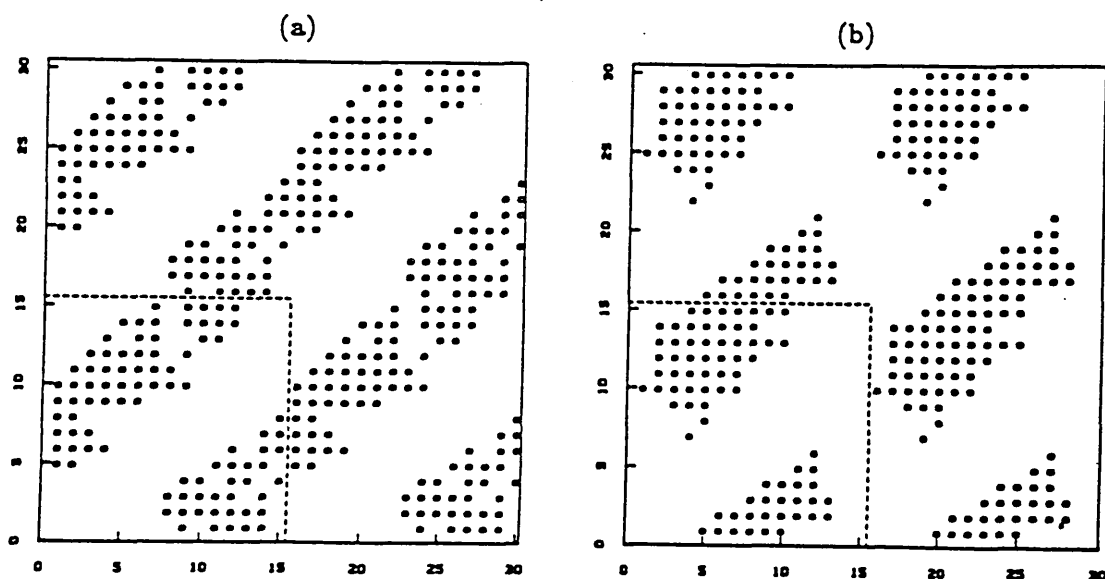


Figure 3.13 : Typical slices through the lattice with (a) 80% amphiphile concentration and (b) 70% amphiphile concentration [Larson 1988].

NB. The dashed squares in figures 3.13a and 3.13b contain the simulated region; the rest of the image being formed by periodic translations.

Larson has successfully shown the self assembly of ordered solution structures using a simple lattice model, but these structures have not been fully characterised. The structures are identified by inspection

of the lattice at equilibrium and no quantitative information is given on the size and shape of the clusters or on the conformation of the chains.

Care (1987a)(1987b) determined the cluster size distribution of an amphiphile and solvent mixture as a function of temperature and head-solvent interaction for a 128 X 128 square lattice with three segment amphiphiles using the model described in chapter 4. The potential energy of the system may be written

$$U/kT = \beta(n_{TS} + \gamma n_{HS} + \xi n_{HH}) \quad (3.22)$$

where n_{HS} , n_{TS} , n_{HH} are the total number of head-solvent, tail-solvent and head-head bonds. The parameter β is the ratio of the tail-solvent bond energy to kT , γ is the ratio of the head-solvent to tail-solvent bond energy and ξ is the ratio of the head-head to tail-solvent bond energy.

In the results presented the head-head bond interaction was omitted ($\xi = 0$). A random initial configuration was obtained at a high temperature which was reduced in steps of $\beta^{-1} = 0.02$ to a low temperature configuration. At each temperature 500 MC steps were discarded as thermalisation and 1500 MC steps were used to obtain data. Each MC step consisted of 5×10^4 attempted moves.

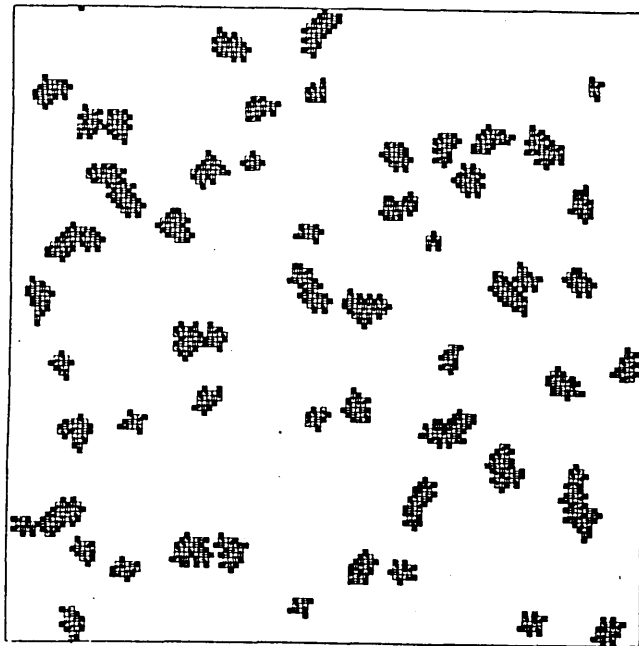


Figure 3.14 : Typical low temperature configuration for solvophilic head-solvent interactions ($\gamma=-0.7$) [Care 1987b]

It was found that a sufficiently solvophilic head-solvent interaction resulted in a large number of micelle-like clusters at low temperatures. This is shown in figure 3.14 [Care 1987b]. The micelles observed were more irregular and had a higher polydispersity than is commonly assumed for micelle systems.

Figures 3.15 (a-h) show the cluster size distribution obtained for $\gamma = -1.6$ and -0.6 at different temperatures [Care 1987b]. Figure 3.15(g) clearly shows both a minimum and maximum in the micelle size distribution. This is considered an indication of true micelle behaviour [Wennerström & Lindman 1978], but was found not to be as sharply defined as current models predict. It was suggested by Care (1987b) that the micelle size is determined by competition between a reduction in energy associated with an ordered micelle and increase in entropy associated with a disordered structure. Figure 3.15(h) shows the onset of freezing.

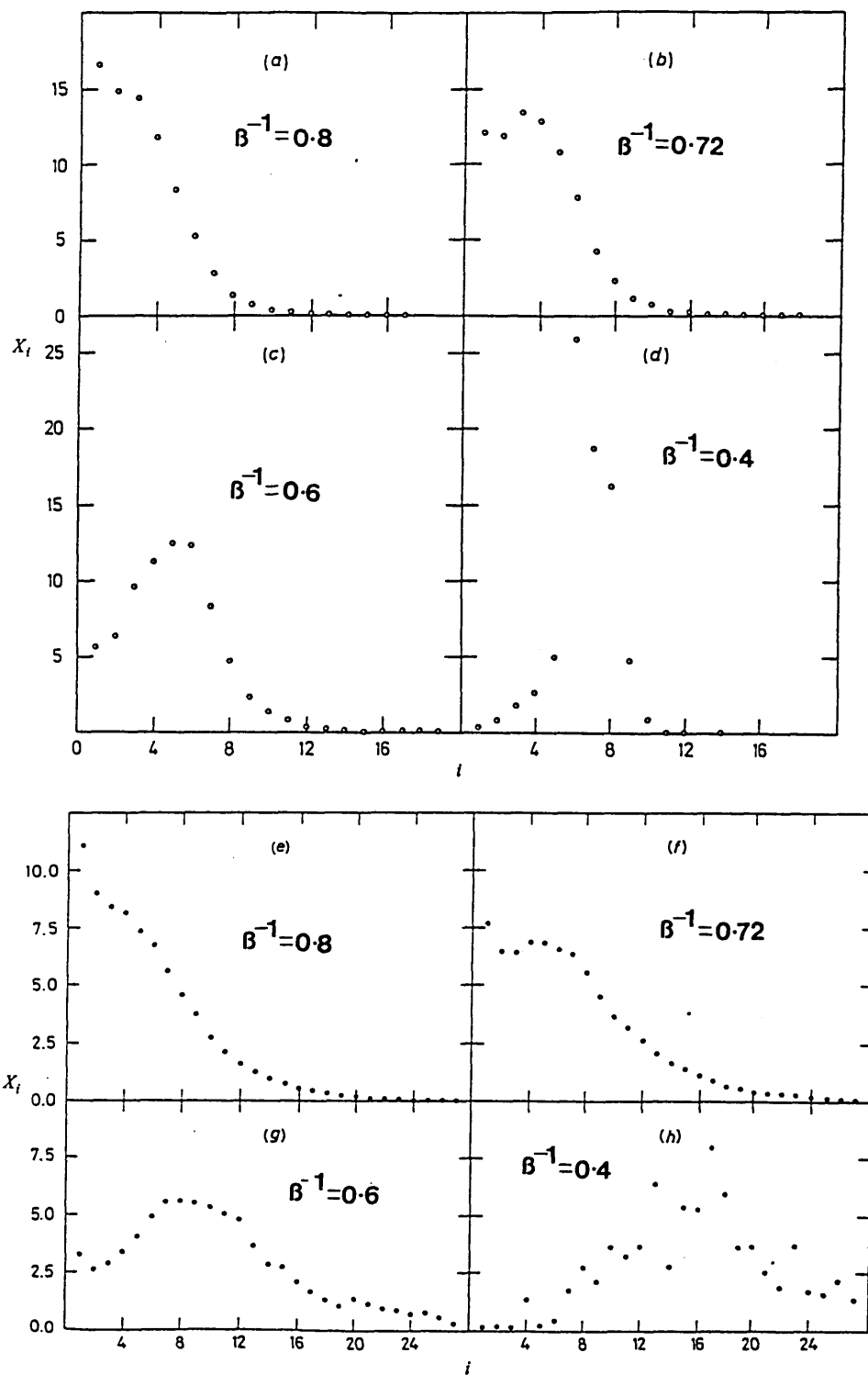


Figure 3.15 : Variation of concentration of monomers in clusters of size i , X_i , with i for (a-d) $\gamma = -1.6$, (e-h) $\gamma = -0.6$. Scales for X_i are arbitrary, but same on all figures [Care 1897b].

The results of Care (1987b) have modelled the self assembly of micelle-like aggregates. However the validity of the results is reduced because only short chains are considered and, as with the similar simulation of Kazakov & Kazakova (1990), the simulation was carried out on two dimensional lattice.

The single micelle Monte Carlo model of Owenson & Pratt (1984) suggests that a lattice model can predict chain conformations similar to those predicted by the more complex molecular dynamics simulations, although Vacatello & Yoon (1990) suggest that the results of their MC simulation indicate that solvent molecules should be explicitly included in future work.

Monte Carlo simulations which describe the amphiphile and solvent molecules by a simple lattice model have shown self assembly to different surfactant structures [Larson 1988]. However there is still much work to be done to properly characterise these structures and to investigate the fundamental driving forces for their formation.

3.4 STATISTICAL MECHANICAL MODELS

Statistical mechanical treatments include analytical approximations, mean field approximations and phenomenological models. Models based on a mean field approximation are reviewed in Chapter 6.

3.4.1 Analytical Treatments

Care (1989) has derived the cluster partition function for the above model using analytical approximations. As with his Monte Carlo simulation head-head interactions were omitted. It was shown that the cluster partition function for n monomers is given by

$$Q_n(T) = [q(T)]^n \sum_{p=p^-}^{p^+} \sum_{n_{HS}=0}^{n_{HS}^+} g_n(p, n_{HS}) e^{-\beta(p-n_{HS})} e^{-\beta\gamma n_{HS}} \quad (3.23)$$

where $g_n(p, n_{HS})$ is the total number of clusters of size n with p surface bonds and n_{HS} head-solvent bonds, γ is the ratio of the head-solvent bond energy to tail-solvent bond energy and β is the ratio of tail-solvent bond energy to kT . The term $q(T)$ is the non-configurational partition function for each monomer.

The central problem was the determination of $g_n(p, n_{HS})$. This was written as

$$g_n(p, n_{HS}) = d_{ns}(p) c_n(p, n_{HS}) \quad (3.24)$$

where $d_{ns}(p)$ is the number of possible clusters of size ns with p surface bonds, and $c_n(p, n_{HS})$ is the number of ways of arranging n monomers on a cluster of ns sites and p surface bonds to give n_{HS} head-solvent bonds. As $d_{ns}(p)$ is only tabulated for small n , a piecewise linear approximation was made. The combinational term $c_n(p, n_{HS})$ was estimated assuming that the bonds within a cluster were independent. The term then becomes the product of the number of ways of arranging n_{HS} head-solvent bonds among p surface sites and the remaining head bonds among the internal bonds.

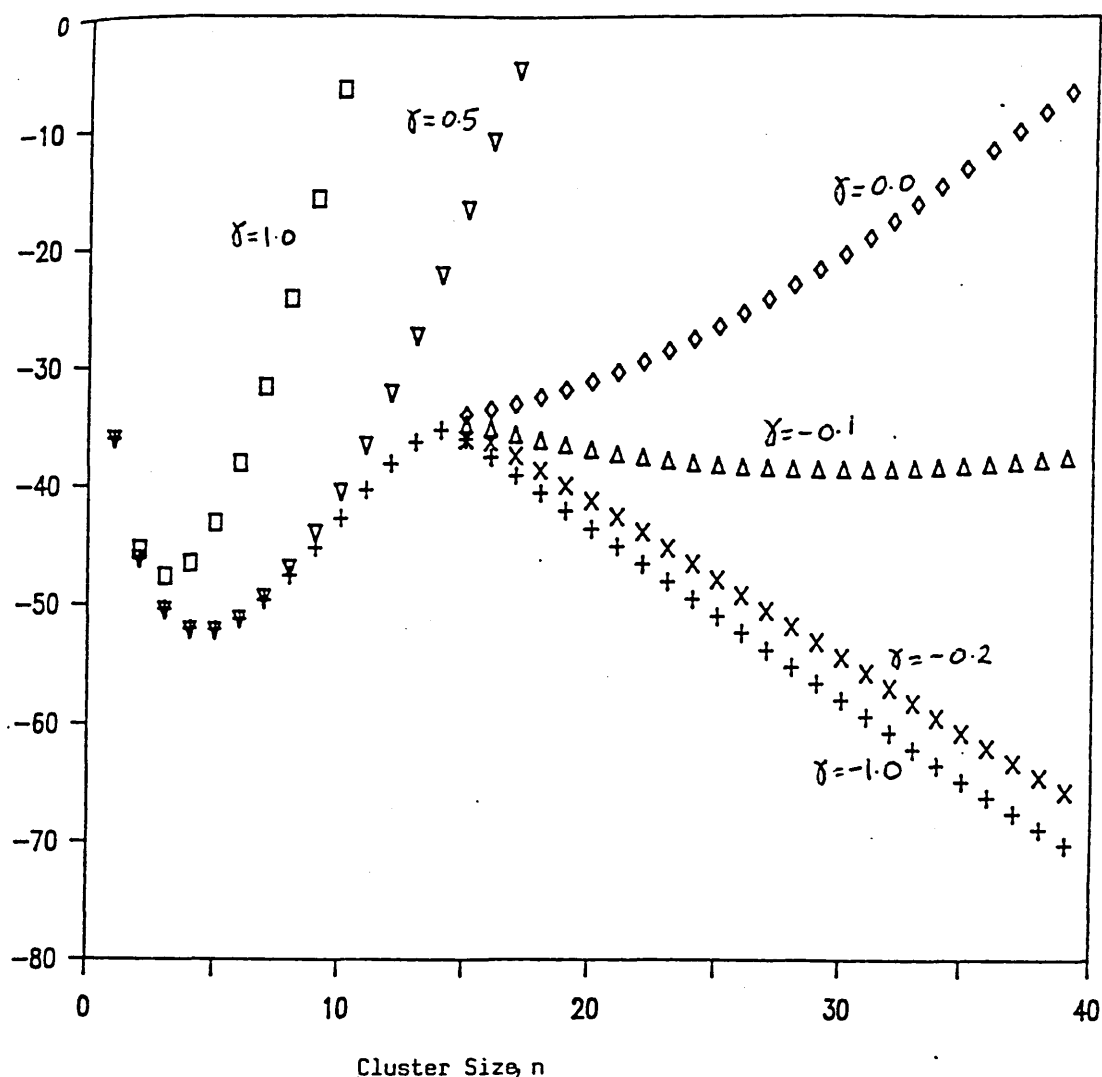


Figure 3.16 : Variation of mole fraction of monomers in clusters of size n , X_n , with n . The monomers have chain length $s=4$ and the reduced temperature $\beta^{-1}=0.18$. [Care 1989]

The cluster partition function of equation 3.18, with the above approximations, yielded a cluster size distribution showing a micellar phase for sufficiently solvophilic head-solvent interactions. The cluster size distribution for various values of γ is shown in figure 3.16. The $\gamma = -1.0$ case clearly shows both the minimum and maximum in

cluster size indicative of micellar systems. The micelle size was shown to be limited by entropy alone. The model exhibited a c.m.c which decreased with increasing amphiphile chain length in agreement with experiment. However the temperature dependence of the c.m.c in the model was much stronger than that observed experimentally and the predicted c.m.c are unphysically small.

Statistical mechanical treatments of micelle formation, (e.g. Hoeve & Benson (1957), Aranow (1963), Poland & Scheraga (1965)), have investigated the contributions necessary to the Helmholtz free energy function to yield a free energy minimum at some limiting degree of aggregation. In each case, this involved making assumptions as to the form of the partition function in the canonical ensemble.

These models are in essence fairly similar. However, the results of Poland and Scheraga (1965) give best agreement with experiment and are therefore examined in more detail here.

Poland and Scheraga consider the micelle to be formed from monomers having uncharged polar heads which lie on the surface of a sphere. The interior of the sphere is made up of the amphiphile tails which are assumed to have similar properties to the liquid hydrocarbon. The tails are partially coiled and interact with each other by means of hydrophobic bonds. It is also assumed that the polar heads serve only to solubilize the detergent molecules in water and do not contribute to the free energy of the micelle. Ignoring the fact that there will be a distribution of micelle sizes, the partition function for the solution is given by :

$$Q = \frac{Q(s)^{N/s}}{(N/s)!} \quad (3.25)$$

where s is the number of monomers in the micelle, $Q(s)$ is the partition function for a single micelle and N is the number of monomers in the system.

Poland and Scheraga express $Q(s)$ as the product of three partition functions representing contributions from (i) the external energy levels of the micelle itself, (ii) from the interaction of the micelle with the solvent, and (iii) from the internal energy levels of the micelle.

$$Q(s) = Q(s)_{\text{ext}}Q(s)_{\text{solv}}Q(s)_{\text{int}} \quad (3.26)$$

The external partition function, $Q(s)_{\text{ext}}$, is taken as the product of the classical partition functions for the translation and rotation of the micelle as a whole. It is shown that

$$Q(s)_{\text{ext}} = \frac{(3\pi^4(32/5)^{3/2}v_0m_0^3(kT)^3)V_f s^4}{4h^6} \quad (3.27)$$

where V_f is the free volume, and v_0 and m_0 are the volume and mass of a surfactant monomer. The values of v_0 and m_0 are calculated from Courteauld's space filling models by taking the volume of a CH_2 group to be 21 \AA^3 and its mass 14. V_f is taken to be a small fraction (about 10^{-2}) of the total system volume V . k is the Boltzmann factor, T is

absolute temperature and h is Planck's constant.

The solvent interaction partition function was given by

$$Q(s)_{\text{solv}} = \exp[-s\Delta F_{\text{H}\Phi}\theta(s)_{\text{H}\Phi}/RT] \quad (3.28)$$

where $\Delta F_{\text{H}\Phi}$ is the free energy of formation of a hydrophobic bond per monomer, and $\theta(s)_{\text{H}\Phi}$ is the fraction of the total hydrocarbon surface involved in hydrophobic bonding. R is the gas constant. The authors show that $Q(s)_{\text{ext}}$ and $Q(s)_{\text{solv}}$ are not sufficient to account for stable micelles at large values of s . It is necessary to include the internal partition function.

$Q(s)_{\text{int}}$ corresponds to the internal freedom of the micelle arising from the motions of the hydrocarbon tails. The term $\Delta F_{\text{H}\Phi}$ in $Q(s)_{\text{solv}}$ already contains the contribution due to the internal rotation of the tails, so this is not included here. Following Hoeve & Benson (1957), it is assumed that the translational motion of the monomers within the micelle could be treated very much like an imperfect gas in terms of a free volume expression. The internal partition function is shown to approximate to the form

$$(1/s) \ln Q(s)_{\text{int}} = A - (1/3) \ln s \quad (3.29)$$

where, $A = (\text{internal free energy per monomer})/RT$, and is treated as an unknown parameter.

Combining the three partition functions allows the calculation of the variation of free energy with micelle size which gives good empirical

agreement with experiment. The model also yields the correct trends for the variation of micelle size with concentration and temperature and of the variation of the c.m.c with temperature. The results can only be considered empirical as they depend on the "fixing" of an unknown constant using experimental results. For example in the variation of the c.m.c with temperature for C_8E_6 , the unknown constant was found by inserting the experimental c.m.c of Corkill et al (1964) at 30°C. A comparison of the calculated and experimental c.m.c at different temperatures is shown below.

-log c.m.c (exptl.)	T / °C	-log c.m.c (calcd.)	T / °C
2.35	18	2.34	20
2.46	30	2.46	30
2.55	40	2.56	40

Table 3.2 : Dependence of cmc on temperature [Poland & Scheraga 1965]

The statistical mechanical treatments of micelle formation of Hoeve & Benson (1957), Aranow (1963), Poland & Scheraga (1965)) contain increasing levels of detail. However they are not quantitatively sufficiently accurate to be of great practical importance in describing micelle formation.

3.4.2 Phenomenological And Decorated Lattice Models

In the phenomenological approach e.g. Talmon & Prager (1978), de Gennes *et al* (1982), Widom (1984), oil and water are considered to be continuum liquids in which the interface is described either as a flexible sheet or in a microscopic manner similar to that of insoluble

Langmuir monolayers.

For a given composition of oil, water and surfactant, the free energy is calculated and a phase diagram is generated. The oil/water domains are often described in terms of a coarse grained lattice.

A model developed by Taylor *et al* (1988)(1989) combines a lattice statistics calculation of the excluded volume effects of a polydisperse system of hard spheres, rods and plates with a phenomenological description of amphiphilic assemblies.

The system is confined to a 3-dimensional cubic lattice. An amphiphile monomer is described by a cube of edge length one whose edges lie parallel to the orthogonal axes of the lattice. Spherical aggregates are approximated as $D \times D \times D$ cubes of monomers, rod-like aggregates as $D \times D \times l$ ($l > D$) arrays of monomers and plate-like aggregates as $D \times l_1 \times l_2$ ($l_1, l_2 > D$) arrays of monomers.

The contribution to the free energy arising from the system configuration is described in terms of the number concentrations of monomers, c_o , quasispherical aggregates, c_s , and of aggregates of dimensions $\{D, l_1, l_2, \}$ ($l_1 \geq D$), ($l_2 > D$) in the three lattice dimensions by

$$\begin{aligned}
 f_{\text{config}} = & c_o(\ln c_o - \xi) + c_s(\ln c_s - \xi) \\
 & + \sum_{i=1}^3 \sum_{l_1=D}^{\infty} \sum_{l_2=D1}^{\infty} c_{il_1 l_2} (\ln c_{il_1 l_2} - \xi) \\
 & + \sum_{i=1}^3 a_i \lambda_i
 \end{aligned} \tag{3.30}$$

where a_i is the total particle cross-sectional area per unit volume perpendicular to the lattice axis i , and λ_i is the total particle edge length per unit volume parallel to the lattice axis i . ξ is a parameter dependent on the volume fraction of the amphiphiles, v_p , and the mesh size, ϵ . It is given by

$$\xi = [1 - 3 \ln \epsilon + \ln(1 - v_p)] \quad (3.31)$$

The free energy contribution due to interactions between monomers in an aggregate is obtained from a phenomenological model. The associated free energy gain in placing a monomer into a given aggregate geometry is considered. Thus,

$$\begin{aligned} f_{\text{assoc}} = & -c_s \phi_o D^3 - \sum_{i=1}^3 \sum_{l_1=D}^{\infty} \sum_{l_2=D+1}^{\infty} c_{i1} l_1 l_2 \{ \phi_o D^3 \\ & + \phi_1 D^2 [(l_1 - D) + (l_2 - D)] \\ & + \phi_2 D (l_1 - D)(l_2 - D) \} \end{aligned} \quad (3.32)$$

where the average free energy of monomers in spherical, cylindrical and planar geometries are given by $-\phi_o kT$, $-\phi_1 kT$ and $-\phi_2 kT$ respectively.

The total free energy of the system, in units of kT , is given by

$$f = f_{\text{config}} + f_{\text{assoc}} \quad (3.33)$$

Minimising f with respect to all possible particle size and orientation distributions $\{c_o, c_s, c_{i1}\}$ subject to the constraint that v_p

is a constant gives the equilibrium distribution function of the system

$$c_{i1}l_1l_2 = c_s P_{i+1}^{(1-D)} P_{i2+1}^{(1-D)} Q_i^{(1-d)(1-D)} \quad 0 \leq (P_i, Q_i) < 1 \quad (3.34)$$

where P_i is the probability for 1 dimensional growth parallel to lattice axis i and Q_i is the probability for 2 dimensional growth perpendicular to lattice axis i .

The minimisation of the free energy may be carried out over $\{c_0, P_i, Q_i\}$ parameter phase space varying c_s to satisfy the constraint on v_p .

The equilibrium state is characterised according to the system orientation symmetry as follows

$P_i = P_j = P_k$	isotropic
$Q_i = Q_j = Q_k$	
$P_i > P_j = P_k$	axial symmetry
$Q_i < Q_j = Q_k$	
$P_i = P_j > P_k$	planar symmetry
$Q_i = Q_j < Q_k$	
$P_i > P_j > P_k$	biaxial symmetry
$Q_i < Q_j < Q_k$	

The particle size distribution is characterised by the average aggregate dimensions $\langle l_{\max} \rangle$, $\langle l_{\text{mid}} \rangle$ and $\langle l_{\min} \rangle$; the maximum, middle and minimum aggregate edge lengths averaged over all aggregates in the

system. Also the average anisotropy is given by $\langle l_{\max}/l_{\min} \rangle$.

Figure 3.17 shows phase diagrams for the model with $D=4$, $\Phi_0=24.0$ and $\epsilon=0.1$ for different values of $\Phi_2-\Phi_1$ which controls the competition between aggregate growth in one and two dimensions. The figures show that for $\Phi_1 > \Phi_2$ rod-like aggregates dominate while for $\Phi_1 < \Phi_2$ plate-like aggregates are dominant.

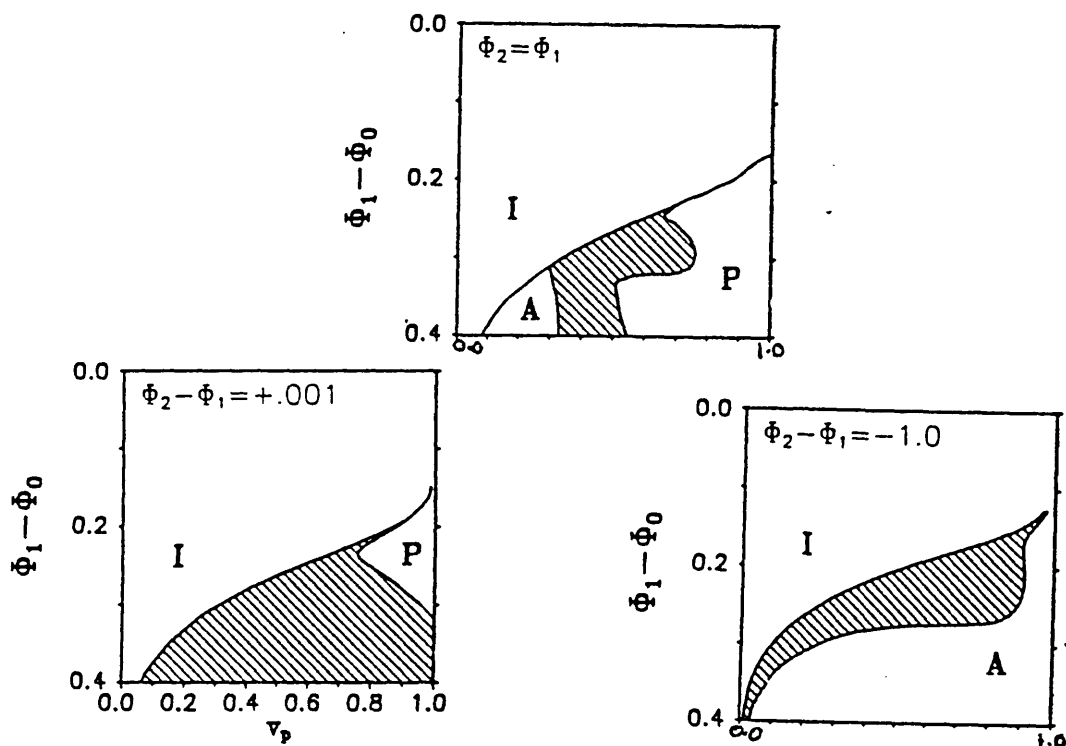


Figure 3.17 : Phase boundaries for different values of $\Phi_2-\Phi_1$. Phases are identified as I for isotropic micellar, A for axial anisotropic, and P for planar anisotropic. Regions of phase coexistence are shaded. [Taylor *et al* 1989]

In decorated lattice models, the amphiphiles, oil and water are modelled by a single site or single bond. This simplification allows mapping onto systems in which the solutions are already known. Some of these models are reducible to the spin - 1/2 Ising model and can be solved exactly [Wheeler 1975] [Alexander 1978] [Widom 1986]. Others

are solved by mean field or MC approximations [Chen *et al* 1988] [Gompper & Schick 1989]. These models have the advantage that they can provide very detailed phase diagrams, but are restricted because of the unrealistic molecular structure of the components.

This type of model is of interest here because it has been extended to apply to micellar systems. For example, Robledo (1987) extended a Widom-type model [Widom 1986] which he solved in a mean field fashion. Widom-type models describe a lattice of bifunctional molecules; A-A, B-B, A-B. The molecules are confined to the bonds of the (simple cubic) lattice, filling every bond once. Only molecular ends of the same type are allowed to meet at a given lattice site and there are no repulsions or attractions between these ends. These restrictions make the model equivalent to a spin-1/2 Ising model.

Robledo extended this model, allowing finite end-end interactions between different molecules. Two species **a-b** and **A-A** were considered in which the amphiphile **a-b** has molecular ends that differ from those of the solvent **A-A**. The system has six different inter-molecular potentials : ϵ_{AA} , ϵ_{Aa} , ϵ_{Ab} , ϵ_{aa} , ϵ_{ab} and ϵ_{bb} . Thus the model is no longer represented by a spin-1/2 Ising model, but by spin-1, which has a strong affect on the phase behaviour.

The global phase behaviour of the binary **A-A + a-b** mixture is examined under a mean-field approximation when two interpenetrating sublattices are condensed. This enables use of the global phase diagram of the Furman-Dattagupta-Griffiths (FDG) three-component model. The lattice is shown below, figure 3.18(a), and consists of two primary lattices **P** and **Q** and two secondary lattices **o** and **x**.

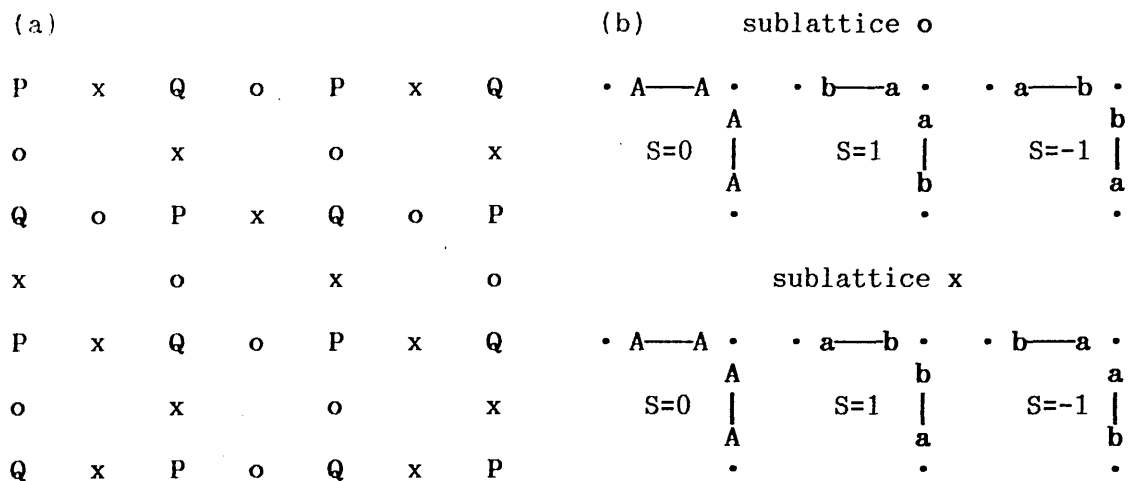


Figure 3.18 : (a) Sublattice arrangement for primary (P & Q) and secondary (o & x) sites. (b) Spin values of molecular orientations in the two sublattices [Robledo 1987]

The bonds of the molecules are centred on the secondary sites and the end-to-end interactions occur at the primary sites. The model restricts non-zero interaction potentials to pairs of molecules placed on perpendicular neighbouring bonds.

The Ising spins are at the secondary sites of the lattice (bonds) and are assigned the values $S=0, 1$ and -1 according to the molecular occupations shown in figure 3.18(b). Reversing the assignment of the orientation for the different secondary sublattices ensures uniquely determined contributions to the total energy. The energy values for each configuration are given in table 3.3 below.

S_i	S_j	sites P ϵ_{ij}	sites Q ϵ_{ij}
0	0	ϵ_{AA}	ϵ_{AA}
1	0	ϵ_{Aa}	ϵ_{Ab}
-1	0	ϵ_{Ab}	ϵ_{Aa}
1	1	ϵ_{aa}	ϵ_{bb}
1	-1	ϵ_{ab}	ϵ_{ab}
-1	-1	ϵ_{bb}	ϵ_{aa}

Table 3.3 : Sin-spin interaction energies

This system is equivalent to the spin-1 Hamiltonian

$$H = -J S_i S_j - K S_i^2 S_j^2 - C (S_i^2 S_j + S_i S_j^2) + \Delta S_i^2 \quad (3.35)$$

with fields

$$\begin{aligned} J &= \frac{1}{2}\epsilon_{ab} - \frac{1}{4}(\epsilon_{aa} + \epsilon_{bb}) \\ K &= \epsilon_{ab} + \epsilon_{Aa} - \epsilon_{AA} - \frac{1}{2}\epsilon_{ab} - \frac{1}{4}(\epsilon_{aa} + \epsilon_{bb}) \\ \pm C &= \frac{1}{2}(\epsilon_{Ab} - \epsilon_{AA}) - \frac{1}{4}(\epsilon_{aa} - \epsilon_{bb}) \\ \Delta &= \frac{1}{2}(\epsilon_{Ab} - \epsilon_{AA}) + \frac{1}{2}(\epsilon_{Aa} - \epsilon_{AA}) - \mu \end{aligned} \quad (3.36)$$

where μ is the chemical potential difference between the two species and C is a staggered field which is positive if the spin pair belong to primary sites P and negative for sites Q.

Equations (3.36) can be mapped onto the FDG model of a ternary mixture of components x, y and z with interaction energy parameters a, b and c, and chemical potential differences μ_{x-z} and μ_{y-z} . In this mapping, x and y represent the two orientations of the amphiphile a-b and z the solvent A-A. If the additional constraint that $\mu_{x-z} = \mu_{y-z}$ is added, the relationships below are derived

$$\begin{aligned}
a_P = b_Q &= \epsilon_{Ab} - \frac{1}{2}(\epsilon_{AA} + \epsilon_{bb}) \\
b_P = a_Q &= \epsilon_{Aa} - \frac{1}{2}(\epsilon_{AA} + \epsilon_{aa}) \\
c_P = c_Q &= \epsilon_{ab} - \frac{1}{2}(\epsilon_{aa} + \epsilon_{bb}) \\
\mu_{x-y} = \mu_{y-z} &= \mu + \frac{1}{2}(2\epsilon_{AA} - \epsilon_{bb} - \epsilon_{aa}) = \bar{\mu}
\end{aligned}
\tag{3.37}$$

Using these relationships, the phase behaviour of the system is given by the symmetrical sections of the FDG model. Figure 3.19 shows a typical phase diagram. It exhibits an ordered AA-rich phase and an isotropic region.

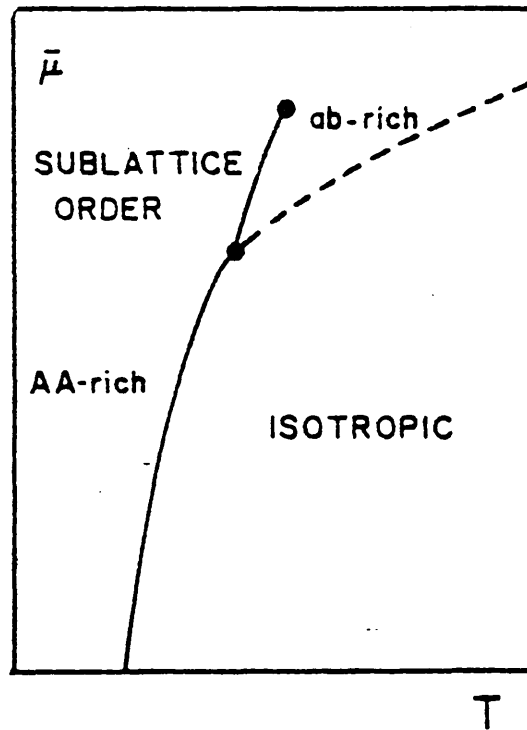


Figure 3.19 : A typical phase diagram in the $(\bar{\mu}, T)$ for the ab + AA mixture. [Robledo 1987]

The phenomenological and decorated lattice models have produced phase diagrams which show evidence of ordered phases. However, the practical use of these models is limited to describing those features of the

system which do not depend upon the details of the chain length or the nature of the chain packing because they do not consider the amphiphile chains to have any structure. The effect of an extended chain plays an important part in the behaviour of surfactant systems.

4.1 INTRODUCTION

A Monte Carlo simulation of a three dimensional lattice model of an amphiphile-solvent mixture in the canonical ensemble has been developed as an extension of earlier work in two dimensions [Care 1987a,b] who determined the cluster size distribution for a range of temperatures, amphiphile concentrations and intermolecular interaction energies. Larson (1988) has done similar work in three dimensions and observed spherical, cylindrical and bilayer structures. These structures, and others, have been observed in the present work. However in this work the clusters are characterised according to their size, shape and surface roughness. This characterisation is an important extension of the work of Larson who only observed the structures in a single configuration. The method allows characterisation of phase transitions.

This section introduces the model used and describes the important features of the program. As Monte Carlo simulations are computer intensive, the parallel computer architecture of transputers was used and the code was written in occam. The parallelisation of the problem is important and is discussed here.

4.2 THE MODEL

A lattice model of an amphiphile and solvent mixture is being considered. It represents an incompressible solution of N_A amphiphiles and N_S solvent molecules. The molecules occupy the sites of a regular

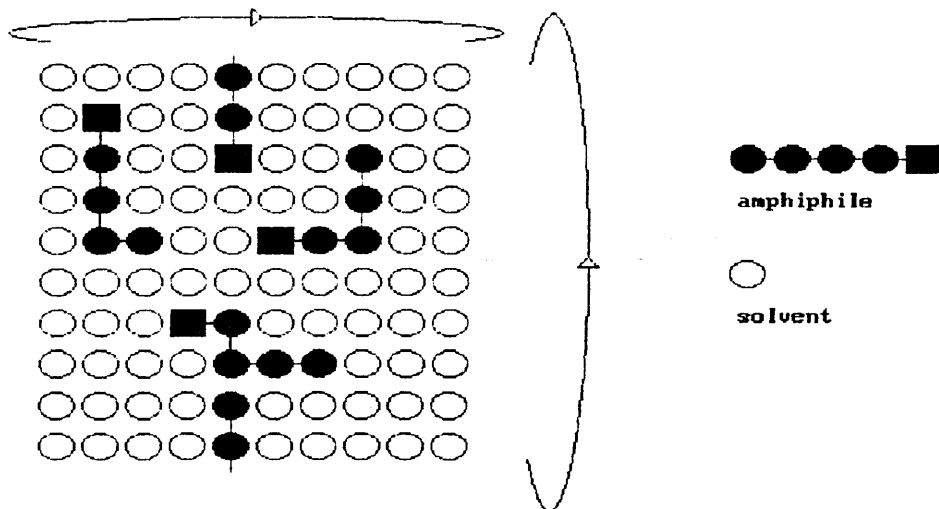


Figure 4.1 : Example lattice

lattice with co-ordination number c . Periodic boundary conditions apply. Each amphiphile is represented by a flexible chain of s adjacent sites with one site on the end of the chain representing the solvophilic head and the remaining $(s-1)$ sites representing the flexible solvophobic tail. The remaining sites in the lattice each represent a solvent molecule. There are no unoccupied sites. Figure 4.1 shows an example lattice with co-ordination number 4. The total number of sites on the lattice is $M = sN_A + N_S$. Only nearest neighbour interactions are assumed and the potential energy of the system may then be written

$$U = n_{HH}E_{HH} + n_{TS}E_{TS} + n_{HS}E_{HS} + \sum_i E_C^i \quad (4.1)$$

where n_{HH} , n_{TS} , n_{HS} are the total number of head-head, tail-solvent and head-solvent bonds; E_{HH} , E_{TS} and E_{HS} are the corresponding interaction energies. E_C^i is the energy associated with the conformation of

the i^{th} molecule. It can be shown [Care 1987a] that (4.1) is the most general form of potential for nearest neighbour interactions. It is thought that chain stiffness will have little effect on the ordering of the system [Szleifer *et al* 1986] and we assume the chains to be fully flexible. Hence, the potential energy of the system reduces to

$$\frac{U}{kT} = \beta(n_{\text{TS}} + \gamma n_{\text{HS}} + \xi n_{\text{HH}}) \quad (4.2)$$

where $\beta = E_{\text{TS}}/kT$, $\gamma = E_{\text{HS}}/E_{\text{TS}}$ and $\xi = E_{\text{HH}}/E_{\text{TS}}$. In order to represent amphiphilic behaviour the tail-solvent interaction is chosen to be solvophobic ($\beta > 0$) and the head-solvent interaction is chosen to be solvophilic ($\gamma < 0$). For $\gamma > 0$, the model shows the complete phase separation of two immiscible liquids at low temperatures.

It is often assumed that the head-head repulsion is responsible for limiting the micelle size. However, the results of Care (1987b) show low temperature configurations of micelles with limited head-head interaction, suggesting that this is unlikely to have a significant effect for short range head-head interactions. Following Care, the simulations assume zero head-head interaction, $\xi=0$. Equation (4.2) thus reduces to

$$\frac{U}{kT} = \beta(n_{\text{TS}} + \gamma n_{\text{HS}}) \quad (4.3)$$

This simplified form facilitated the use of several programming techniques to minimise the program execution time, while still retaining the essential features of an amphiphilic system.

4.3 THE SIMULATION

The model is simulated using the Metropolis (1953) Monte Carlo (MC) technique in the canonical, constant NVT, ensemble.

4.3.1 The Metropolis Algorithm

The generation of each configuration is an important part of the program and is done using the Metropolis MC algorithm. A random move is attempted on a particle in the system and the change in internal energy, ΔU , of the system due to this move is calculated. If $\Delta U < 0$ the move is accepted, otherwise the move is accepted according to a Boltzmann distribution. The Boltzmann probability is given by

$$w = \exp\{-\Delta U/kT\} \quad (4.4)$$

In order to ensure that each successive generated configuration is sufficiently different to the previous one for the purposes of calculating thermal averages, moves are attempted on several particles before calculating new configurational properties. The number of moves attempted for each configuration is known as a Monte Carlo step. In the present work a Monte Carlo step is equal to the number of particles in the system so that, on average, an attempted move is made on each particle once during each Monte Carlo step. Larger intervals may be adopted if equilibration is slow. The pseudo-code for a general form of this algorithm is shown below.

pseudo-code : metropolis algorithm

begin

set moves = 0

while (moves < mc step)

 attempt to move particle in system

 set ΔU = internal energy difference due to move

 if ($\Delta U < 0$) then

 accept move

 else

 set $w = \exp\{-\Delta U / kT\}$

 set z = random number with uniform distribution (0,1)

 if ($z < w$) then

 accept move

 else

 reject move

 end if

 end if

 set moves = moves + 1

end while

end

The simulation described here usually starts from a random configuration of amphiphiles on the lattice at a high temperature, and is cooled in small temperature steps until a low temperature configuration is reached. The starting configuration of the current temperature is the final configuration at the previous temperature. The simulation has also started from an ordered low temperature configuration and heated to check for hysteresis, which is evidence of a first order transition. An algorithm for the simulation is shown below.

pseudo-code : the simulation

begin

set temperature = high temperature
generate random lattice configuration

while (temperature > low temperature)

 set thermalisation step = 0
 while (thermalisation step < no. of thermalisation steps)
 do a monte carlo step
 set thermalisation step = thermalisation step + 1
 end while

set configuration = 0

while (configuration < configurations in average)

 do a monte carlo step
 include configuration in averaging
 set configuration = configuration + 1

 end while

do ensemble averaging
set temperature = temperature - temperature step
end while
end

At each temperature a number of Monte Carlo steps are rejected to allow the system to equilibrate before any ensemble averaging takes place. The number of steps required for thermalisation was investigated by plotting the variation in the mean cluster size with the number of Monte Carlo steps for runs with various, s , γ , and β . The mean cluster size was seen initially to change sharply, but began to fluctuate around a mean value after about 5,000 Monte Carlo steps. No further change was seen after continuing up to 100,000 Monte Carlo steps, indicating that the system had equilibrated after 5,000 Monte Carlo steps at the temperatures reported in this work. In practice, between 20,000 and 50,000 Monte Carlo steps were rejected for thermalisation.

Of particular interest is the change in internal energy when the system is perturbed from a state i to another state j . This is given by

$$\Delta U/kT = \beta(\Delta n_{TS} + \gamma\Delta n_{HS}) \quad (4.5)$$

where Δn_{TS} is the number of tail-solvent bonds in state j minus the number of tail-solvent bonds in state i , and Δn_{HS} is the difference in the number of head-solvent bonds.

4.3.2 Describing The Amphiphiles

An important feature of the present model is that the amphiphiles consist of connected sites. It is necessary to describe the amphiphiles in a manner which retains this connectivity and also allows their nearest neighbour sites to be determined easily in the calculation of the internal energy change. To achieve this, the amphiphiles are stored both on a lattice and in a separate table.

The lattice is an array whose elements contain values which describe the occupancy of the sites as in the model lattice. It does not contain any information about the connectivity of the chains, but enables us easily to determine whether a given site is occupied by a solvent, head or tail segment.

The connectivity of the amphiphiles is stored in a table. For each amphiphile of length s , the table holds the absolute lattice positions of the head and of the $(s-1)$ tail segments. It does not store the

positions of solvent sites.

The table is used when randomly selecting amphiphiles and to determine the location of the amphiphile's nearest neighbour sites on the lattice. It is also used when calculating the ensemble averages of the bond order parameters, which depend on the chain connectivity.

In principle, it is not necessary to store the amphiphile and solvent sites in the form of the lattice, but determining the nature of nearest neighbour sites from the table would be very time consuming. The lattice is also very useful when determining cluster statistics.

To reduce the memory requirements of simulating large lattices, multi-spin coding techniques are used. Thus since each lattice site has only 3 possible states; head, tail or solvent, each site is represented by 2 bits: head=10, tail=01 and solvent=00. Rather than using the 3 coordinate system to address the lattice sites, the sites are indexed from 1 to M. This method of indexing reduces the storage needed for the table of amphiphile conformations as each amphiphile of length s can be described by s integers which are the indices to the positions of the head segment and $(s-1)$ tail segments.

After each temperature step in the simulation, the amphiphile table is stored on disk. This can be used either to regenerate the lattice to continue the simulation or for graphics. Storing the lattice directly would be wasteful of memory as the solvent sites are effectively redundant.

4.3.3 Random Number Generation

An important feature of the Monte Carlo (MC) algorithm, in respect of coding, is the generation of random numbers. For each attempted move three random numbers are generated. The first two are used to randomly select an amphiphile and the type of move to be attempted with that amphiphile on the lattice. The third random number is generated in cases where the acceptance of the move is with a Boltzmann probability. It is therefore essential to use a fast random number generator with the maximum possible cycle length.

Maximum-length binary sequences generated by linear-feedback shift registers are often used to produce random numbers for simulation. The statistics of maximum length sequences are fairly well understood and they can be generated quickly as only the logic exclusive-or operation is involved.

The linear-feedback shift register of Kirkpatrick and Stoll (1981) was implemented. A table is generated of 521 random integers between 1 and 2^{31} (maximum machine integer) using a simple random number generator. If x is the table of 521 random numbers, then the k^{th} random number in the sequence is given by

$$x_k = x_{k-32} \oplus x_{k-521} \quad (4.6)$$

where the table is assumed to be cyclic.

The statistical properties of maximum length sequences generated by linear-feedback shift registers are investigated by Compagner & Hol-

land (1987). They judge non-randomness by considering the complete hierarchy of correlation numbers of any order. Although persistent deviations from pure randomness exist, both the pair correlations between bits of the sequence and the number of runs of a certain size are almost what they should be. All maximum length sequences of the same length are found to be equally random, although their suitability depends on their particular application.

In the present application three random numbers are used for each attempted move. Kirkpatrick & Stoll (1981) have tested the uniformity of successive triples generated by their algorithm. Each triple of random numbers was assigned to a cell (i,j,k) in a unit cube with a resolution of 32x32x32 cells. The cell to cell variation was measured by the χ^2 -like quantity

$$\varphi = L^{-3} \sum_{\substack{\text{cells} \\ i,j,k=1}}^L [n(i,j,k)-n_0]^2/n_0 \quad (4.7)$$

where $n(i,j,k)$ is the number of triples falling into cell (i,j,k) and n_0 is the mean number of triples per cell. For independently distributed triples $\varphi \approx 1$. Taking several samples of 10^6 numbers each a value of $\varphi = 1.00 \pm 0.005$ was obtained for this generator.

4.3.4 Moving The Amphiphile

A restriction imposed on a move made in a Metropolis MC simulation is that the conditions of a Markov chain are obeyed. The probability of a move from state i to state j must equal the probability of the reverse

move

$$p(a_{ij}) = p(a_{ji}) \quad (4.8)$$

This restriction means that moving flexible molecules in MC is more difficult than moving rigid molecules. A further restriction imposed on the movement of the amphiphiles is that the system must be ergodic i.e. it must be possible to sample all regions of phase space.

Care (1987b) simulated short chains ($s=3$) at low densities. The chains were allowed to move by translation or by changing to a new conformation. The probabilities for change to each of the possible conformations were equal to ensure that equation (4.8) was satisfied. This approach is, however, inapplicable at high densities as the rejection rate would be too high due to frequent hard-core interactions.

A better method at high densities was suggested by Wall & Mandel (1975). The chains are moved by reptation which involves moving one end of the chain to a nearest neighbour site on the lattice with all other segments of the chain moving forward along the old contour. The end of the chain must move onto a solvent site as hard core interactions are not permitted. In this implementation, if the head of the amphiphile attempts to move onto a site occupied by the last segment of its own tail, it is not considered a hard core interaction as this site is no longer occupied by the tail at the end of the move. The same is true for a move made in the reverse direction.

Reptation is equally valid for all chain lengths, but is not as efficient as allowing complete molecule translation at low densities. It

has been used previously in the simulation of multiple chains e.g. Bishop *et al* (1980), Larson (1988).

4.3.5 The Internal Energy Change

In practice, it is not necessary to calculate the internal energy change due to an attempted move. To save processing time, only the change in the number of head-solvent bonds, Δn_{HS} , and tail-solvent bonds, Δn_{TS} , are counted. These alone are needed to determine the Boltzmann weighting factor, as shown below. As only reptation moves are allowed there are changes in the nearest neighbour environment of only 3 lattice sites, independent of chain length. This easily shown with a two dimensional example.

Consider a chain lying on the lattice as shown below. The head group is represented by H and each tail segment by T. The chain is to be moved head first into the site marked S, which must be a solvent site. The nearest neighbour sites affected by the move are labelled a-n, but their type remains unspecified.

```

. . . . .
. . b d f h j l . .
. . a T T T T H S n .
. . c e g i k m . .
. . . . .

```

After the move has taken place the lattice will be as below. The site previously occupied by the end of the tail becomes a solvent site.

```

. . . . .
. . b d f h j l . .
. . a S T T T T H n .
. . c e g i k m . .
. . . . .

```

If xy signifies a bond between a sites of type x and y , then the nearest neighbour bonds of interest before the move are given by

$$B = T(a+b+c) + T(d+e+f+g+h+i) + H(j+k) + S(l+m+n) \quad (4.9)$$

and after the move by

$$A = S(a+b+c) + T(d+e+f+g+h+i) + T(j+k) + H(l+m+n) \quad (4.10)$$

Of interest is the difference between the nearest neighbour bonds before and after the move. Subtracting (4.9) from (4.10) gives

$$A - B = (S-T)(a+b+c) + (T-H)(j+k) + (H-S)(l+m+n) \quad (4.11)$$

Using equation (4.11) it is possible to determine Δn_{HS} and Δn_{TS} for the attempted move given information about the sites a, b, c, j, k, l, m and n . This information can be obtained from the lattice. Equation (4.11) is equally valid for the reverse move, (tail first), if both sides are multiplied by -1 . It can easily be extended to 3 dimensions.

4.3.6 The Boltzmann Weighting Factor

To increase the speed of the simulation all possible Boltzmann weighting factors were calculated a priori and placed in a look-up table. Substituting equation (4.5) into (4.4) gives

$$w = \exp\{-\beta (\Delta n_{TS} + \gamma \Delta n_{HS})\} \quad (4.12)$$

where w is the Boltzmann factor. The values of Δn_{TS} and Δn_{HS} , when only reptation moves are allowed, fall in tightly bound ranges; in 3-dimensions $-10 \leq \Delta n_{TS} \leq 10$ and $-10 \leq \Delta n_{HS} \leq 10$. A simple hashing algorithm is used to calculate a unique index for each combination of Δn_{TS} and Δn_{HS} , and the appropriate Boltzmann factor is placed in the look-up table at this index. Thus, for a given move on the lattice the index is calculated using the hashing formula and the Boltzmann probability is read directly from the table.

4.3.7 Accepting The Move

Accepting an energetically favourable move involves both updating the lattice and updating a table of amphiphile conformations. The sites on the lattice are specified by a 2 bit binary number, therefore it is possible to change the occupancy of a site by simple logical operations. As reptation moves are used it is only necessary to update 3 sites on the lattice and the positions of the two ends of the chain in the conformation table.

4.3.8 Data Analysis

The results of Larson (1988), suggest we should expect a range of structures from the simulation e.g. spheres, cylinders and bilayers. This was indeed the case so methods of numerically characterising these different structures were developed; namely the cluster size

distribution and the principal moments of inertia. Other properties measured are the surface roughness and the bond order parameters. Each of these are discussed separately below, but they all depend on being able to count the number and size of clusters.

The cluster counting routine is a version of the 'ant in the labyrinth' algorithm [Dewar & Harris 1987]. The lattice is scanned until a site occupied by a head or a tail segment is found. Using the 'ant' analogy, the ant sits on this site and lays eggs on each of its nearest neighbour sites that are occupied by an amphiphile segment. These eggs hatch and lay more eggs on amphiphile sites not previously visited. This process is repeated until there are no longer any free sites in the cluster. Counting the number of ants determines the cluster size. The cluster is then deleted from the lattice and the lattice again scanned to find another cluster.

4.3.9 Cluster Size

At low concentrations we are interested in the cluster size distribution as the existence of a maximum and a minimum in the distribution has been suggested as an effective indicator of a micellar region.

At higher concentrations, such as in the bilayer region, the cluster size distribution is very narrow. The mean cluster size is of more interest here. Plotting contours of the ratio of the mean cluster size to the total number of amphiphiles, N_A , on a temperature-composition diagram has helped determine the phase boundary of a lamellar region.

The number-average cluster size, \bar{n} , and the root-mean-square devia-

tion, σ , of the cluster size distribution are given by

$$\bar{n} = \frac{\sum_{i=1}^{\infty} i n_i}{\sum_{i=1}^{\infty} n_i} \quad (4.13)$$

and

$$\sigma^2 = \frac{\sum_{i=1}^{\infty} i^2 n_i}{\sum_{i=1}^{\infty} n_i} - (\bar{n})^2 \quad (4.14)$$

where n_i is the total number of clusters containing i amphiphiles and σ is a measure of the width of the cluster size distribution.

Assuming each observed cluster is an independent sample taken from some underlying cluster size distribution, the standard error, δ_1 , in \bar{n} is given by

$$\delta_1 = \frac{\sigma}{\left[\sum_{i=1}^{\infty} n_i - 1 \right]^{\frac{1}{2}}} \quad (4.15)$$

Following Care (1987b), the uncertainty of the Monte Carlo results may be estimated by comparing the standard error, δ_1 , with the error, δ_2 , obtained by dividing the data collecting MC steps into p blocks of q steps such that pq is the total number of MC steps at each temperature. Typically $p=500$ and $q=50$. The number average cluster size after each q steps is \bar{n}^j and an alternative estimate of the number-average cluster size is given by \bar{n}' , where

$$\bar{n}' = \frac{\sum_{j=1}^{\infty} \bar{n}^j}{p} \quad (4.16)$$

and the error, δ_2 , in \bar{n}' is

$$\delta_2 = \left[\frac{\sum_{j=1}^{\infty} (\bar{n}^j - \bar{n}')^2}{p(p-1)} \right]^{\frac{1}{2}} \quad (4.17)$$

The values of the errors in \bar{n} and \bar{n}' should be similar provided that the \bar{n}^j are independent. Failure of this condition indicates that there is strong correlation between successive \bar{n}^j and corresponds physically to the persistence of clusters through several configurations.

The size of the choice of the subblock, p , is discussed by Bishop & Frinks (1987). They conclude statistical efficiency cannot be calculated accurately for either small or large values of p . The subblocks are correlated when p is too small and when p is too large there are too few subblocks for accurate analysis.

4.3.10 Principal Moments Of Inertia

The size and shape of aggregates are often described in terms of the principal components of the moments of the inertia tensor I . The inertia tensor is found to have diagonal components

$$I_{\alpha\alpha} = \sum_{i=1}^{\infty} m_i (r_i^2 - \alpha_i^2), \quad \alpha = x, y, z \quad (4.18)$$

the subscript i referring to the mass m_i . The diagonal components are given by the products of inertia

$$I_{\alpha\beta} = - \sum_{i=1}^{\infty} m_i \alpha_i \beta_i = I_{\beta\alpha}, \quad \begin{array}{l} \alpha = x, y, z \\ \beta = x, y, z \\ \alpha \neq \beta \end{array} \quad (4.19)$$

For any point in a rigid body, a set of Cartesian axes exist for which the inertia tensor will be diagonal. These axes are the principal axes and the corresponding diagonal elements are the principal moments of inertia, I_x , I_y and I_z . The principal moments of inertia are the eigenvalues of I , and are found by solving

$$\begin{vmatrix} I_{xx} - I_x & I_{xy} & I_{xz} \\ I_{xy} & I_{yy} - I_y & I_{yz} \\ I_{xz} & I_{yz} & I_{zz} - I_z \end{vmatrix} = 0 \quad (4.20)$$

The summations I_{xx} , I_{xy} , I_{xz} etc. are done in the cluster counting routine, (see section 4.3.8). In cases where the cluster completely spans the lattice in one or more directions, periodic boundary conditions mean there is no 'edge' to the cluster. The cluster perimeter is determined by the order in which sites are found by the 'ant in a labyrinth' algorithm.

We are interested in distinguishing between spheres, cylinders and planes and consider the principal moments of inertia for a sphere, a thin rod and a circular disk

$$\begin{aligned}
I_x = I_y = I_z &= (2/5)MR^2 & : \text{ sphere} \\
I_x = I_y = 0, I_z &= (1/12)ML^2 & : \text{ rod} \\
I_x = I_y &= (1/4)MR^2, I_z = (1/2)MR^2 & : \text{ disk}
\end{aligned} \tag{4.21}$$

Measuring the principal moments of inertia from the simulation involves averaging over many clusters of different sizes and orientations. We therefore sort the moments of each cluster into ascending order and normalise them to sum to unity. Thus

$$I_L + I_M + I_S = 1, \quad I_L \geq I_M \geq I_S \tag{4.22}$$

where I_L , I_M , I_S are the largest, middle and smallest principal moments of inertia of a cluster in the ensemble.

The mean principal moments, I_L , I_M and I_S , are weighted by the cluster size, i

$$I_\alpha = \frac{\sum_{i=1}^{\infty} i I_{\alpha i}}{\sum_{i=1}^{\infty} I_{\alpha i}}, \quad \alpha = L, M, S \tag{4.23}$$

Similarly to 4.14 and 4.15 the root-mean-square deviation and standard error are given by

$$\sigma = \left[\frac{\sum_{i=1}^{\infty} i^2 I_{\alpha i}}{\sum_{i=1}^{\infty} I_{\alpha i}} - (I_\alpha)^2 \right]^{\frac{1}{2}} \tag{4.24}$$

and

$$\delta = \left[\frac{\sigma}{\omega \sum_{i=1} n_i - 1} \right]^{\frac{1}{2}} \quad (4.25)$$

For the normalised principal moments of inertia, equations (4.21) become

$$\begin{aligned} I_S = I_M = I_L = 1/3 & \quad : \text{ sphere} \\ I_S = I_M = 0, I_L = 1 & \quad : \text{ rod} \\ I_S = I_M = 1/4, I_L = 1/2 & \quad : \text{ disk} \end{aligned} \quad (4.26)$$

The ratio of the smallest to the largest moment (sphere=1, rod=0, disk=0.5) are plotted on contour diagrams to show change in structure with respect to temperature and concentration. These ratios were used as a measure of aggregate shape fluctuation in the molecular dynamics simulation of micelles of Woods *et al* (1986).

4.3.11 Surface Roughness

The surface roughness of micelles has been an area of contention and is also something which can be determined from the simulation. A convenient representation of the surface roughness is the ratio of the number of amphiphile-solvent bonds to the number of amphiphile sites in contact with solvent. Three forms of the surface roughness are determined : the total surface roughness, ρ_{total} , and the corresponding contributions from the head and tail sites, ρ_{head} and ρ_{tail} , which

are referred to as the head roughness and the tail roughness. The three surface roughness terms are defined in equations 4.27(a-c) below

$$\rho_{\text{total}} = \frac{\text{total number of amphiphile-solvent bonds}}{\text{total amphiphile sites with solvent contact}} \quad (4.27a)$$

$$\rho_{\text{head}} = \frac{\text{total number of head-solvent bonds}}{\text{total head sites with solvent contact}} \quad (4.27b)$$

$$\rho_{\text{tail}} = \frac{\text{total number of tail-solvent bonds}}{\text{total tail sites with solvent contact}} \quad (4.27c)$$

As with the principal moments of inertia, the surface roughness is weighted by cluster size and the root-mean-square deviation and standard error are measured.

$$\sigma = \left[\frac{\sum_{i=1}^{\infty} i^2 \rho_{xi}}{\sum_{i=1}^{\infty} n_i} - (\bar{\rho}_x)^2 \right]^{\frac{1}{2}} \quad (4.28)$$

x= total,head,tail

and

$$\delta = \left[\frac{\sigma}{\sum_{i=1}^{\infty} n_i - 1} \right]^{\frac{1}{2}} \quad (4.29)$$

4.3.12 Bond Order Parameters

Bond order parameters which describe the orientation of the chain

bonds with respect to the first bond where calculated in some cases. This was largely for comparison with mean field models, rather than structure characterisation. The bond order parameter S_k , is given by

$$S_k = \langle 3/2 \cos^2\theta_k - 1/2 \rangle \quad (4.30)$$

where θ_k is the angle between the first and k^{th} bonds. When $S_k = 0$ all bond directions are equally probable. For $1 \geq S_k > 0$ there is preferential ordering in the direction of the first bond, whilst for $-0.5 \leq S_k < 0$ the k^{th} bond prefers to order in the direction of the normal to the first bond.

4.4 CHOICE OF PARALLEL ALGORITHM

Monte Carlo simulations are demanding of computer resources. The use of parallel computing is seen as a convenient way of obtaining the necessary computer power. Parallel computers are defined as computers having processors working simultaneously under the control of an application programme [Fincham 1987]. Such computers can be broadly classified as either SIMD (Single Instruction stream/Multiple Data stream) or MIMD (Multiple Instruction stream/Multiple Data stream).

SIMD machines run the same code on each processor, although the data on each may be different. An example of a SIMD computer is the Digital Array Processor (DAP). Lattice simulations are suited to the DAP as lattice sites can be identified directly with processing elements, although, in our case, the existence of the amphiphile chains will make the algorithm complex in practice.

Unlike SIMD, MIMD machines are able to run different code on each processor simultaneously. This makes them very versatile, providing the opportunity to use different techniques in exploiting parallelism. An example of a MIMD machine uses Inmos transputers. This is a high performance microprocessor designed specifically for concurrent processing. Each transputer has four links enabling "arrays" of transputers to be connected together in various topologies. Each transputer processes its own code, communicating data to and from other processors via the bi-directional links as necessary. The transputer also has the advantage of its own concurrent programming language based on the occam model of concurrency. The transputer is being used to provide the computing power required in the simulation considered here both because of its suitability and because it is readily available.

In many problems suitable for parallel programming there are several distinct ways to obtain concurrency and it is not always obvious which method will be best suited to the particular problem. As very significant speed increases can be obtained by optimising the parallelism, it is necessary to evaluate the different options available before starting to write the code.

There are three common categories of parallel algorithms which are used in scientific computing; processor farms, geometric parallelism and algorithmic parallelism. Both the geometric and algorithmic methods of parallelism take advantage of the inherent parallelism in the Metropolis Monte Carlo technique.

In the Monte Carlo simulation a molecule is taken at random and an

attempted move is made. The move is accepted or rejected according to the change in energy of the system. As we have only nearest neighbour interactions this energy change can be calculated by examining only a small part of the lattice. Thus, in principal, there is no reason why moves may not be attempted on two or more non-interacting molecules concurrently.

In considering parallel algorithms and architectures a distinction is made between processes and processors. In the occam model a system is decomposed into parallel processes. Each processor (transputer) is able to run one or more processes.

4.4.1 Processor Farm

In order to run a Metropolis Monte Carlo simulation on a processor farm, each processor runs the same programme but with different starting conditions. If the time for thermalisation is T_t and the production time on a single processor is T_p , the total effective simulation time on a farm of N processors is T_F where

$$T_F = T_t + T_p/N \quad (4.31)$$

This method has the advantage that only a small time is spent on communications, but the fixed thermalisation time limits the value of the method.

4.4.2 Geometric Parallelism

If geometric parallelism is used for this problem, the lattice is divided into cells and each cell is assigned to a different processor. The transputers must communicate in order to move amphiphiles which lie at the boundary of two or more cells. The simulation time for N processors in a geometric array will be

$$T_G = \frac{1}{N} \frac{(T_t + T_p)}{\text{Eff}} \quad (4.32)$$

where Eff is the efficiency of the geometric algorithm and is a function of N. Note that $0 \leq \text{Eff} \leq 1$.

If we assume that $T_t = T_p$, the geometric algorithm will be superior to the farm method provided

$$\text{Eff} > (2/N + 1) \quad (4.33)$$

Unfortunately, for the model considered here, the amphiphiles will form clusters and this may cause severe load matching problems in a geometric array. Thus one transputer may be responsible for the Monte Carlo moves of significantly more amphiphiles than its neighbouring transputers. To overcome these problems a form of algorithmic parallelism was considered.

4.4.3 Algorithmic Parallelism

The simulation algorithm was decomposed such that the selection of the amphiphiles, the testing of the Monte Carlo criterion and the subsequent updating of the amphiphiles on the lattice were separate proc-

esses. The lattice was placed on a single transputer along with the selection and update processes, whilst the MC process was replicated on a farm of transputers. Each selected amphiphile was taken from the lattice along with its nearest neighbour sites and was sent to a vacant MC process, where a move was attempted. The updated section of the lattice was then returned to update the main lattice. Assuming enough transputers in the MC farm, the program speed would be limited by the time taken to remove and add amphiphiles to the lattice.

In practice, there were overheads involved with the selection of amphiphiles as amphiphiles with an overlapping region of nearest neighbour interaction could not be processed simultaneously. This meant that the selection process took a large amount of time compared to the time taken to do the MC test. For this reason the program was abandoned and an algorithm based on the processor farm method described above was adopted.

4.5 IMPLEMENTATION OF PARALLEL SYSTEM

The transputers are configured, as shown in figure 4.2, such that the farm consists of replicated pairs of processes, numbered 1 to P, where P is the number of simulations that may be run concurrently. Each pair of transputers is initialised with unique starting conditions and is responsible for the MC simulation and the statistics of a single, complete simulation.

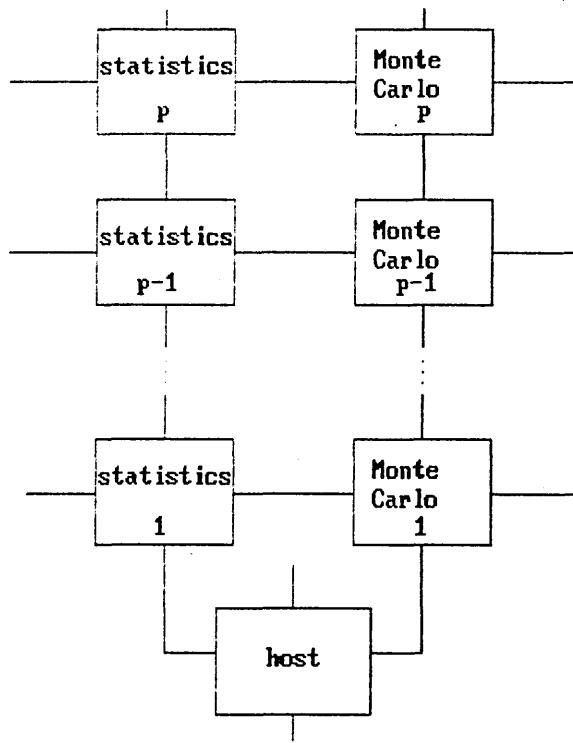


Figure 4.2 : the transputer configuration

At present $P = 15$, but may easily be increased if more transputers become available as P is merely a constant in the program.

4.5.1 The Monte Carlo Process

A data flow diagram of the MC process is shown in figure 4.3. The input buffer receives data from the host which is tagged with the processor identity. If the identity tag matches the number of the processor the data is passed to the main process, otherwise it is passed on to the next MC processor in the farm. At each temperature the MC process periodically dumps its lattice to the statistics routine where cluster counting and averaging takes place. Optimal load balancing occurs when time period between successive dumps of the lattice equals the time taken for the statistics process to analyse

the lattice.

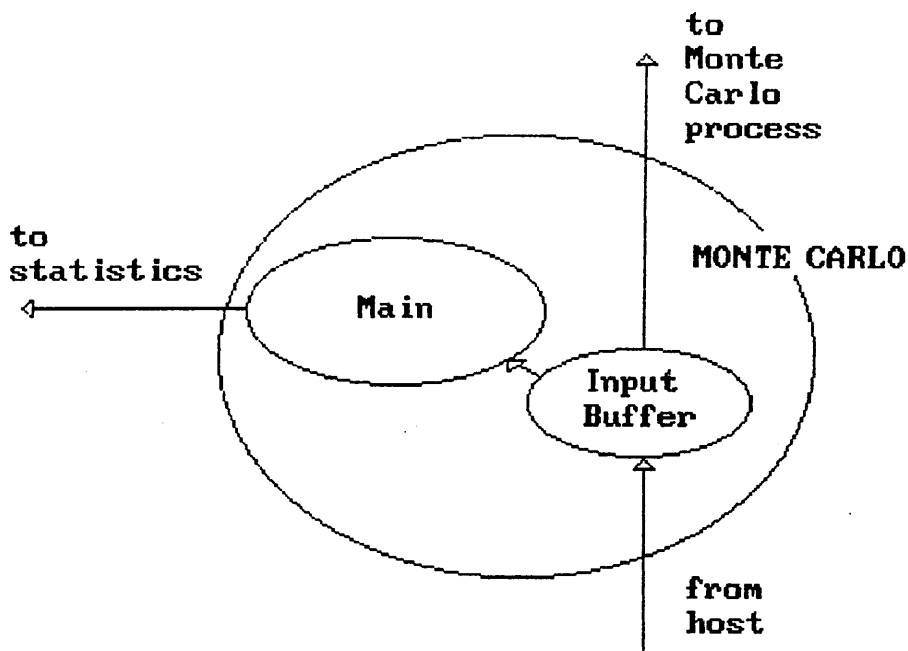


Figure 4.3 : Data flow diagram of the Monte Carlo process

In addition to new initial conditions, the MC processes receive user requests for information on the progress of the simulation. This information is passed back to the host via the statistics processor.

4.5.2 The Statistics Process

The statistics processor, as shown in figure 4.4, has three main processes. The input buffer diverts lattices from the MC process to the main process, where the cluster counting takes place. Other data is passed directly to the output buffer. The output buffer also receives statistics from the main process and from the previous statistics process in the farm, which it passes to the host. Averaged sta-

tistics are dumped to the host for filing at the end of each temperature step. In addition, the state of the lattice and random tables are dumped, enabling the system to be restarted from any temperature.

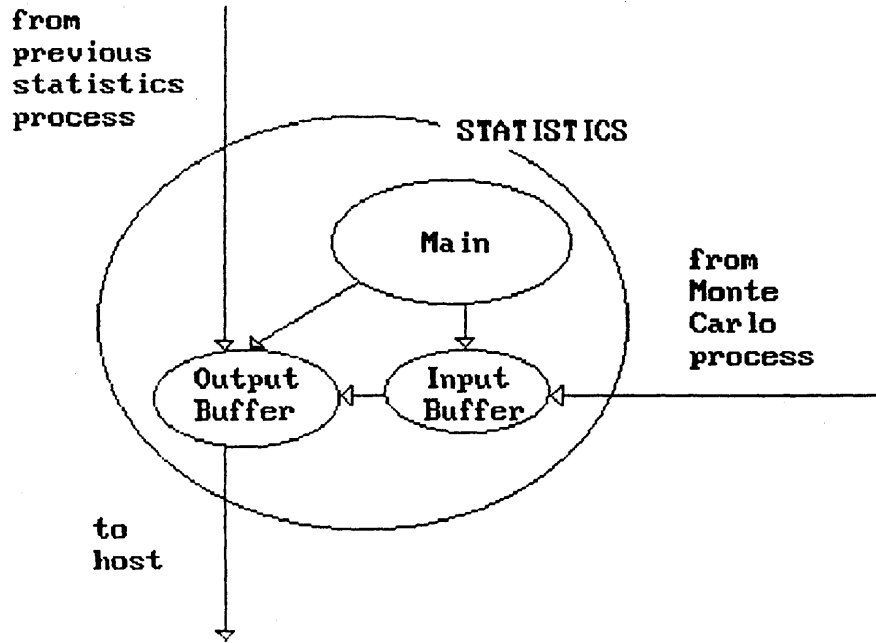


Figure 4.4 : Data flow diagram of the statistics process

4.5.3 The Host Process

The host processor provides the user interface to the farm and is responsible for file handling. The main processes involved are shown in figure 4.5. The control process is menu driven and allows the user to initialise and interrogate processes. It is linked to the lattice and random filers to enable MC processes to be initialised from previous configurations. The input buffer filters all data from the farm and distributes it to the appropriate filing process, or to the screen, via the control process.

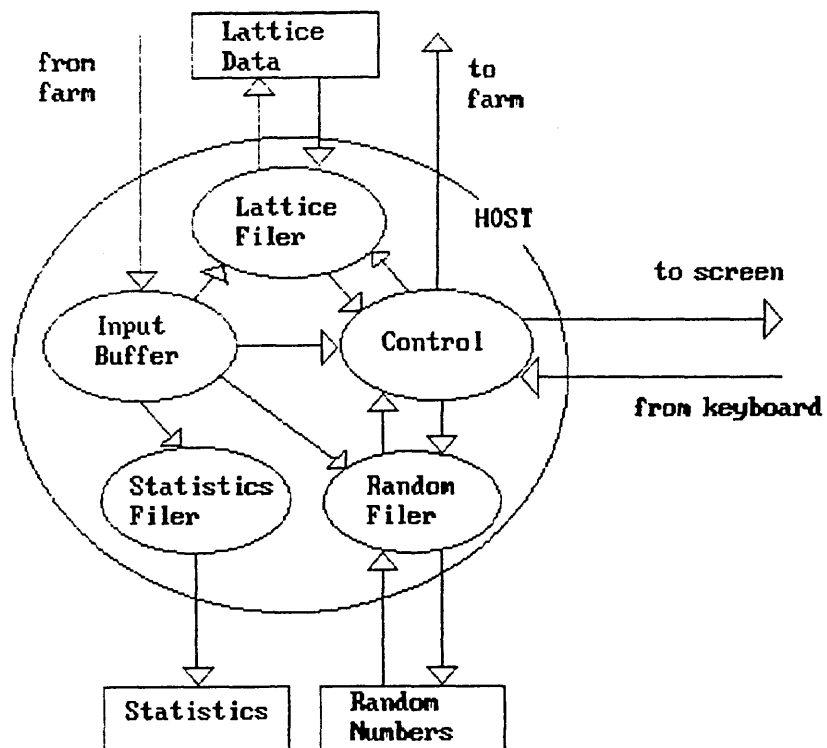


Figure 4.5 : Data flow diagram of the host process

5.1 INTRODUCTION

The model described in Chapter 4 has a number of parameters which can be investigated : the head-solvent interaction γ , the reduced temperature β^{-1} , the number of amphiphiles N , and the chain length s . However, the simulations have a long run time as they are slow to equilibrate particularly at high amphiphile concentrations where there is a low success rate of attempted moves. For this reason, only a small region of the parameter space of the model has been investigated in detail.

Initially the model was simulated in 2-dimensions on a square lattice of 128×128 sites, populated with 512 amphiphiles with chain length $s=3$ and the results compared with those of Care (1987b). Having established agreement between our results and the results of Care (1987b), the equivalent 3-dimensional system was examined for similar values of γ . All further runs were made in 3 dimensions.

The $s=3$ system showed evidence of both micelles and a bilayer. Encouraged by these results, a preliminary investigation was made giving a general appreciation of how the model behaves. These simulations were at fairly low concentrations and revealed a variety of structures such as micelles, cylinders, single bilayers and a vesicle-like structure. The structures were sensitive to changes in s and γ .

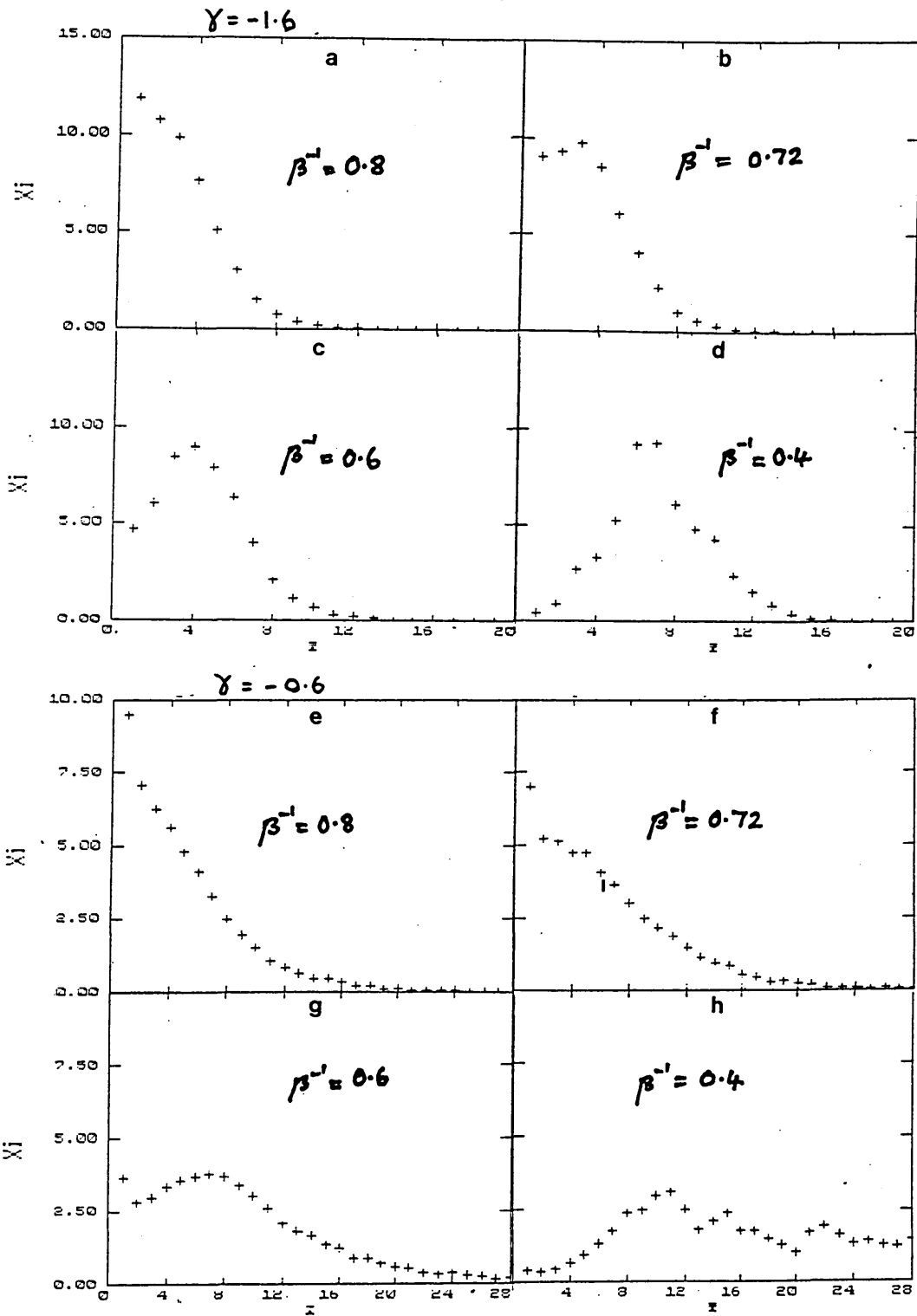


Figure 5.1 : Variation of concentration of monomers in clusters of size i , X_i , with i . Arbitrary units for X_i , but same units used on all figures.

The majority of the work presented here concerns the detailed examination of the $s=4$ system, particularly with $\gamma=-2.0$. This system was simulated over a wide range of amphiphile concentrations, for temperatures between $\beta^{-1} = 1.5$ and $\beta^{-1} = 0.8$. At low concentrations the most common low-temperature structures were cylinders, with a micellar region in the mid-temperature range. At high concentrations ($\approx 50\%$) a lamellar region comprising of several bilayers was found at low temperatures. Unlike the preliminary work, these structures were characterised by examining their principal moments of inertia as well as their mean cluster sizes and cluster size distribution curves. The ratio of the smallest to the largest principal moments of inertia were plotted as a function of temperature and amphiphile concentration to construct a phase diagram of the $s=4$, $\gamma=-2.0$ system. Similar diagrams were plotted using the mean cluster size and the surface roughness, as defined in Chapter 4, equation (4.27).

5.2 TESTING THE SIMULATION IN 2-D

To check that the simulation was working correctly, results from the 2-D work of Care (1987b) were reproduced. Cluster size distributions were obtained for systems of 512 amphiphiles with a chain length $s=3$ on a lattice of dimensions 128×128 sites. Values of the head-solvent interaction, γ ranging between 1.0 and -1.7 were considered and the simulations were cooled from $\beta^{-1}=1.4$ to $\beta^{-1}=0.4$ in steps of 0.02. At each temperature 2.56×10^7 attempted moves were made to thermalise the system and a further 7.68×10^7 attempted moves were used to obtain data. The initial configuration at $\beta^{-1}=1.4$ was generated ran-

domly. At all other temperatures the initial configuration is the final configuration of the previous temperature.

The uncertainty in the Monte Carlo results was estimated by comparing the standard error in the mean cluster size, δ_1 (equation 4.15), with the standard error, δ_2 obtained by dividing the data into blocks, (equation 4.17). Over the temperature range considered δ_1 and δ_2 are similar indicating that the clusters are not persistent through several configurations. The fractional errors corresponding to δ_1 and δ_2 do not exceed 0.8% for these results.

When the head was solvophobic the amphiphiles condensed to a single cluster at low temperatures in which the heads were distributed approximately evenly throughout the cluster. For negative γ , cluster size distributions were obtained with a minimum and maximum, characteristic of a micelle formation. The cluster size distributions for $\gamma = -0.6$ and -1.6 are shown in figure 5.1. Figures 5.1(g) clearly shows a minimum and maximum in the cluster size distribution. Although the minimum is shallow, its position is reproducible. The results compare well with those of Care (1987b), see figure 3.14, but are less well defined. The poorer statistics may be due to the reduced efficiency incurred when moving the amphiphiles by reptation only.

There was also evidence for the formation of small bilayer-type clusters for $\gamma < -1$. Encouraged by these results, the simulation was run in three dimensions over the same range of γ .

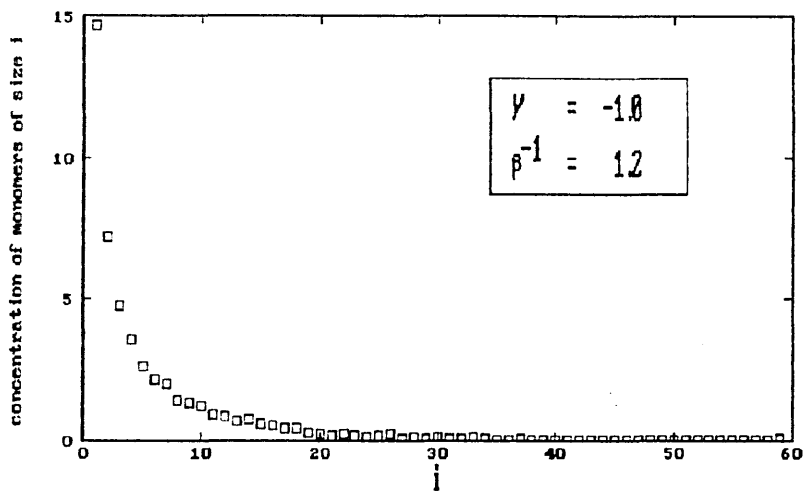
5.3 COMPARISON OF 2-D AND 3-D

The parameters for these initial 3-D simulations were chosen to be approximately equivalent to those used in the 2-D simulations described above. The simulations were carried out for 512 amphiphiles, with chain length $s=3$, on a $32 \times 32 \times 32$ lattice. Values of the head-solvent potential γ ranging between 1.0 and -1.7 were considered and the simulations were cooled from $\beta^{-1}=2.0$ to $\beta^{-1}=0.8$ in steps of 0.02. The starting configuration at the highest temperature was generated randomly and the starting configuration for each new temperature was the last configuration from the previous temperature. 2.56×10^7 attempted moves were discarded as thermalisation and 1.024×10^8 attempted moves were used to collect data.

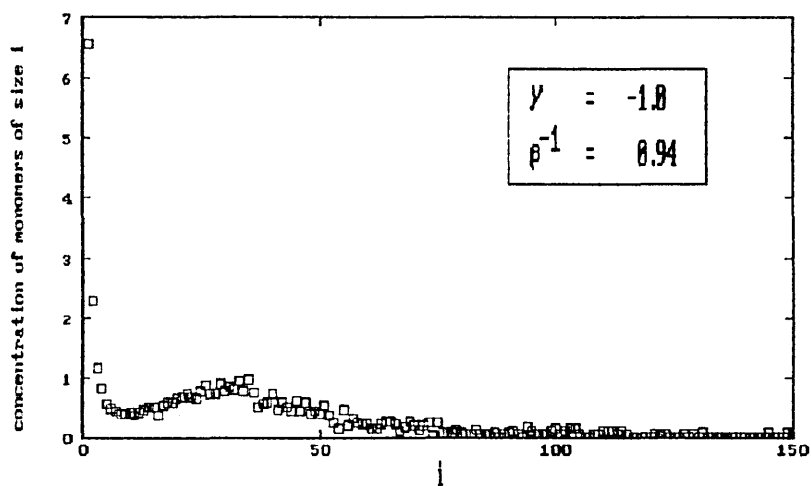
The standard errors in the mean cluster size δ_1 and δ_2 , (equations 4.15 & 4.17), are similar except at very low temperatures where δ_2 is significantly smaller than δ_1 . This is because the cluster configuration becomes almost 'frozen' and hence, although the spread of cluster sizes in a configuration is significant, there is little change in this spread over successive blocks of configurations.

For γ between 1.0 and -0.6, condensation into a single cluster was observed with no evidence of micelle formation in the cluster size distribution. Evidence of a micellar size distribution, however, was observed at $\gamma = -1.0$. Figure 5.2(a-c) shows size distribution curves ($\gamma = -1.0$) at different temperatures. At reduced temperature $\beta^{-1} = 0.94$ a weak minimum and maximum were observed, (figure 5.2(b)). On lowering β^{-1} past this point, the system quickly starts to 'freeze' which is indicated by noise in the cluster size distribution curve, (figure 5.2(c)).

(a)



(b)



(c)

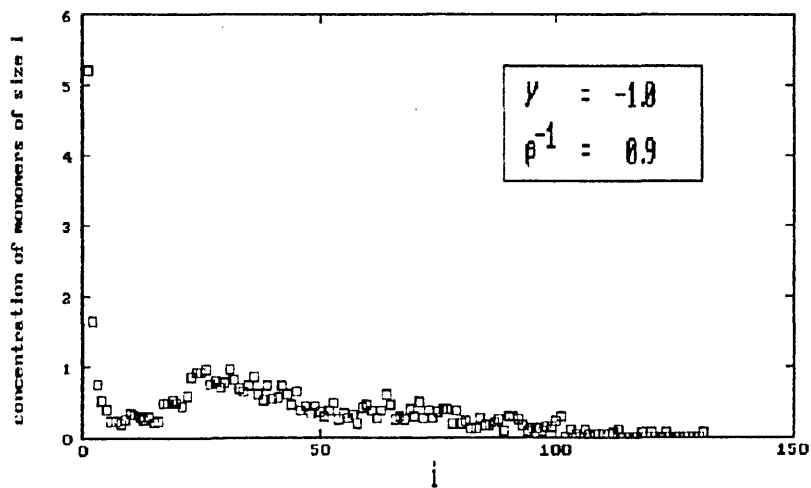
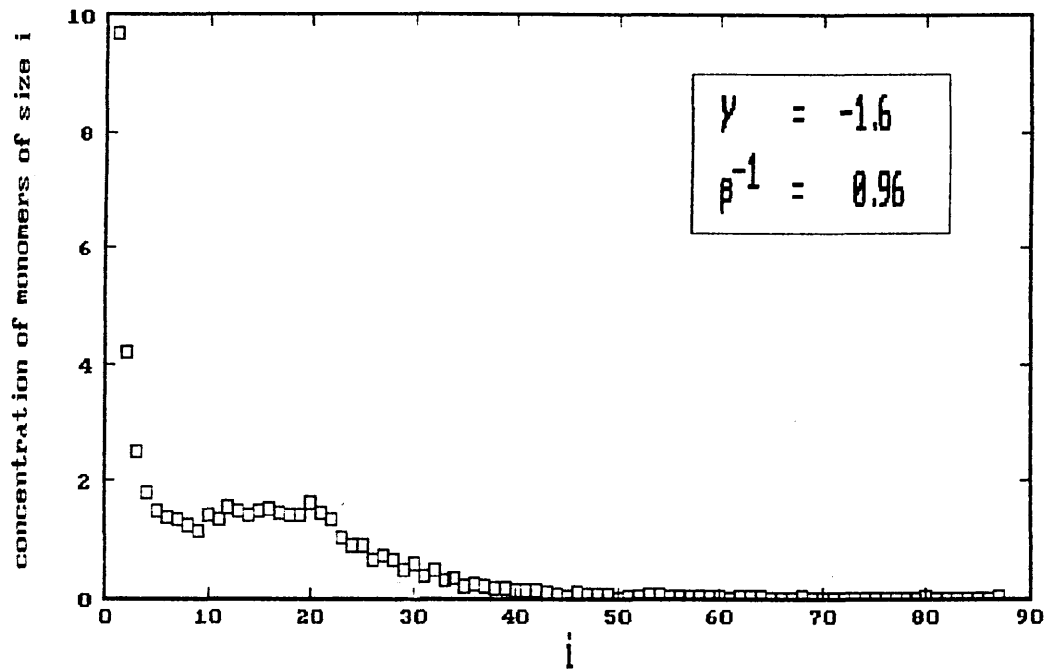


Figure 5.2 : Cluster size distributions from 3D simulations;
 $\gamma = -1.0$

(a)



(b)

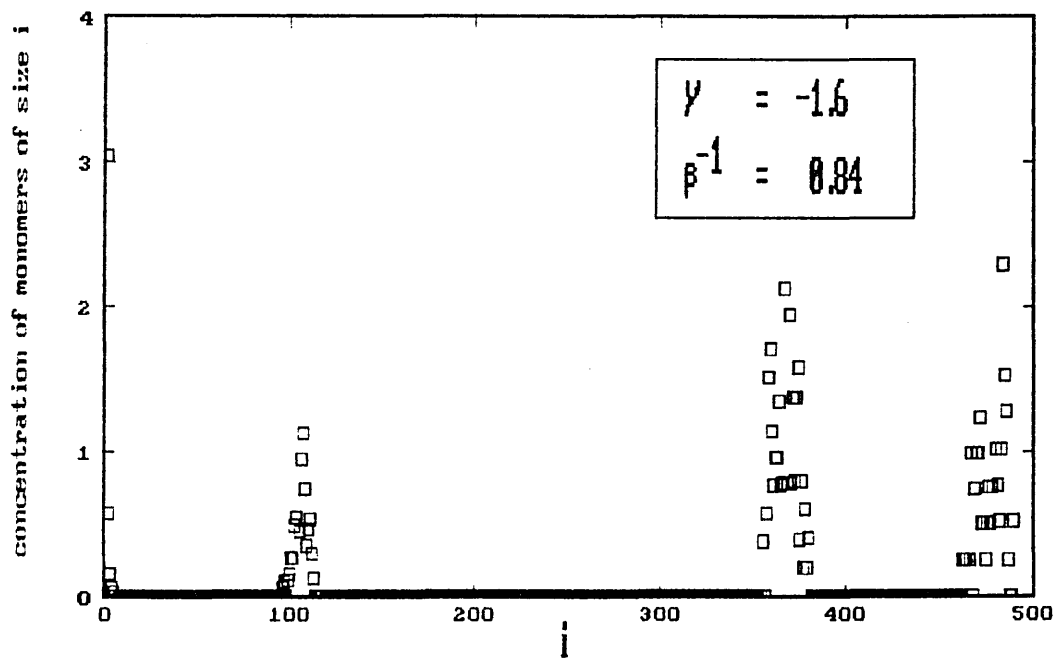


Figure 5.3 : Cluster size distributions from 3D simulation;
 $\gamma = -1.6$

Following the pattern of the two dimensional simulation, it seemed likely that a curve similar to figure 5.2(b) would occur as the head-solvent interaction was made more solvophilic. This did not happen as indicated by figure 5.3(a) which shows the most prominent minimum and maximum obtained for $\gamma = -1.6$. However, when the temperature was lowered further, the system formed two large clusters of about 100 and 400 monomers. Figure 5.3(b) shows the cluster size distribution for $\gamma = -1.6$ at $\beta^{-1} = 0.84$. The apparent cluster of about 500 monomers is due to the two smaller clusters touching each other during the statistical averaging.

Examination of the large clusters revealed castellated bilayer structures which occupied four planes of the lattice. Figure 5.4 represents successive slices through the lattice in the z-direction, reading from top left to bottom right. A distinct bilayer is clearly seen as a layer of heads followed by two layers of tail sites and another layer of head sites. This result, which is similar to results obtained by Larson (1988) at much higher amphiphile concentrations, is significant as it represents the self assembly of a bilayer from a random initial configuration.

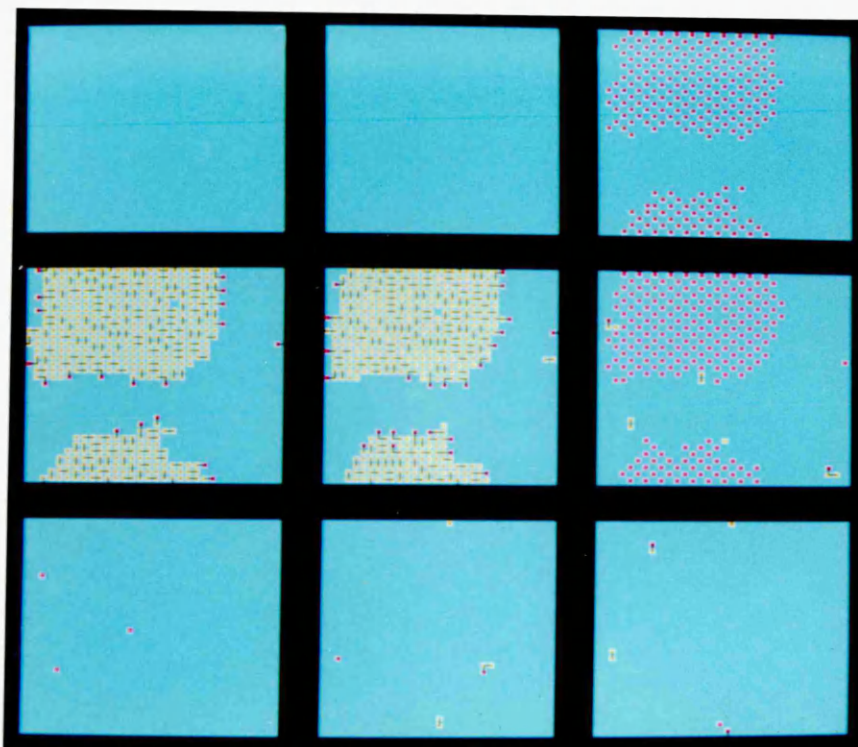


Figure 5.4 : Sections of the lattice at $\gamma = -1.6$ and $\beta^{-1} = 0.84$ showing the castellated bilayer. (red = head sites, yellow = tail sites and blue = solvent sites)

5.4 PRELIMINARY INVESTIGATION

In the preliminary investigation only the cluster size and surface roughness were measured, therefore the different structures were identified by viewing individual 'snap-shots' of the lattice at the end of each temperature step. Chains of lengths $s=4, 5, 6$ and 8 were considered. At each chain length simulations were made on a cubic lattice of $32 \times 32 \times 32$ sites with $N=512$ amphiphiles and with head-solvent interaction $\gamma=-1.0$ and -1.5 . The systems were cooled in fairly large steps of 0.1 in reduced units. The starting configuration of the first temperature was generated randomly and for each new temperature was the final configuration of the previous temperature. A Monte Carlo

step was defined to be 512 attempted moves which means that on average a single move is attempted on each amphiphile per Monte Carlo step. 50,000 Monte Carlo steps were discarded for thermalisation and 200,000 Monte Carlo steps were used to collect data.

The cluster size distribution and mean cluster surface roughness, (equation 4.27), were determined at each temperature. The standard error, δ_1 , (equation 4.15) was determined for the mean cluster size, but for these preliminary results a measure of the error in the surface roughness was not determined. As the simulation is cooled, the standard error in the mean cluster size generally increases to a maximum of about 7% at low temperatures. In some of the runs, ($\gamma = -1.0$), δ_1 reaches a maximum at a low temperature. As the system is cooled further δ_1 rapidly falls to zero. This is because the system cools to a single aggregate and the variation in cluster size is therefore zero.

There is no evidence of a micellar region for the chain lengths $s > 4$ at the values of γ considered. However a minimum in the cluster size distribution curve is observed for chain length, $s=4$, with $\gamma = -1.5$. The behaviour of the $s=4$ system with the less solvophilic head-solvent interaction, $\gamma = -1.0$, was unexpected by comparison with the $s=3$ system. It cools to a castellated bilayer structure, similar to the $s=3$ bilayer, but has 3 layers of tail sites between the planes of heads, instead of 2. The heads were also less ordered than in the $s=3$ system.

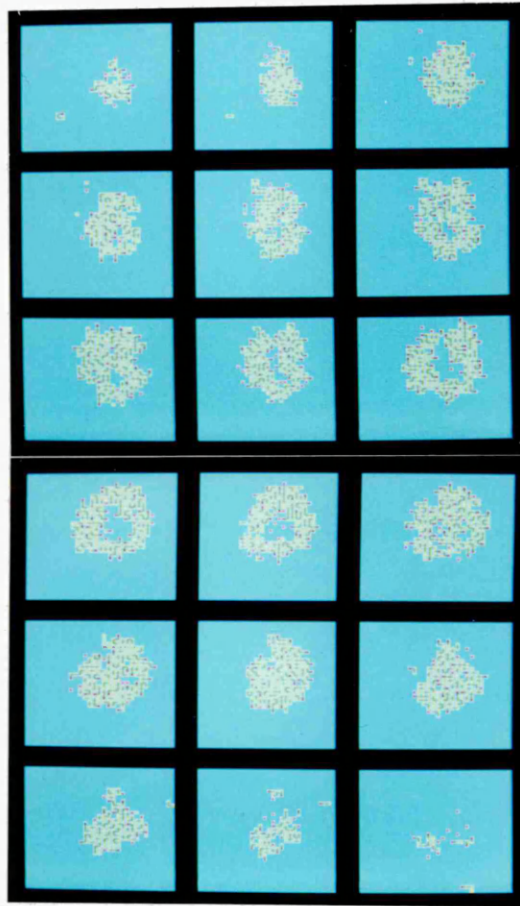


Figure 5.5 : Cross-sections of a vesicle; $s=6$, $\gamma=-1.0$, $\beta^{-1}=1.1$

The $s=5$ system produced a bilayer at both $\gamma=-1.5$ and $\gamma=-1.0$. The bilayer has a rough surface and is more flexible than those seen for shorter chains. The extra length allows the bilayer planes to lie off the principal lattice planes. The increasing flexibility and roughness of the bilayers continues at $s=6$ and $s=8$ with $\gamma=-1.5$. However when $\gamma=-1.0$, these longer chains yield different low temperature configurations. The $s=8$, $\gamma=-1.0$ system cooled to a large cylinder, while the $s=6$, $\gamma=-1.0$ system cooled to a vesicle. This is surprising as it is usually thought that a mixture of chain lengths are required to facilitate the layer curvature needed in a bilayer. One possible reason for seeing them here is that the chains are fully flexible and could mimic a mixed system by folding some of the tails.

Figure 5.5 shows successive cross sections through the vesicle. The vesicle is a roughly spherical shell with a solvent interior. The head groups mainly lie at the inner and outer surfaces of the vesicle.

Figure 5.6 shows the variation in mean cluster sizes with temperature for the different chain lengths with $\gamma=-1.0$. In each case, the mean cluster size increases as the system cools. Decreasing the chain length lowers the temperature at which larger clusters are formed and makes the transition between small and large clusters steeper. However, it must be noted that the simulations were run with a constant lattice size and a constant number of amphiphiles. Thus the $s=8$ system will have twice the amphiphile concentration of the $s=4$ system and some of the trends seen may be due to these changes concentration.

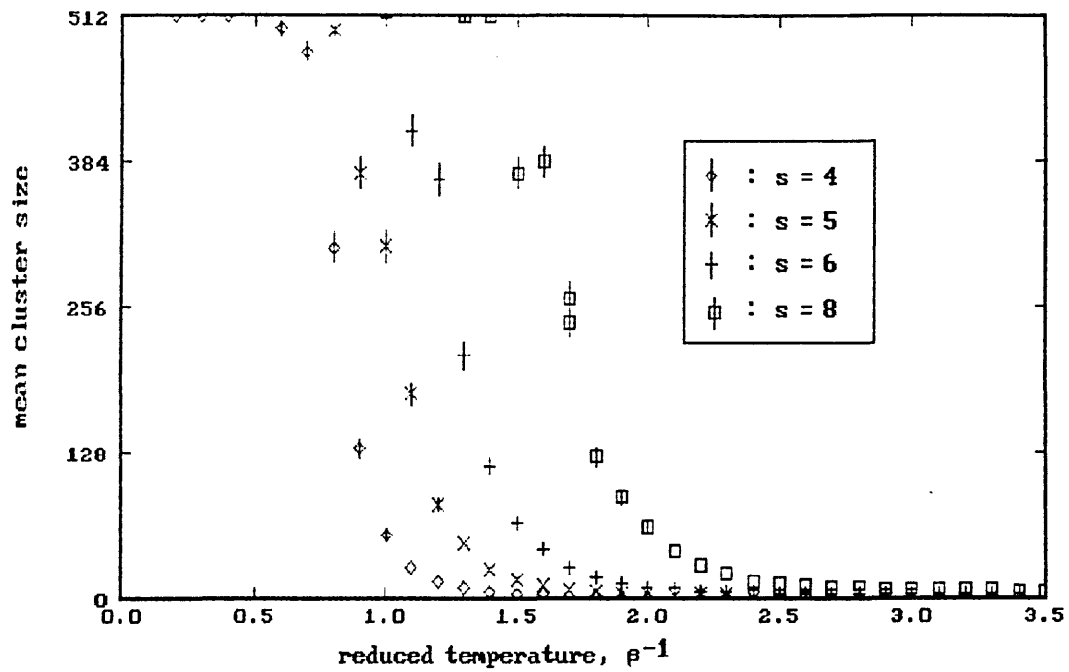


Figure 5.6 : Variation of mean cluster size with temperature for $s=4,5,6$ and 8

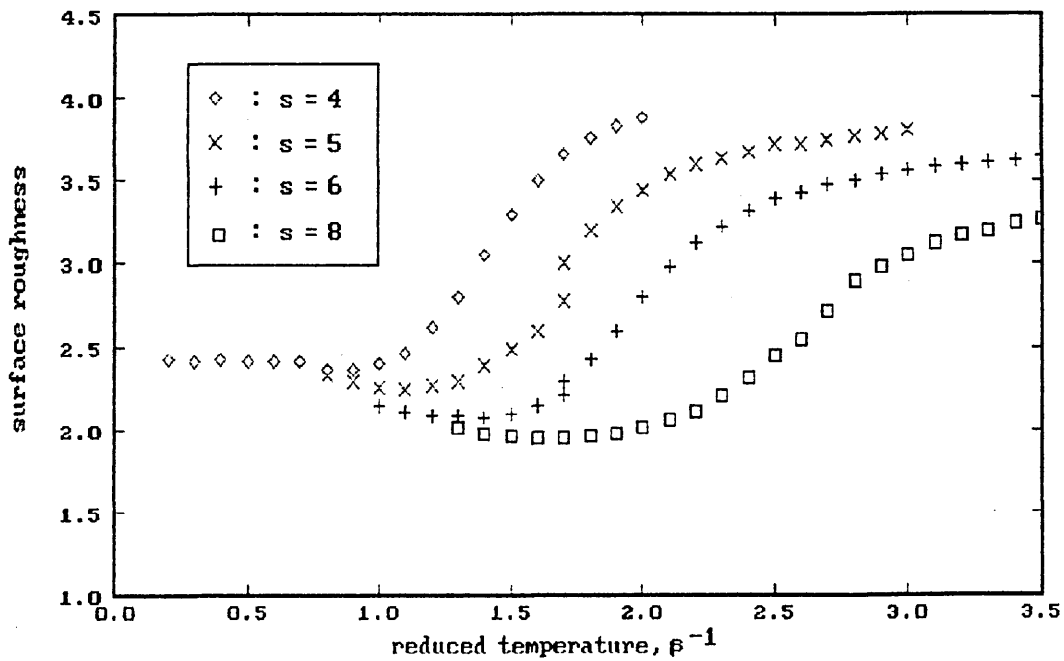


Figure 5.7 : Variation in surface roughness with temperature for $s=4,5,6$ and 8

The transition between small and large clusters has an observable effect on the surface roughness, figure 5.7. The figure shows that the surface roughness decreases as the monomers pack into larger clusters. This would be expected as the monomer tails have maximum surface contact with the solvent. At low temperatures there is a slight upturn in the surface roughness. This is possibly due to the head groups becoming fully solvated.

These early results indicate that the model can predict the formation of several different recognisable structures. Different structures have been seen for changes in chain length and head-solvent interaction, however a change from one recognisable structure to another has not been observed on cooling a system with fixed γ and s . The model appears to be very sensitive to the value of γ chosen, but the dependency is not yet fully understood.

The effect of γ is examined more closely for systems with a chain length of 4. The low temperature configurations observed so far, apart from the micelles, have all been single structures. It is preferable to model multi-bilayer systems, as seen in lamellar phases, rather than a single bilayer. Therefore the $s=4$ system is examined at higher concentrations.

5.5 HEAD-SOLVENT POTENTIAL, γ

The effect of increasing the head-solvent interaction was examined both at low amphiphile concentration (6.25%) and at high concentration (50%).

5.5.1 Low Concentration

Figure 5.8 shows the mean cluster size as the system is cooled for $\gamma = -1.0$, -1.5 and -2.0 . There is a clear difference between the $\gamma = -1.0$ case and $\gamma = -1.5$ and -2.0 cases. The more solvophilic interactions show evidence of a micellar region before freezing out into large clusters.

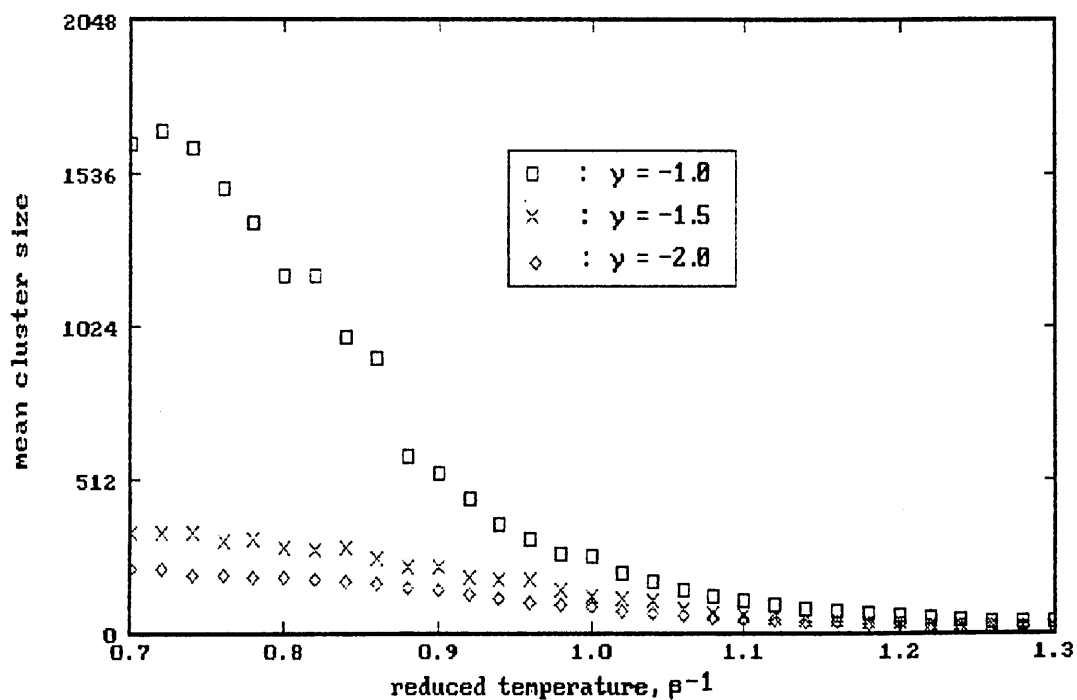
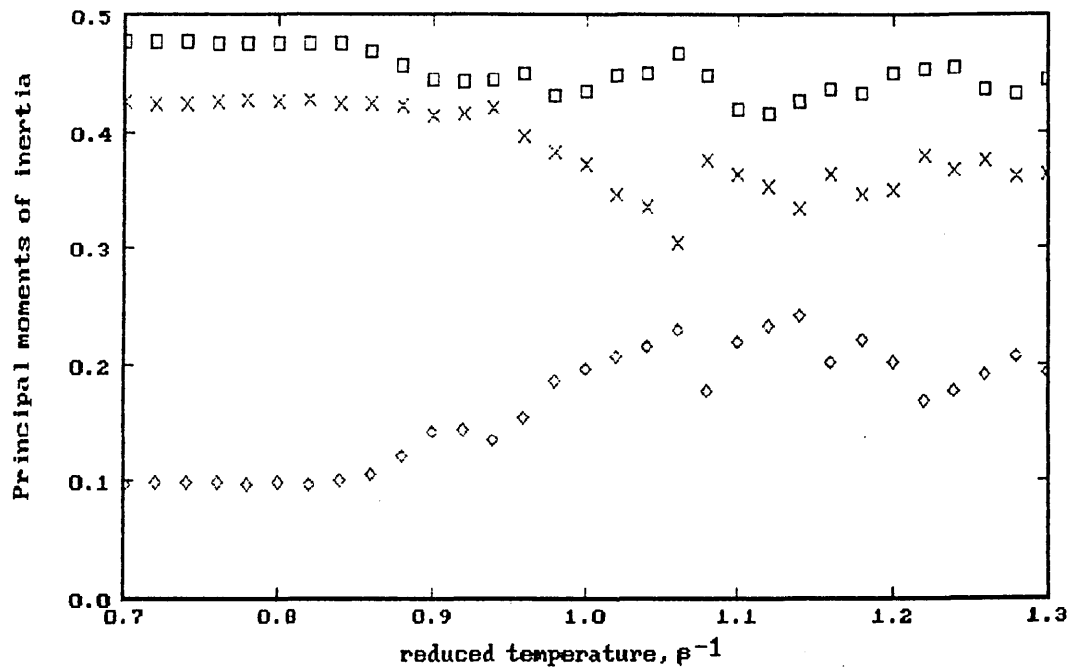


Figure 5.8 : Variation in mean cluster size with temperature, $s=4$, $\gamma=-1.0, -1.5, -2.0$

The $\gamma = -2.0$ system shows a clearer minimum in its cluster size distribution curve.

The $\gamma = -1.0$ run confirms the preliminary examination in that it does not form micelles, as may have been predicted from comparison with the equivalent $s=3$ system. Figure 5.8 shows that the mean cluster size rises much quicker with $\gamma = -1.0$ than $\gamma = -1.5$ or -2.0 .

(a)



(b)

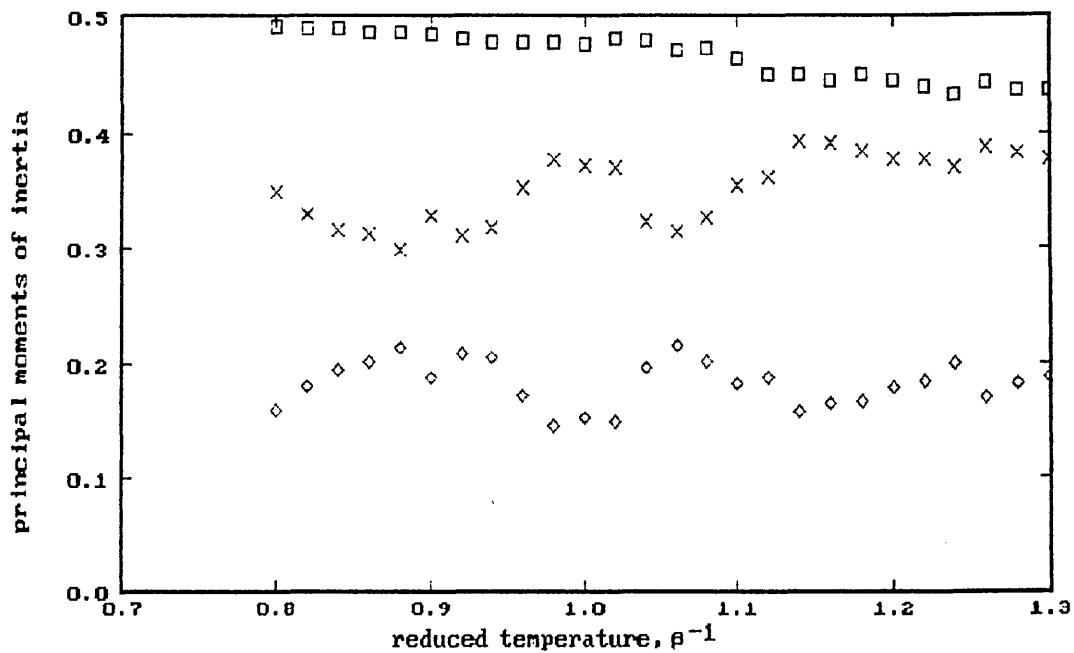


Figure 5.9 : Variation of the principal moments of inertia with temperature; $\gamma=-1.0$, $s=4$, (a) and (b) represent different starting configurations

Examination of the principal moments of inertia, figure 5.9(a), reveals that on cooling the structure initially oscillates between a rough bilayer and a cylinder, finally settling as a cylinder at low temperatures.

Figure 5.9(b) shows the same system with a different random start. The oscillation between bilayer and cylinder continues at lower temperatures and the final low temperature configuration is better described as a rough bilayer rather than a bilayer.

Figure 5.10 displays the variation of the number of head-solvent bonds, for head sites in contact with solvent, as a function of temperature. This "head roughness" becomes progressively closer to 5, (which is the maximum value for a lattice with coordination number $c=6$), as γ is made increasingly solvophilic and is virtually saturated when $\gamma=-2.0$. This saturation point is not reached in the $\gamma=-1.0$ case, possibly accounting for the difference seen in the final configuration when starting from different random configurations.

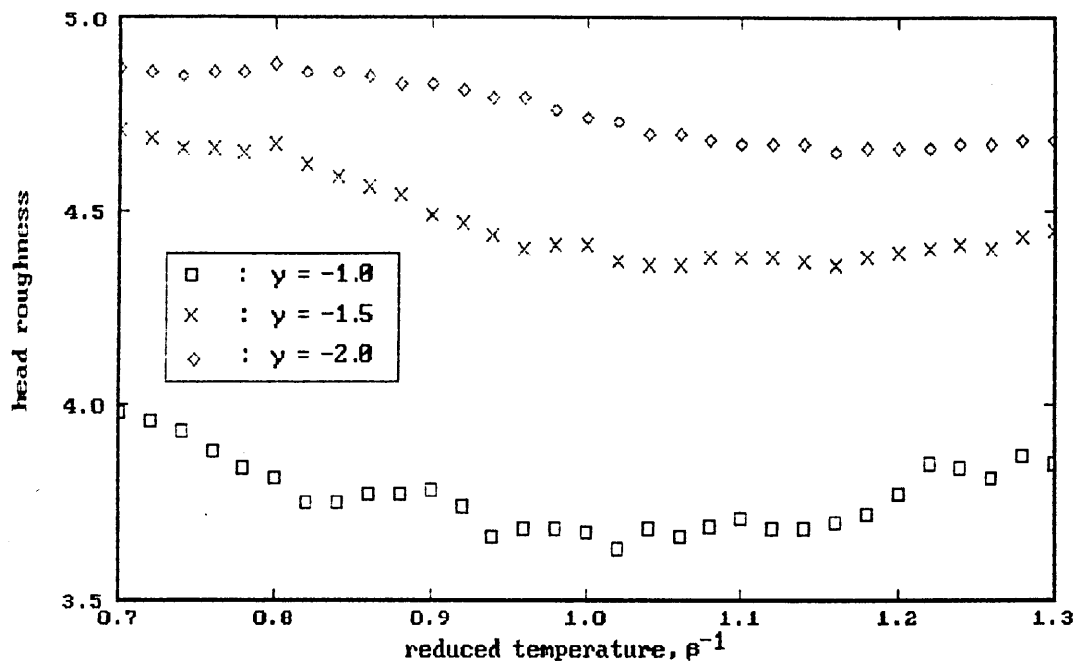


Figure 5.10 : Variation of "head roughness" with temperature;
 $\gamma = -1.0, -1.5, -2.0$ and $s=4$

It is evident, that the $s=4$, $\gamma=-1.5$ and $\gamma=-2.0$ cases are similar to the $s=3$, $\gamma=-1.0$ case as this is where micelles are found. The $s=4$, $\gamma=-1.0$ results describe a region where the head-solvent interaction is too weak to promote micelles. They are equivalent to the large cluster seen for $s=3$, $\gamma=-0.6$. This increase in the head solvent interaction needed to yield an equivalent phase (mesophase) can be explained by noting that the internal energy of the system depends on a balance between the tail-solvent repulsion and the head-solvent attraction. Longer tails therefore necessitate greater head-solvent attraction. Following the analogy with the $s=3$ results, it is expected that making γ more negative than $\gamma=-2.0$ would cause the amphiphiles to assemble into a well ordered bilayer.

5.5.2 High Concentration

At amphiphile concentrations around 50%, the $s=4$ $\gamma=-2.0$ system undergoes a transition from a large amorphous cluster to a lamellar phase. Figure 5.11 shows the moments of inertia for such a transition.

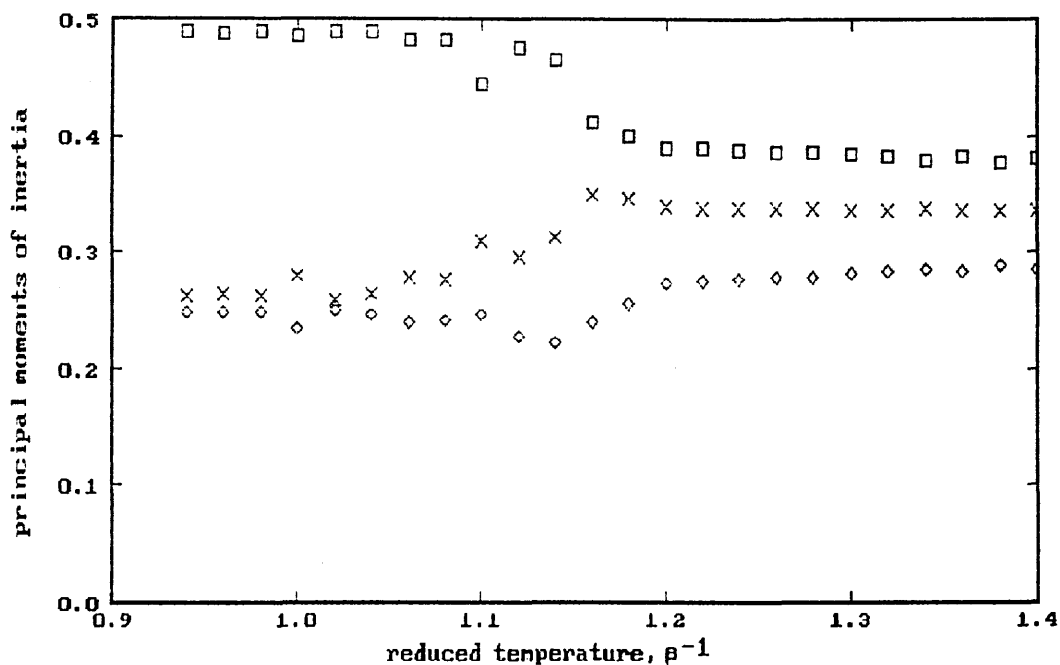


Figure 5.11 : Variation of the principal moments of inertia with temperature (50% amph. conc.); $\gamma=-2.0$, $s=4$

If however, γ is made too negative, the system does not undergo the transition (figure 5.12) as the head-solvent bonds become saturated in the amorphous cluster at high temperature and these interactions dominate the internal energy expression.

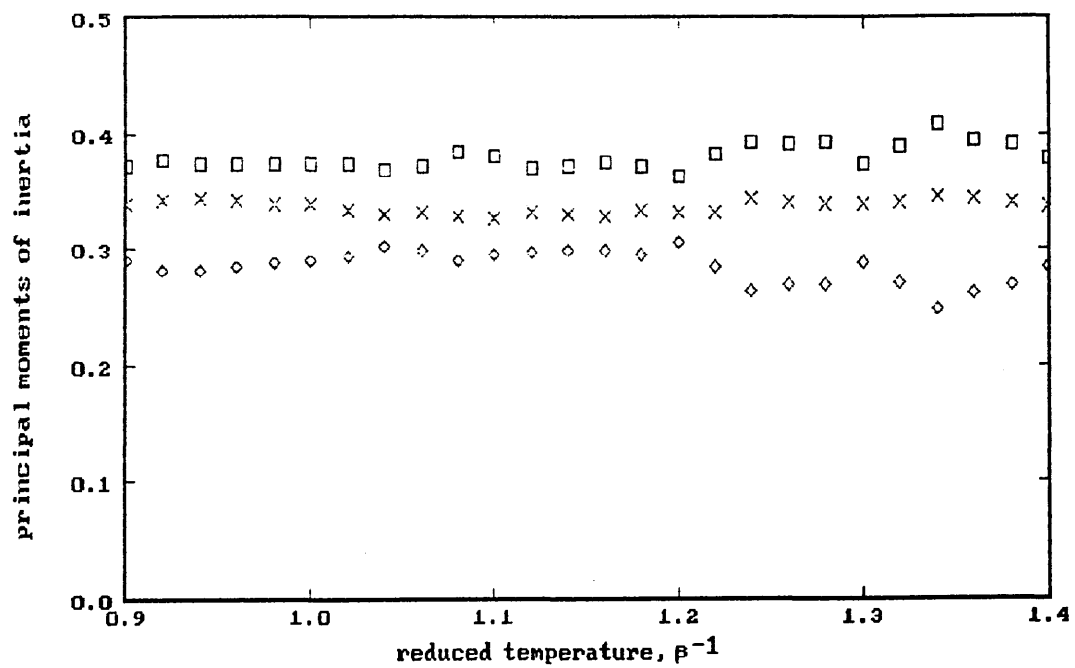


Figure 5.12 : Variation of principal moments of inertia with temperature (50%); $\gamma=-5.0$, $s=4$

Figure 5.13 shows the early saturation of the head-solvent bonds and the lack of change in the tail-solvent interaction.

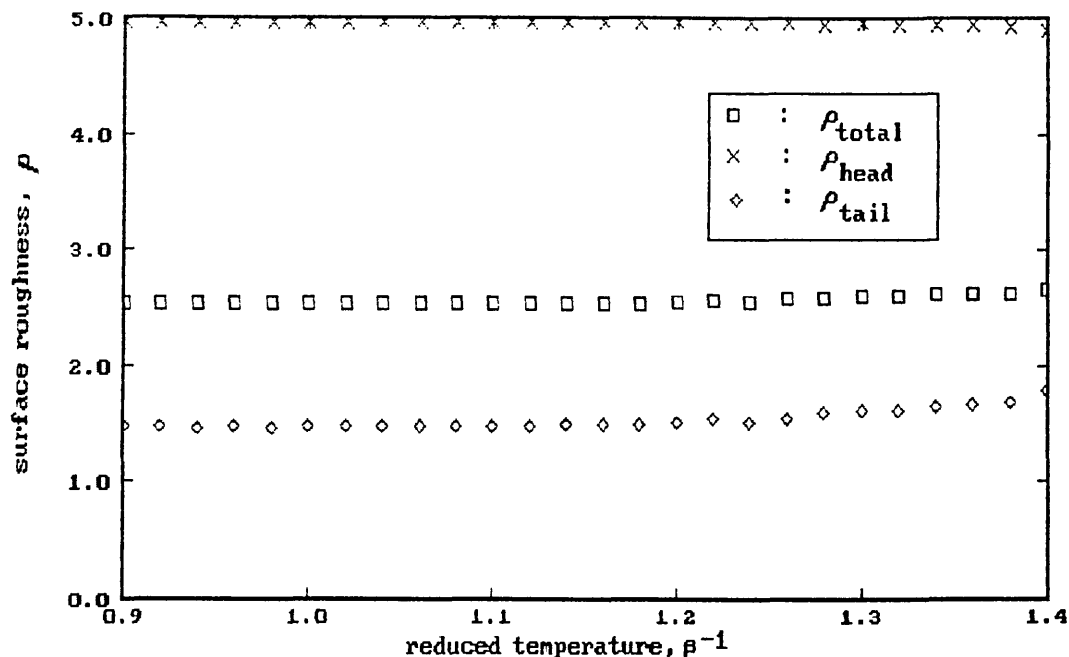


Figure 5.13 : Surface roughness terms versus temperature (50);
 $\gamma=-5.0$, $s=4$

5.5.3 Summary

The value of γ is critical. If the value chosen is too low the heads do not become fully solvated and the amphiphiles are not able to reach their preferred structure. If γ is too high they will be rapid solvation of the heads at the expense of the ordering of the tails. When $\gamma=-2.0$, $s=4$ a micellar region is observed at low concentrations and a lamellar region at high concentrations. Thus this system was chosen for detailed investigation over the full concentration range.

5.6 THE $s=4$, $\gamma=-2.0$ SYSTEM

The $s=4$, $\gamma=-2.0$ system has been studied in detail for amphiphile concentrations ranging from 0.78% to 75%. In most of these simulations

the system was cooled from $\beta^{-1}=1.4$ to $\beta^{-1}=0.8$ in steps of $\beta^{-1}=0.02$. Table A1, (Appendix A), lists the run conditions of the simulations used to construct a temperature-concentration phase diagram. In most runs each temperature step involved 20,000 Monte Carlo Steps rejected for thermalisation and 200,000 Monte Carlo steps used to collect data. (A Monte Carlo step is taken to be N moves, where N is the number of amphiphiles in the system.)

Distinct regions of the phase diagram have been found, but the transition between the mesophases is not sharp in each case. These regions include micellar, cylindrical, bicontinuous and multiple bilayer regions and are characterised by shape, size and surface roughness.

5.6.1 The Micellar Region

The existence of a micellar region is initially determined from the cluster size distribution curves. As stated previously, a minimum in the cluster size distribution curve has been proposed to be evidence of micelle formation [Wennerström & Lindmann 1979]. This minimum is predicted to be deep, as shown in figure 2.4 (Chapter 2) where the aggregate concentration is plotted on a logarithmic scale. However, the minima obtained in this model are weaker than those predicted by usual interpretations of experimental data. Also the distribution in cluster sizes obtained from the simulation is broader than commonly accepted. The c.m.c values determined by observing a minimum in the cluster size distribution curve are compared with those determined by plotting the monomer concentration against the total amphiphile concentration as in figure 2.3 (Chapter 2).

At high temperatures the cluster size distributions fit the Fischer model of condensation [Fischer 1967]. As the system is cooled a shoulder is formed, which on further cooling becomes a peak. The temperature at which this shoulder occurs was initially taken as the upper temperature boundary of the micellar region. The lower temperature boundary of the micellar region is assumed to occur at the temperature when the cluster size distribution curve is no longer smooth. This indicates that permanent clusters have started to form. Sample cluster size distribution curves from within the micellar region are shown in Appendix A, figures A1-A12. The figures are scaled such that the areas under a distribution curve equals the total amphiphile (% volume) concentration.

Figures A1-A5 show the temperature dependence on the cluster size distribution for a total amphiphile concentration of 3.125%. The cluster size distribution curve at $\beta^{-1}=1.24$ shows a shallow shoulder starting to occur at a cluster size of about 10 amphiphiles. The clusters are in equilibrium with a large number of monomers. As the system is cooled to $\beta^{-1}=1.16$ there is a reduction in the number of monomers and a corresponding increase in the number of clusters of about size 25 amphiphiles. On further cooling the width of the distribution becomes broader and less smooth (figure A5).

Figures A6-A12 show the effect of amphiphile concentration on the cluster size distribution curves at a fixed temperature of $\beta^{-1}=1.24$. At the lowest amphiphile concentration considered, (0.78%), a distinguishable minimum is not formed. This concentration must therefore be considered to be below the c.m.c. for the model at $\beta^{-1}=1.24$. Increas-

ing the amphiphile concentration reduces the monomer concentration and increases the height and width of the distribution. The distributions also become increasingly less smooth. At 20% amphiphile concentration, figure A12, there is no longer a maximum in the distribution.

As the minima observed in the cluster size distribution curves are shallow, the curves do not give a very sensitive measure of the c.m.c. Thus the variation in the concentration of monomers with total amphiphile concentration was plotted as shown in figure 5.14.

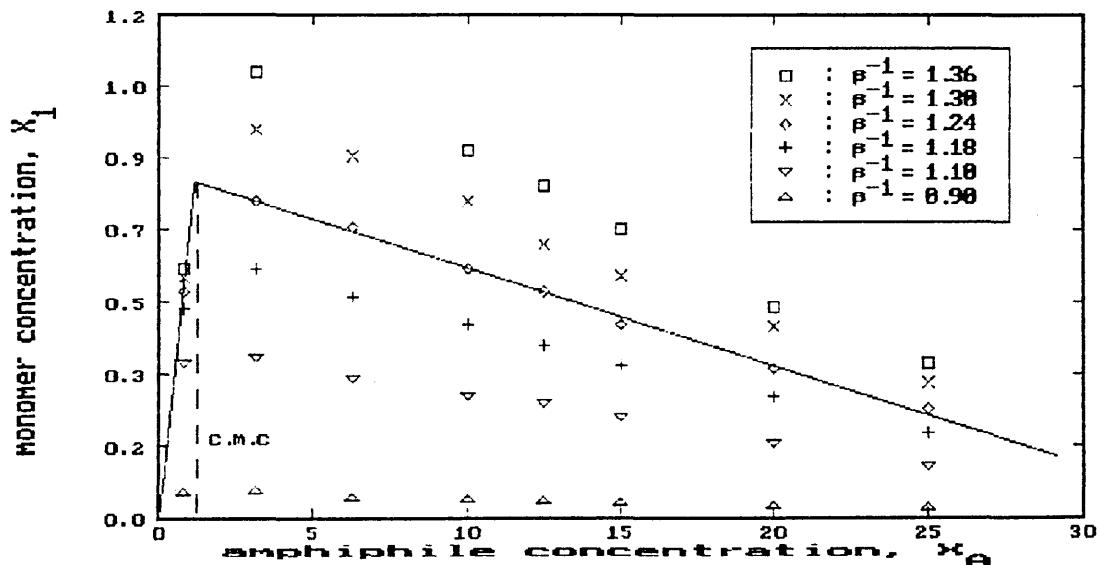


Figure 5.14 : variation in monomer concentration with total amphiphile concentration for the $s=4$, $\gamma = -2.0$ system

Temperatures above $\beta^{-1}=1.1$ show evidence of a c.m.c. As indicated by the solid lines for $\beta^{-1}=1.24$, there is an initial increase in the monomer concentration with increasing total amphiphile concentration up to about 1% amphiphile concentration. It is reasonable to assume this region is linear as there will be very little interaction between

monomers at such low concentrations. Above this limiting concentration, which is the c.m.c, there is a significant decrease in the monomer concentration with added amphiphile. The slope of the decreasing concentration becomes increasingly negative with increasing temperature. At the temperature $\beta^{-1}=1.1$ it is possible that the c.m.c is below the minimum amphiphile concentration (0.78%) considered.

The c.m.c is seen to increase with temperature. However, as with experimental results, the dependence of the c.m.c on temperature is only slight. In contrast to experimental results the monomer concentration appears to undergo a sharp transition at the c.m.c. It is also noticeable that the negative slopes in figure 5.14 converge at an amphiphile concentration of about 35%. This suggests that the concentration at which it is no longer favourable for the amphiphiles to exist as monomers is independent of temperature.

The shape of the curves in figure 5.14 are significantly different from that of the thermodynamic model described in Chapter 2, figure 2.3. However there is experimental evidence to support the results obtained from the simulation. Johnson *et al* (1987) used an electrostatic cell model proposed by Jönsson & Wennerström (1981) to evaluate calorimetric results. They found it necessary to take into account the decreasing monomer concentration after the c.m.c in order to derive correct values for the enthalpy of micelle formation for ionic sodium dodecyl sulphate (SDS) amphiphiles.

Differential enthalpies of a dilution of 28wt% aqueous SDS solution were measured accurately using a titration microcalorimeter. Titration curves were obtained at three different temperatures at concentrations

around the c.m.c. These titration curves were compared with theoretical curves determined from the cell model.

In the electrostatic cell model the micellar solution is divided into spherical cells which each contain a spherical micelle and the appropriate amount of water and electrolyte to give the desired overall concentration. It is necessary to specify some of the properties of the system to be studied. These include the temperature, the amphiphile volume, the c.m.c, the number of monomers in the micelle and the counterion valance. The model is solved using the Poisson-Boltzmann equation to give the monomer concentration at various values of the concentration of amphiphile in the micellar state. The chemical potentials for the amphiphile in water and in a micelle are determined.

When monomer concentrations were calculated assuming a constant number of monomers in micelles, the theoretical titration curves did not give satisfactory agreement with experimental results. A much better fit was obtained by assuming the number of monomers in a micelle increased above the c.m.c. Figure 5.15 shows a comparison between calculated and experimental titration curves at 35°C.

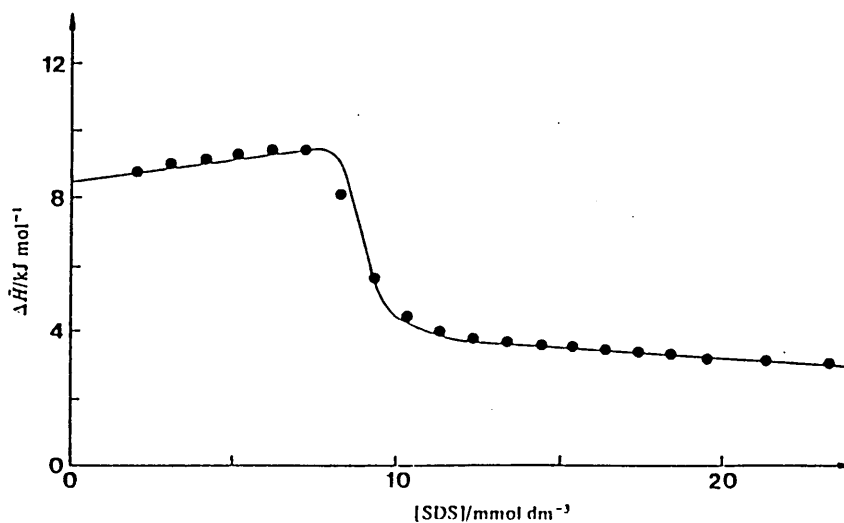


Figure 5.15 : Comparison between calculated and experimental titration curves at 35°C [Johnson *et al* 1987].

The variation of the cell model monomer concentration with total SDS concentration is shown in figure 5.16. As in figure 5.14, the monomer concentration decreases significantly with increasing total amphiphile concentration above the c.m.c. Thus the concentration of amphiphile in micelles increases more rapidly than the total amphiphile concentration.

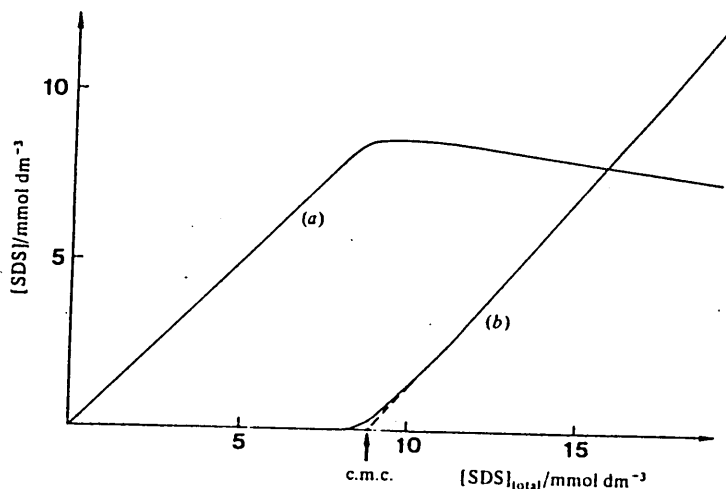


Figure 5.16 : Concentration of SDS in monomer (a) and micellar (b) states as a function of total concentration calculated from the electrostatic cell model [Johnson *et al* 1987]

There is thus evidence to support the variation in monomer concentration with total amphiphile concentration obtained from the Monte Carlo simulation. The modelling of experimental results by Johnson *et al* (1987) also supports the result that the mean micelle aggregation number increases with increasing amphiphile concentration.

The simulation shows that the narrow distribution in micelle sizes and the deep minimum in the cluster size distribution curves are not necessary consequences of experimental results. It has been shown that the observed behaviour of the monomer concentration around the c.m.c may be a result of a system with a broad distribution in micelle sizes and only a weak minimum in the cluster size distribution curve.

5.6.2 The Phase Diagram

Plotting the ratio of the smallest to largest principal moments of

inertia as contours on a temperature-amphiphile concentration diagram proved to be a successful technique for deriving the phase diagram, figure 5.17(a). The figure has four regions marked (A-D) representing different types of amphiphile aggregation. Region (A) is a region of small quasi-spherical clusters, which includes the micellar region. In region (B) the aggregates are large cylinders. On cooling from region (C) to region (D) there is a transition from a bicontinuous structure to a lamellar phase. The hashed region marks the extent of the micellar region as determined from figure 5.16 and the cluster size distribution curves.

Evidence of these regions is presented by considering the behaviour of the principal moments of inertia, the mean cluster size and the surface roughness, which are shown in figure A13-A34 (Appendix A). Photographs of sample lattice configurations are also presented.

5.6.3 The Principal Moments Of Inertia

The standard errors for the three principal moments of inertia were calculated according to equation 4.23. The standard errors generally increased on cooling, but never rose above 0.2% of the mean values. This is probably an underestimate of the errors involved.

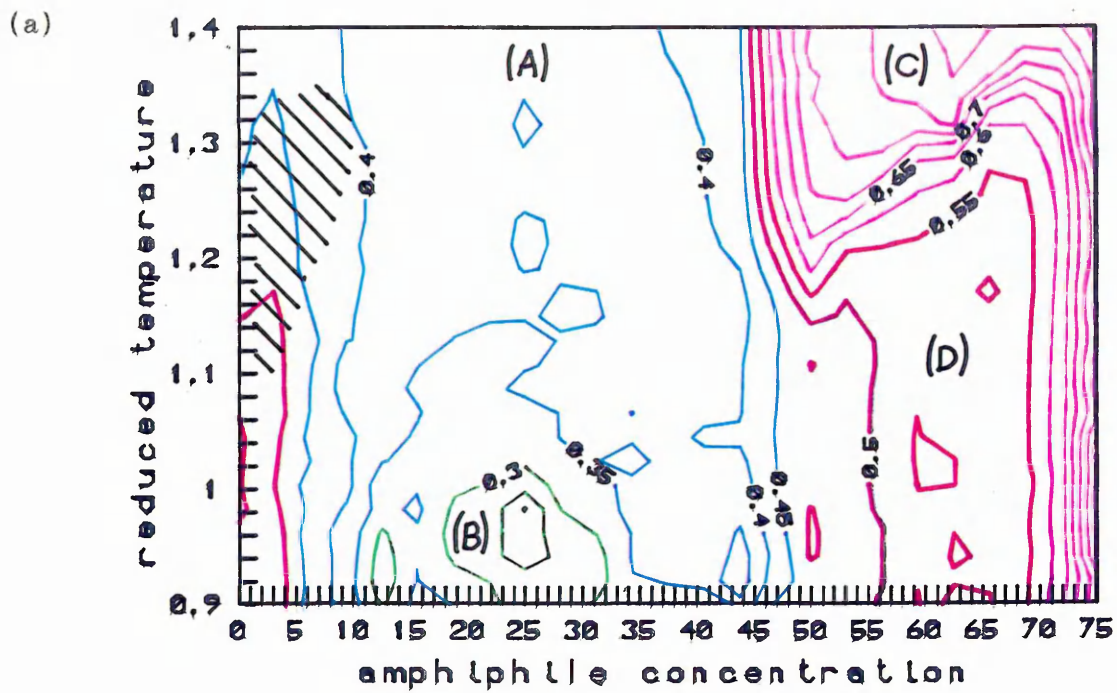
Figures 5.17(a)(b) are plots of the ratio of the smallest to the largest principal moments of inertia as a function of temperature and amphiphile concentration. Figure 5.17(b) is the same as figure 5.17(a) except that the contours are plotted on a vertical scale. The different regions (A-D) are shown in different colours; the colours being

the same in both diagrams.

The values of the contours range from 0.2 region (B), representing cylindrical clusters, to 0.9 region (C) which describes a cluster with little preferential growth along one particular axis or another. In region (D), the contour levels ≈ 0.5 , suggesting planar clusters which is consistent with a lamellar region. The contours in the region (A) have values around 0.35 which suggests aggregates with moments of inertia somewhere between those of a cylinder and those of a plane.

Figure 5.17(b) indicates that there are a sharp transitions when cooling from the bicontinuous region (C) to the lamellar region (D) and when increasing the concentration from region (A) to regions (C) and (D). The order of the former transition is discussed in the next section and the latter transition is similar to the percolation point seen in percolation theories.

The micellar region is not identified by the contours in figure 5.17(a) suggesting that a tightly confined shape is not a necessary condition for micellar stability.



(b)

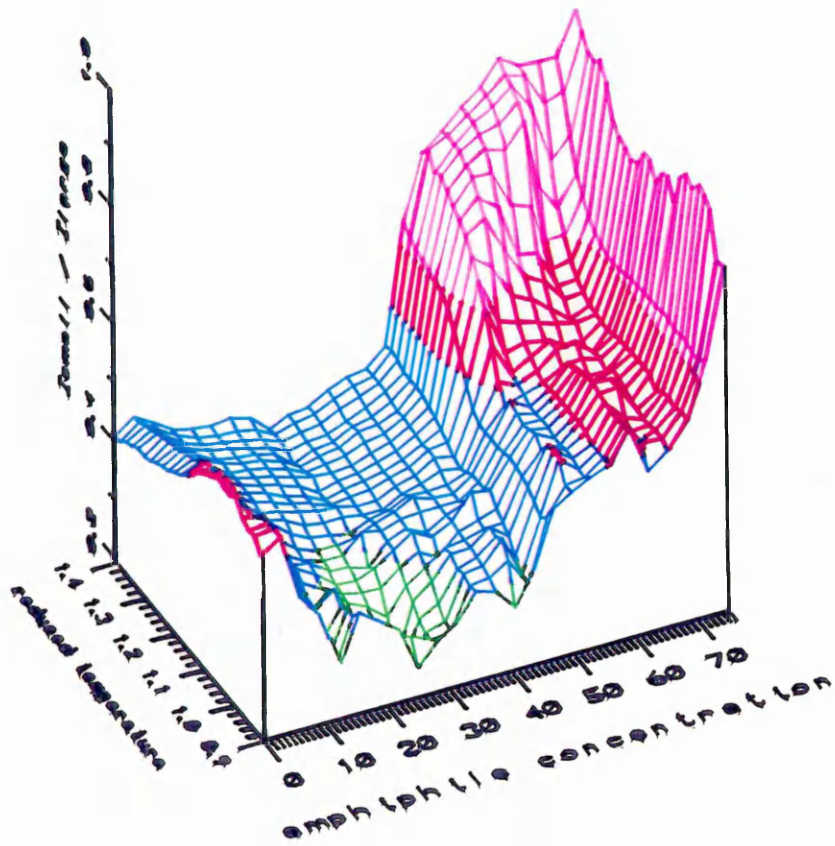
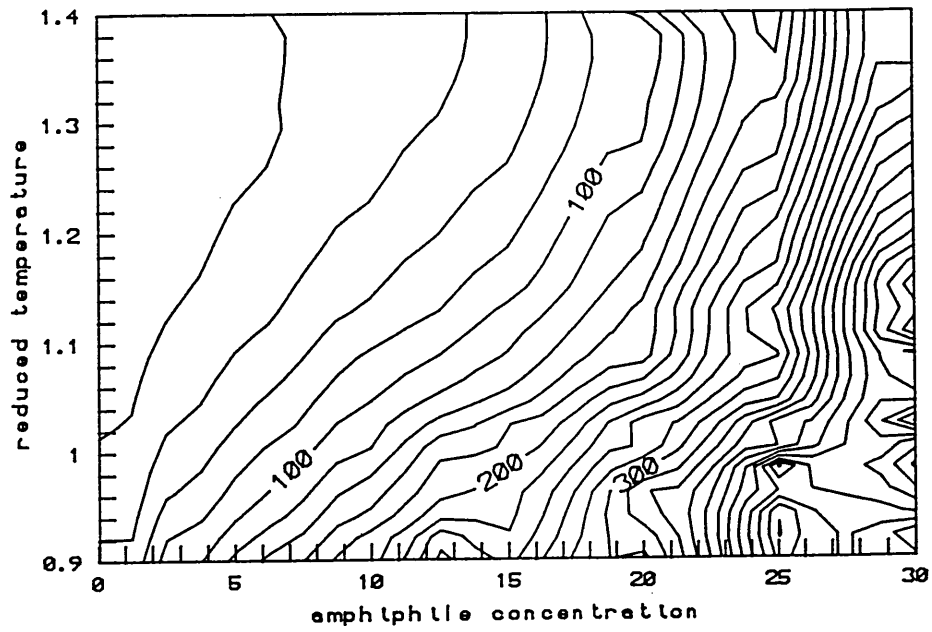


Figure 5.17 : The dependence of the ratio of the largest to smallest principal moments of inertia (contour lines) on reduced temperature (y axis) and amphiphile concentration (x axis). ((a)=2D, (b)=3D)

(a)



(b)

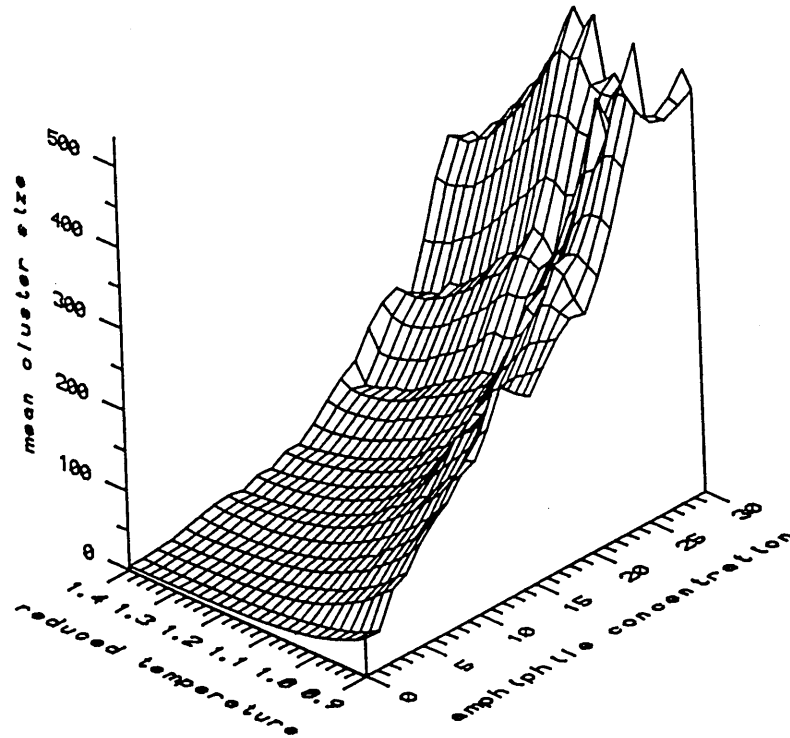


Figure 5.18 : The dependence of the mean cluster size (contour lines) on reduced temperature (y axis) and amphiphile concentration (x axis). ((a)=2D, (b)=3D)

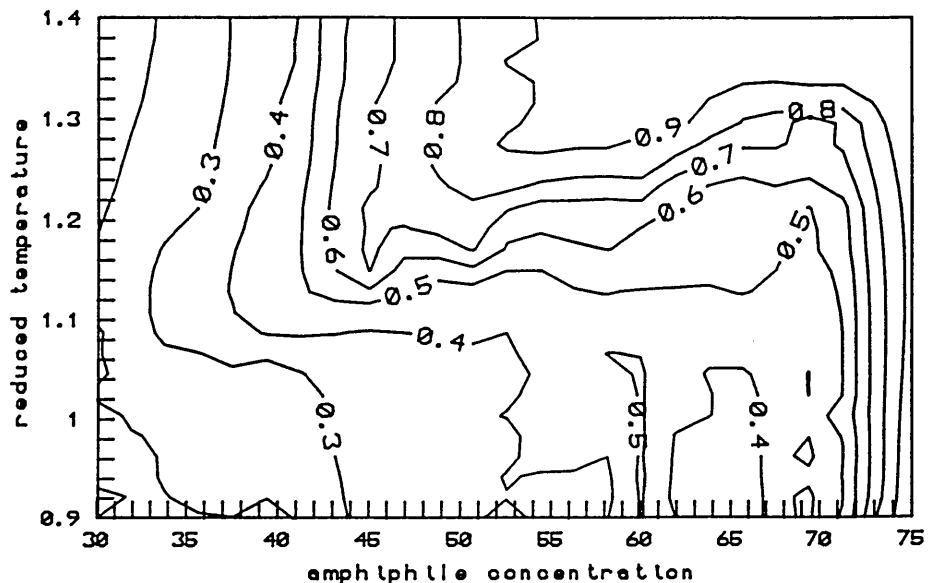
5.6.4 The Mean Cluster Size

At low amphiphile concentrations, there is good agreement between the standard errors δ_1 and δ_2 (equations 4.15 & 4.17) indicating that the statistics are good. As a percentage the standard error, δ_1 , is about 0.5%. At lower temperatures $\delta_2 \approx 0$ and significantly less than δ_1 which suggests persistence of clusters. At amphiphile concentrations around 50% there is a transition from a bicontinuous to lamellar region. In both these regions there is a persistence of clusters, however the percentage value of the standard error, δ_1 , in the mean cluster size is less than 7%.

A comparison of the mean cluster size and the alternative estimate of the mean cluster size, (equations 4.13 & 4.16), within the micellar region is shown in figures A14-A17. The agreement between the two estimates is best at lower concentrations and higher temperatures.

As expected, the micellar region shows some consistency in mean cluster size as indicated in figure 5.18(a). The plot shows contours of equal mean cluster size on the temperature-amphiphile concentration diagram. The diagram is limited to concentrations up to 30% as finite size effect start to dominate at higher concentrations as the cluster sizes begin to approach the number of monomers in the system. The figure shows that the micelles have a mean of about 10 monomers (or 40 lattice sites).

(a)



(b)

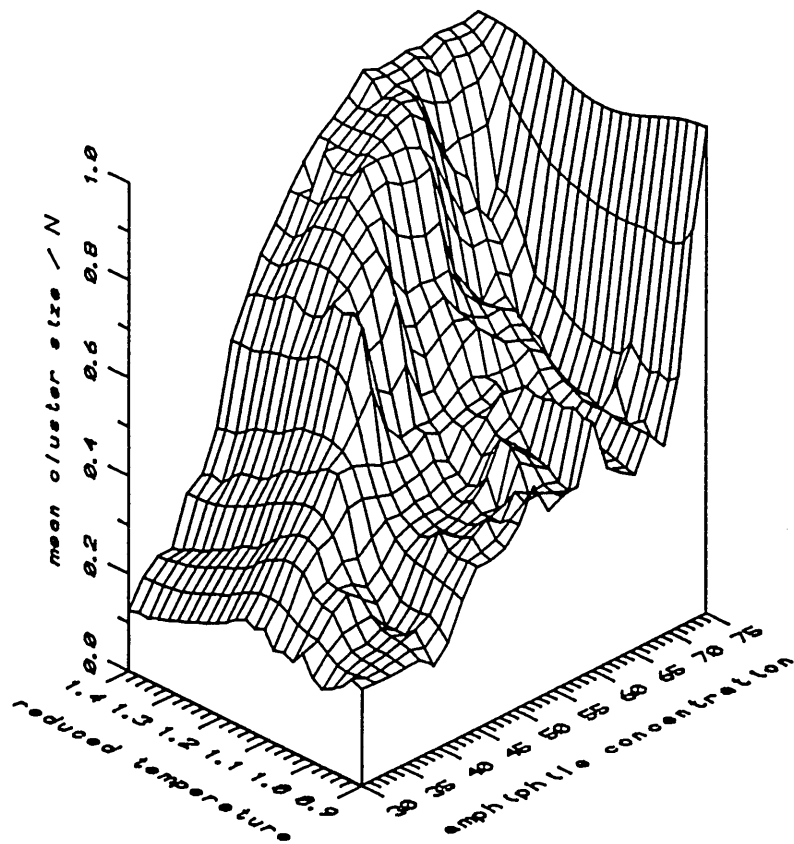


Figure 5.19 : The dependence of the ratio of the mean cluster size to the total number of monomers (contour lines) on reduced temperature (y axis) and amphiphile concentration (x axis). ((a)=2D), (b)=3D)

Figure 5.18 also shows that region (B), figure 5.17, contains large clusters and examination of sample lattice configuration does indeed confirm the existence of large cylindrical aggregates

To overcome some of the problems of large errors in the mean cluster size at high amphiphile concentrations an equivalent plot to figure 5.18 was made using the ratio of the mean cluster size to the number of amphiphiles in the system as the contours, figure 5.19. This plot reveals that when the system is cooled from region (C) of figure 5.17 to region (D), there is a transition from a single cluster to multiple clusters. This is consistent with the proposal that region (D) is a multiple bilayer region. The order of the transition was investigated by examining the system for hysteresis.

Figure 5.20 shows the variation of the mean cluster size with temperature at an amphiphile concentration of 50.0%. The line with the square symbols represents a system cooled from an initial random configuration at $\beta^{-1}=1.4$ to a low temperature configuration at $\beta^{-1}=0.9$. The system was reheated from this low temperature configuration up to $\beta^{-1}=1.4$. The resulting mean cluster sizes are represented by crosses on the graph.

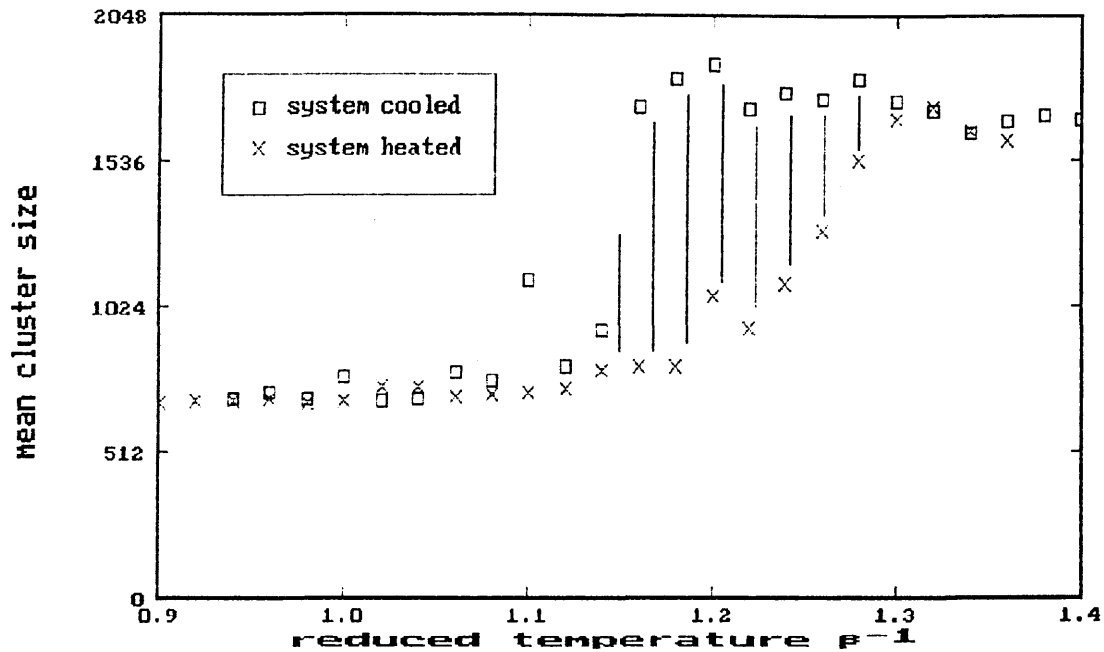


Figure 5.20 : Hysteresis in the mean cluster size for the $\gamma=-2.0$, $s=4$, $N=512$ system (amphiphile % conc.=50%)

The figure shows that there is substantial hysteresis in the mean cluster size due to cooling and heating the system. The presence of hysteresis is evidence of a first order transition.

5.6.5 The Surface Roughness

The standard errors, δ , measured for the mean surface roughness, (equations 4.27(a-c)), are less than 0.2% for all for the temperatures and concentrations considered. They increase slightly on cooling but change little with concentration.

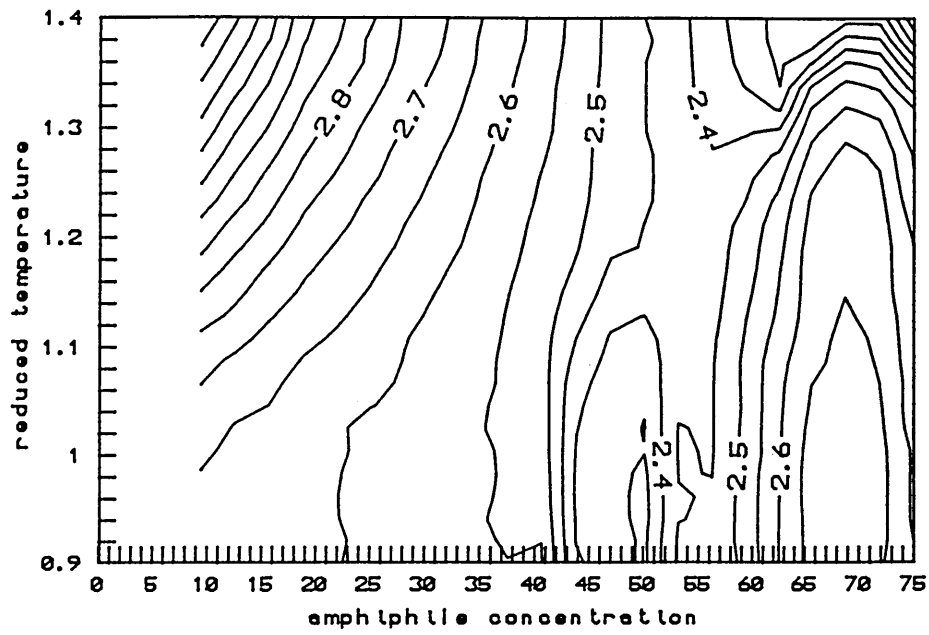
Further information about the system is available from a contour plot of the surface roughness, figure 5.21. The figure indicates that the region (A) has a fairly high surface roughness and that the micellar

region is reasonably well bound by the contours. The figure also shows some evidence of the transition from region (C) to region (D). A clearer picture emerges by considering the separate contributions of the head sites and tail sites individually

Figure 5.22 considers the mean number of head solvent bonds for head groups in contact with the solvent. The contour levels are thus constrained to lie between 1.0 (minimal head-solvent contact) and 5.0 (total head saturation). Generally it is clear that the head solvent contact increases as the system is cooled. This is because a high head-solvent contact helps to minimise the internal energy of the system. The increase in head-solvent interaction upon cooling is most prominent when moving from region (C) to region (D). There is a transition from moderate solvation to almost total solvation of the head groups.

Examination of the equivalent diagram for tail sites, figure 5.23, reveals the opposite behaviour. The number of solvent sites in contact with tail sites decreases with cooling and with increasing amphiphile concentration. It is evident that the micellar region is bounded by tail roughness contours. It is also clear that the transition from region (C) to (D) is one of moderate (≈ 1.6) to very low (≈ 1.1) tail roughness.

(a)



(b)

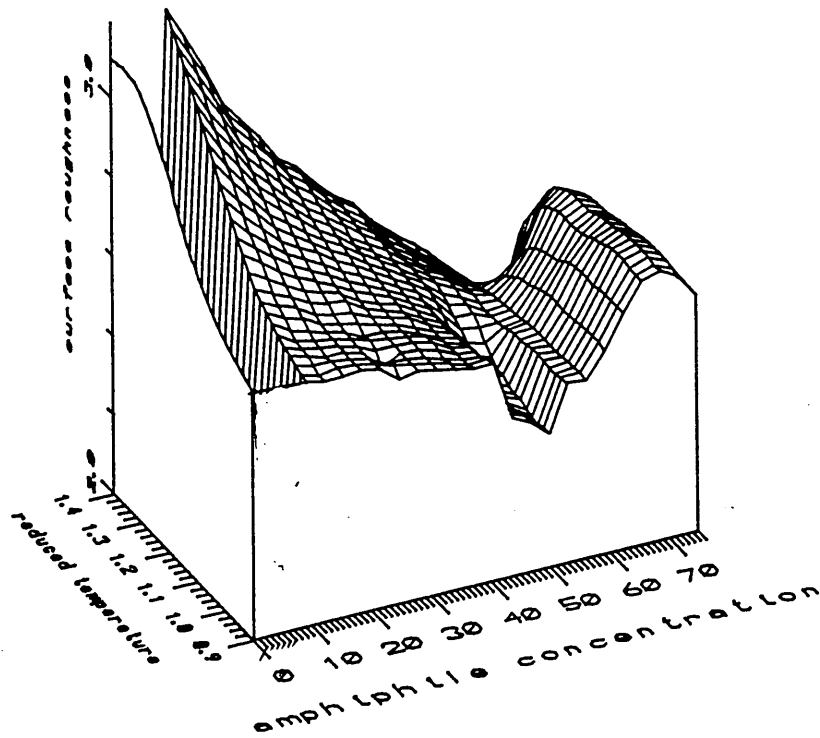
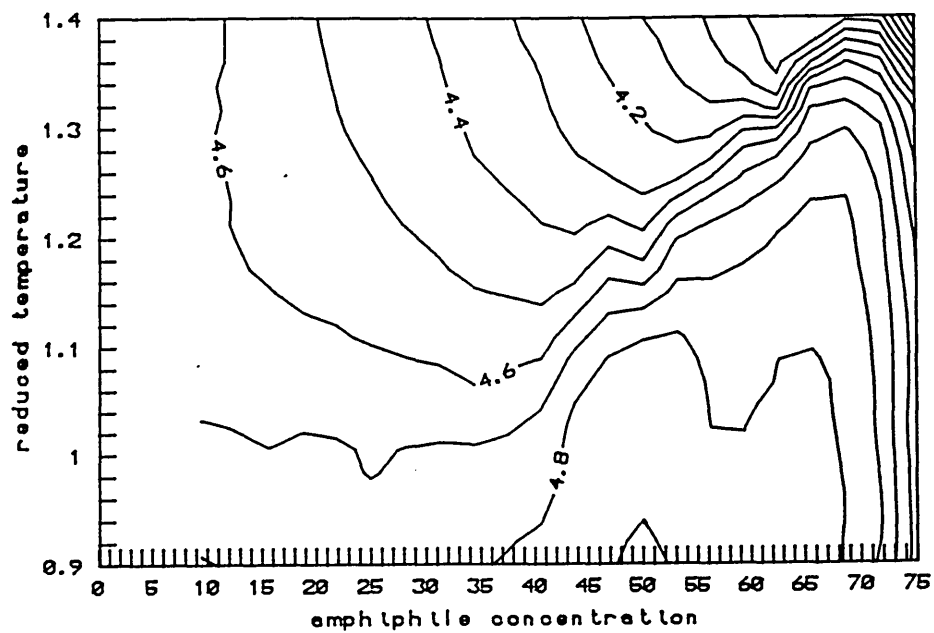


Figure 5.21 : The dependence of the surface roughness (contour lines) on reduced temperature (y axis) and amphiphile concentration (x axis). ((a)=2D, (b)=3D)

(a)



(b)

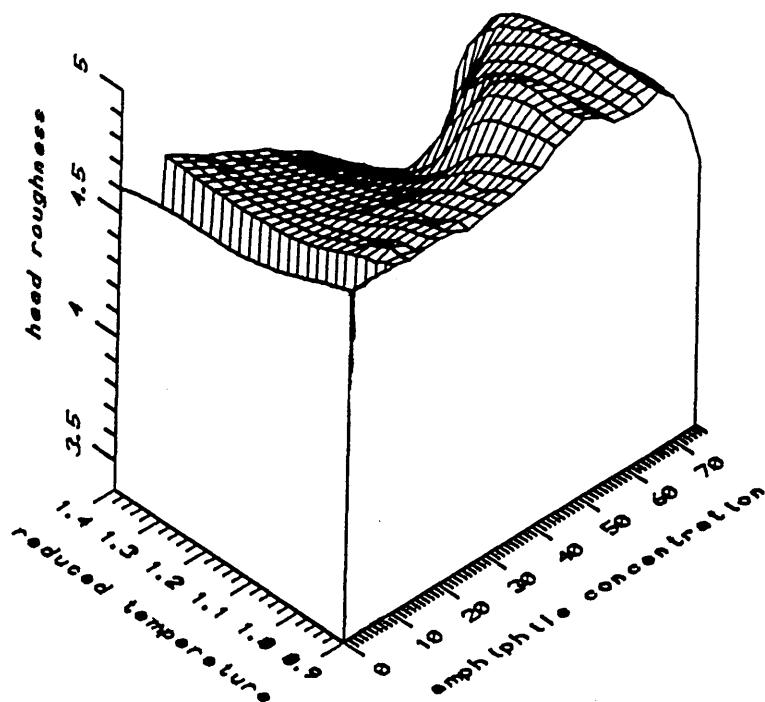
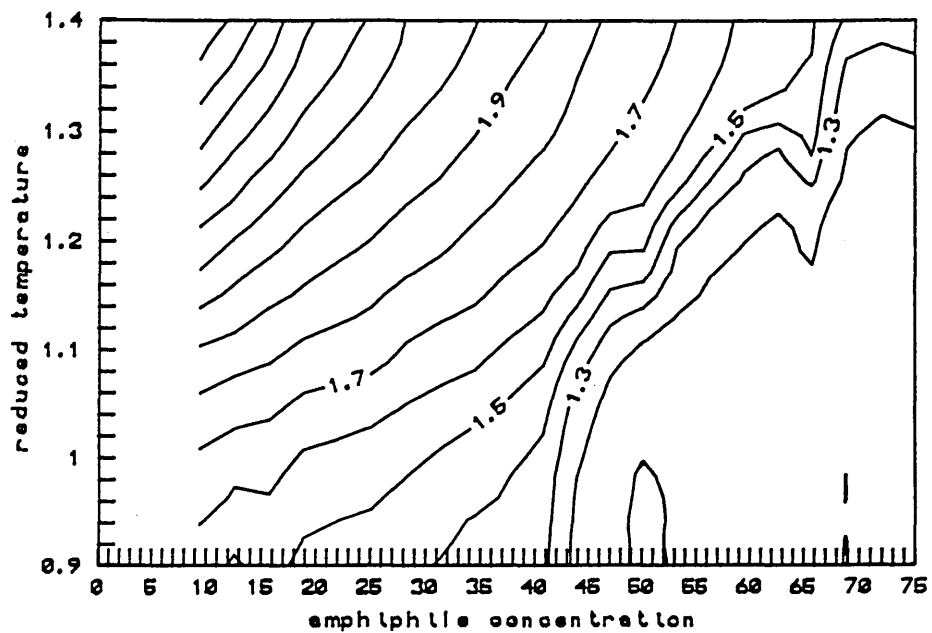


Figure 5.22 : The dependence of the head roughness (contour lines) on reduced temperature (y axis) and amphiphile concentration (x axis). ((a)=2D, (b)=3D)

(a)



(b)

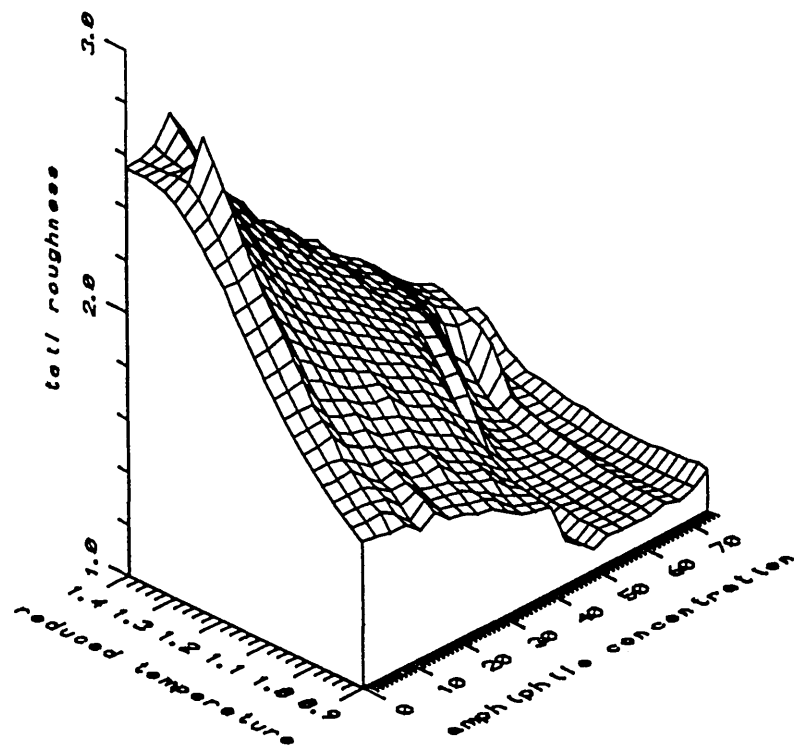


Figure 5.23 : The dependence of tail roughness (contour lines) on reduced temperature (y axis) and amphiphile concentration (x axis). ((a)=2D, (b)=3D)

5.6.6 Comparison With Experiment

The model phase diagram exhibits much of the phase behaviour of real systems. A typical phase diagram is that of the binary water-(dodecane - pentaoxyethylene dodecyl ether) system [Harusawa *et al* 1974], shown in figure 2.6, Chapter 2.

At low amphiphile concentrations the $C_{12}E_5$ - water phase diagram shows an isotropic solution. The region marked L1 is the micellar region which is consistent with the micellar region obtained from the simulation. At high amphiphile concentration (>50%) there is a lamellar region. This is again in agreement with the simulation.

At moderate amphiphile concentrations the $C_{12}E_5$ - water system has a hexagonal phase at low temperatures. The simulation produces large cylindrical aggregates in this region, but the systems studied were not large enough to draw any conclusions about the packing of the cylinders. Similarly the simulation shows some evidence of the L2 region of figure 2.6, but the simulation statistics are very poor at the high amphiphile concentrations of this region.

5.6.7 Effect Of Lattice Dimensions

The simulations at concentrations around 25% were run on lattices in which the dimensions were not equal. This is because the simulation code was written, for the sake of efficiency, with the restriction that the lattice dimensions must be an exact power of two. At amphiphile concentrations around 25%, it is necessary to use a large lattice in order to have a sufficiently high number of amphiphiles if the

lattice dimensions are equal. Such simulations run very slowly and are difficult to run with the available memory on the transputers. Thus lattices with unequal dimensions were used.

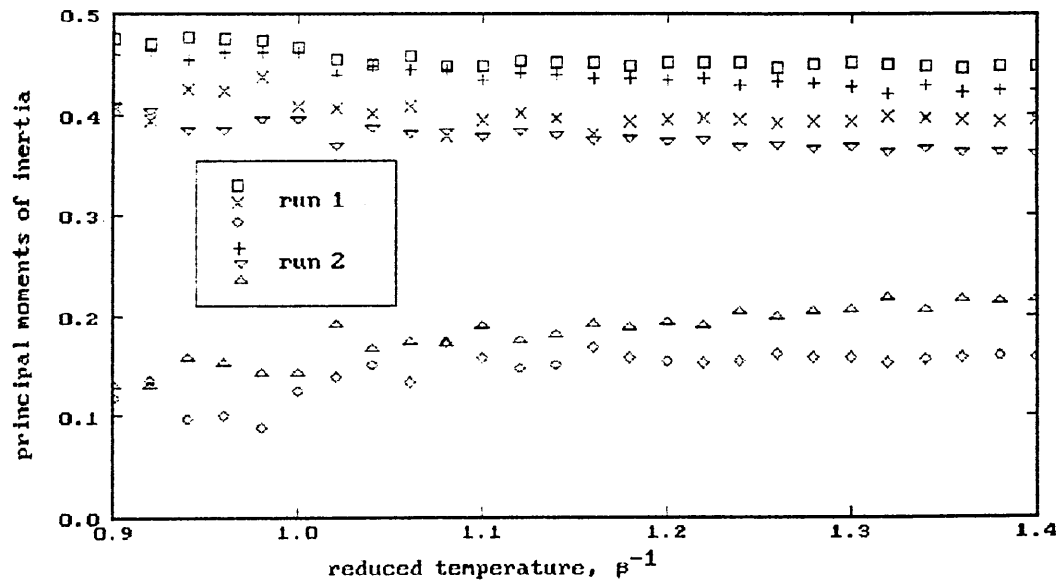


Figure 5.24 : Principal moments of inertia on different shaped lattice. Amphiphile concentration=25%, $s=4$, $\gamma=-2.0$. Dimensions : [run 1] 32x16x16, [run 2] 32x32x32

Figure 5.24 show a comparison between the principal moments of inertia of two simulations at 25% amphiphile concentration with a chain length $s=4$ and head-solvent potential $\gamma=-2.0$. In [run 1] 512 amphiphiles occupied a lattice with dimensions 32x16x16, whereas in [run 2] 2048 amphiphiles occupied a 32x32x32 lattice. All other conditions were the same.

The figure indicates good agreement between the two cases suggesting that the lattice shape does not have a significant affect on the shape of the clusters at the amphiphile concentration considered.

5.6.8 Summary

The micelles have mean cluster sizes between 5 and 12 monomers and are non-spherical with moments of inertia which suggest their shape is between a cylinder and a plane. The micelles have a rough surface, with surface roughness values lying between approximately 3.0 and 3.1. The head-solvent interaction is moderately high, but the heads are not fully solvated. The micelle size increases with concentration and they do not show a deep minimum in their cluster size distribution curves. Example micelles are shown in figure 5.25.

At low temperatures and amphiphile concentrations around 25%, the clusters have condensed into large cylinders. The cylinders are between about 100 and 200 monomers in size, which accounts for about 1/5 to 1/2 of the total number of amphiphiles in the system. The clusters are not very rough, although the head groups are almost completely solvated. A cross-section of the cylindrical aggregates is shown in figure 5.26.

At amphiphile concentrations above about 45% the amphiphiles form a large connected cluster at high temperatures, in which many of the faces of the head groups are obscured from the solvent. Examination of sample lattice configurations suggests that this structure is bicontinuous.

At low temperatures the large single cluster of the bicontinuous region divides into smaller clusters (e.g. 3), with a planar geometry. The head-solvent contact is at a maximum and the tail-solvent contact is minimised. This region is a lamellar region. Figure 5.27 shows a

sample lattice configuration at an amphiphile concentration of 50%. As the amphiphile concentration is increased the bilayers become wider until, at 75% amphiphile concentration, they merge (figure 5.28). It is possible that the model may show a gel region for amphiphile concentrations above 75%, but it is difficult to run the simulation at such high temperatures because the packed lattice severely restricts the movement of the amphiphiles.

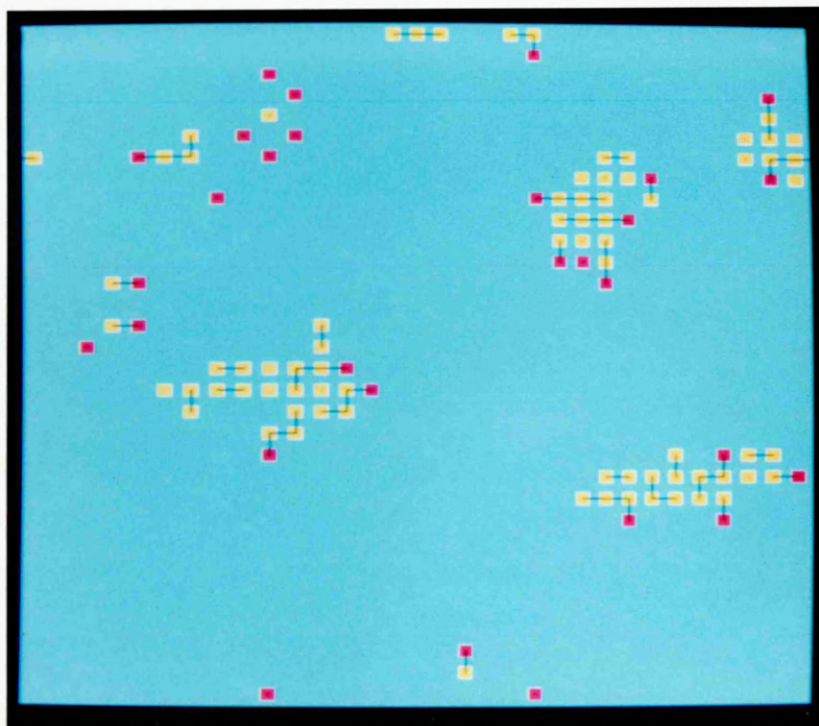


Figure 5.25 : Sample lattice section in the micellar region. $s=4$, $N=512$, $\gamma=-2.0$, $\beta^{-1}=1.26$, amphiphile conc.=6.25%

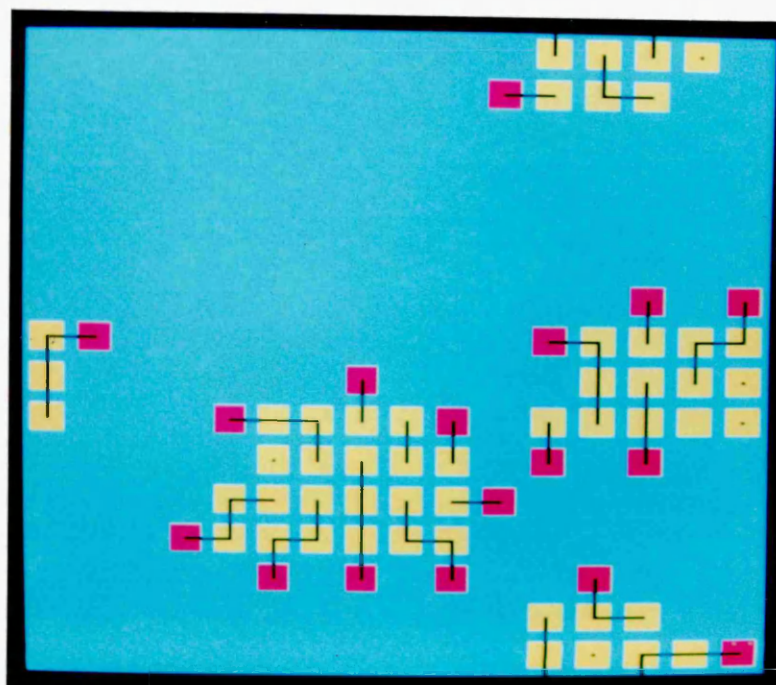


Figure 5.26 : Sample lattice section in the cylindrical region. $s=4$, $N=512$, $\gamma=-2.0$, $\beta^{-1}=0.9$, amphiphile conc.=25%

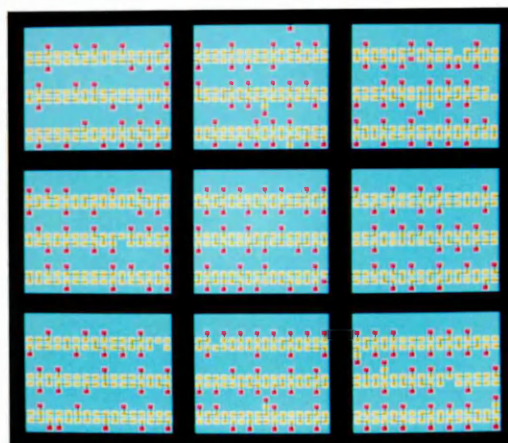


Figure 5.27 : Sample lattice section in the lamellar region. $s=4$,
 $N=512$, $\gamma=-2.0$, $\beta^{-1}=0.9$, amphiphile conc.=50%

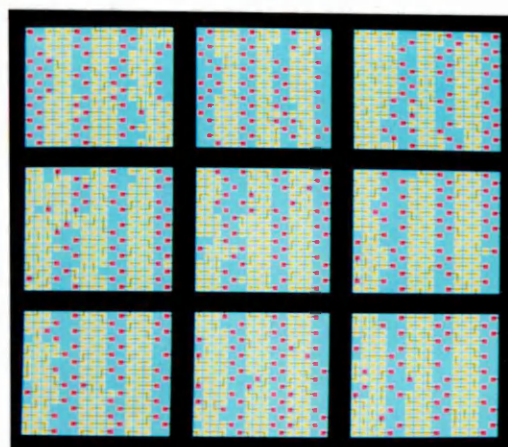


Figure 5.28 : Sample lattice section in the lamellar region. $s=4$,
 $N=768$, $\gamma=-2.0$, $\beta^{-1}=0.9$, amphiphile conc.=75%

6.1 INTRODUCTION

Mean field models of amphiphilic systems determine the best conformational probability distribution of a single chain by considering the packing constraints imposed by its neighbours in a mean field approximation. They are often referred to as single chain theories. As only the singlet probability distribution function, pdf, is provided by these theories, the thermodynamic properties can only be evaluated approximately. The packing constraints imposed by a particular geometry may be simplified by placing the chains on an appropriate lattice.

Chains confined to a particular geometry (e.g. bilayer, cylinder or sphere) are subject to packing constraints imposed by the presence of neighbouring chains. This results in a distribution in probabilities over different chain conformations which can be used to calculate any desired chain property as well as estimate thermodynamic properties such as the conformational free energy per chain.

In this section a review is made of the theory needed for a calculation which allows comparison between simulation and mean field approaches to modelling bilayers. The review considers both lattice and off-lattice mean field models as the new calculation combines features of the two approaches.

A mean field model is presented in which tail segments at the surface experience a hydrophobic free energy cost and head groups experience a hydrophilic free energy reduction proportional to their exposure to

the solvent. The model is a lattice model similar to that described by Ben-Shaul *et al* (1984) with additional interaction parameters equivalent to those used in the Monte Carlo simulation. The model shows a temperature dependent head roughness.

Results of the mean field model are obtained over a range of temperatures and compared with those of the Monte Carlo simulation (Chapter 5). Plots of the head roughness, equation (4.27b), against temperature suggest a phase transition to a bilayer, indicated by a point of inflection as seen in the Monte Carlo work. This is novel behaviour in a mean field lattice model of a bilayer. Models of monolayers which do not consider the effects of surface roughness have been reported with intermolecular potentials between the chains and solvent e.g. Cantor & McIlroy (1989).

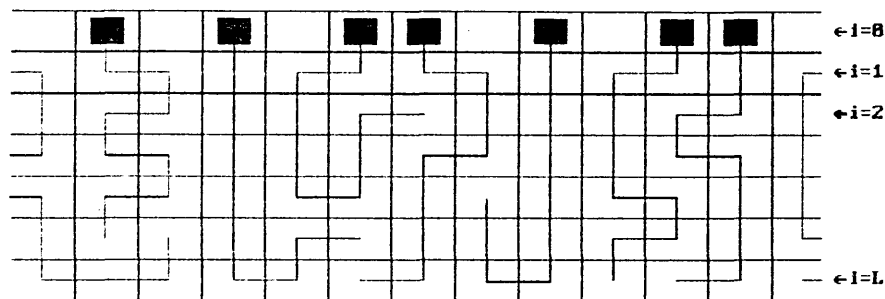
6.2 LATTICE MODELS

Lattice models have been studied extensively by the groups of Ben-Shaul *et al* and Dill *et al* [Dill & Flory 1980a,b] [Ben-Shaul *et al* 1984,1985a,b] [Szleifer *et al* 1985] [Dill *et al* 1988] [Naghizadeh & Dill 1988]. Systems of N identical amphiphilic chains are considered. The amphiphiles consist of s segments connected by $s-1$ flexible bonds, with the first site designated as the head group and the remaining $s-1$ sites represent the hydrocarbon tail. The amphiphiles are placed on the lattice with each segment occupying a single lattice site.

Spherical and cylindrical lattices are used to represent micelles, and cubic lattices are used for bilayers or monolayers. The chains are

placed on the lattice with their heads on the surface and their tails occupying the lattice core. The hydrocarbon core is divided up into L equally spaced layers, parallel to or concentric with the aggregate surface.

(a)



(b)

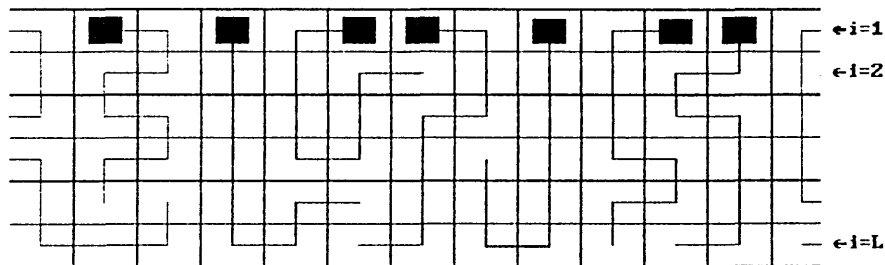


Figure 6.1 : Equivalent Schematic representations of a monolayer
 (a) heads lie on surface layer and do not contribute to packing constraints, (b) heads lie in layer $i=1$ and are considered in packing.

Figures 6.1(a),(b) show alternative schematic ways of representing a monolayer, similar to that suggested by Dill & Flory (1980). In figure 6.1(a), the head groups sit in a surface layer, $i=0$, with their first bond downwards to layer $i=1$. The packing constraints apply to layers

$1 \leq i \leq L$ only, and are thus equivalent to those of figure 6.1(b) in which the head segment replaces the first tail segment of the chain. Chains in representation 6.1(b) are one segment shorter than those in 6.1(a). To keep the notation consistent for both representations n is defined to be the number of chain segments contributing to the packing constraints. In figure 6.1(a) $n=s$, while in 6.1(b) $n = s-1$.

Ben-Shaul *et al* (1984) developed expressions for the chain conformational probabilities using the maximal entropy principle. According to the maximal entropy principle, the pdf of chain conformations, $P(a)$, is that which maximises the entropy function

$$S = -k \sum_a P(a) \ln[P(a)/g(a)] \quad (6.1)$$

subject to appropriate constraints on $P(a)$, where $g(a)$ is the degeneracy of chain conformation a , and k is the Boltzmann constant.

The constraints are the normalising condition

$$\sum_a P(a) = 1 \quad (6.2)$$

and the packing constraints imposed by the aggregate geometry.

To include packing constraints the number of lattice sites in each layer of the particular geometry is considered. Ben-Shaul *et al* (1984) expressed these as

$$\begin{array}{ll}
 M_i = M_1 & \text{plane} \\
 M_i = 3h[2(L - i) + 1] & \text{cylinder} \\
 M_i = 4[3(L - i)^2 + 3(L - i) + 1] & \text{sphere}
 \end{array} \quad (6.3)$$

where M_i is the number of sites in layer i and h is the height of the cylinder in lattice sites. These equations are derived by considering the volume occupied by the i^{th} layer as shown in figure 6.2.

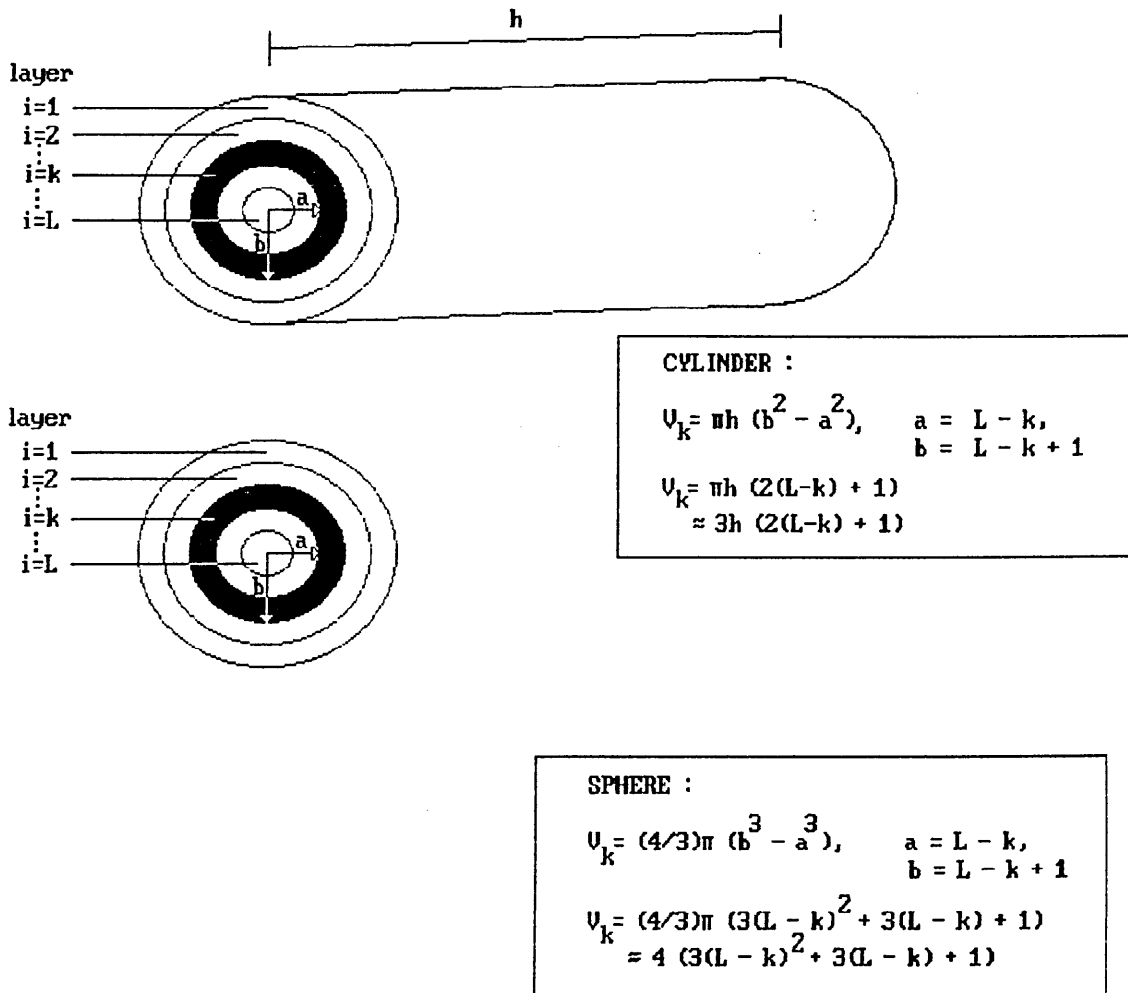


Figure 6.2 : Volumes occupied by layers in cylindrical and spherical aggregates

Assuming uniform (liquid hydrocarbon) density in the aggregate core,

each lattice site is occupied by a chain segment. Hence, the average number of segments per chain in layer i , $\langle \phi_i \rangle$, is expressed as

$$\langle \phi_i \rangle = \sum_a P(a) \phi_i(a) = m_i, \quad i = 1, \dots, L \quad (6.4)$$

where $\phi_i(a)$ is the number of segments in layer i of conformation a and $m_i = M_i/N$. N is the number of amphiphiles. These equations provide L constraints on $P(a)$, but only $L-1$ of these are linearly independent as $\sum_i \langle \phi_i \rangle = n$, where n is the chain length.

The distribution which maximises S subject to the normalisation condition and the $L - 1$ packing constraints is

$$P(a) = g(a) \exp\left[-\sum_{i=1}^{L-1} \lambda_i \phi_i(a)\right] / Q = g(a) \prod_{i=1}^{L-1} \alpha_i^{\phi_i(a)} / Q \quad (6.5)$$

$$Q = \sum_a g(a) \exp\left[-\sum_{i=1}^{L-1} \lambda_i \phi_i(a)\right] = \sum_a g(a) \prod_{i=1}^{L-1} \alpha_i^{\phi_i(a)}$$

where $\alpha_i = \exp(-\lambda_i)$, λ_i are the Lagrange multipliers conjugate to the m_i 's and Q is the conformational partition function of the chain in the aggregate.

All amphiphile conformations may be generated systematically using a computer program enabling the determination of $\phi_i(a)$ and $g(a)$. The $L-1$ simultaneous non linear equations

$$\sum_a g(a) [m_i - \phi_i(a)] \prod_{i=1}^{L-1} \alpha_i^{\phi_i(a)} = 0, \quad i = 1, \dots, L-1 \quad (6.6)$$

may then be solved numerically to give the α_i 's. Once solved, the α_i 's are substituted into equation 6.5 to determine the pdf $P(a)$, which in

turn is used to yield the partition function and bond conformation averages. In the work presented the L-1 non linear equations are solved by Newton-Raphson iteration.

In practice the $\phi_i(a)$ and $g(a)$ are only determined approximately for long chains as the method used does not exclude all hard core interactions between chain segments. For a given chain length, n , in which the chain segments are numbered 1 to n , Ben-Shaul *et al* (1985b) generate all chain conformations of the form $\{a\} = \{i_1, i_2, \dots, i_k, \dots, i_n\}$, where i_k is the layer in which segment k is placed. The degeneracy of each conformation is calculated assuming four possible bond positions between lateral sites and a single bond between sites connected vertically. The method is only correct for hard core interactions between chain segment k and segment $k-1$ and is therefore not exact for chains longer than 4 segments.

Having determined the chain conformations $\{a\}$, it is necessary to express the packing constraints. The number of downward, lateral and upward transitions in layer i due to each chain conformation, $d_i(a)$, $r_i(a)$ and $u_i(a)$ are counted using the set $\{a\}$. Equation 6.4 is reexpressed as

$$\langle \phi_i \rangle = \langle d_i \rangle + \langle r_i \rangle + \langle u_i \rangle = m_i \quad (6.7)$$

where $\langle d_i \rangle$, $\langle r_i \rangle$ and $\langle u_i \rangle$ are the average number of downward, lateral and upward transitions per chain in layer i . Each of these averages can be expressed in terms of $P(a)$ i.e.

$$\begin{aligned}
\langle d_i \rangle &= \sum_a P(a) d_i(a) \\
\langle r_i \rangle &= \sum_a P(a) r_i(a) \\
\langle u_i \rangle &= \sum_a P(a) u_i(a)
\end{aligned}
\tag{6.8}$$

Expressing the packing constraints in this way enables chain conformational averages to be calculated. For example, the distribution of chain ends is given by the probability of finding the n^{th} chain segment in layer i , t_i . This can be expressed as

$$t_i = (\langle d_i \rangle + \langle u_i \rangle) + (\langle d_{i+1} \rangle + \langle u_{i-1} \rangle) \tag{6.9}$$

Figure 6.3 [Ben-Shaul *et al* 1985b] shows example chain distributions for a chain of length $n=7$ in different aggregate geometries.

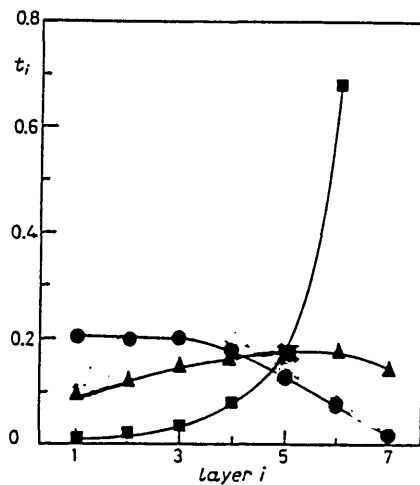


Figure 6.3 : Probabilities of chain termination of 7-segment chains in (a) a bilayer of half-thickness, $L=6$, (squares), (b) a cylinder, $L=7$, (triangles) and (c) a sphere, $L=7$, (circles). [Ben-Shaul *et al* 1985b]

Dill *et al* expressed the constraints on the system in a slightly different way. They apply the conservation of length

$$\sum_i (d_i(a) + r_i(a) + u_i(a)) = n \quad (6.10)$$

together with the constraint of chain connectivity which enables the use of a matrix method to generate the chain conformations. Again a maximal entropy approach was used to determine the pdf of chain conformations, although in the original work of Dill & Flory (1980)(1981) this was not necessary as chain reversals were ignored which fully constrained the system. Dill *et al* estimate the surface density term, m_1 , from experimental data. Their value is primarily dependent on the temperature, solvent and chemical structure of the chains.

Figure 6.4 shows layer order parameters calculated for a monolayer with different values of surface density. [Dill & Flory 1980]. The layer order parameter for layer i , S_i , is defined as

$$S_i = \langle 3/2 \cos^2(\theta_i) - 1/2 \rangle \quad (6.11)$$

where θ_i is the angle of a bond in layer i with respect to the normal of the layer surface. The brackets $\langle \dots \rangle$ indicate averaging over all conformations. On a cubic lattice there are only two possible bond angles, 0° and 90° , and thus equation 6.11 reduces to

$$S_i = 1 - 3/2 \sum_a P(a) r_i(a) \quad (6.12)$$

where $\sum_a P(a) r_i(a)$ is the fraction of sites in layer i occupied via lateral bond placements.

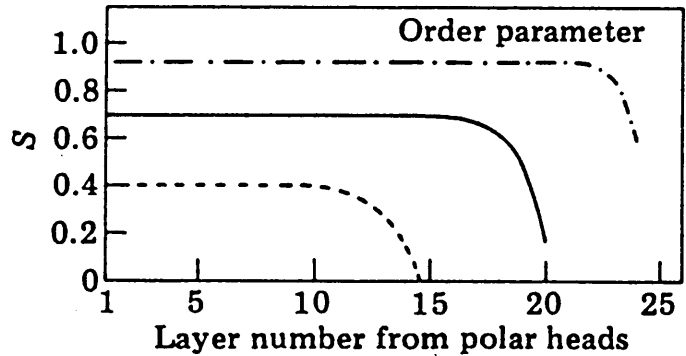


Figure 6.4 : Layer order parameters for a monolayer with $n=25$:
 $m_1=0.60$ (---), $m_1=0.80$ (—), $m_1=0.95$ (-·-)
 [Dill & Flory 1980]

It is seen that the layer order is dependent on the surface density chosen, which is effectively determining the layer thickness, L . The figure indicates that the layer order parameter remains constant over the initial layer. This is probably due to the exclusion of chain reversals.

In the case of interdigitating bilayers [Ben-Shaul *et al* 1985a], the expression for $P(a)$, equation 6.5, remains valid provided the $\phi_i(a)$ are replaced by

$$\bar{\phi}_i(a) = \phi_i(a) + \phi_{2L-i+1}(a) \quad (6.13)$$

Ben-Shaul *et al* also pointed out that the formulation could be extend-

ed to include chain conformation energies.

$$P(a) = g(a) \exp[-E(a)/kT - \sum_{i=1}^{L-1} \lambda_i \phi_i(a)] / Q \quad (6.14)$$

where $E(a)$ is an internal energy which is dependent solely on the conformation, a , of the chain. It is proportional to the number of kinks in the chain and is equivalent to a gauche bond energy cost. The internal energy is expressed as

$$E(a) = k_0(a)x_0 + k(a)x \quad (6.15)$$

where x is the energetic cost assigned to each kink in the tail, x_0 is the energetic cost assigned to a kink in the first bond $k_0(a) = 0$ or 1 if there is or is not a kink between zeroth and first bonds. $k(a)$ is the number of internal kinks in conformation a . Equation 6.5 now becomes

$$P(a) = g(a)w_0^{k_0(a)}w^{k(a)} / Q \quad (6.16)$$

where $w = \exp(-x/kT)$ and $w_0 = \exp(-x_0/kT)$.

Figure 6.5 displays bond order parameters for bilayers of different thickness [Szeleifer *et al* 1985] and shows the effect of interdigitation. The bond order parameters are similar to the layer order parameters but consider the order along the chain as opposed to the order through the aggregate. The bond order parameter, S_k , is defined as

$$S_k = \langle 3/2 \cos^2(\theta_k) - 1/2 \rangle \quad (6.17)$$

where θ_k is the angle of a bond in layer i with respect to the normal of the layer surface. On a cubic lattice, equation 6.17 reduces to

$$S_k = 3/2P_k'' - 1/2 \quad (6.18)$$

where P_k'' is the overall probability of finding the k^{th} bond parallel to the normal of the layer surface.

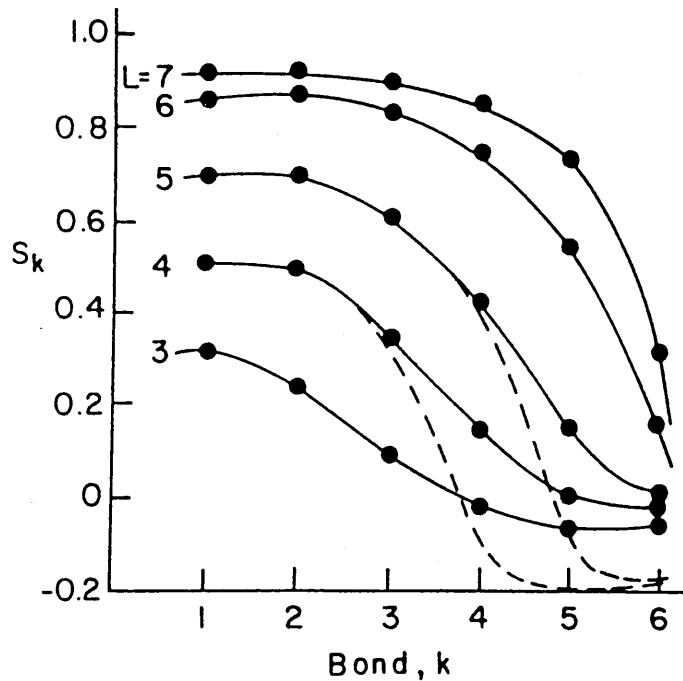


Figure 6.5 : Bond order parameters for a planar bilayer with kink energy parameters $x_0=0.7$, $x=0.3$. The dashed curves refer to chains prevented from crossing the midplane (no interdigitation). [Szeifer *et al* 1985]

Interdigitation in bilayers is shown to be significant, but that chain stiffness effects were found to play a secondary role to packing constraints.

Gruen (1985a,b) extended the single chain models to include a more

realistic model of the amphiphile chain, which involved taking it off-lattice.

6.3 OFF LATTICE MODELS

An off-lattice single chain model was described by Gruen (1985a,b) and similar models have been used by others in recent years e.g Szleifer *et al* (1986)(1988) and Ben-Shaul *et al* (1987). As with the lattice models, described above, the amphiphiles are constrained to a hydrophobic core. The amphiphilic molecules are of the form $X-(CH_2)_{n-1}-CH_3$ where X denotes the hydrophilic head. The chain conformations, a , are obtained by randomly sampling from bond sequences generated according to the rotational isomeric (RIS) scheme [Flory 1969]. In the RIS model, the conformation of a chain is fully specified by the sequence of trans/gauche bonds along the backbone and the three Euler angles describing the orientation of the chain relative to the interface. It is necessary that the sample of conformations is large enough for properties of the sample to be almost independent of the sample used.

As with the lattice models described above, the chains are placed on planar, spherical or cylindrical geometries to represent the hydrophobic core of a bilayer or spherical or cylindrical micelle. The hydrophobic cores are divided into layers, $i=1$ to 7, parallel to or concentric with the aggregate surface.

The model is constrained such that when the ensemble average is taken over all conformations, the aggregate is packed at liquid hydrocarbon density. Head group positions are randomly sampled within a small interval normal to the interface, thus allowing some chain conforma-

tions with part of the chain outside the hydrophobic core, but these conformations are subject to a hydrophobic free energy cost.

In describing the packing constraints, Gruen (1985a,b) takes into account that the volume of the chain terminal, CH₃, segment has greater volume than a CH₂ segment. The packing constraints are described by the product $(\prod_j (a_i)^{V_j})$, where a_i is associated with layer i and is adjusted to comply with the packing constraints. V_j is the ratio of the volume of the j^{th} segment over the volume of a CH₂ group. $V_j=1$ except for the methyl group.

The probability of a chain in conformation a , $P(a)$, is given by

$$P(a) = (\prod_j (a_i)^{V_j}) \exp[-E(a)/kT] / Q \quad (6.19)$$

where k is the Boltzmann constant, Q is the partition function and $E(a)$ is the energy of conformation a . $E(a)$ is given by

$$E(a) = E_{\text{int}}(a) + \sum_j w_j(a) \quad (6.20)$$

$E_{\text{int}}(a)$ is the internal energy of the chain (cf. equation 6.15) and is of the form

$$E_{\text{int}}(a) = n_g(a)E_g \quad (6.21)$$

where $n_g(a)$ is the number of gauche bonds in conformation a , and E_g is the energy of a gauche bond.

The hydrophobic free energy cost for chains protruding outside the core is modelled by the term $\sum_j w_j(a)$. It is assumed

$$w_j(a) = (1 - \Phi_{\text{HC}}(r_j)) f_j(a) F_{\text{HC-W}} \quad (6.22)$$

where $\Phi_{\text{HC}}(r)$ is the fractional increase in the chain water contact due to the position of chain segment j and $F_{\text{HC-W}}$ is the free energy cost of transferring CH_2 groups from bulk hydrocarbon to water. $\Phi_{\text{HC}}(r)$ is modelled as

$$\Phi_{\text{HC}}(r) = A \exp(-r / l) \quad (6.23)$$

where A and l are adjustable parameters.

The results are generated by an iterative technique. After each iteration, the partition function for the chain is evaluated and ensemble averages are calculated.

Extensive comparison was made with the molecular dynamics simulation of van der Ploeg and Berendsen (1983) and with experiment. Good quantitative agreement was achieved, but this required some parameter adjustment. In Gruen (1985b), the results are fitted to experimental data by multiplying the pdf by a factor $(\sin\theta)^x$, where θ is the angle of the bond between the head group and the first chain segment with the z axis, and x is an adjustable parameter depending on the amphiphile in question.

Szleifer *et al* (1986), also use the RIS description of amphiphile

chains, but model surface roughness differently. They introduce a density profile, $\{\rho_i\}$, into the packing constraints. Equation 6.4 now becomes

$$\langle \phi_i \rangle = \rho_i m_i, \quad i=1, \dots, L \quad (6.24)$$

where ρ_i is the average segment density in layer i of the hydrophobic core. Layers towards the centre of the core had density $\rho_i = 1$, whilst those near the surface were given densities $0 < \rho_i \leq 1$. The model also includes a gauche bond energy cost, $E_{int}(a)$.

Equations 6.6 are reexpressed as

$$\sum_a [\phi_i(a) - \rho_i m_i] \omega(a) \prod_{i=1}^L \phi_i(a) = 0, \quad i=1, \dots, L-1 \quad (6.25)$$

where $\omega(a)$ is related to the internal energy of the chain, $E_{int}(a)$, by

$$\omega(a) = \exp(-E_{int}(a)/kT) \quad (6.26)$$

Results are obtained as with the lattice models without the need for ensemble averaging.

By adjusting the density profile accordingly, Szleifer *et al* achieved good agreement with experimental results and with Gruen (1985a,b). They also compared chains with a gauche bond energy against flexible chains and found that the effect of the internal energy on the bond order profile was qualitative rather than quantitative. They concluded

that the qualitative nature of the results using RIS model chains were identical to those derived for the approximate lattice model chains.

A further development has been to study aggregates with chains of mixed lengths [Ben-Shaul *et al* 1987] [Szleifer *et al* 1988]. Bending energies for bilayers with chains of different lengths were calculated. Their results indicate that the bending energy of a bilayer with chains of two different lengths is less than that of bilayers occupied solely by either of the two chain lengths used. See figure 6.6.

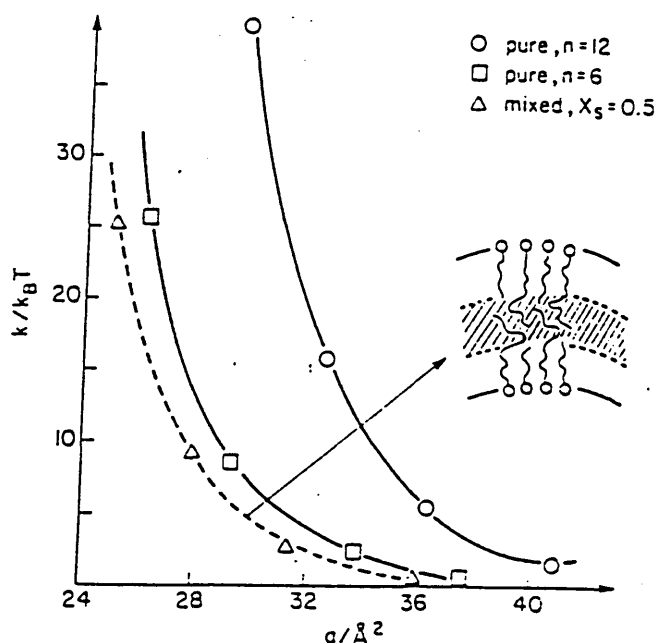


Figure 6.6 : Bending energy k vs. area per molecule for two single component bilayer systems and their equimolar mixture. [Szleifer *et al* 1988]

6.4 EXTENSION TO MODEL

It has been observed in the reported Monte Carlo simulation of an amphiphile and solvent system, that the transition from a bicontinuous region to a lamellar region can be characterised by the change in

surface roughness, particularly the head roughness.

At high temperatures, in the bicontinuous region, the heads remain partly buried in the hydrophobic core but on cooling to the lamellar region the head groups are forced out of the surface and are fully solvated. In figure 6.7 the temperature dependence of the second differential of the head roughness for the $s=4$, $N=512$, $\gamma=-2.0$ system is plotted with the temperature dependency of the mean cluster size for the same system. (See figures A26, Appendix A).

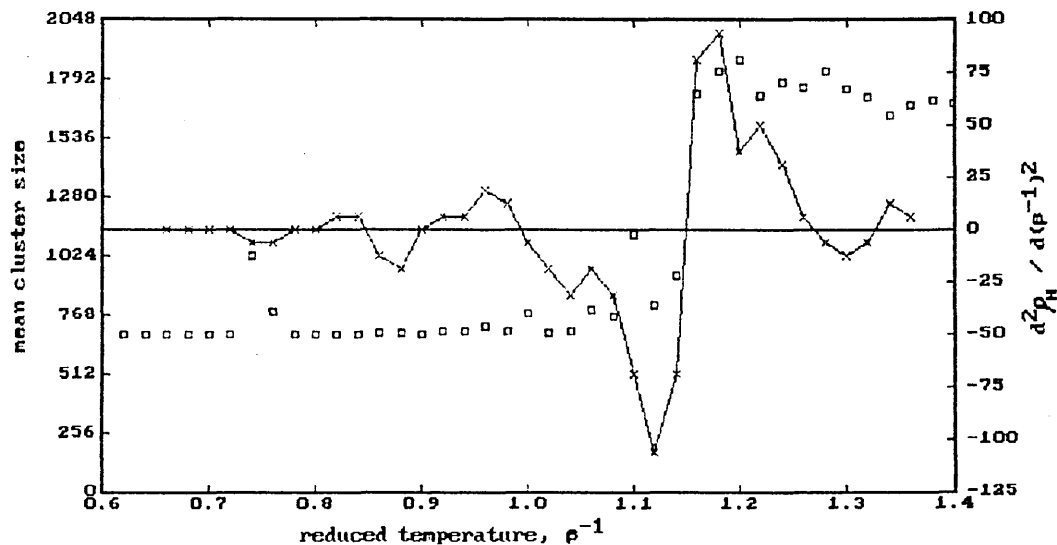


Figure 6.7 : Phase transition of the $s=4$, $\gamma=-2.0$, 50% amphiphile concentration system on cooling (crosses represent $d^2\rho_H/d(\beta^{-1})^2$, where ρ_H is the head roughness and squares represent the mean cluster size.

The phase transition is seen as the main point of inflection on the temperature-head roughness plot. (At a point of inflection the second differential crosses the $y=0$ axis.) The tail-solvent interaction remains minimal in both bicontinuous and lamellar regions.

A mean field model is presented which has a temperature dependent surface roughness similar to that of the simulation. An important variation from previous mean field lattice models is that the head groups are allowed to lie in either layers 0 or 1 of the lattice, where they experience different exposure to solvent. Figure 6.8 is a schematic representation of the lattice.

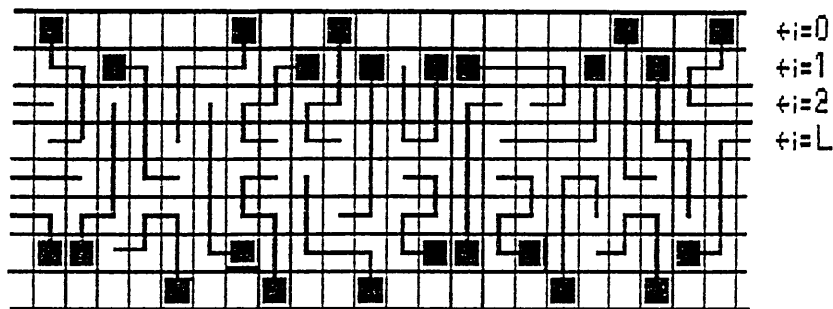


Figure 6.8 : Schematic representation of lattice

For simplicity, it is desirable that the hydrophobic free energy costs and reductions acting on a given chain are a function of the chain conformation, a , only. This can be achieved by making the following assumptions which are consistent with results from our Monte Carlo simulations made :

- (i) Layer $i=0$ contains only head sites.
- (ii) Each head site in layer $i=0$ is fully solvated.
- (iii) Layers $1 \leq i \leq L$ are fully packed, i.e they have no vacant sites.
- (iv) Layer $i=1$ contains both head and tail sites.

(v) Layers $2 \leq i \leq L$ are occupied by tail sites only.

The solvent sites are not modelled explicitly, but are assumed to occupy all sites in layer $i=0$ not occupied by head segments.

The internal energy of conformation, a , $U(a)$ is modelled by

$$U(a) = n_{\text{HS}}(a)E_{\text{HS}} + n_{\text{TS}}(a)E_{\text{TS}} \quad (6.27)$$

E_{HS} and E_{TS} are the interaction energies associated with single nearest neighbour head-solvent and tail-solvent bonds. $n_{\text{HS}}(a)$ and $n_{\text{TS}}(a)$ are the number of head-solvent and tail-solvent bonds associated with conformation, a . Chain conformations with a head group in layer $i=0$ have $n_{\text{HS}}(a)=5$ and those in layer $i=1$ have $n_{\text{HS}}(a)=1$. The value of $n_{\text{TS}}(a)$ is equivalent to the number of tail segments of conformation, a , lying in layer $i=1$, except for those with heads in layer $i=1$. In such cases it is the number of tail segments in layer $i=1$ minus one.

In reduced units, equation (6.27) becomes

$$U(a)/kT = \beta(n_{\text{TS}}(a) + \gamma n_{\text{HS}}(a)) \quad (6.28)$$

where $\beta = E_{\text{TS}}/kT$ and $\gamma = E_{\text{HS}}/E_{\text{TS}}$. The $L-1$ packing constraints are described by a modification of equations 6.6 to include equation 6.28 as

$$\sum_a g'(a) \{m_i - \sigma_i(a)\} \prod_{j=1}^{L-1} \alpha_j^{\sigma_j(a)} = 0, \quad i = 1, \dots, L-1 \quad (6.29)$$

where $g'(a)$ may be thought of as an effective degeneracy and is given by

$$g'(a) = g(a) \exp(-U(a)/kT) \quad (6.30)$$

Similarly, by analogy with equation 6.5, the probability of a conformation, a , $P(a)$ is

$$P(a) = g'(a) \exp\left[-\sum_{i=1}^{L-1} \lambda_i \phi_i(a)\right] / Q = g'(a) \prod_{i=1}^{L-1} \alpha_i^{\phi_i(a)} / Q \quad (6.31)$$

$$Q = \sum_a g'(a) \exp\left[-\sum_{i=1}^{L-1} \lambda_i \phi_i(a)\right] = \sum_a g'(a) \prod_{i=1}^{L-1} \alpha_i^{\phi_i(a)}$$

6.5 THE PROGRAM

The extended mean field model was coded in Fortran. A top level algorithm is given below.

pseudo code : mean field model of surface roughness

begin

input chain length(n), number of layers(L)

input γ , β

generate all chain conformations for given chain length

set $a = 0$

while ($a <$ number of conformations)

set $a = a + 1$

calculate degeneracy of conformation a

determine number of segments in each layer due to conformation a

weight degeneracy of conformation a by $\exp\{-\beta(n_{TS}(a) + \gamma n_{HS}(a))\}$

end while

determine probability of each conformation
calculate head roughness (or any other thermodynamic property)

end

6.5.1 Generating Chain Conformations

To model a rough surface two distinct sets of chain conformations are used. We consider all chain conformations with the head segment in layer $i=0$ to be of type-A and those with the head segment in layer $i=1$ to be type-B chains.

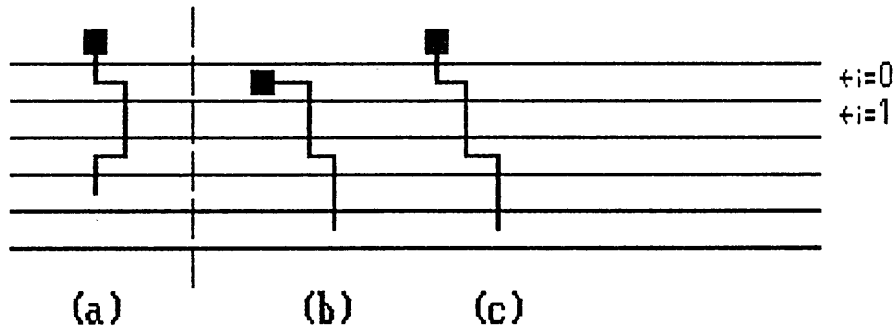


Figure 6.9 : Distinct chain conformations: (a) type-A with head group in layer $i=0$, (b) type-B with head group in layer $i=1$, (c) type-A equivalent conformation of (b)

Figure 6.9 shows an example of the two chain types. In order to be consistent with the Monte Carlo simulation, the head group size is set equal to the size of a tail segment. Thus the packing constraints of a type-B chain of length n are equivalent to a type-A chain of length $(n+1)$.

All possible two dimensional chain conformations for chain lengths n

and $(n+1)$ are generated in the form $\{a_A\} = \{i_1, i_2, \dots, i_k, \dots, i_n\}$ and $\{a_B\} = \{i_1, i_2, \dots, i_k, \dots, i_n, i_{n+1}\}$, where i_k is the layer in which the k^{th} segment is placed. A recursive algorithm is used which ensures all possible chain conformations are generated. Chain conformations in which there are immediate reversals, i.e. an upward bond directly succeeds a downward bond, are rejected.

6.5.2 Determining The Degeneracies

The chain conformations are degenerate because a lateral site placement in a given layer can be in any of four directions for a cubic lattice. For each chain conformation, a_A or a_B , the degeneracies $g(a_A)$ and $g(a_B)$ are determined by multiplying the individual degeneracies due to each bond in the conformation. Consider the chain conformation shown below.

$$\begin{aligned} \{a\} &= \{1 \ 1 \ 2 \ 3 \ 3 \ 3 \ 3\} \\ \text{degeneracy} &= 4 \times 1 \times 1 \times 4 \times 3 \times 3 = 144 \end{aligned}$$

The first two tail segments lie in layer $i=1$; thus the bond between them is a horizontal one, which has a degeneracy of 4. The next two bonds are downward bonds reaching layer $i=3$. These vertical bonds are not degenerate. The remaining three sites in the chain are all in layer $i=3$, which implies there are three consecutive horizontal bonds. The first of these bonds is assigned a degeneracy of 4 as there are four possible lattice directions it can occupy. In the case of the second horizontal bond one of the four directions is occupied by the previous site, thus this bond has a degeneracy of three. The determination of the correct degeneracy for further successive horizontal

bonds becomes increasingly complicated and is usually evaluated by making approximations [Ben-Shaul 1985b]. Thus hard core interactions are ignored between sites separated by a segment or more, and each successive horizontal is assigned bond a degeneracy of 3.

6.5.3 Conformational Probabilities

The conformation probabilities are found by solving for the α_i 's in equation 6.29 and substituting in equation 6.31. The α_i 's are found by Newton-Raphson iteration as shown in Appendix B.

6.5.4 Head Roughness

The main property of interest is the mean head roughness, $\langle \rho_H \rangle$. This is defined to be consistent with equation 4.27b as follows

$$\langle \rho_H \rangle = \sum_a P(a) n_{HS}(a) \quad (6.32)$$

where $n_{HS}(a)$ is the number of head-solvent bonds associated with conformation a.

6.6 RESULTS

The model is examined to show the variation with temperature of the amphiphile chain length, bilayer thickness and head-solvent interaction on the bilayer. The model is also compared to results from the Monte Carlo simulation for a bilayer with chain length $s=6$.

6.6.1 The Head-Solvent Interaction, γ

The mean field model was solved over a range of temperatures for bilayers with half thickness $L=4$ occupied by chains of length $s=6$. The head roughness was determined with three different head-solvent potentials, $\gamma=-0.5$, -1.0 and -2.0 . The results are shown below in figure 6.10.

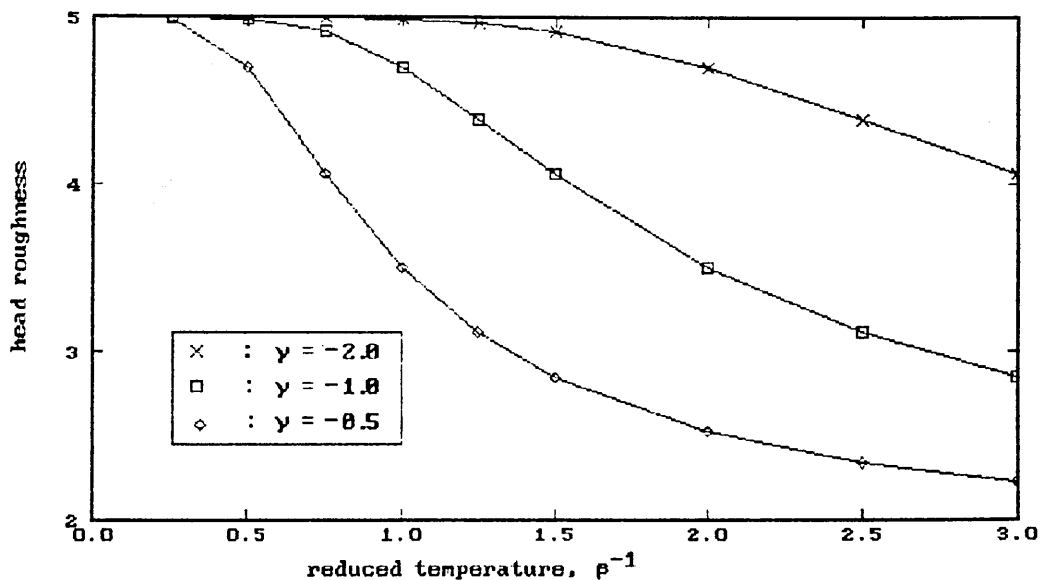


Figure 6.10 : Temperature dependence of head roughness for various γ . $n=6$, $L=5$.

The point of inflection marking the transition to a bilayer is clearly seen. Doubling γ almost exactly doubles the temperature at which the point of inflection occurs. This is because the head roughness is effectively a measure of the average number of head solvent bonds per amphiphile.

6.6.2 Effect Of Chain Length

The variation of head roughness with temperature for chains of lengths

$n=6$ and 7 was investigated for a bilayer half thickness, $L=5$ and head-solvent potential, $\gamma=-1.0$. The variation was only slight; the head roughness is lower at high temperatures for the longer chain amphiphiles. At high temperatures the tail-solvent interactions are less significant and conformations of chains are possible with some tail-solvent contact.

6.6.3 The Bilayer Thickness

The temperature dependence of the head roughness was examined for amphiphiles of length $n=6$ and head-solvent potential, $\gamma=-1.0$, for bilayers with widths $L=2, 3, 4$ and 5 . The variation of head roughness with L was negligible. This is because the tail-solvent interactions are not significant and the head roughness depends only on the value of γ and the temperature. Although the head roughness values vary little with the bilayer thickness the chain conformations are distinctly different. This is shown in figure 6.11.

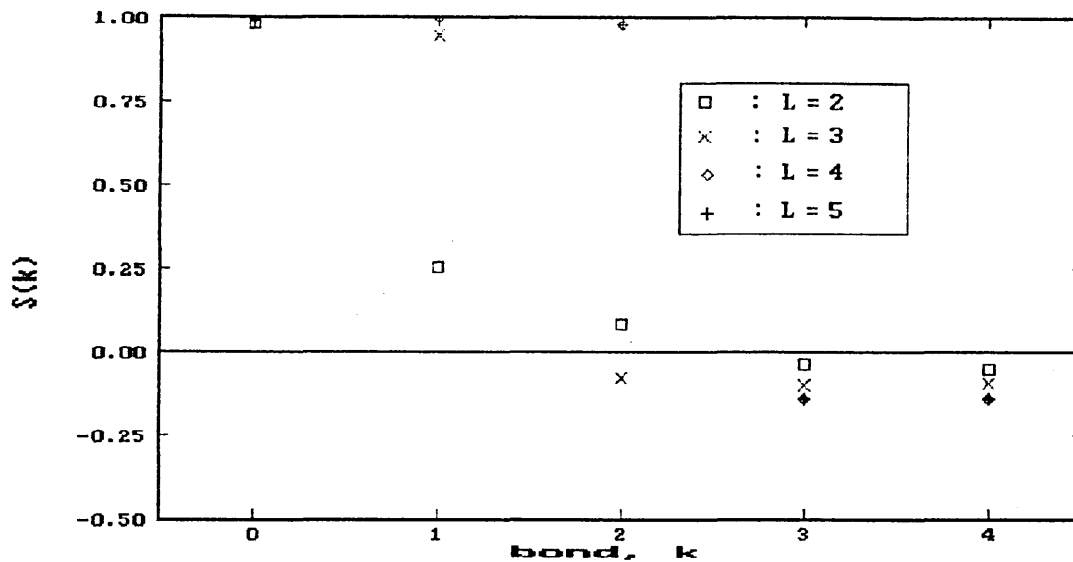


Figure 6.11 : Bond order parameters from mean field calculations of bilayers. $n=6$, $\gamma=-1.0$, $\beta^{-1}=0.75$

The figure shows that bond 0, (the bond between the head group and first tail group), is well ordered. It lies perpendicular to the surface of the bilayer. The bond order decreases moving down the chain. The thicker bilayers force order on bonds lower down the chain than thinner ones.

6.6.4 Comparison With Simulation

The mean field model of a bilayer described cannot be applied to bilayers with half-thickness $L < 2$. This prevents a direct comparison with the results from the Monte Carlo simulation for the chain length $s=4$, which was studied in most detail, as the bilayers produced have a maximum thickness, $2L = 3$.

To enable a direct comparison between mean field and Monte Carlo models, results were obtained using the simulation for the $n=6$, $\gamma=-2.0$

system at an amphiphile concentration (60%), which yields a bicontinuous to lamellar phase transition. The resulting bilayers have half-thickness $L=2$ and can thus be compared with the mean field model. Figure 6.12 shows the variation of head roughness with temperature for the $n=6$, $\gamma=-2.0$ system as obtained from the simulation. The crosses indicate the temperature dependence of the mean cluster size and show the phase transition temperature.

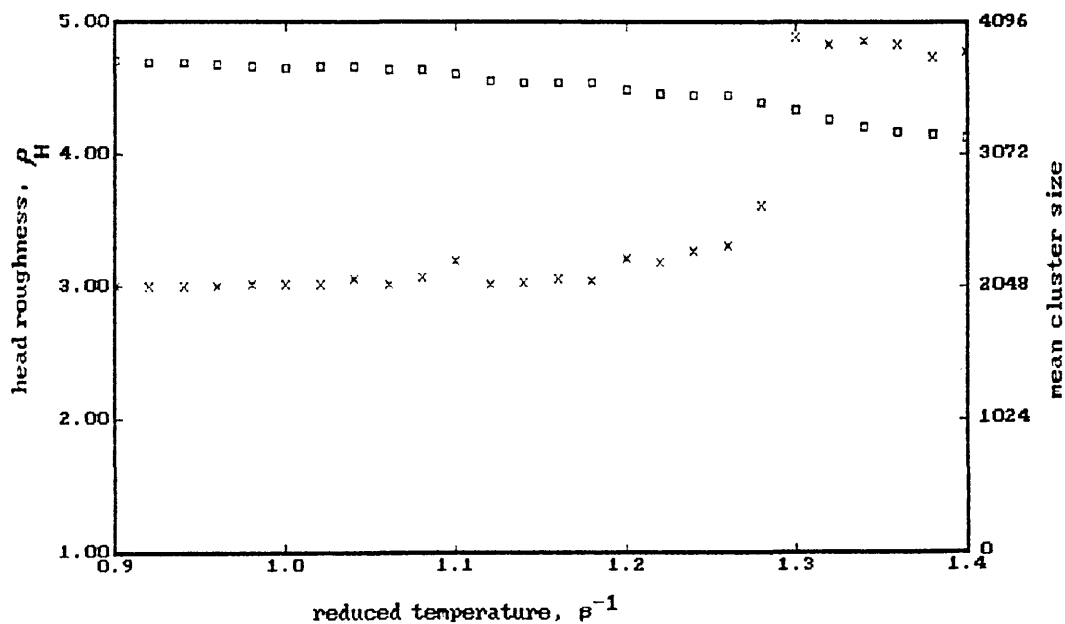


Figure 6.12 : The temperature dependence of the head roughness (squares) and the mean cluster size (crosses) from a simulation bilayer with $n=6$, $L=2$ and $\gamma=-2.0$.

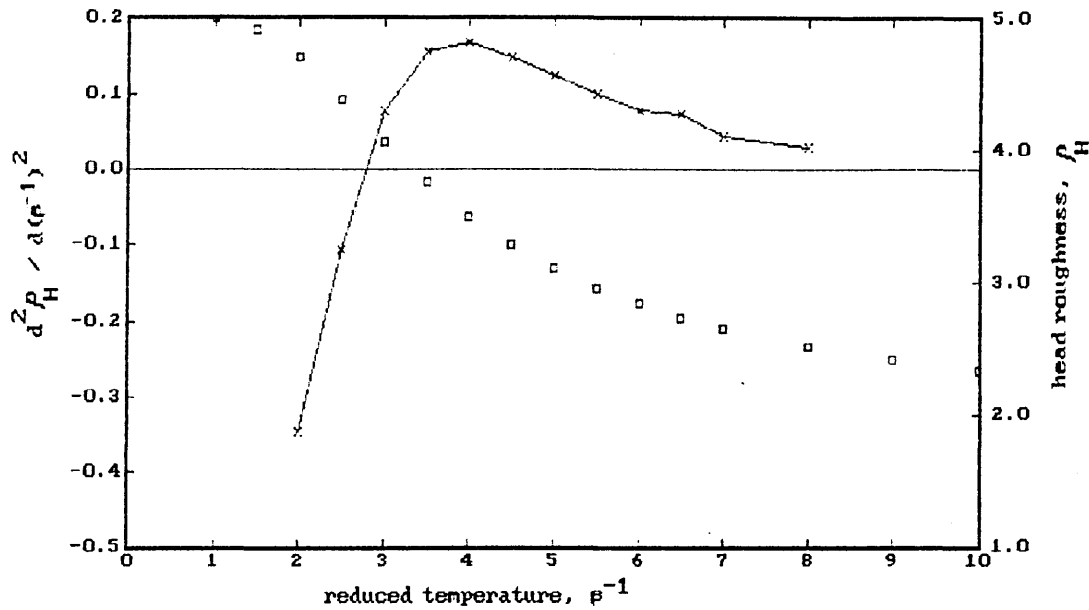


Figure 6.13 : Mean field temperature dependence of the head roughness (squares) and its second differential (solid line). $n=6$, $\gamma=-2.0$, $L=2$.

The equivalent system is examined in the mean field approximation and the resulting head roughness is shown in figure 6.13. The figure shows a similar point of inflection, but it occurs at a higher temperature. Interestingly, decreasing the magnitude of the head-solvent interaction to $\gamma=-1.0$ shifts the point of inflection to approximately coincide with that produced by the simulation. This is shown below in figure 6.14.

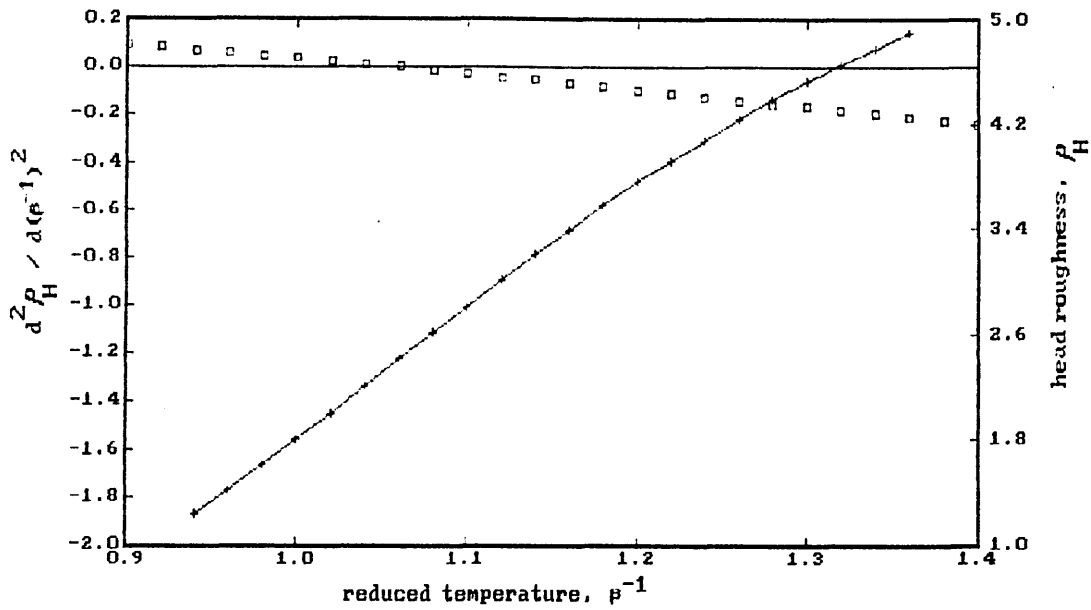


Figure 6.14 : Mean field temperature dependence of the head roughness (squares) and its second differential (solid line). $n=6$, $\gamma=-1.0$, $L=2$.

The reason for the difference in the phase transition temperature obtained, with the same n , L and γ , from the simulation and from the mean field calculation is unclear. However, it should be noted the simulations model multiple bilayers and that the temperature of the transition to the bilayers is dependent on the total amphiphile concentration; a parameter not included in the mean field calculation.

Figure 6.15 compares the order parameters of simulation and mean field models at high and low temperatures. The mean field results use a value of γ scaled such that the transition to the bilayer occurs at approximately the same temperature that in the simulation.

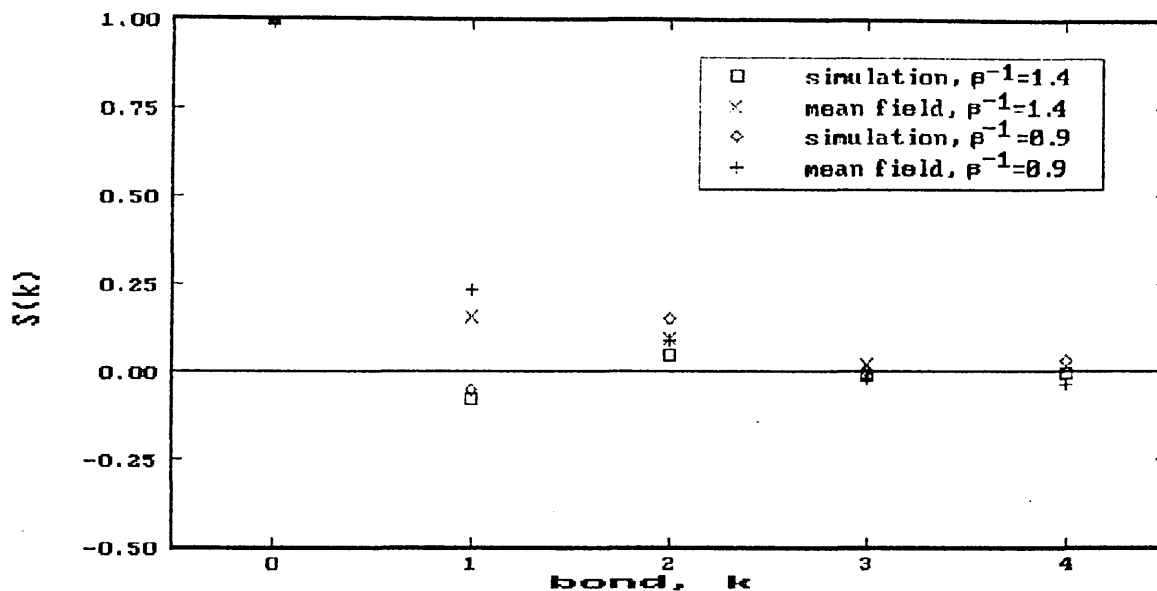


Figure 6.15 : Order parameters from simulation and mean field models at high and low temperatures.

The order parameters derived from the mean field model are in reasonable agreement with those of the simulation, although the mean field model is not able to predict the almost complete lack of order shown in the simulation results for bond, $k=1$. In both approaches the order parameters indicate greater chain order at the lower temperature.

6.7 SUMMARY

The phase transition temperature to an ordered bilayer of a mean field model has been determined as being the point of inflection of a plot of head roughness against temperature. For a given head-solvent potential, γ , the phase transition temperature predicted by the mean field model is approximately twice that observed in the simulation. Good agreement for the variation of head roughness with temperature is achieved by solving the mean field model with a value of head-solvent interaction set to half of that used in the simulation. However, the

reason for this is unclear. Reasonable agreement is obtained between bond order parameters of the simulation and mean field model, although the mean field approach tends to 'smooth out' the fine detail.

A three dimensional lattice model of an amphiphile-solvent mixture has been developed which displays the essential features of real lyotropic systems. Monte Carlo simulations have been used to investigate the effect of the model parameters i.e the head-solvent interaction, γ , the reduced temperature, β^{-1} , the amphiphile concentration and the chain length, s on a range of observables. The chains are completely flexible. The amphiphile concentration was controlled by varying the number of amphiphiles in the system, N , or by changing the size of the lattice. Because of the large number of parameters in the model it has not been possible to examine all the parameter space in detail.

In most of the simulations the amphiphiles were allowed to self-assemble by cooling from a high temperature random configuration to a low temperature ordered configuration. Aggregates observed include small roughly spherical micelles, large cylindrical micelles, ordered multiple bilayers and a vesicle.

The different structures obtained from the simulations are classified according to their size, shape and surface roughness. The ratio of the smallest to the largest principal moments of inertia has been shown to be a useful way of characterising amphiphilic aggregates according to their shape. The ratio provides a clear distinction between spherical, cylindrical and planar structures. Contour maps of this parameter plotted as a function of reduced temperature and amphiphile concentration are a good way of showing the phase diagram. The measurement of cluster size is particularly important in determining a micellar

region as micelles are characterised by a minimum in their cluster size distribution.

The temperature-concentration phase diagram has been determined for amphiphiles with chain length $s=4$ and head-solvent interaction, $\gamma=-2.0$. This value of head-solvent interaction was chosen because it is sufficiently solvophilic for micelle formation at low amphiphile concentrations and for the formation of multiple bilayers at high amphiphile concentrations. The phase diagram shows many of the features associated with real systems, particularly a critical micelle concentration and a lamellar region.

Small micelles are observed at low amphiphile concentrations. The micelles have mean cluster sizes between 5 and 12 monomers and are non-spherical with moments of inertia which suggests their shape is between a cylinder and a plane. The micelles have a rough surface, but the heads are not fully solvated. In contrast to common models of micelle formation, the micelle size increases significantly as the amphiphile concentration is increased above the critical micelle concentration and only a weak minimum is observed in their cluster size distribution curves. The cluster size distribution is also broader than that assumed in thermodynamic models. It is shown that a head-head repulsion is not necessary for limiting micelle size. Growth of the simulation micelles appears to be limited by entropy.

At high amphiphile concentrations ($\approx 45\%$) there is a transition from a bicontinuous structure to a multiple bilayer region as the system is cooled. This is a sharp transition and the existence of hysteresis

when the system is cooled and then reheated, observed in plots of the temperature dependence of the mean cluster size, suggests this transition may be first order. A plot of the temperature dependence of ratio of the number of head-solvent bonds to the number of head sites in contact with solvent sites, referred to as the head roughness, shows a point of inflection at the transition temperature of the bicontinuous to lamellar regions.

Some other regions have been investigated in a preliminary way and the following has been noted.

The model is particularly sensitive to the value of the head-solvent interaction, γ . When γ is solvophobic and there is a low amphiphile concentration, the amphiphiles condense into a single cluster on cooling in which the head groups are evenly distributed throughout the cluster.

At low concentrations for slightly solvophilic and moderately solvophilic values of γ , (e.g. $-1.0 > \gamma > -0.5$ for $s=4$), the system again undergoes a phase separation in which the amphiphiles form a single large cluster. However the chains pack with most of the head groups on the surface of the cluster. This ordering of the head groups increases with shorter chains and more solvophilic head-solvent interactions.

At amphiphile concentrations less than approximately 15%, systems with chains of length $s=3$ and $s=4$ have formed small micelle-like clusters when γ is strongly solvophilic e.g. $\gamma=-2.0$. It is likely that micelles would occur with longer chain lengths, but the model has not been simulated using long chains with sufficiently high head-solvent inter-

actions. Increasing the chain length will require increasingly solvophilic values of γ if micelles are to be observed. This is because increasing the chain length increases the tail-solvent interactions and these repulsions dominate the simulation at the expense of the head-solvent interactions which are not able to equilibrate fully.

At high amphiphile concentration, (above $\approx 50\%$ by volume), chains of length $s=4$ cool to form multiple bilayers when head-solvent interaction, $\gamma=-2.0$. In the bilayers the head groups are almost totally solvated, thus γ must be sufficiently solvophilic. However, if γ is too solvophilic, (e.g $\gamma=-5.0$), the head groups quickly become fully solvated at high temperatures and there is no further ordering of the tails on cooling. The possibility of obtaining multiple bilayers using amphiphiles with chain lengths other than $s=4$ has not been investigated. For longer chains the simulations would require a larger lattice than those considered here and would thus be more expensive in computer resources.

A mean field lattice model of a bilayer has been developed which has similar interaction energies to the Monte Carlo model. The model has temperature dependent head-solvent and tail-solvent interactions at the bilayer surface and shows a transition to an ordered bilayer on cooling. The transition temperature is given by the temperature at which the main point of inflection occurs in a plot of the head roughness against temperature.

For a given head-solvent potential, γ , the phase transition temperature predicted by the mean field model is approximately twice that

observed in the simulation. Good agreement for the variation of head roughness with temperature is achieved by solving the mean field model with a head-solvent interaction set to half of that used in the simulation. However, the reason for this is unclear. Reasonable agreement is obtained between bond order parameters of the simulation and mean field model, although the simulation tends to 'smooth out' the fine detail.

The inclusion of the tail-solvent interactions in the mean field calculation had a negligible effect on the chain ordering in the bilayer. The interactions remained at their minimum value except at very high temperatures where the energy cost of having an increased tail-solvent interaction is small.

The phase diagram obtained for amphiphiles with a chain length of 4 could be improved by studying larger systems for longer runs. This is particularly the case at high amphiphile concentrations and low temperatures where the simulation statistical errors are greatest. Studying a larger system may provide evidence for a hexagonal phase.

The micelles observed in the current work show a wide cluster size distribution. A sharper distribution may be obtained by including a long range head-head repulsion term. Including this term may give a better representation of amphiphiles with ionic head groups. Alternatively systems could be studied in which the head group is larger than a tail segment.

In the current work interesting structures such as 'curly bilayers' and a vesicle have been observed for systems with longer chain amphiphiles. A possible area of future work would be to examine in detail the factors which cause curvature in bilayers. A phase diagram which included a vesicle would be of great interest as the self-assembly of a vesicle by computer simulation has not been shown previously and there is still much to learn about the mechanism of their formation. To this end, it would be of interest to run simulations with mixed amphiphile chain lengths as this is known to cause bending in bilayers. It could be achieved with only minor alterations to the existing simulation code.

A further refinement would be to simulate the amphiphiles off-lattice using molecular dynamics. This would remove any artifacts caused by

the lattice and allow dynamic information to be obtained. This should also allow better comparisons to be made with experiment, but will be at the limit of what is possible with current computers.

REFERENCES

- Adam C D, *J. Chem. Soc. Faraday Trans. 1*, **80**, (1984)
- Alexander S, *J. Phys. (Paris)*, Lett **39**, L-1, (1978)
- Aranow R H, *J. Chem. Phys.*, **67**, 556, (1963)
- Baxter R J, "Exactly Solved Models In Statistical Mechanics", Academic Press (1982)
- Ben-Shaul A, Szleifer I and Gelbart W M, *Proc. Natl. Acad. Sci. USA*, **81**, 4601, (1984)
- Ben-Shaul A and Gelbart W M, *Am. Rev. Phys. Chem.*, **36**, 179, (1985)
- Ben-Shaul A, Szleifer I and Gelbart W M in "Physics of Amphiphiles: Micelles, Vesicles and Microemulsions", Degiorgio V and Corti M (eds), North-Holland, (1985a)
- Ben-Shaul A, Szleifer I and Gelbart W M, *J. Chem. Phys.*, **83**, 3597, (1985b)
- Ben-Shaul A, Szleifer L and Gelbart W M, "Springer Proceedings in Physics, Vol. 21, Physics of Amphiphile Layers", Springer-Verlag, (1987)
- Benedouch D, Chen S H, Koehler W C and Lin T S, *J. Chem. Phys.*, **76**, 5022, (1982)
- Benedouch D, Chen S H and Koehler W C, *J. Chem. Phys.*, **87**, 153, (1983)
- Berendsen H J C, Postma J P M, Van Gunsteren W F and Hermans J, in : "Intermolecular Forces", Pullman B (ed), Reidel, Dordrecht (1981)
- Binder K (ed), "Monte Carlo Methods in Statistical Methods", Topics in Current Physics 7, Springer-Verlag (1979)
- Binder K (ed), "Applications of the Monte Carlo Method in Statistical Physics", Topics in Current Physics 36 (2nd ed.), Spinger-Verlag (1987)
- Bishop M, Ceperley D, Frisch H L and Kalos M H, *J. Chem. Phys.*, **72**, 3228, (1980)
- Cabane B, Duplessix R and Zemb T, *J. Phys. (Paris)*, **46**, (1985)
- Cantor R S and McIlroy P M, *J. Chem. Phys.*, **90**, 4431, (1989)
- Care C M, *J. Chem. Soc. Faraday Trans. 1*, **83**, 2905, (1987a)
- Care C M, *J. Phys. C: Solid State Phys.*, **20**, 689, (1987b)
- Care C M, *J. Phys. Cond.*, **1**, 8583, (1989)

- Caspar D L D and Kurschner D A, *Nature, New Biol.*, **231**, 46, (1971)
- Chen K, Ebner C, Jayaprakash C and Pandit R, *Phys. Rev. A*, **38**, 6240, (1988)
- Chevalier Y and Chachaty C, *J. Chem. Phys. Lett.*, **89**, 875, (1985)
- Compagner A and Hoogland A, *J. Comp. Phys.*, **79**, 391, (1987)
- Corkill J M, Goodman J F and Tate J R, *Trans. Faraday Soc.*, **60**, 996, (1964)
- Cotterill R M J, *Biochem. Biophys. Acta*, **433**, 246, (1976)
- De Gennes P G and Taupin C, *J. Phys. Chem.*, **86**, 2294, (1982)
- Dewar R and Harris C K, *J. Phys. A*, **20**, 985, (1987)
- Dill K A and Flory P J, *Proc. Natl. Acad. Sci. USA*, **77**, 3115, (1980)
- Dill K A and Flory P J, *Proc. Natl. Acad. Sci. USA*, **78**, 676, (1981)
- Dill K A, Naghizadeh J and Marquesse J A, *Ann. Rev. Phys. Chem.*, **39**, 425, (1988)
- Eicke H F (ed), "Modern Trends of Colloid Science in Chemistry and Biology", Birkhauser Verlag (1985)
- Fincham D, *Molecular Simulation*, **01**, 1, (1987)
- Fischer M E, *Physics*, **3**, 225, (1967)
- Flory J P, "Statistical Mechanics of Chain Molecules", Interscience, New York (1969)
- Gompper G and Schick M, *Phys. Rev. Lett.*, **62**, 1647, (1989)
- Gruen D W R, *J. Phys. Chem.*, **89**, 146, (1985a)
- Gruen D W R, *J. Phys. Chem.*, **89**, 153, (1985b)
- Gunn J R and Dawson K A, *J. Chem. Phys.*, **91**, 6393, (1989)
- Haan W and Pratt R, *Chem. Phys. Lett.*, **79**, 436, (1981)
- Haile J M and O'Connell J P, *J. Phys. Chem.*, **88**, 6363, (1984)
- Hansen J P and McDonald I R, "Theory of Simple Liquids", Academic Press (1976)
- Harusawa F, Nakamura S and Mitsui T *Colloid and Polymer Sci.*, **252**, 613, (1974)
- Hill T L, "An Introduction to Statistical Thermodynamics", Addison - Wesley, (1962)

- Hoeve C A J and Benson G C, *ibid.*, **61**, 1149, (1957)
- Johnson I, Olofsson G and Jönsson B, *J. Chem. Soc., Faraday Trans. 1*, **83**, 3331, (1987)
- Jönsson B and Wennerström H, *J. Colloid Interface Sci.*, **80**, 482, (1981)
- Jönsson B, Edholm O and Teleman O, *J. Chem. Phys.*, **85**, 2259, (1986)
- Karaborni S and O'Connell J P, *J. Phys. Chem.*, **94**, 2624, (1990)
- Kazakov V A and Kazakova N F, *Kolloidn. Zh.*, **52**, 29, (1990)
- Kazakova N K, *Kolloidn. Zh.*, **52**, 39, (1990)
- Kirkpatrick S and Stol E P, *J. Comp. Phys.*, **40**, 517, (1981)
- Kox A J, Michels J P J and Wiegel F W, *Nature*, **287**, 317, (1980)
- Larson R G, Scriven L E and Davis H T, *J. Chem. Phys.*, **83**, 2411, (1985)
- Larson R G, *J. Chem. Phys.*, **89**, 1642, (1988)
- Lawson K D and Flautt T J, *J. Amer. Chem. Soc.*, **89**, 5489, (1967)
- Levine Y K, Bailey A I and Wilkins M H F, *Nature, Lond.*, **220**, 577, (1968)
- Levine Y K and Wilkins M H F, *Nature, New Biol.*, **230**, 69, (1971)
- Lindman B, in: Tadros (1983), 83
- Menger F M, *Acc. Chem. Res.*, **12**, 111, (1979)
- Metropolis N, Rosenbluth A W, Rosenbluth M N, Teller E H and Teller E, *J. Chem. Phys.*, **21**, (1953)
- Mittal K L and Lindman B (eds), "Surfactants in Solution" vols. 1,2, and 3, Plenum Press (1984)
- Mittal K L (ed), "Micellization, Solubilization and Microemulsions" vols. 1 and 2, Plenum Press (1977)
- Mukerjee P and Mysels K J, "Critical Micelle Concentrations of Aqueous Surfactant Systems", U.S. Government Printing Office (1971)
- Naghizadeh J and Dill K A, *J. Chem. Phys.*, (1988)
- O'Connor J, Wallace R G and Ch'ng Beng Tatt, in: Mittal (1984), vol. 2, 875
- Ottewill R H, in: Tadros (1983), 1
- Owenson B and Pratt L R, *J. Phys. Chem.*, **88**, 2905, (1984)
- Ploeg Van Der P and Berendseu H J C, *J. Chem. Phys.*, **76**, 3271, (1982)

- Ploeg Van Der P and Berendsen H J C, *Mol. Phys.*, **49**, 233, (1983)
- Poland D C and Scheraga H A, *J. Phys. Chem.*, **69**, 2431, (1965)
- Robledo A, *Phys. Rev. A.*, **36**, 4067, (1987)
- Ryckaert J P, Ciccotti G and Berendsen H J C, *J. Comput. Phys.*, **23**, 327, (1977)
- Seelig J and Niederburger W, *Biochemistry*, **13**, 1585, (1974)
- Seelig J, *Quart. Rev. Biophys.*, **10**, 353, (1977)
- Szleifer I, Ben-Shaul A and Gelbart W M, *J. Chem. Phys.*, **83**, 3612, (1985)
- Szleifer I, Ben-Shaul A and Gelbart W M, *J. Chem. Phys.*, **85**, 5345, (1986)
- Szleifer I, Ben-Shaul A and Gelbart W M, *NATO ASI Ser., Ser. B*, **174**, 843, (1988)
- Tadros T F (ed), "Surfactants", Academic Press (1903)
- Talmon Y and Prager S, *J. Chem. Phys.*, **69**, 2984, (1978)
- Tanford C, "The Hydrophobic Effect", Wiley-Interscience (1980)
- Taylor M P, Berger A E and Herzfeld J, *J. Chem. Phys.*, **91**, 528, (1989)
- Taylor M P and Herzfeld J, *Langmuir*, **6**, 911, (1990)
- Tiddy G J T, Rendall K and Galsworthy P, *Mol. Crystals Liquid Crystals*, **72**, 147, (1982)
- Tiddy G J T, in: Eicke (1985), pp148
- Toxveard S J, *J. Chem. Phys.*, **67**, 2056, (1977)
- Vacatello M and Yoon Do Y, *J. Chem. Phys.*, **92**, 757, (1990)
- Verlet L, *Phys. Rev.*, **159**, 98, (1967)
- Walderhaug H, Soderman O and Stilbs P, *J. Phys. Chem.*, **82**, 1655, (1984)
- Wall F T and Mandel F, *J. Chem. Phys.*, **64**, 4592, (1975)
- Walsh M F and Tiddy G J T, in: Wynn-Jones (1983), pp151
- Watanabe K, Ferrario M and Klein M I, *J. Phys. Chem.*, **92**, 819, (1988)
- Wennerström H and Lindman B, *Phys. Rep.*, **52**, 1, (1979)
- Wheeler J C, *J. Chem. Phys.*, **62**, 433, (1975)

Widom B, *J. Phys. Chem.*, **88**, 6508, (1984)

Widom B, *J. Chem. Phys.*, **84**, 6943, (1986)

Woods M C, Haile J M and O'Connell J P, *J. Phys. Chem.*, **90**, 1875,
(1986)

amphiphile % vol. conc.	N	lattice dimensions	reduced temperature			thermalisation M.C steps	data collecting M.C steps	No of data dumps
			init.	final	step			
0.78	512	64x64x64	1.5	0.8	0.02	50 000	200 000	100
3.125	1024	64x64x64	1.5	0.8	0.02	50 000	200 000	100
6.25	512	32x32x32	1.3	0.7	0.02	20 000	200 000	200
10.0	819	32x32x32	1.4	0.9	0.02	20 000	200 000	200
12.5	1024	32x32x32	1.4	0.7	0.02	20 000	200 000	200
15.0	1229	32x32x32	1.4	0.9	0.02	20 000	200 000	200
20.0	410	32x16x16	1.4	0.8	0.02	20 000	200 000	200
25.0	512	32x16x16	1.4	0.9	0.02	20 000	200 000	200
30.0	614	32x16x16	1.4	0.9	0.02	20 000	200 000	200
35.0	717	32x16x16	1.4	0.7	0.02	20 000	200 000	200
40.0	819	32x16x16	1.4	0.9	0.02	20 000	200 000	200
45.0	460	16x16x16	1.4	0.9	0.02	20 000	200 000	200
48.0	492	16x16x16	1.4	0.8	0.02	20 000	200 000	200
50.0	512	16x16x16	1.4	0.9	0.02	20 000	200 000	200
52.5	538	16x16x16	1.4	0.9	0.02	20 000	200 000	200
55.0	563	16x16x16	1.4	0.8	0.02	20 000	200 000	200
57.5	589	16x16x16	1.4	0.9	0.02	20 000	200 000	200
60.0	614	16x16x16	1.4	0.9	0.02	20 000	200 000	200
62.5	640	16x16x16	1.4	0.9	0.02	20 000	200 000	200
65.0	666	16x16x16	1.5	0.9	0.02	20 000	200 000	200
70.0	717	16x16x16	1.5	0.9	0.02	20 000	200 000	200
75.0	768	16x16x16	1.4	0.9	0.02	20 000	200 000	200

table A1 : Run conditions for the $s=4$, $\gamma=-2.0$ phase diagram. A Monte Carlo (M.C) step involves N attempted moves, where N is the number of amphiphiles. The number of data dumps is the number of configurations used to sample data.

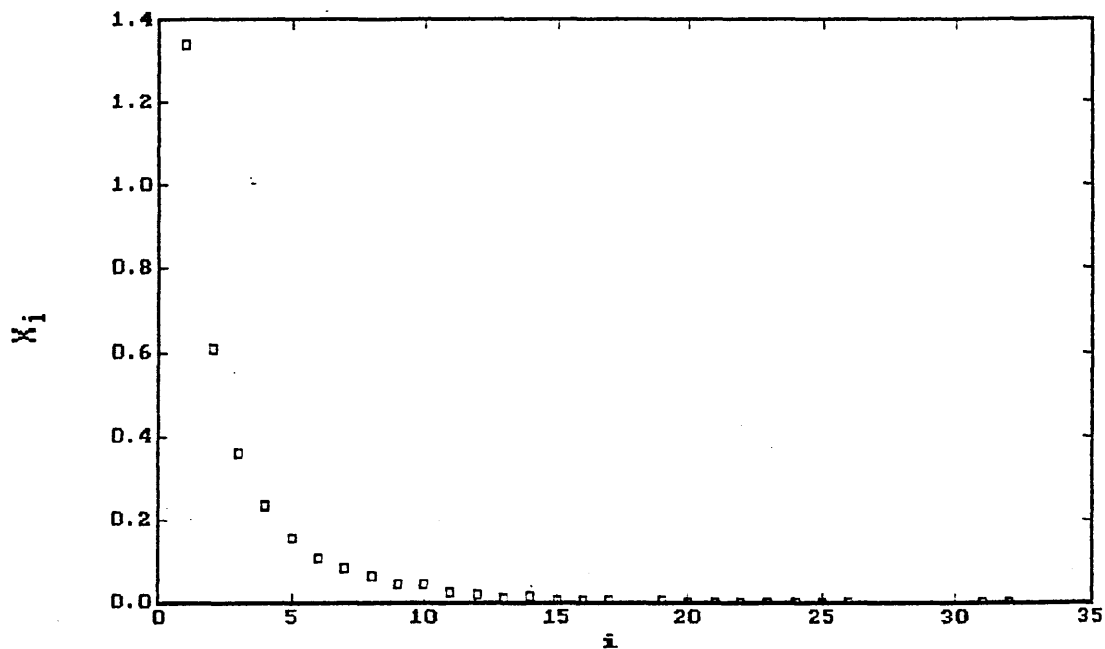


Figure A1 : Variation of concentration of monomers in clusters of size i , X_i , with i . Amphiphile concentration=3.125% chain length=4, $\gamma=-2.0$ and $\beta^{-1}=1.5$

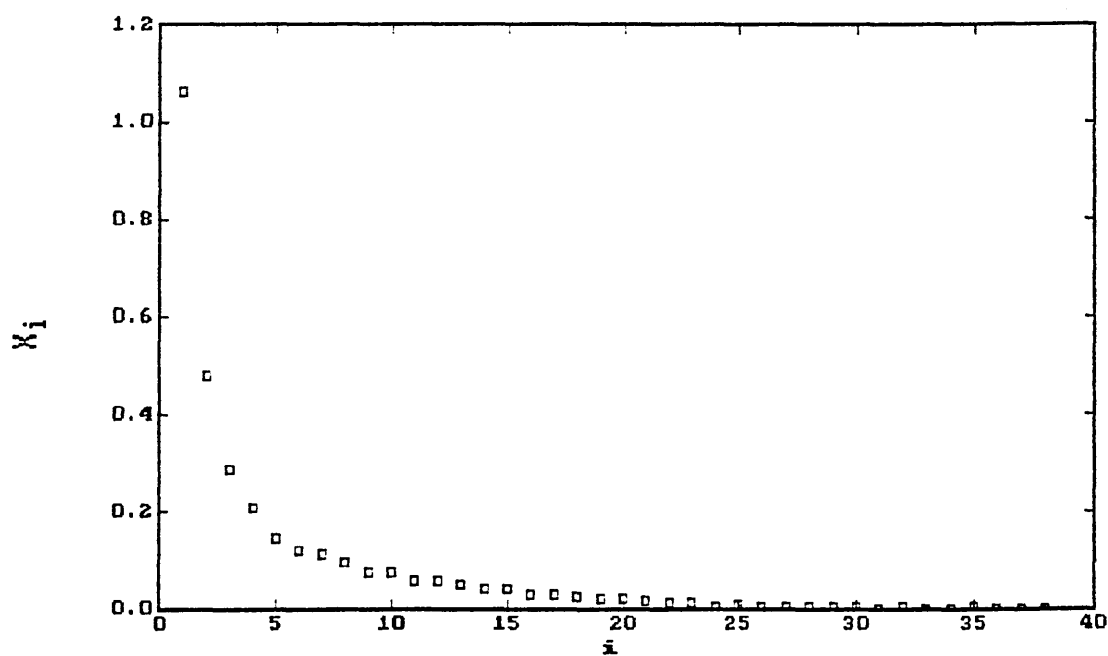


Figure A2 : Variation of concentration of monomers in clusters of size i , X_i , with i . Amphiphile concentration=3.125%, chain length=4, $\gamma=-2.0$ and $\beta^{-1}=1.38$

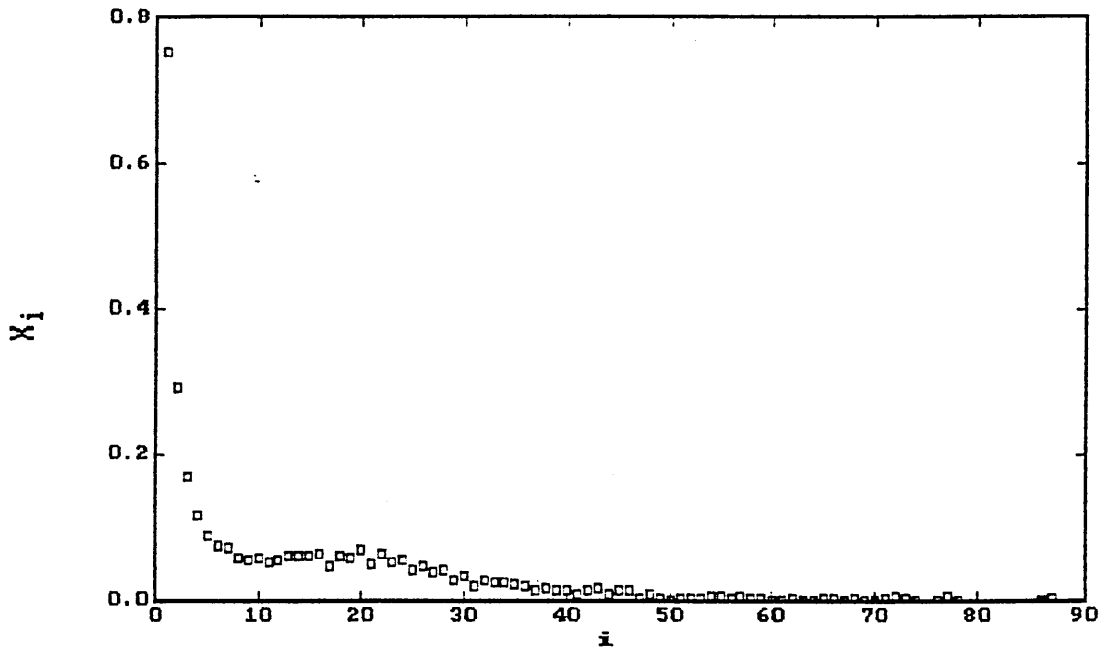


Figure A3 : Variation of concentration of monomers in clusters of size i , X_i , with i . Amphiphile concentration=3.125%, chain length=4, $\gamma=-2.0$ and $\beta^{-1}=1.24$

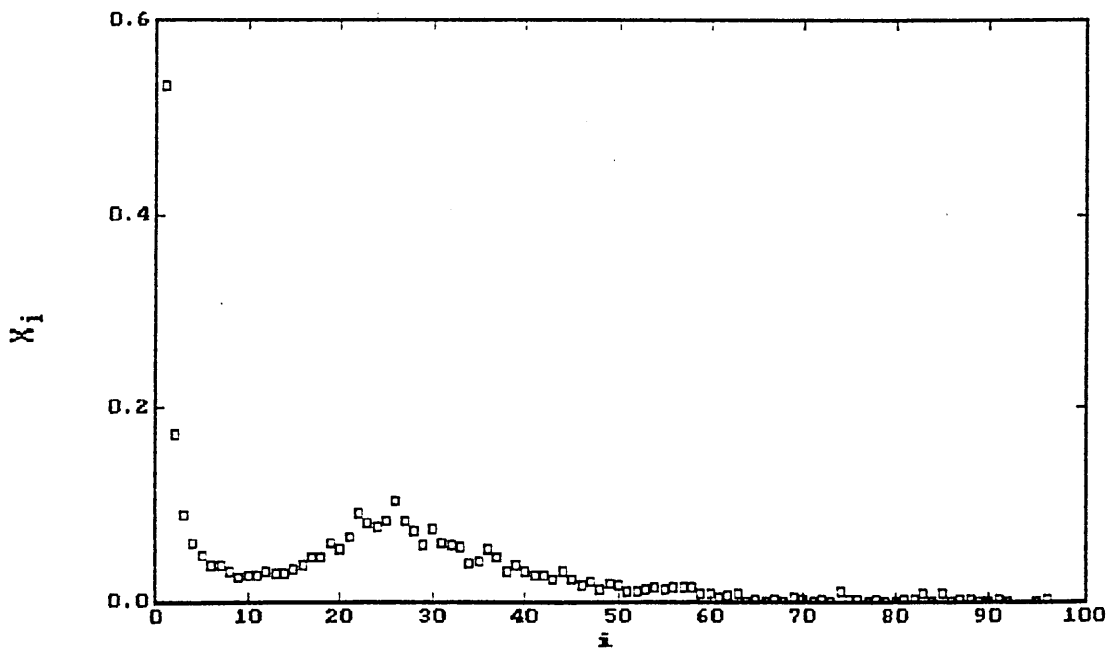


Figure A4 : Variation of concentration of monomers in clusters of size i , X_i , with i . Amphiphile concentration=3.125%, chain length=4, $\gamma=-2.0$ and $\beta^{-1}=1.16$

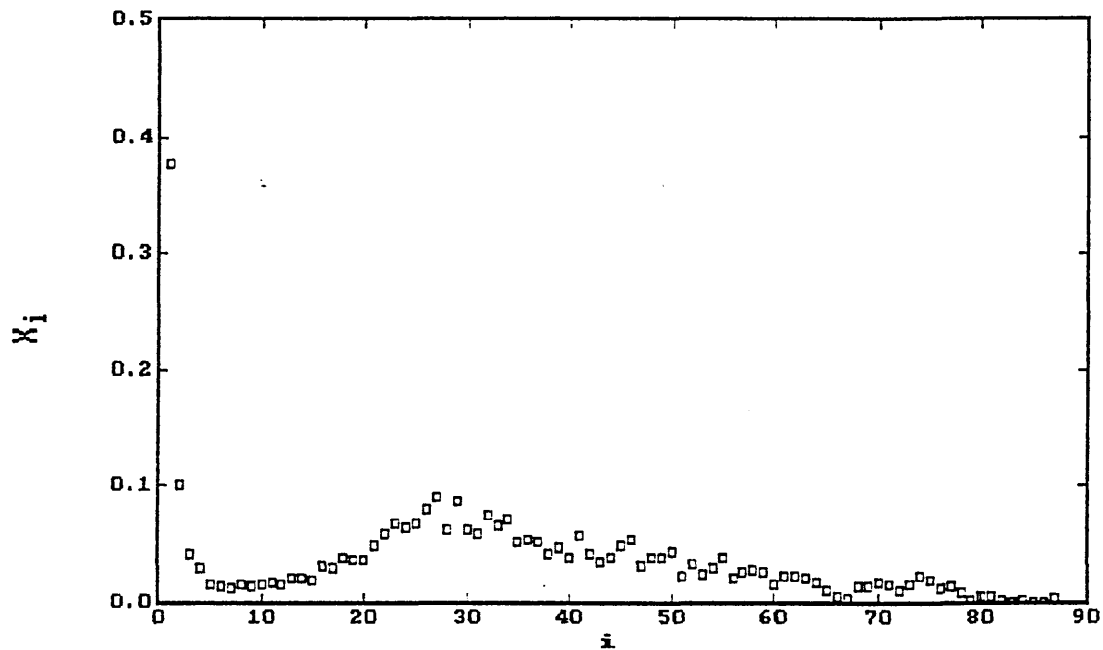


Figure A5 : Variation of concentration of monomers in clusters of size i , X_i , with i . Amphiphile concentration=3.125% chain length=4, $\gamma=-2.0$ and $\beta^{-1}=1.10$

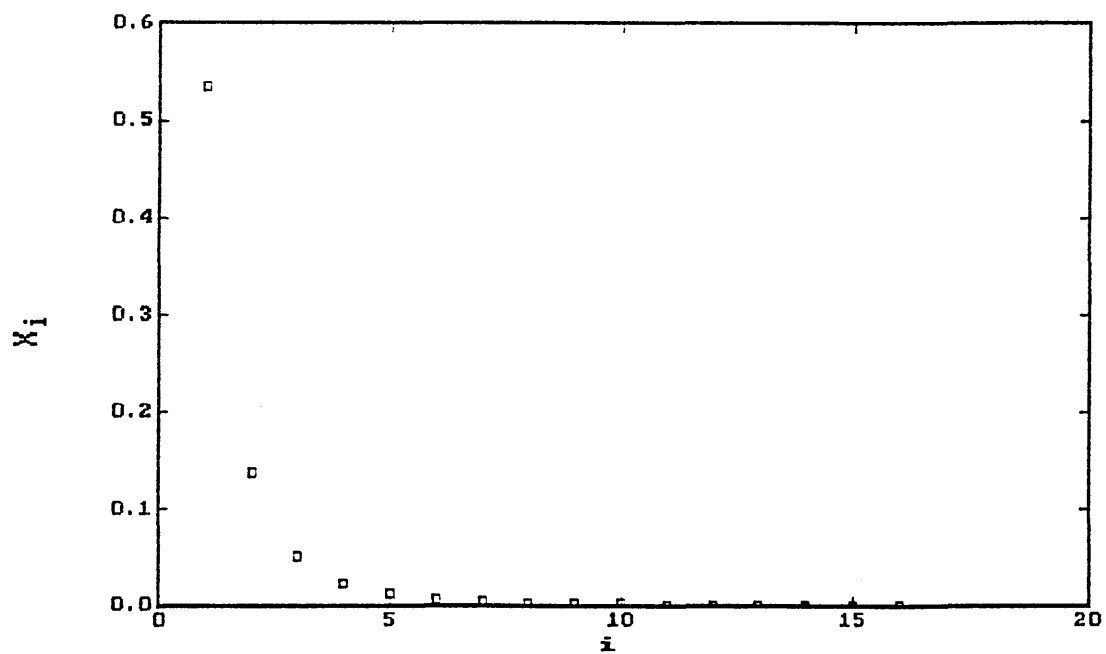


Figure A6 : Variation of concentration of monomers in clusters of size i , X_i , with i . Amphiphile concentration=0.78%, chain length=4, $\gamma=-2.0$ and $\beta^{-1}=1.24$

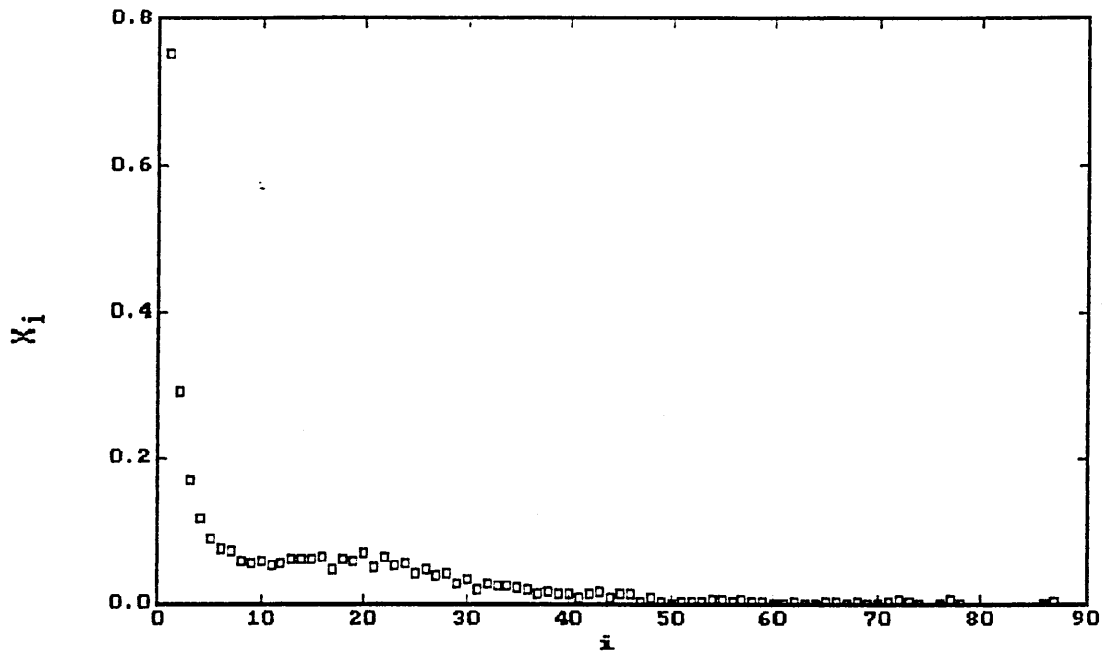


Figure A7 : Variation of concentration of monomers in clusters of size i , X_i , with i . Amphiphile concentration=3.125% chain length=4, $\gamma=-2.0$ and $\beta^{-1}=1.24$

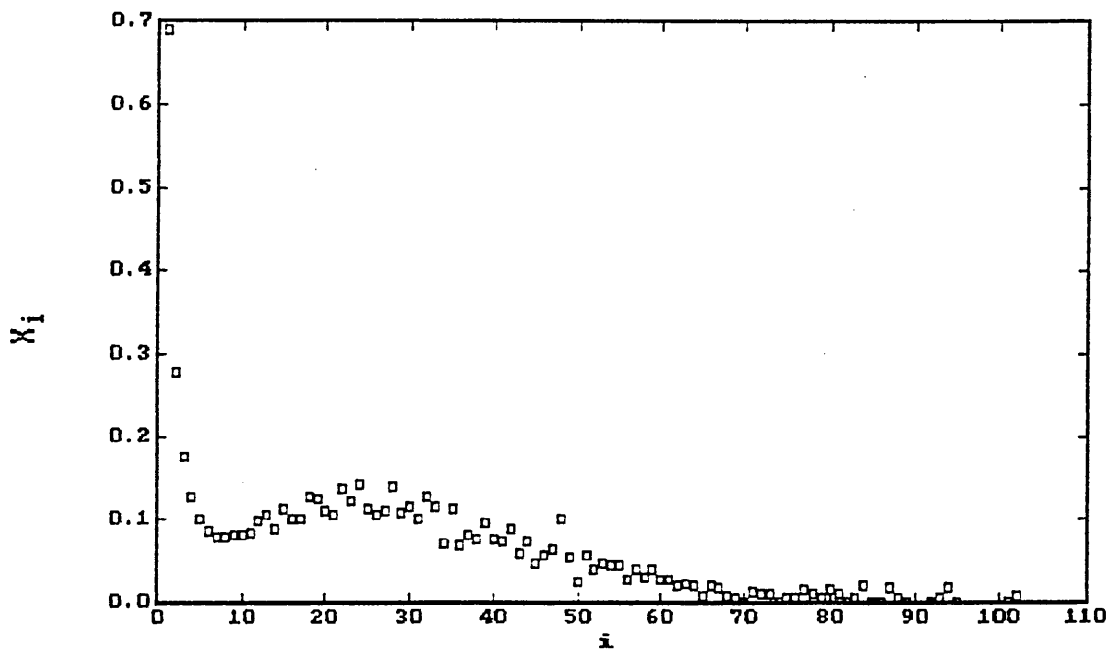


Figure A8 : Variation of concentration of monomers in clusters of size i , X_i , with i . Amphiphile concentration=6.25%, chain length=4, $\gamma=-2.0$ and $\beta^{-1}=1.24$

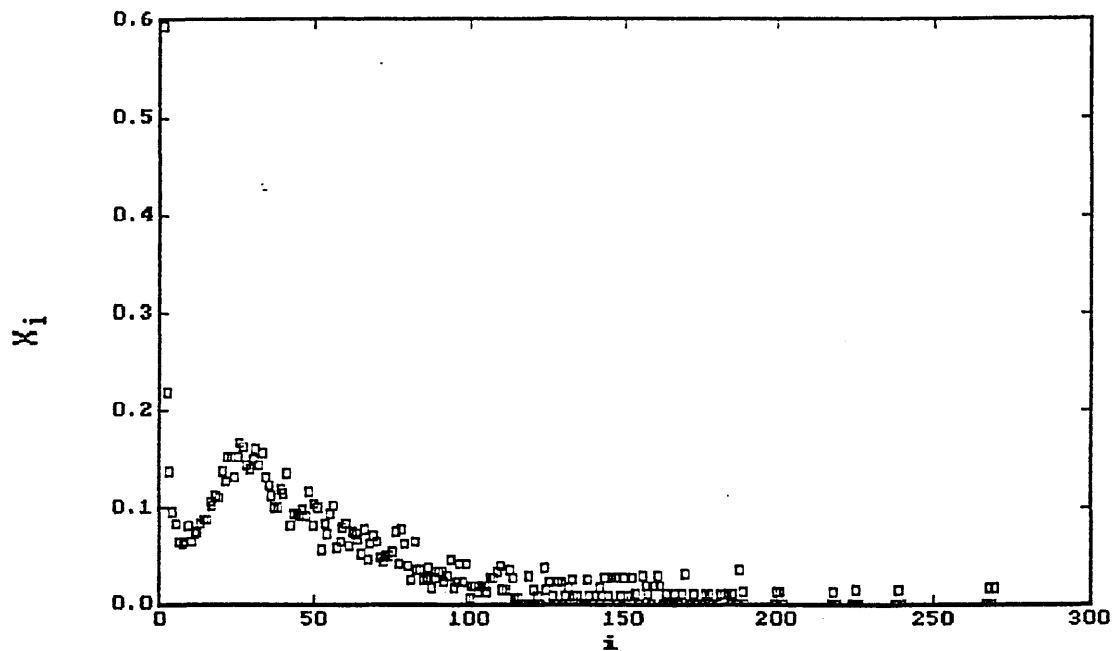


Figure A9 : Variation of concentration of monomers in clusters of size i , X_i , with i . Amphiphile concentration=10.0%, chain length=4, $\gamma=-2.0$ and $\beta^{-1}=1.24$

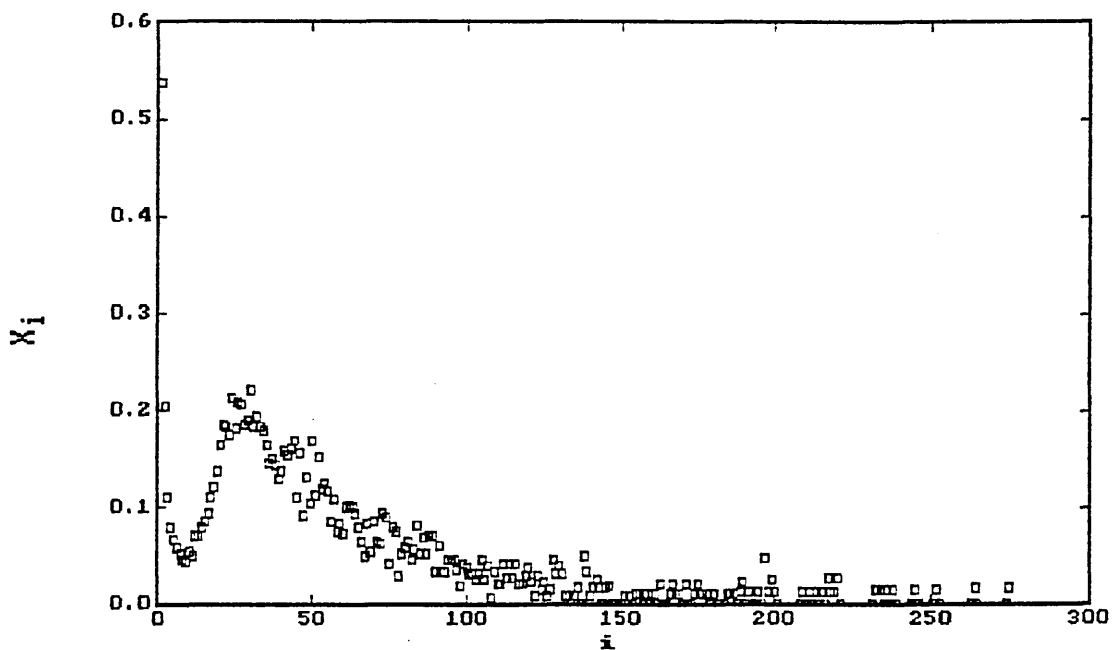


Figure A10 : Variation of concentration of monomers in clusters of size i , X_i , with i . Amphiphile concentration=12.5%, chain length=4, $\gamma=-2.0$ and $\beta^{-1}=1.24$

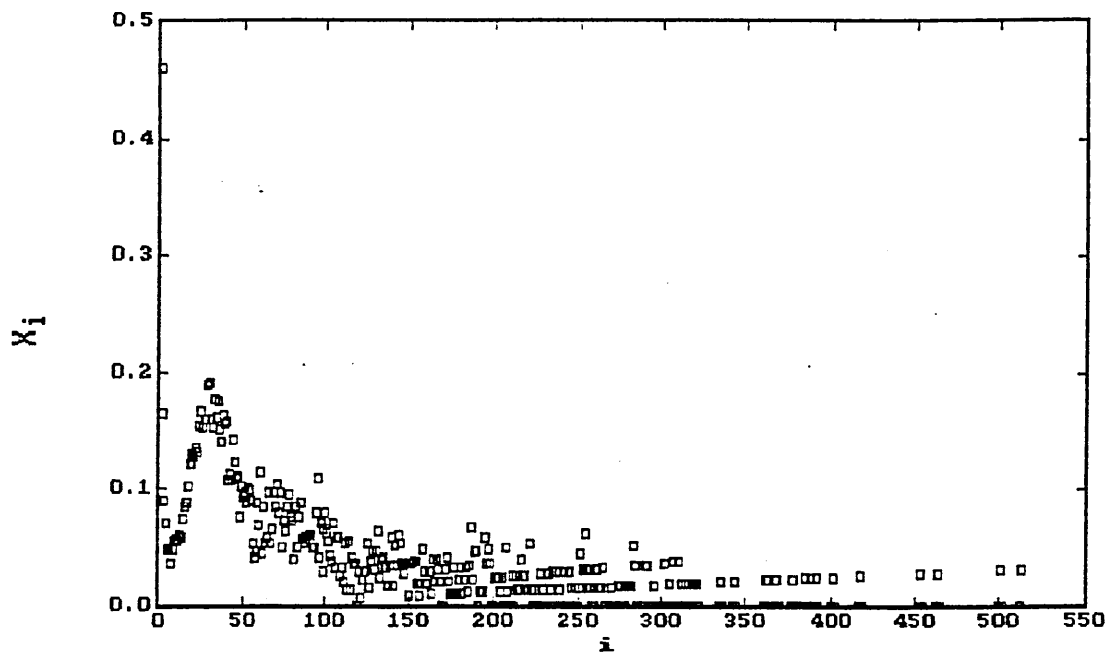


Figure A11 : Variation of concentration of monomers in clusters of size i , X_i , with i . Amphiphile concentration=15.0%, chain length=4, $\gamma=-2.0$ and $\beta^{-1}=1.24$

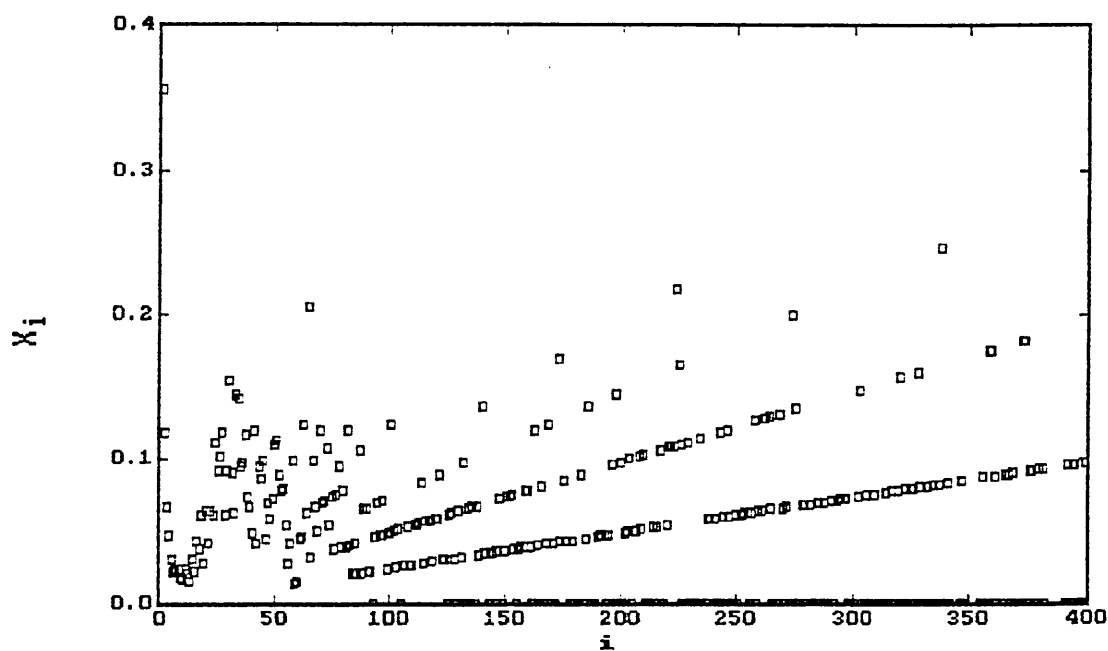


Figure A12 : Variation of concentration of monomers in clusters of size i , X_i , with i . Amphiphile concentration=20.0%, chain length=4, $\gamma=-2.0$ and $\beta^{-1}=1.24$

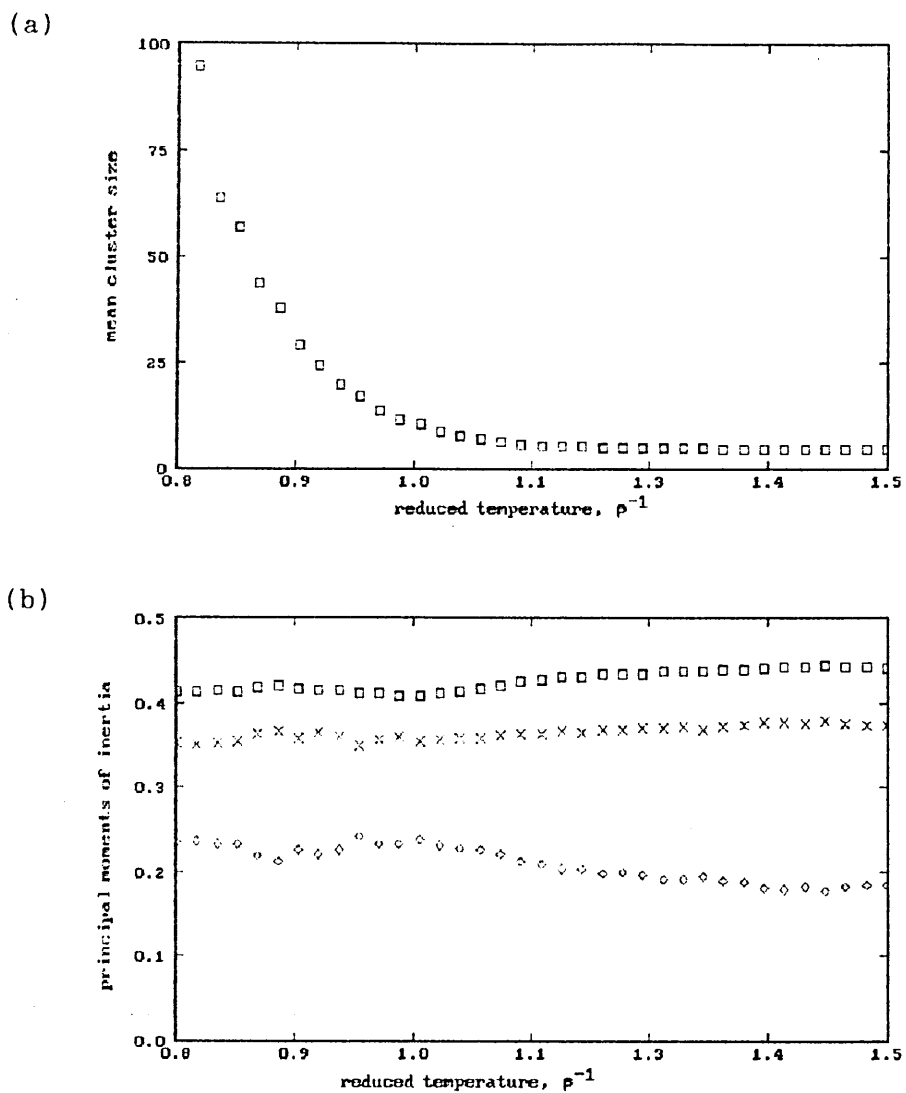
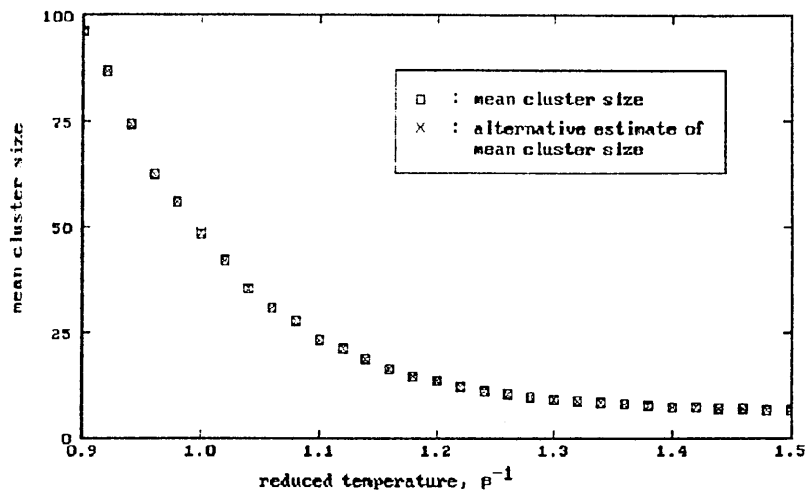


Figure A13 : Behaviour of the $s=4$, $\gamma=-2.0$, 0.78% amphiphile conc. system on cooling. (a) mean cluster size against reduced temperature (b) principal moments of inertia against reduced temperature

(a)



(b)

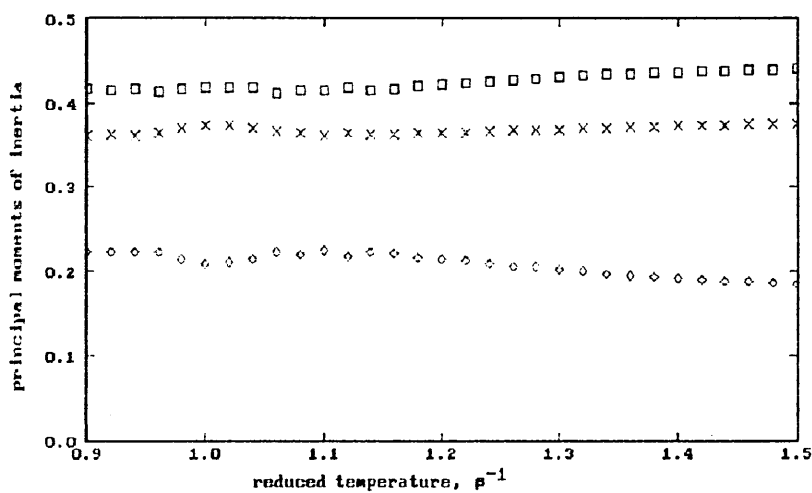


Figure A14 : Behaviour of the $s=4$, $\gamma=-2.0$, 3.125% amphiphile conc. system on cooling. (a) mean cluster size against reduced temperature (b) principal moments of inertia against reduced temperature

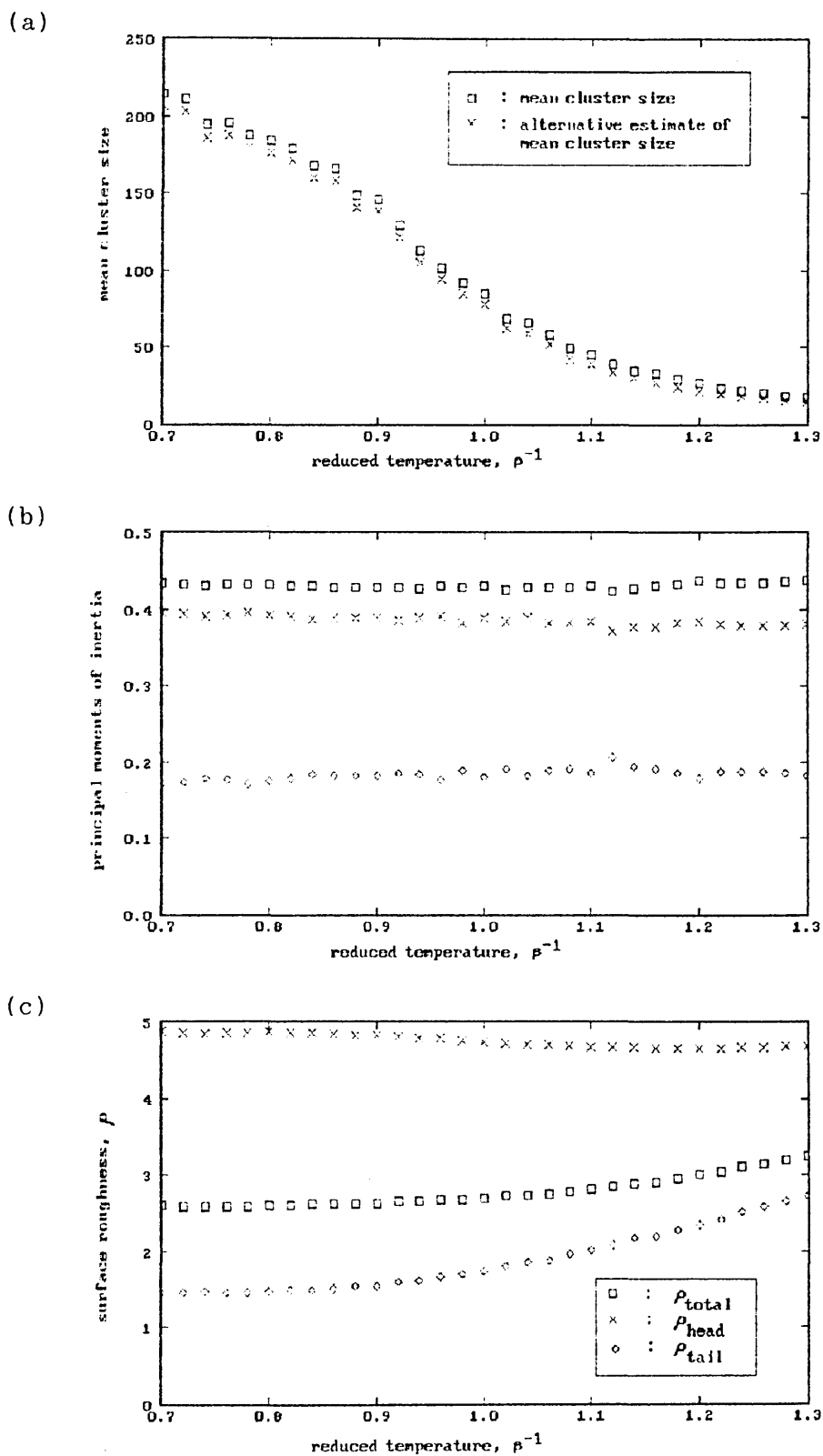


Figure A15 : Behaviour of the $s=4$, $\gamma=-2.0$, 6.25% amphiphile conc. system on cooling. (a) mean cluster size against reduced temperature (b) principal moments of inertia against reduced temperature (c) surface roughness against temperature.

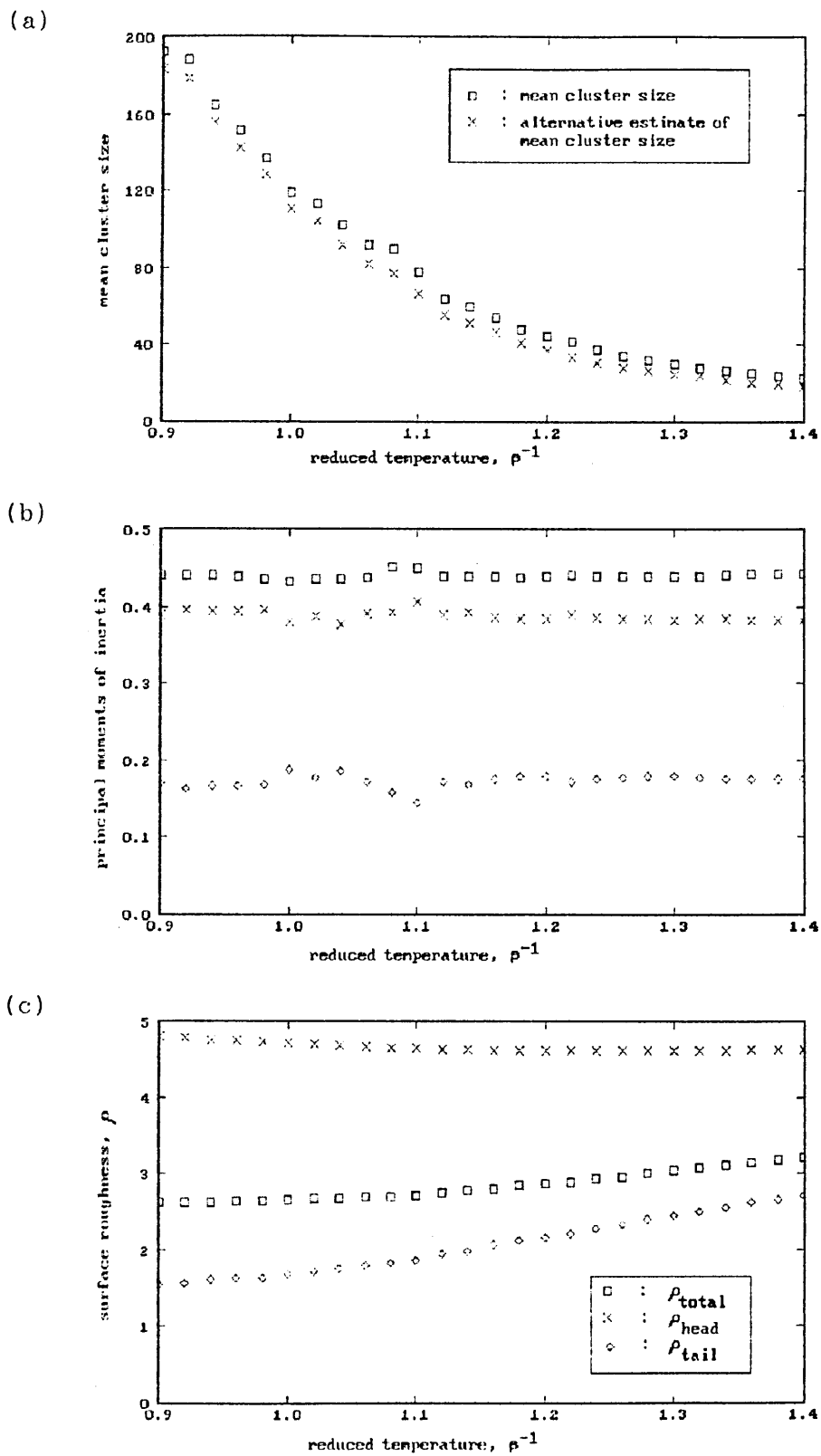


Figure A16 : Behaviour of the $s=4$, $\gamma=-2.0$, 10.0% amphiphile conc. system on cooling. (a) mean cluster size against reduced temperature (b) principal moments of inertia against reduced temperature (c) surface roughness against temperature.

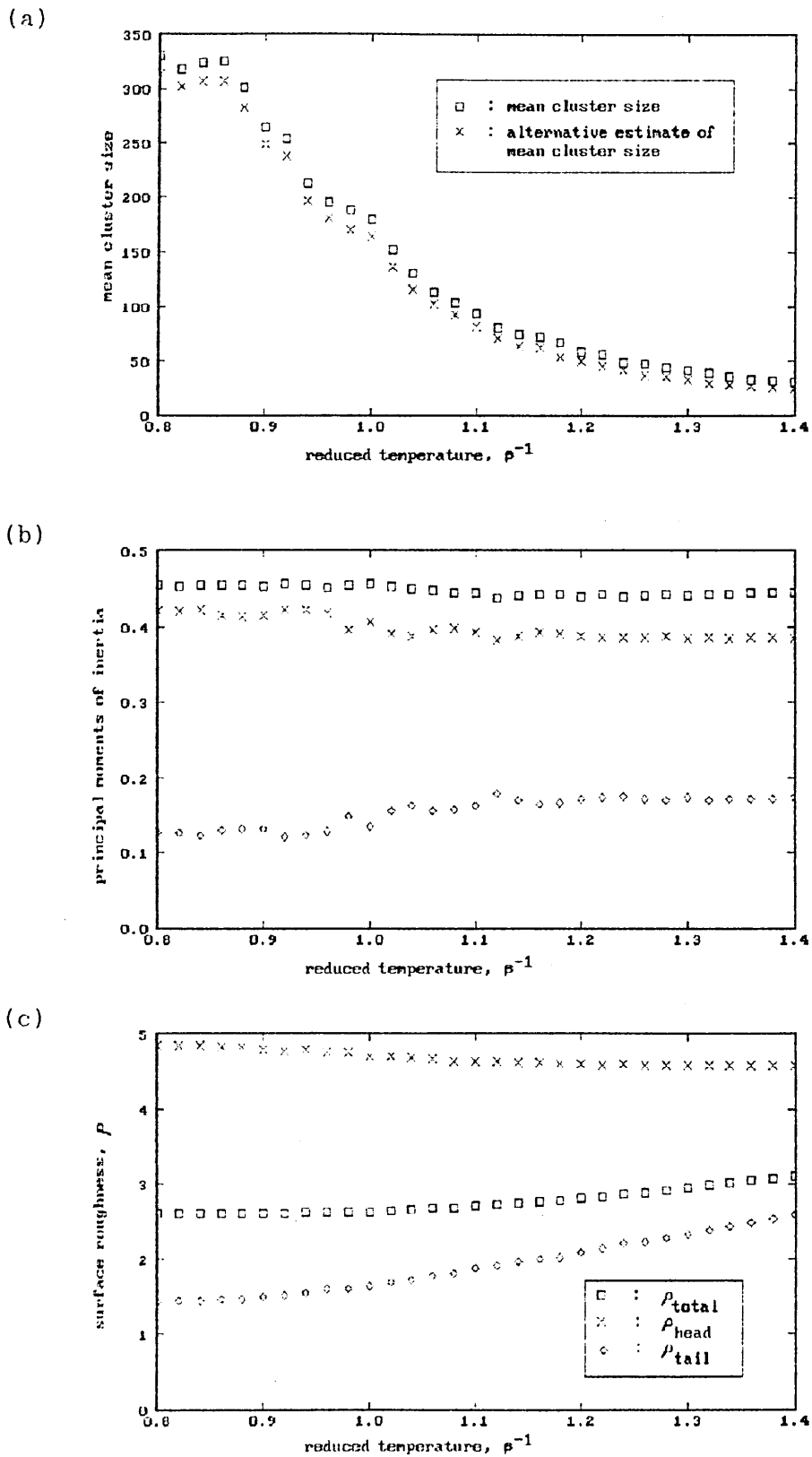


Figure A17 : Behaviour of the $s=4$, $\gamma=-2.0$, 12.5% amphiphile conc. system on cooling. (a) mean cluster size against reduced temperature (b) principal moments of inertia against reduced temperature (c) surface roughness against temperature.

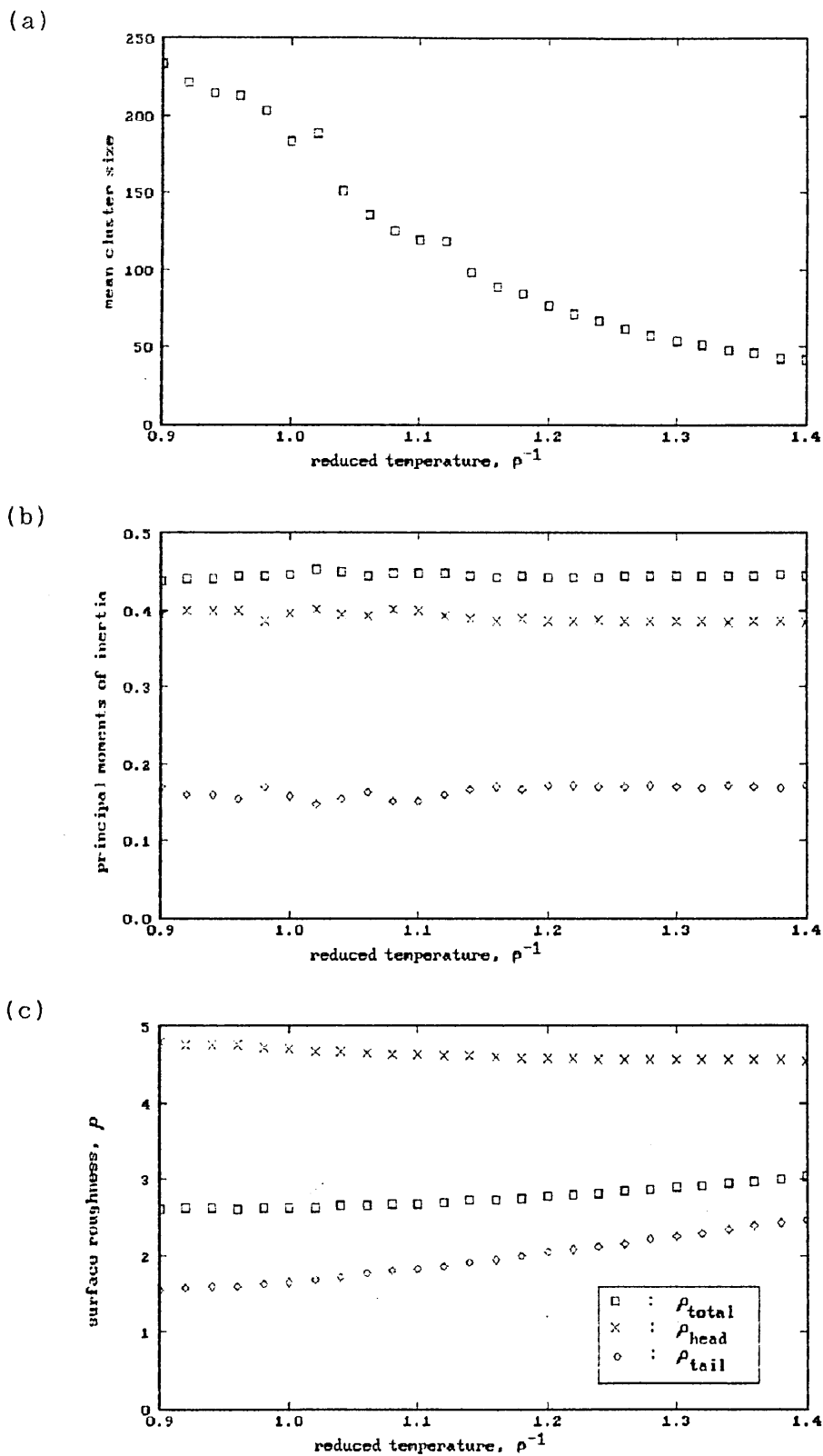


Figure A18 : Behaviour of the $s=4$, $\gamma=-2.0$, 15.0% amphiphile conc. system on cooling. (a) mean cluster size against reduced temperature (b) principal moments of inertia against reduced temperature (c) surface roughness against temperature.

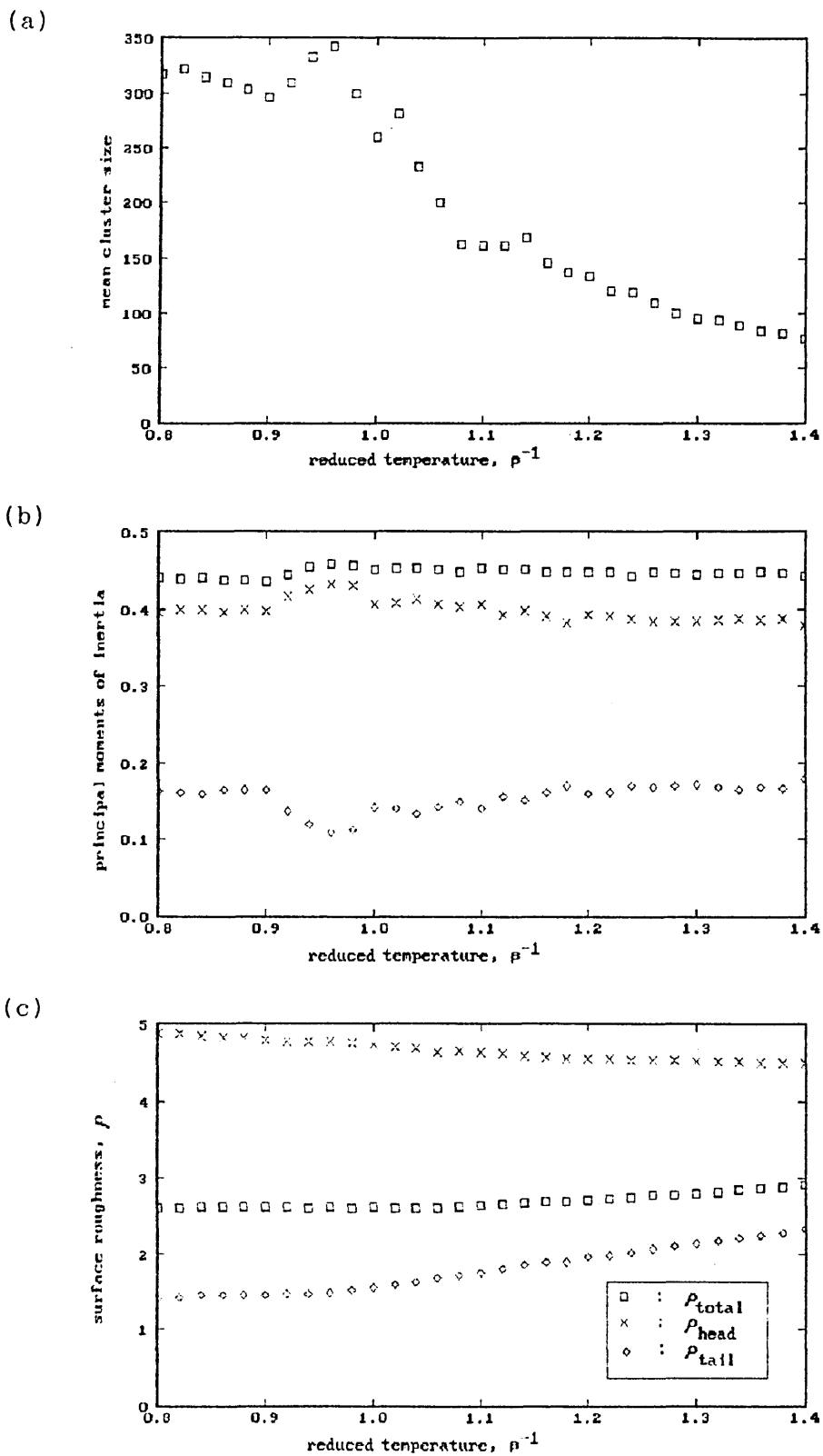


Figure A19 : Behaviour of the $s=4$, $\gamma=-2.0$, 20.0% amphiphile conc. system on cooling. (a) mean cluster size against reduced temperature (b) principal moments of inertia against reduced temperature (c) surface roughness against temperature.

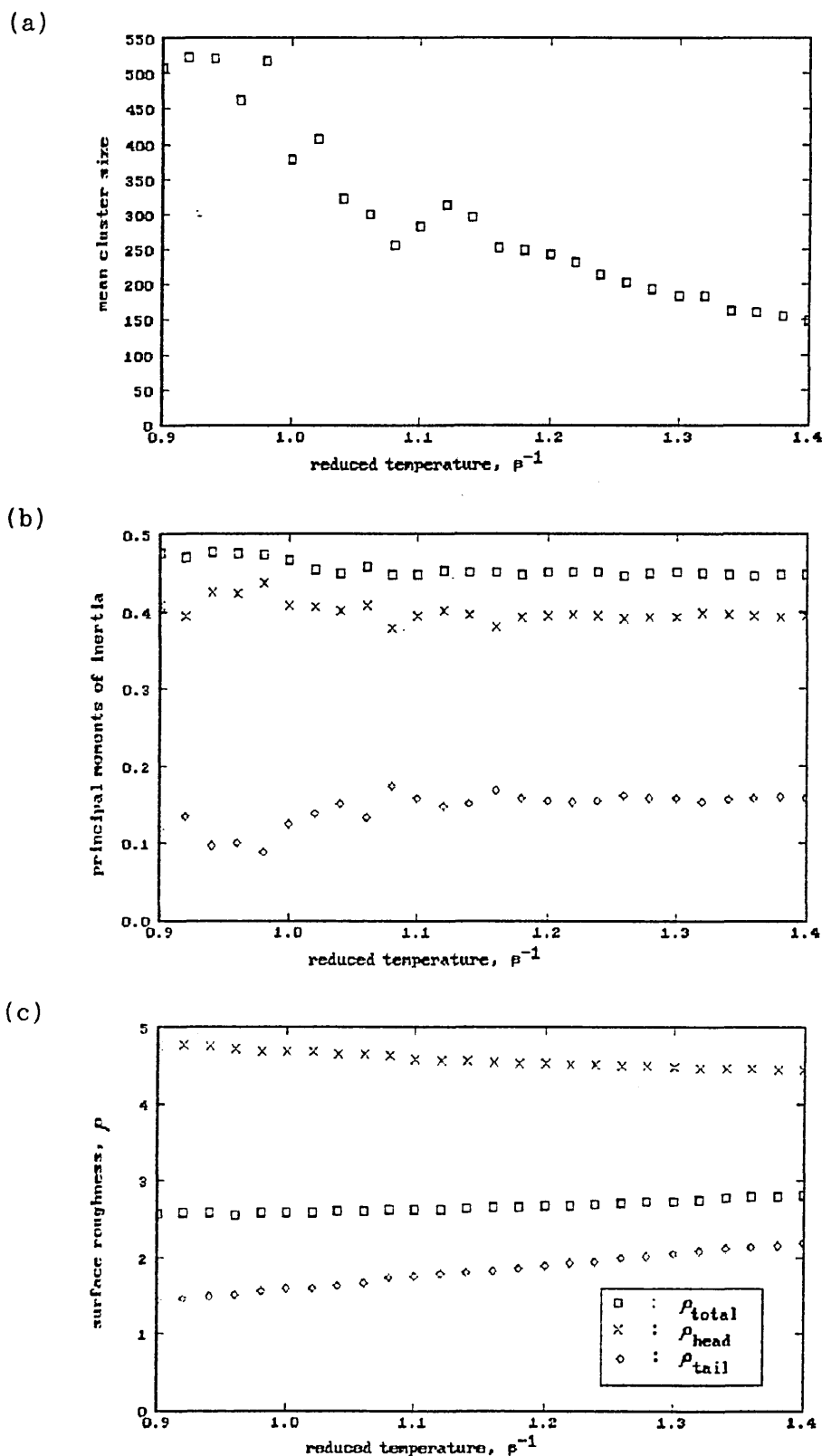


Figure A20 : Behaviour of the $s=4$, $\gamma=-2.0$, 25.0% amphiphile conc. system on cooling. (a) mean cluster size against reduced temperature (b) principal moments of inertia against reduced temperature (c) surface roughness against temperature.

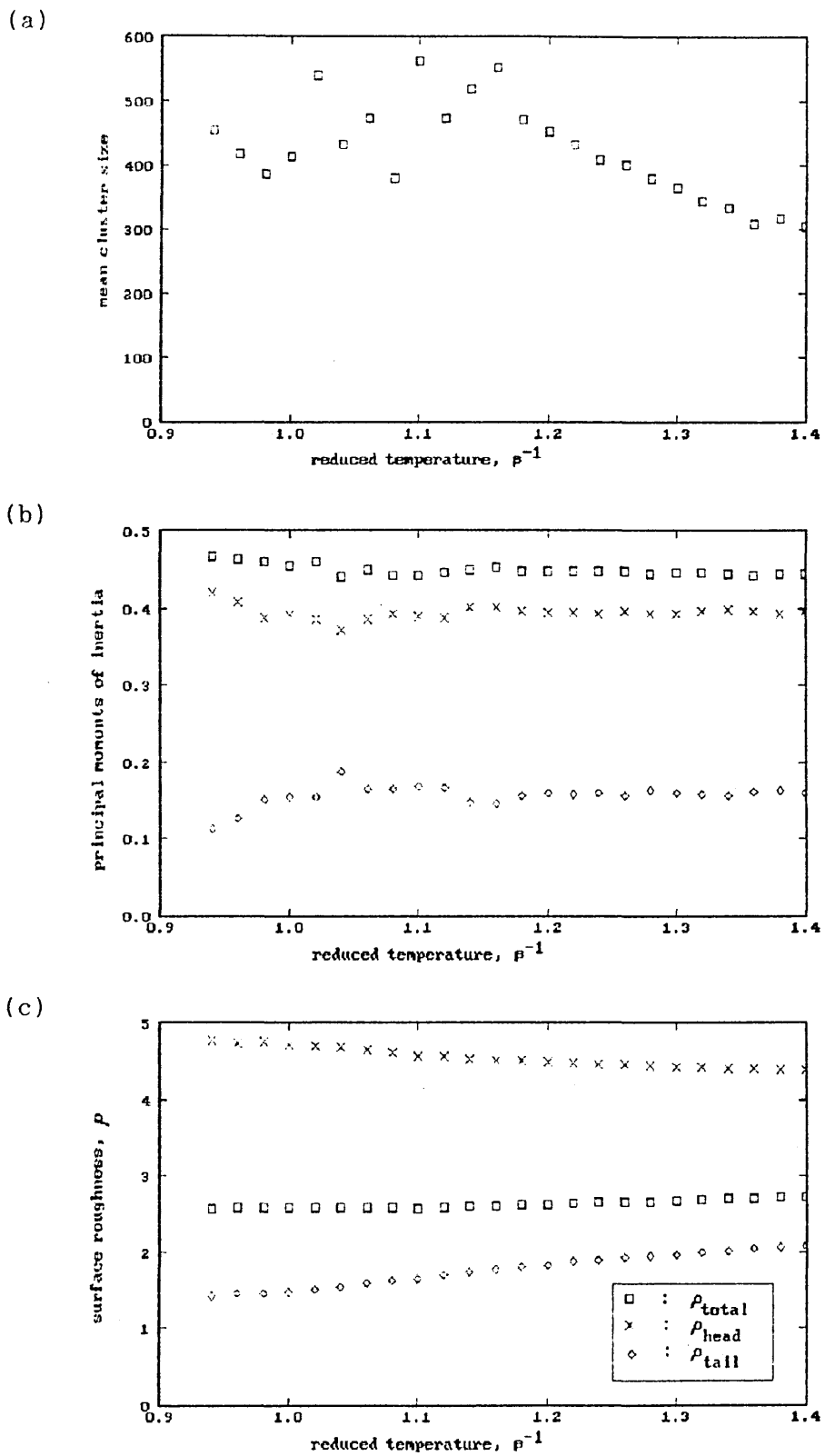


Figure A21 : Behaviour of the $s=4$, $\gamma=-2.0$, 30.0% amphiphile conc. system on cooling. (a) mean cluster size against reduced temperature (b) principal moments of inertia against reduced temperature (c) surface roughness against temperature.

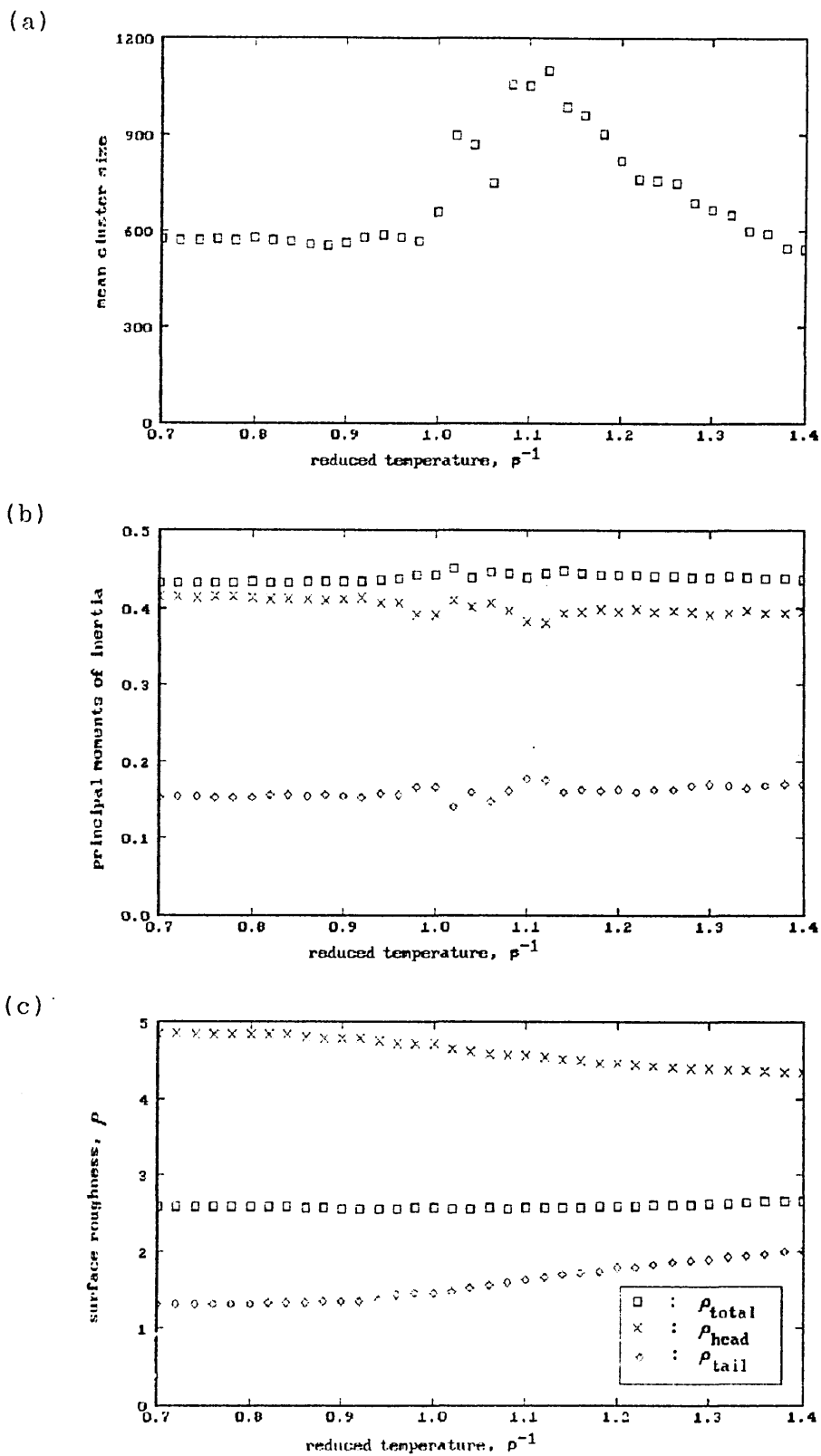


Figure A22 : Behaviour of the $s=4$, $\gamma=-2.0$, 35.0% amphiphile conc. system on cooling. (a) mean cluster size against reduced temperature (b) principal moments of inertia against reduced temperature (c) surface roughness against temperature.

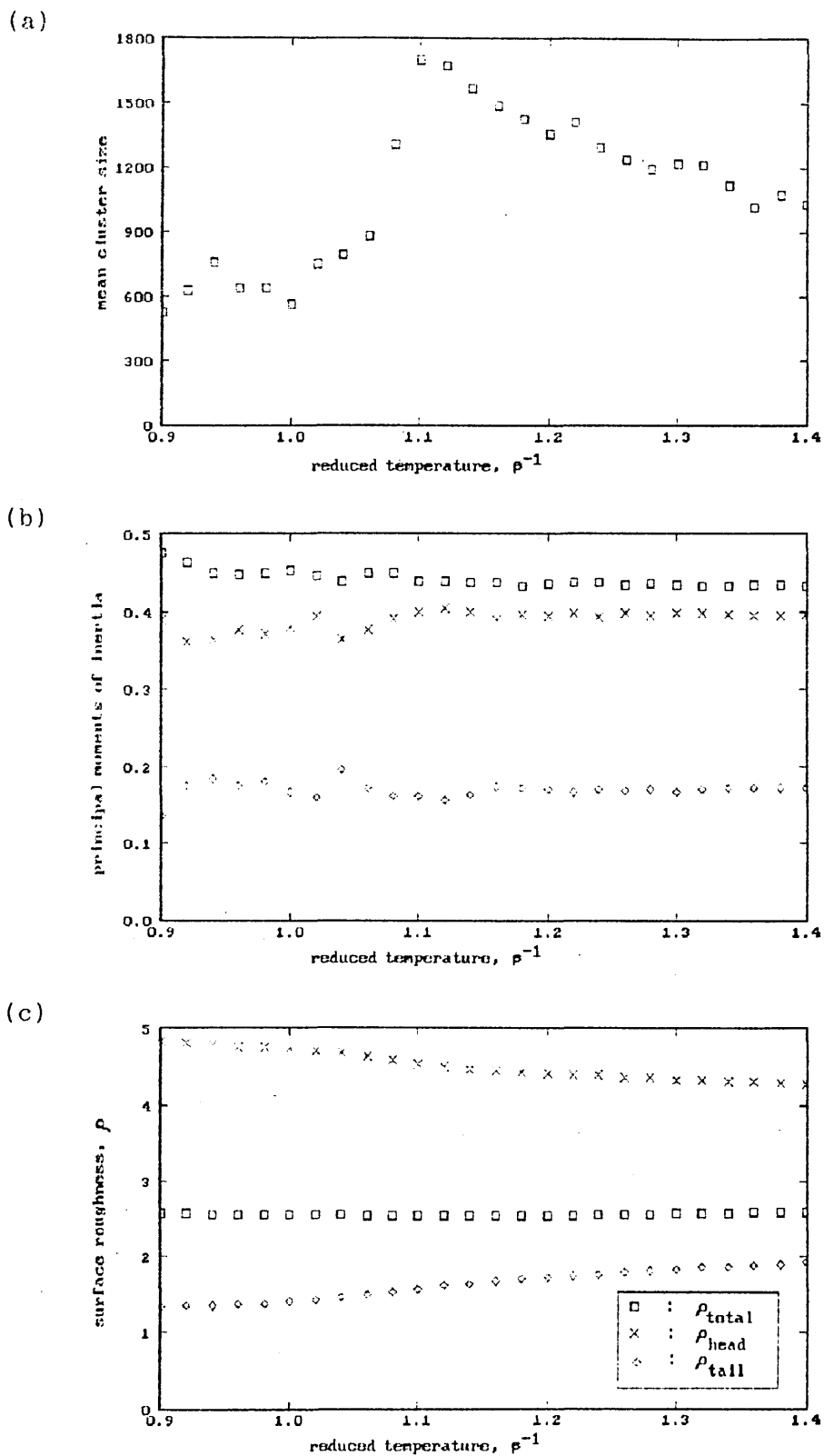
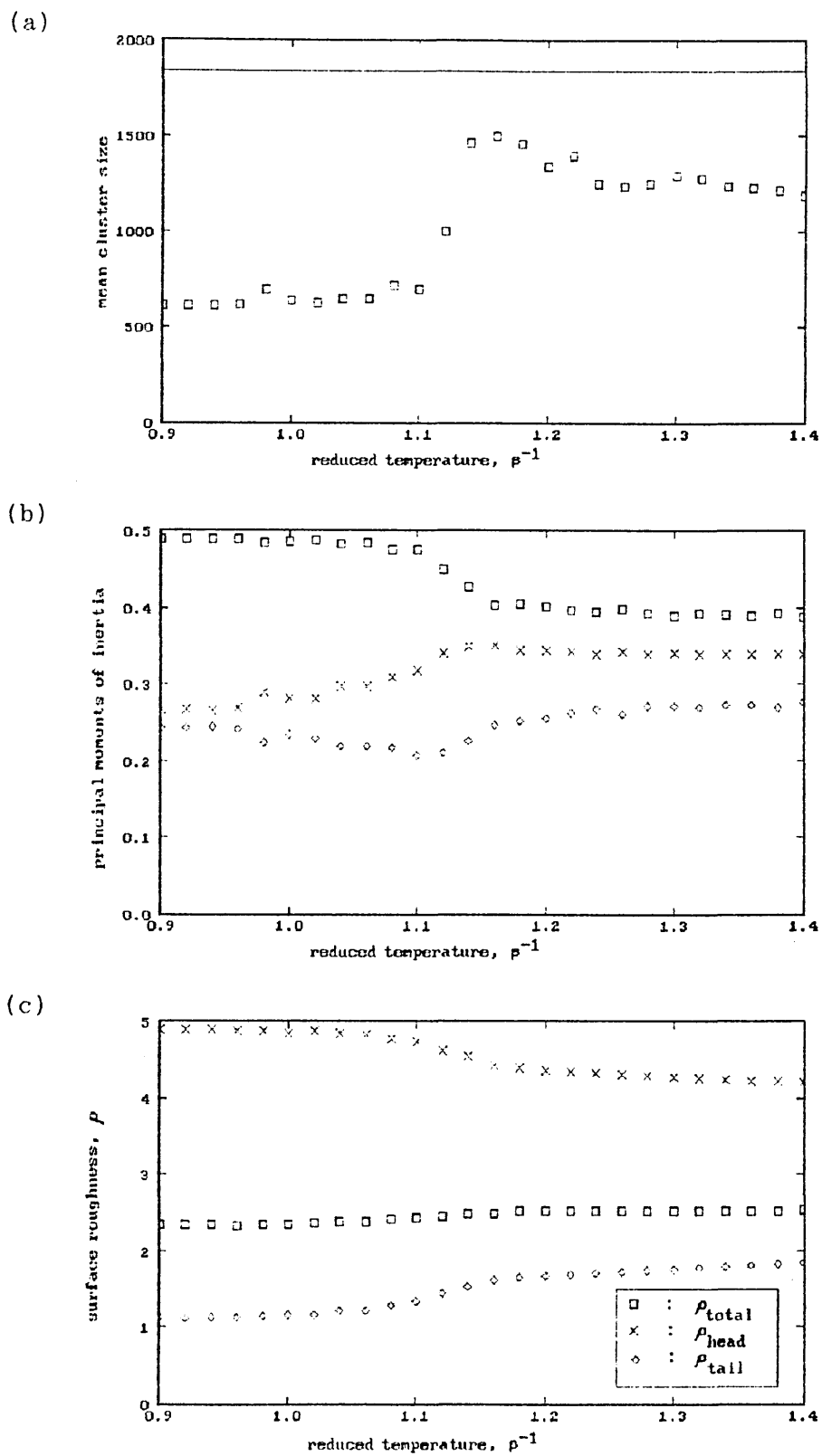


Figure A23 : Behaviour of the $s=4$, $\gamma=-2.0$, 40.0% amphiphile conc. system on cooling. (a) mean cluster size against reduced temperature (b) principal moments of inertia against reduced temperature (c) surface roughness against temperature.



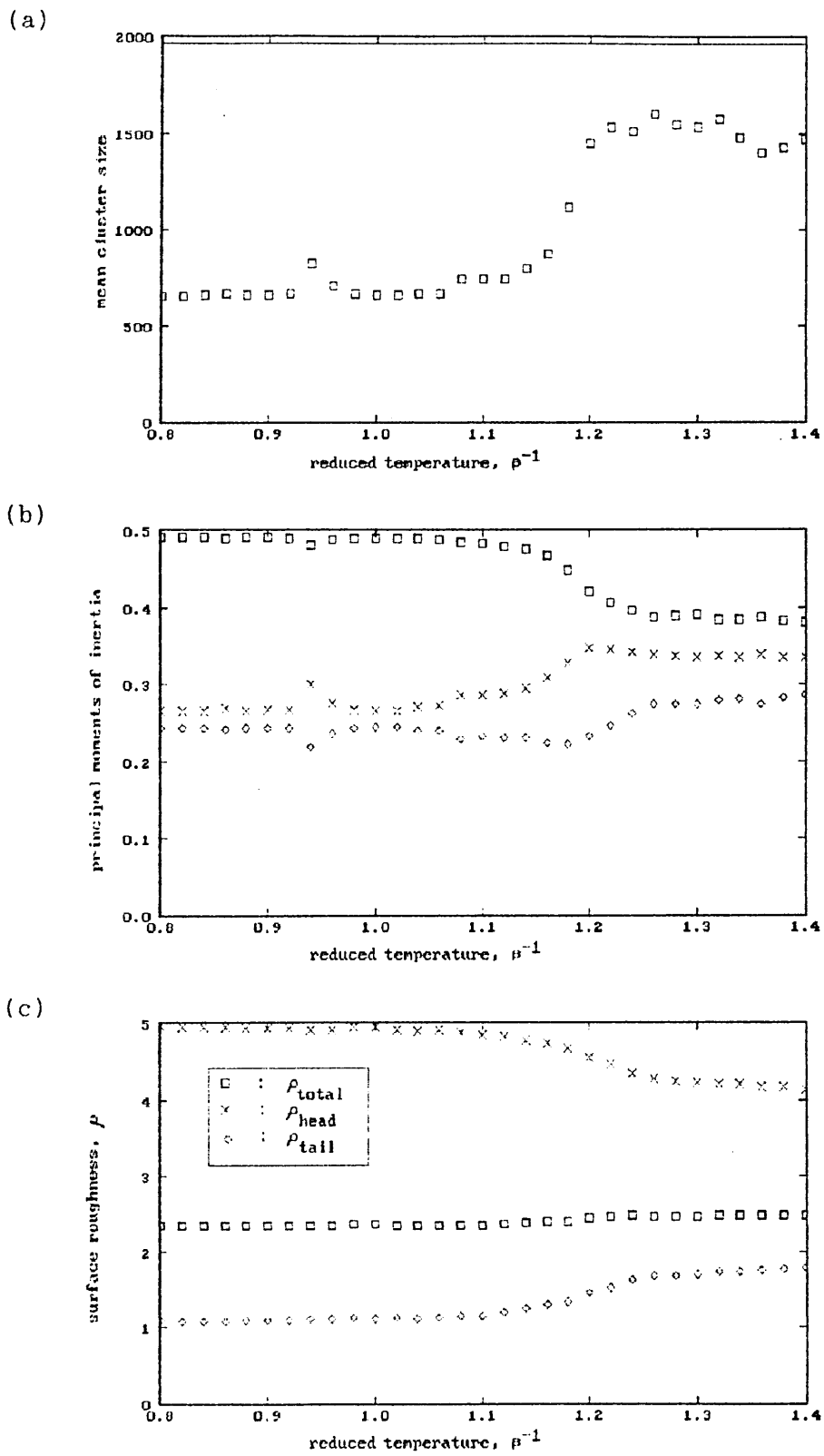


Figure A25 : Behaviour of the $s=4$, $\gamma=-2.0$, 48.0% amphiphile conc. system on cooling. (a) mean cluster size against reduced temperature (b) principal moments of inertia against reduced temperature (c) surface roughness against temperature.

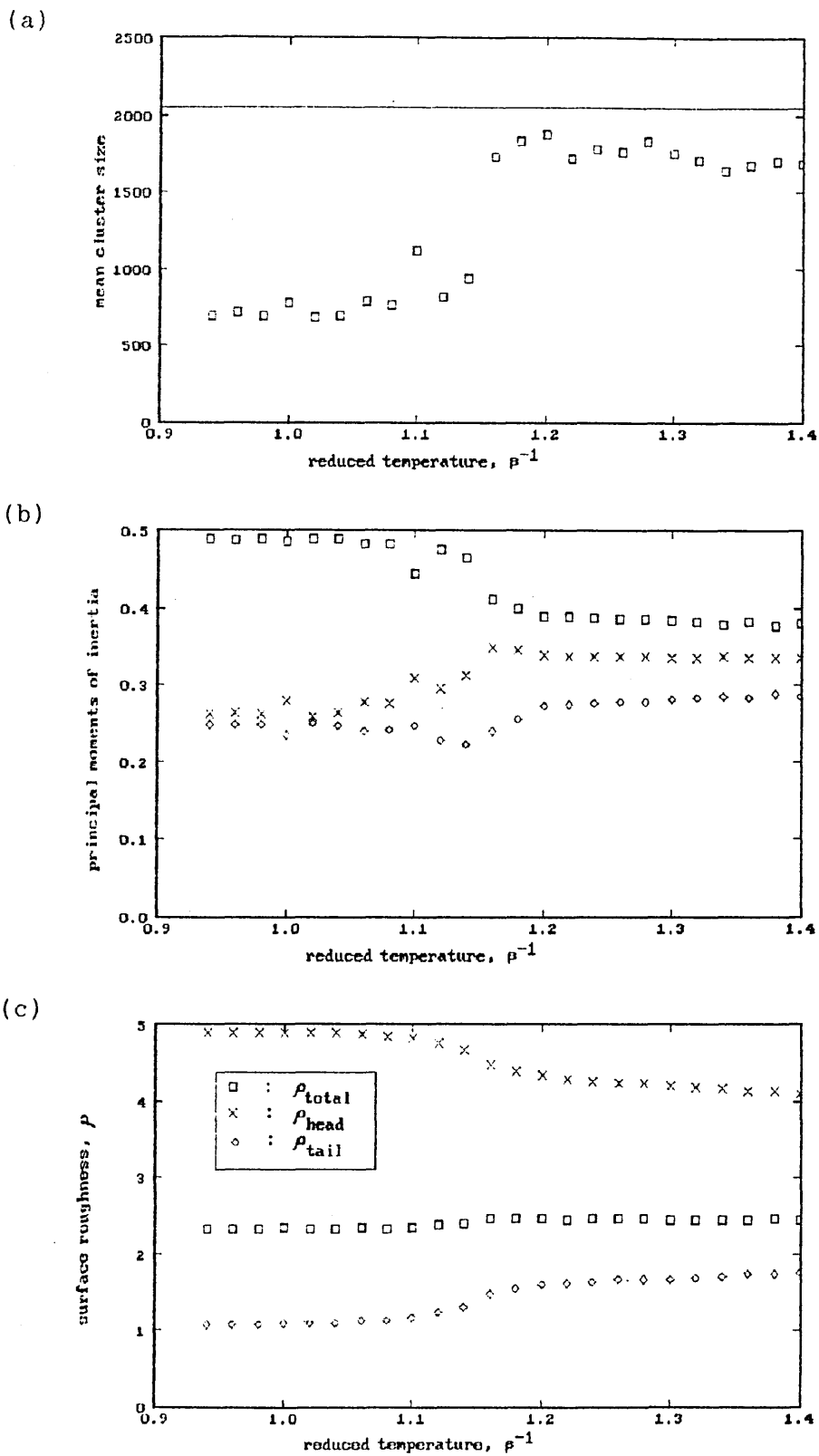


Figure A26 : Behaviour of the $s=4$, $\gamma=-2.0$, 50.0% amphiphile conc. system on cooling. (a) mean cluster size against reduced temperature (b) principal moments of inertia against reduced temperature (c) surface roughness against temperature.

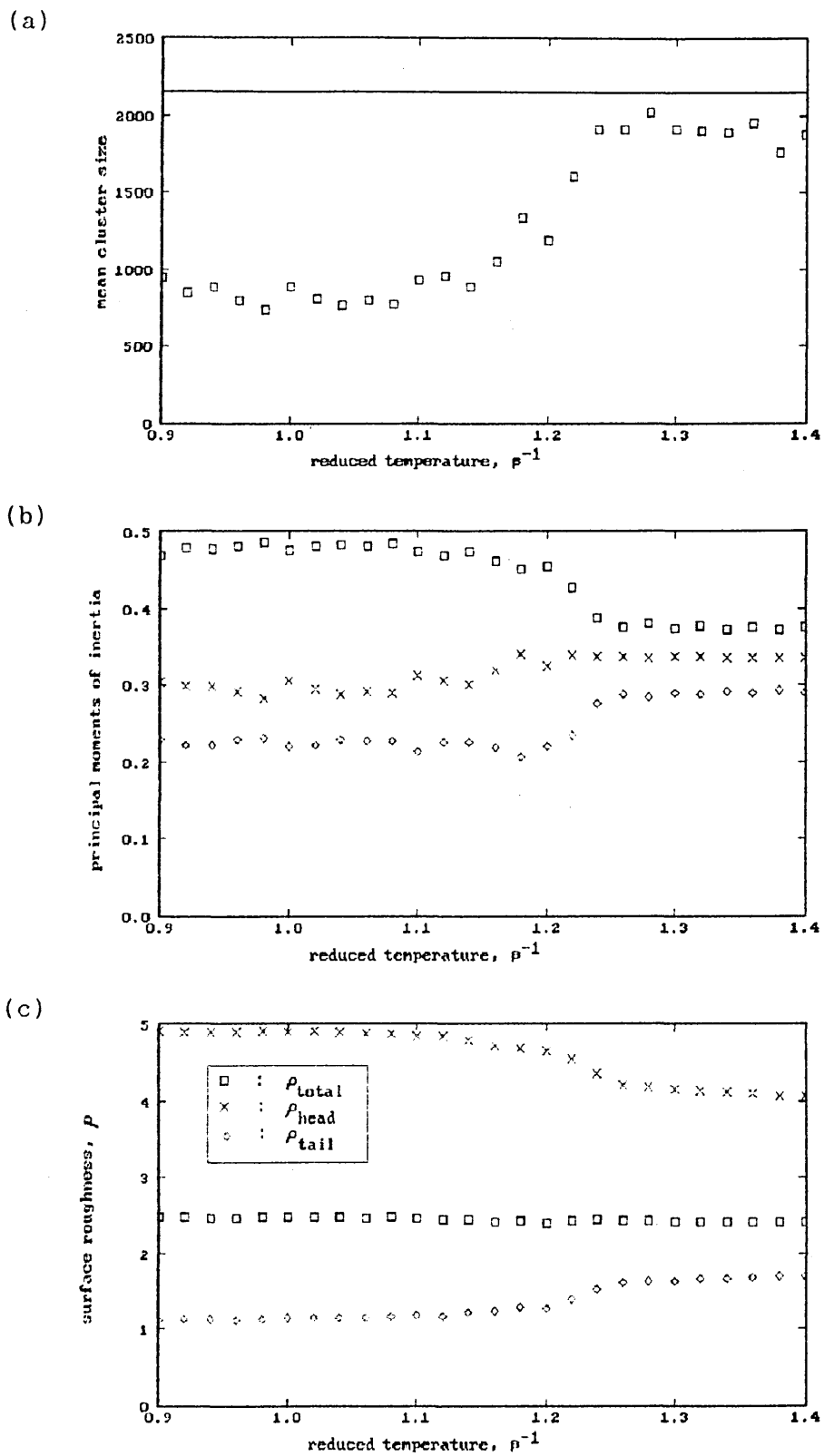


Figure A27 : Behaviour of the $s=4$, $\gamma=-2.0$, 52.5% amphiphile conc. system on cooling. (a) mean cluster size against reduced temperature (b) principal moments of inertia against reduced temperature (c) surface roughness against temperature.

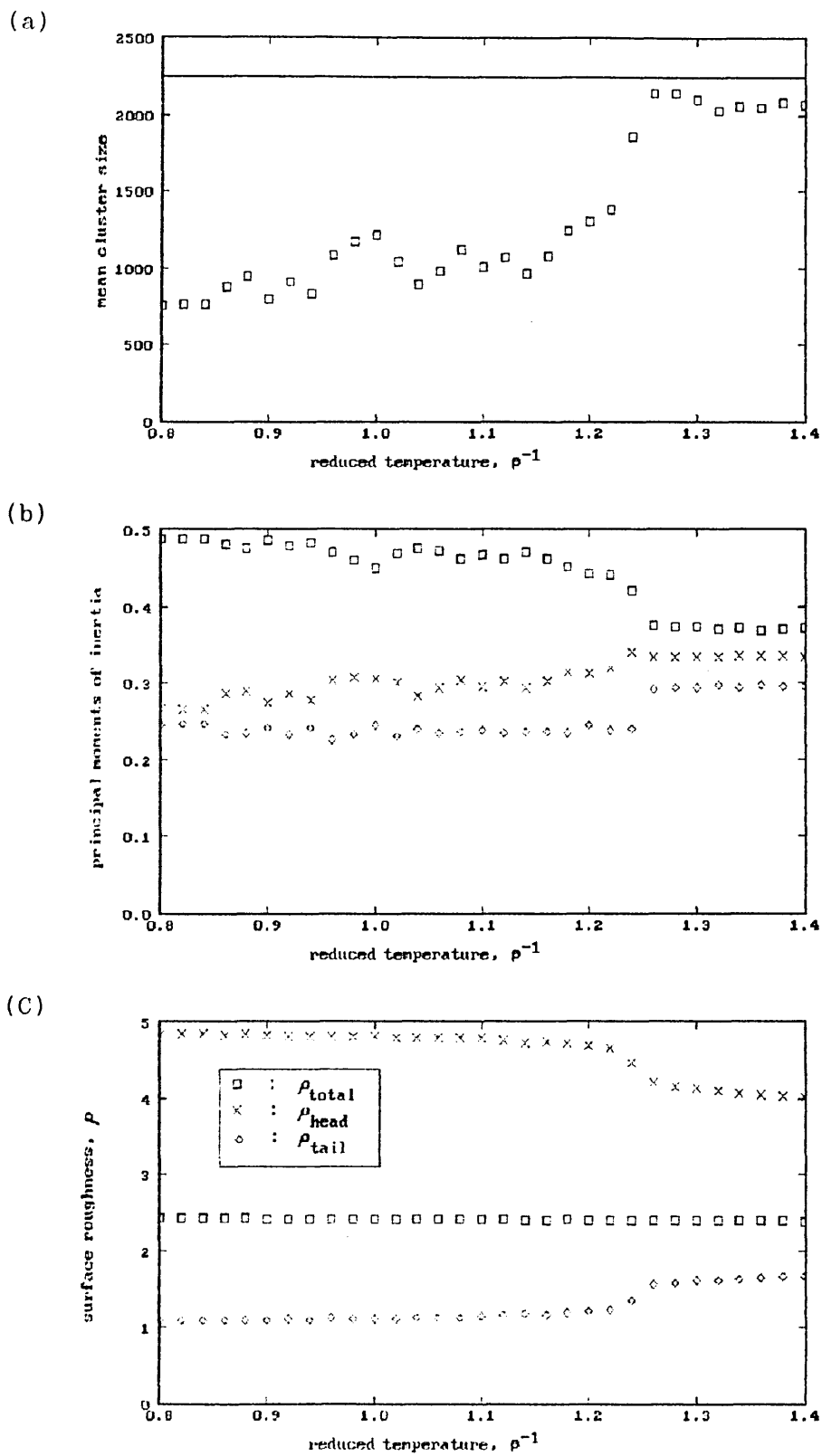


Figure A28 : Behaviour of the $s=4$, $\gamma=-2.0$, 55.0% amphiphile conc. system on cooling. (a) mean cluster size against reduced temperature (b) principal moments of inertia against reduced temperature (c) surface roughness against temperature.

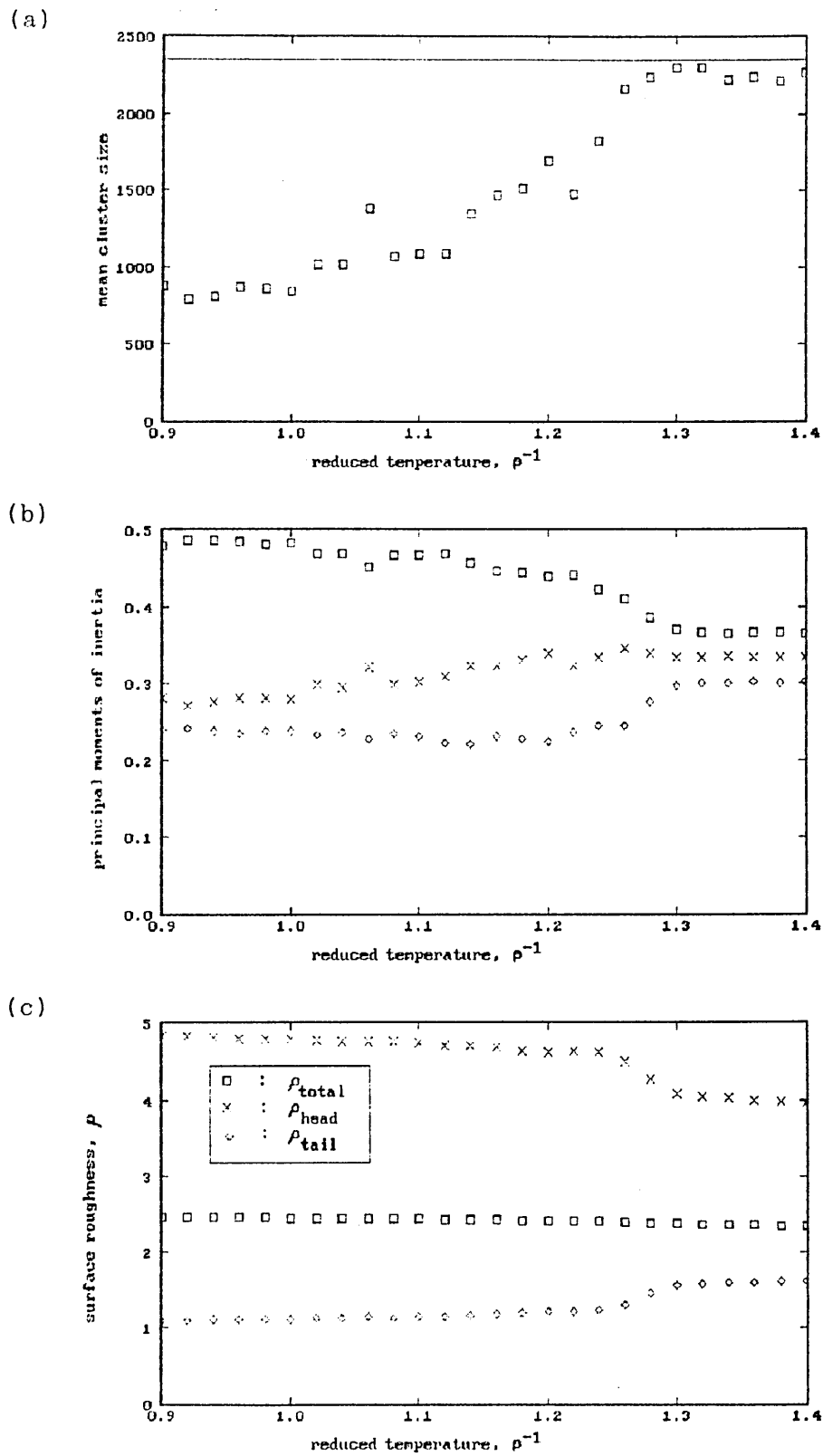


Figure A29 : Behaviour of the $s=4$, $\gamma=-2.0$, 57.5% amphiphile conc. system on cooling. (a) mean cluster size against reduced temperature (b) principal moments of inertia against reduced temperature (c) surface roughness against temperature.

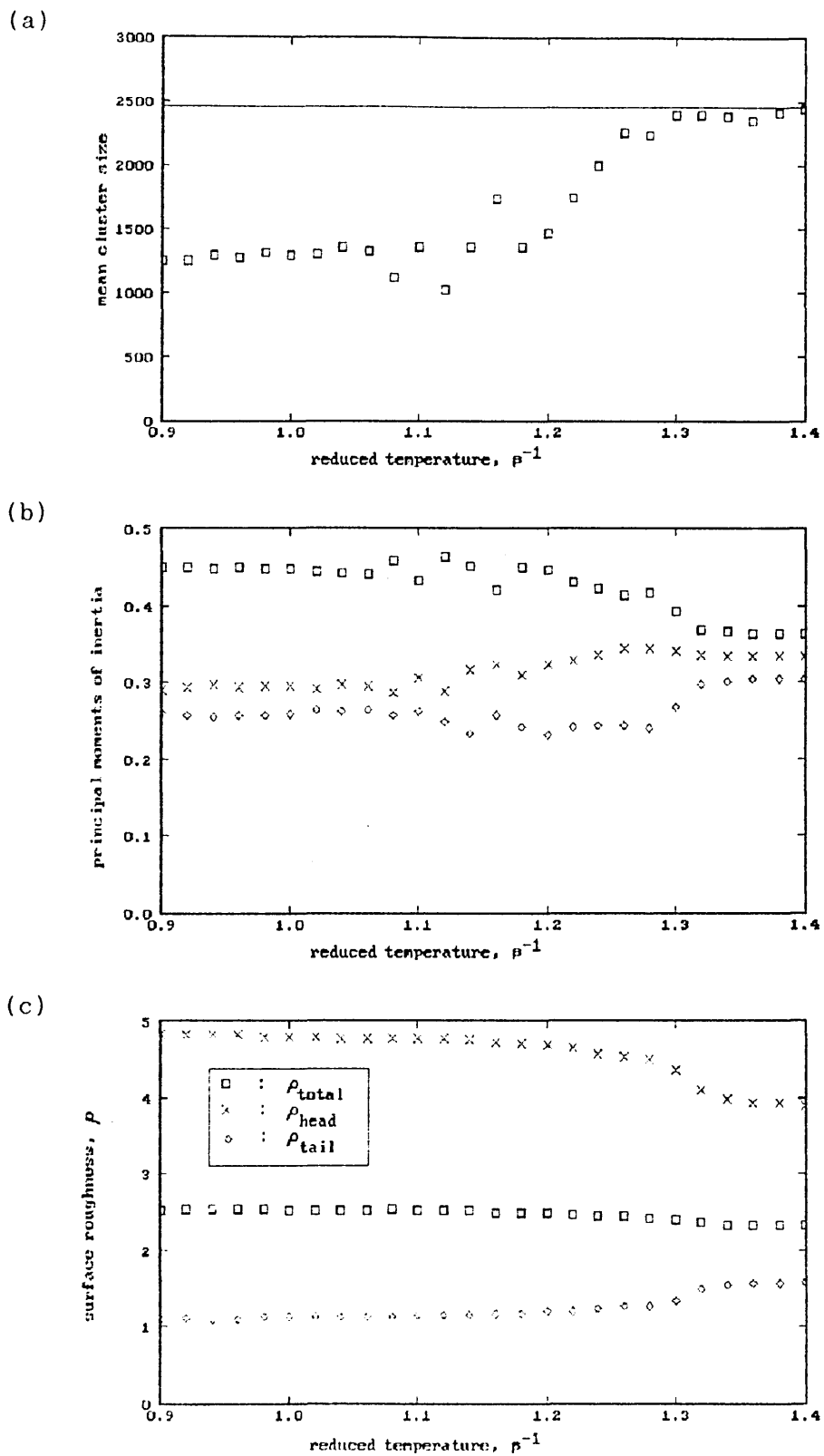


Figure A30 : Behaviour of the $s=4$, $\gamma=-2.0$, 60% amphiphile conc. system on cooling. (a) mean cluster size against reduced temperature (b) principal moments of inertia against reduced temperature (c) surface roughness against temperature.

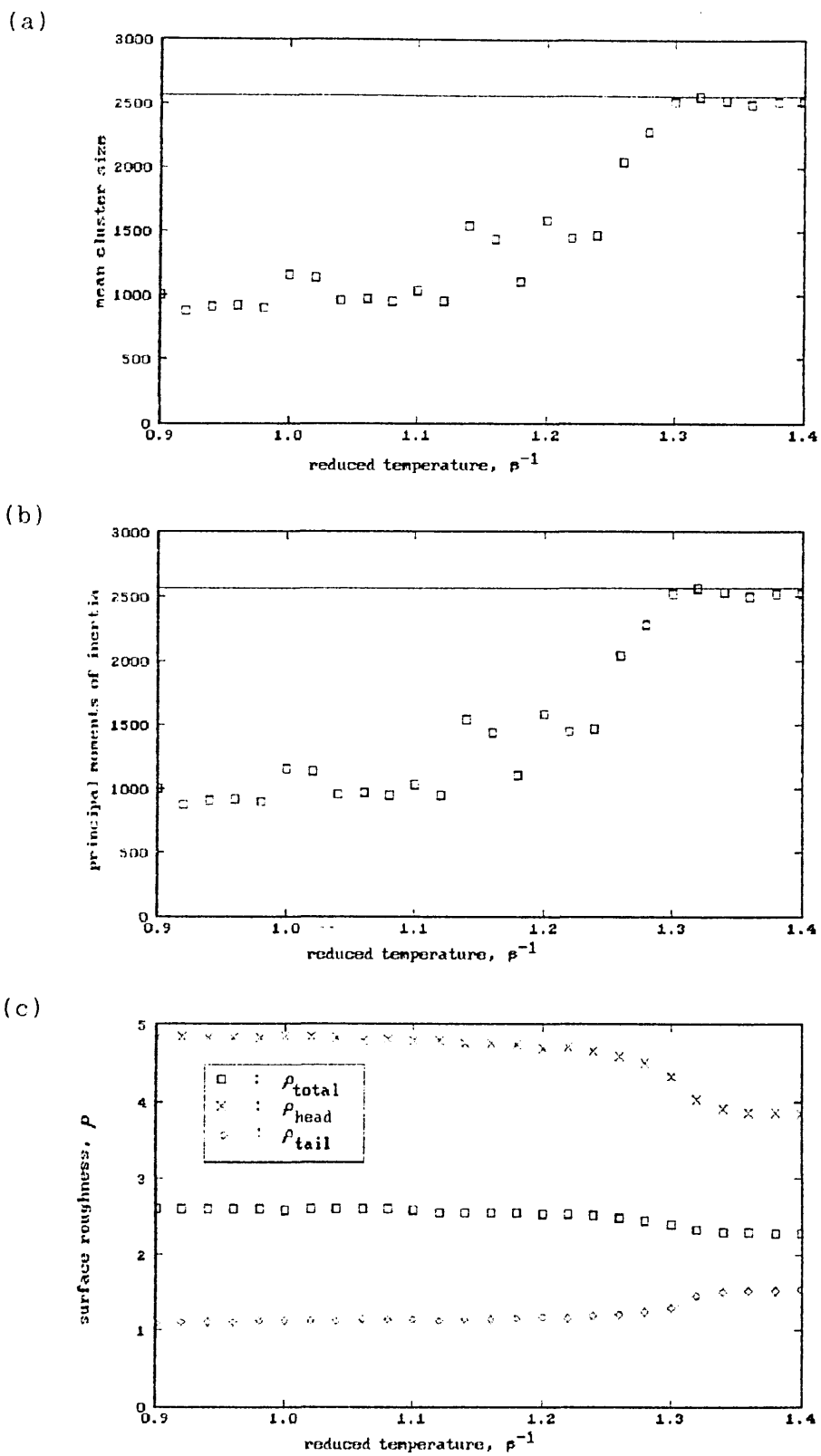


Figure A31 : Behaviour of the $s=4$, $\gamma=-2.0$, 62.5% amphiphile conc. system on cooling. (a) mean cluster size against reduced temperature (b) principal moments of inertia against reduced temperature (c) surface roughness against temperature.

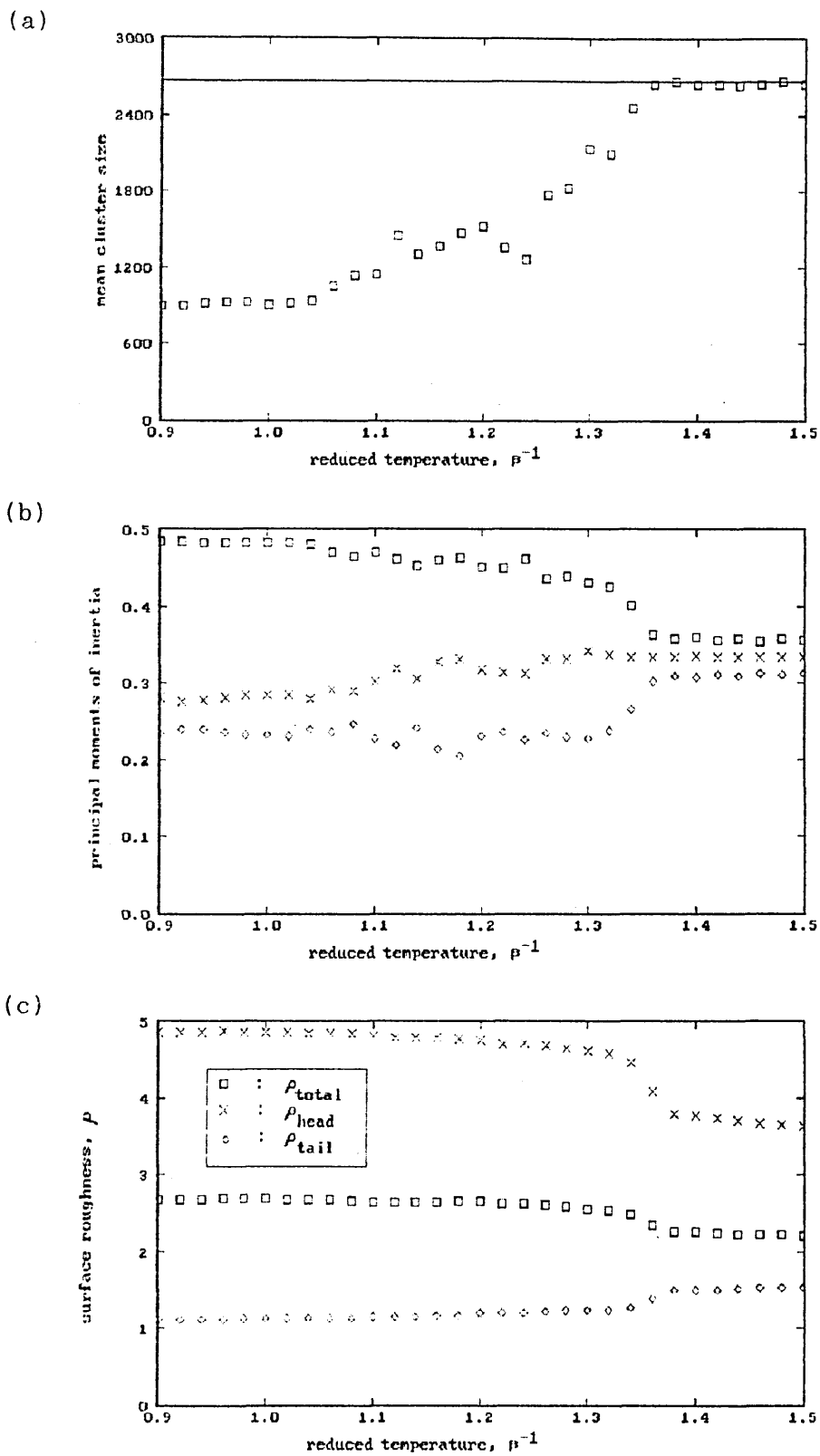
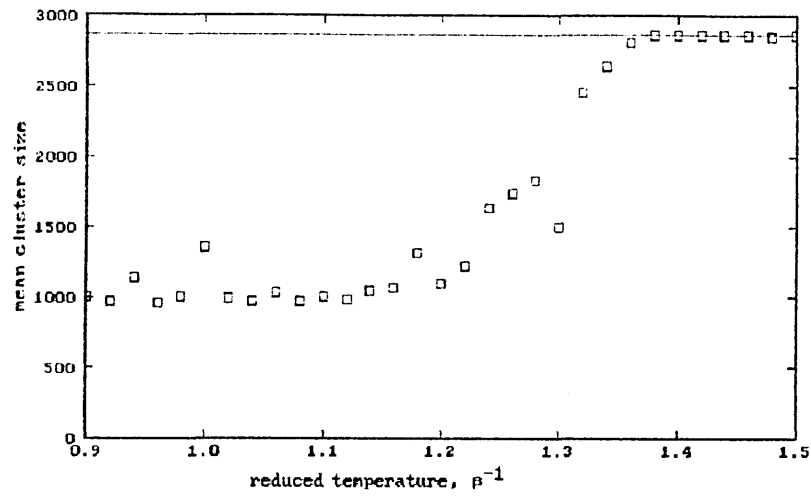
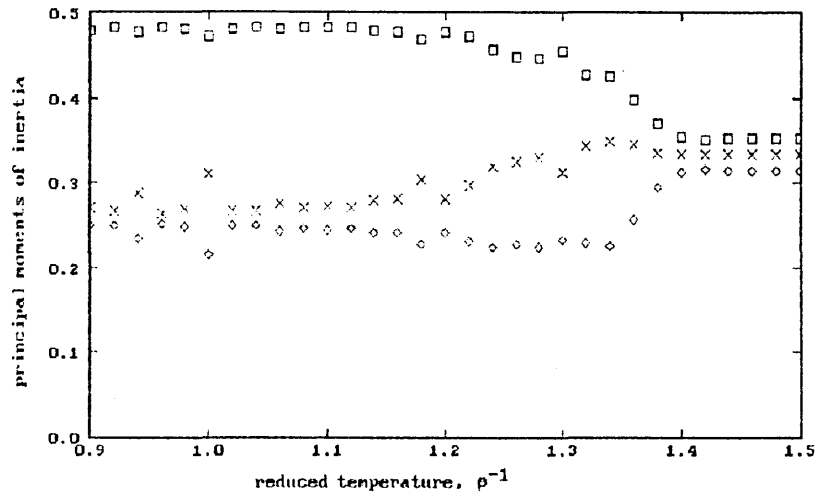


Figure A32 : Behaviour of the $s=4$, $\gamma=-2.0$, 65.0% amphiphile conc. system on cooling. (a) mean cluster size against reduced temperature (b) principal moments of inertia against reduced temperature (c) surface roughness against temperature.

(a)



(b)



(c)

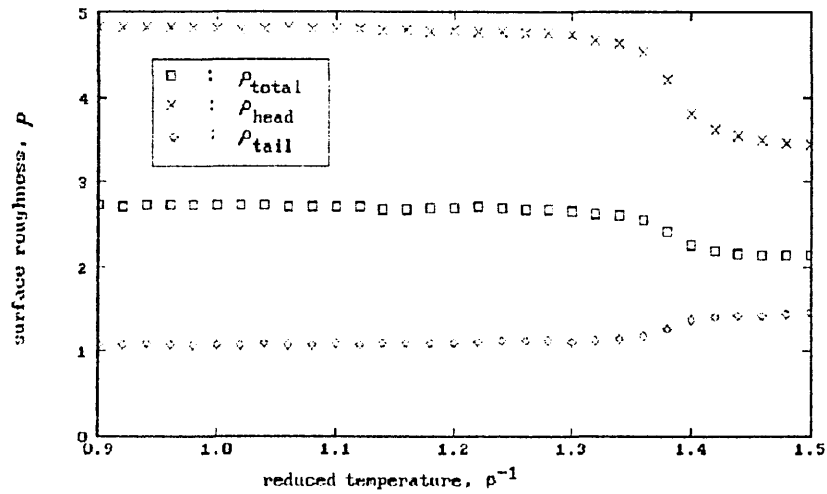


Figure A33 : Behaviour of the $s=4$, $\gamma=-2.0$, 70.0% amphiphile conc. system on cooling. (a) mean cluster size against reduced temperature (b) principal moments of inertia against reduced temperature (c) surface roughness against temperature.

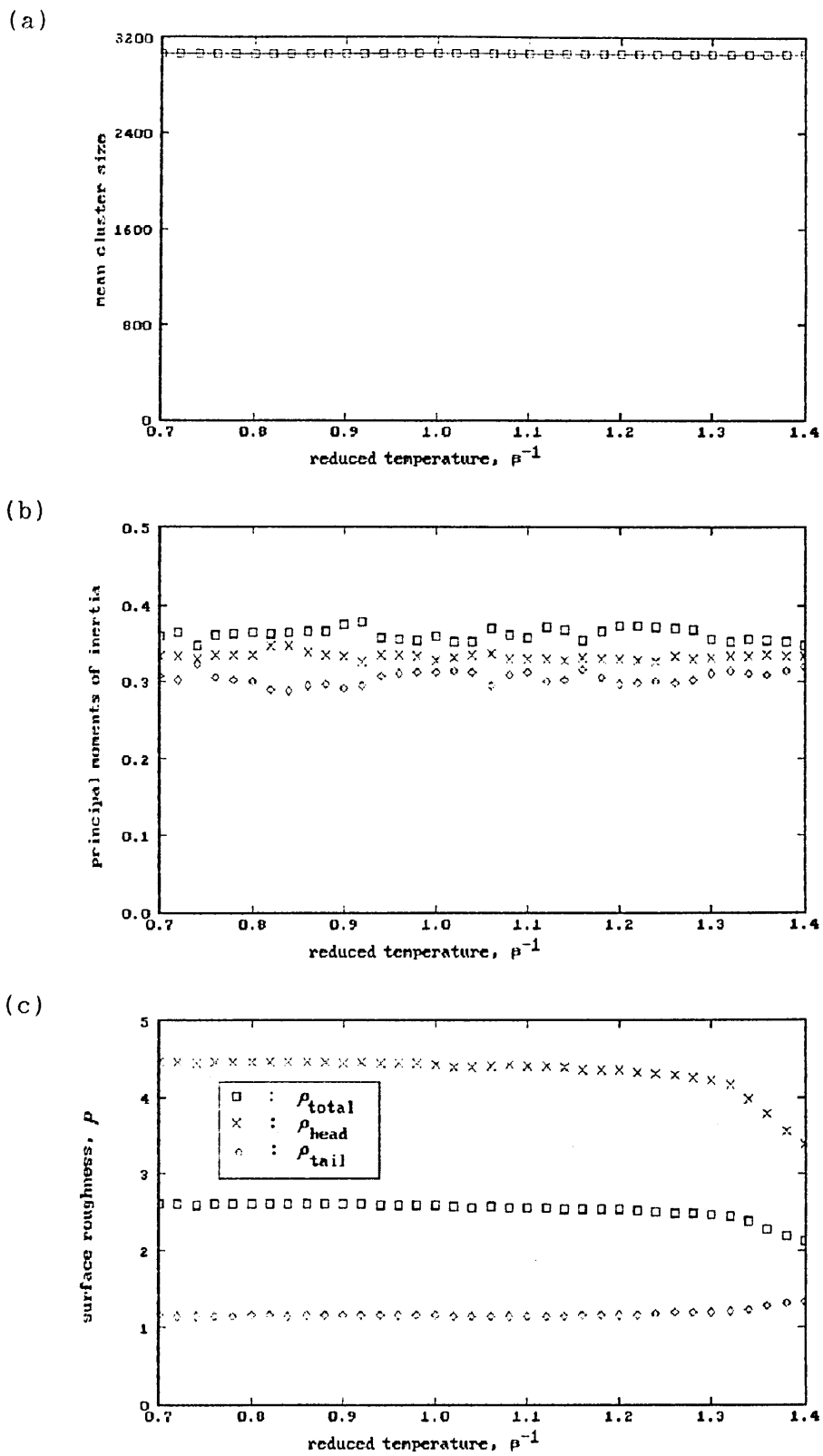


Figure A34 : Behaviour of the $s=4$, $\gamma=-2.0$, 75.0% amphiphile conc. system on cooling. (a) mean cluster size against reduced temperature (b) principal moments of inertia against reduced temperature (c) surface roughness against temperature.

In the mean field model, Chapter 6, it is necessary to determine the roots, α_i , of L-1 simultaneous equations. For simplicity, equations (6.29), Chapter 6, are expressed as

$$F_i(\alpha_1, \alpha_2, \dots, \alpha_{L-1}) = 0, \quad i=1, \dots, L-1 \quad (B1)$$

The Newton-Raphson iteration gives successively better estimates of the α_i using the relationship

$$X = F'^{-1} F \quad (B2)$$

where,

$$F = \begin{bmatrix} F_1 \\ F_2 \\ \vdots \\ F_{L-1} \end{bmatrix}, \quad F' = \begin{bmatrix} \partial F_1 / \partial \alpha_1 & \partial F_1 / \partial \alpha_2 & \dots & \partial F_1 / \partial \alpha_{L-1} \\ \partial F_2 / \partial \alpha_1 & \partial F_2 / \partial \alpha_2 & \dots & \partial F_2 / \partial \alpha_{L-1} \\ \vdots & \vdots & \ddots & \vdots \\ \partial F_{L-1} / \partial \alpha_1 & \dots & \dots & \partial F_{L-1} / \partial \alpha_{L-1} \end{bmatrix}$$

and

$$X = \begin{bmatrix} \alpha_1 - \alpha_{1_1} \\ \alpha_2 - \alpha_{1_2} \\ \vdots \\ \alpha_{L-1} - \alpha_{1_{L-1}} \end{bmatrix}$$

X is a vector of errors given by the difference of the current estimates of α_i and their predicted improved estimates, α_{1_i} . Pseudo-code for estimating the α_i is given below.

pseudo code : Solving α_i

begin

input initial estimates α_i

set $\text{err}_i = 0$

while ($\text{err}_i \neq 0$)

 determine F
 determine F'
 determine F'^{-1}

 set $X = F'^{-1}F$

 set $\alpha_i = \alpha_i$
 set $\alpha_i^1 = \alpha_i - X_i$
 set $\text{err}_i = \alpha_i / \alpha_i^1$

end while

end

The inverse matrix F'^{-1} is determined from F' using Gaussian Elimination with partial pivoting.